



Universität Regensburg

UNIVERSITY OF REGENSBURG

DOCTORAL THESIS

**Musculoskeletal modelling of the
shoulder complex and its application
for EMG assessed pathologies**

Author:

Maximilian AURBACH

Supervisor:

Prof.Dr.-Ing. Sebastian
DENDORFER

*A thesis submitted in fulfilment of the requirements
for the degree of Dr. scientiarum humanarum (Dr. sc. hum.)*

at the

Faculty of Medicine
University of Regensburg

conducted in the

Laboratory for Biomechanics
OTH Regensburg

submitted by

Maximilian Aurbach, M.Sc.

July 2020

Dean	Prof. Dr. Dirk Hellwig
Supervisor	Prof. Dr.-Ing. Sebastian Dendorfer
Mentors	Prof. Dr. med. Tobias Renkawitz Prof. Dr. Rainer Spang

Day of Defence 12.11.2020

Declaration of Authorship

I, Maximilian AURBACH, born at the 23.01.1990 in Heilbronn declare that this thesis titled, “Musculoskeletal modelling of the shoulder complex and its application for EMG assessed pathologies” and the work presented in it are my own. I confirm that:

- This work was done wholly or mainly while in candidature for a research degree at this University.
- Where any part of this thesis has previously been submitted for a degree or any other qualification at this University or any other institution, this has been clearly stated.
- Where I have consulted the published work of others, this is always clearly attributed.
- Where I have quoted from the work of others, the source is always given. With the exception of such quotations, this thesis is entirely my own work. I did not receive paid help from mediation and advisory services e.g. PhD consultants.
- I have acknowledged all main sources of help.
- Where the thesis is based on work done by myself jointly with others, I have made clear exactly what was done by others and what I have contributed myself.

Signed:

Date:

“If I have seen further it is by standing on the shoulders of Giants.”

Isaac Newton

“But I am very poorly today & very stupid & I hate everybody & everything. One lives only to make blunders.”

Charles Darwin

Abstract

The aim and purpose of the presented thesis is with regard to musculoskeletal model improvements of the human shoulder and simulation of pathologies. It addresses three distinct research questions. From a modelling perspective using an inverse dynamics approach, there is a discrepancy between computed glenohumeral joint reaction forces and in-vivo measurements above 90° humeral abduction. In-vivo measurements and muscle activities derived from electromyographic measurements indicate a continuous increase in the joint reaction force above 90° abduction. Models using an inverse dynamics approach however tend to compute decreasing forces above 90° abduction. In order to address this issue, several modelling parameters are tested and compared with regard to their effect on muscle activation and force development in the glenohumeral joint. Two clinical research questions are addressed and simulated with an updated model. The first investigates several operative techniques of a long biceps tendon transposition from a biomechanical perspective. As multiple techniques are used in the clinical practice, it is of interest how they compare in terms of joint reaction forces and whether one technique provides an outcome which is closer to the healthy state of the shoulder-arm complex. The second simulates tears of the m. supraspinatus and evaluates muscle recruitment changes, changes of the joint reaction forces and a comparison to electromyographic measurements. This is done in order to assess, how model predictions compare to observations in the clinical field and whether a generic model can predict these changes. The major outcomes of this thesis are threefold: it postulates the mechanical muscle properties Hill muscle model as key parameter for the force development in the glenohumeral joint during abduction, argues for an insertion of the long biceps tendon at the bicipital groove as superior operative technique from a biomechanical point of view and depicts a discrepancy between simulated symptomatic cases of a tear of the m. supraspinatus with regard to electromyographic measurements.

Zusammenfassung

Die Kernaspekte der vorliegenden Dissertation fokussieren sich auf die muskuloskelettale Modellierung und Simulation von Pathologien des menschlichen Schulterkomplexes. Die Arbeit adressiert innerhalb dieses Kontextes drei spezifische Forschungsfragen. Auf der Simulationsebene wurde die Muskelrekrutierung des Schulterkomplexes und die Kraftentwicklung innerhalb des Glenohumeralgelenks bei der Abduktion des Humerus untersucht. In-vivo Messungen basierend auf instrumentalisierten Endoprothesen des Humeruskopfes zeigen einen kontinuierlichen Anstieg der resultierenden Reaktionskraft im Glenohumeralgelenk bis zu 150° Abduktion. Eine hohe Aktivierung der involvierten Muskulatur bei der Abduktion über 90° wird ebenfalls durch elektromyographische Messungen bestätigt. Muskuloskelettale Modelle der Schulter, welche auf einem inversdynamischen Ansatz beruhen, berechnen jedoch zumeist sinkende Muskelaktivitäten und damit verbunden erniedrigte Gelenkreaktionskräfte. Um dieser Diskrepanz nachzugehen, wurden mehrere kinematische, kinetische und Muskelmodell Parameter auf ihre Auswirkung bezüglich Muskelaktivität und Gelenkreaktionskraft evaluiert und mit experimentellen elektromyographischen Messungen und der Literatur verglichen. Ferner wurde der Muskelfaserverlauf der anterioren, lateralen und posterioren Deltoiden mittels virtueller Torus-Objekte innerhalb des verwendeten Schultermodells für die Abduktion optimiert. Die erste der beiden klinischen Fragestellungen der dargelegten Arbeit bezieht sich auf eine Transposition der langen Bizepssehne. Mehrere verschiedene tenodese Techniken oder eine Tenotomie finden hierbei im klinischen Alltag Anwendung. Eine Untersuchung bezüglich biomechanischer Aspekte der unterschiedlichen Techniken ermöglicht hierbei Einblicke, welche am ehesten dem Normalzustand im Bezug auf Gelenkskraftentwicklung entspricht. Zwei tenodese Techniken und die Tenotomy wurden hierbei während der Ellbogenflexion, Pronation und einer kombinierten Bewegung simuliert, wobei die Reaktionskräfte und Momente im Schulter und Ellenbogengelenk mit einem intakten Modell verglichen wurden. Die zweite klinische Anwendung betrifft eine Ruptur des m. supraspinatus. Die Kinematik und Muskelaktivität gesunder und pathologischer Probanden wurden hierbei experimentell bei 6 verschiedenen Bewegungen gemessen. Die

Probanden wurden in Simulationsmodellen mit und ohne Riss des m. supraspinatus nachgebildet. Hierbei sollte ermittelt werden, ob ein generisches Modell Muskelrekrutierungsänderungen aufgrund einer Ruptur adäquat abbilden kann. Auf Simulationsebene konnte die Arbeit die mechanischen Eigenschaften des Hill Muskelmodells als mögliche physiologische Ursache und Erklärung für die steigenden Reaktionskräfte im Glenohumeralgelenk bei Abduktion $>90^\circ$ identifizieren. Im Bezug auf die biomechanischen Auswirkungen verschiedener Tenodesetechniken der langen Bizepssehne scheint eine Verankerung an der Bicipitalrinne aus mechanischer Sicht am ehesten die Kräfte des gesunden Modells zu erzeugen. Dies liegt an der Präservierung der generellen Richtung des Hebelarmes des langen Bizeps. Der Vergleich zwischen modellierten Aktivitäten mit und ohne Ruptur des m. supraspinatus konnte keine Übereinstimmung der simulierten und experimentellen Unterschiede bei symptomatischen Patienten zeigen. Dies wird auf eine eventuelle Veränderung der Kinematik der Scapula zurückgeführt, welche nicht im verwendeten Modell berücksichtigt wird. Die Erkenntnisse könnten jedoch für asymptomatische Rupturen gültig sein. Hierbei ist die Aussage, dass die Änderung in der Muskelrekrutierung nur geringfügig ist, jedoch die kumulative Erhöhung signifikante Auswirkung auf die Gelenkreaktionskraft hat.

Acknowledgements

First and foremost I would like to thank my supervisor Sebastian Dendorfer. His profound knowledge, demeanour, guidance and humour have inspired me for almost 10 years. I could not have wished for a better mentor and role model. A similar position is occupied by his right-hand man, Franz Süß. His serenity, critical thinking and comprehensive skill-set always were a tremendous help and example. Special thanks also go to Lars Krenkel for the entertaining, constructive discussion rounds and all-round knowledge. My colleagues Simon Auer, Simon Groß, Clemens Birkenmaier, Bernd Gamisch and Melina Tauwald deserve extra credits. The years spent together in hardship and laughter forged friendships which I will always cherish. A special place among these friends has Maximilian Melzner. I cannot thank him enough for his friendship, tremendous support and the awesome time together. Also thanks a lot to all for investing your time in the proofreading. Furthermore, I want to thank the Regensburg Centre of Biomedical Engineering in general and more specific Alexander Leis for providing the organisational framework for this work and giving the best support in all administrative questions. Special acknowledgements also receive all the student assistants which helped in the measurements and various aspects of this work during the years. Their eagerness to learn, enthusiasm and also frustration always made me remember why I started on this path in the first place. The contents of this thesis were created within the framework of the Interreg V, Project 38 by the EFRE, ZIEL-ETZ BY-CZ 2014-2020. In this context I want to thank my clinical and Czech project partners for the years of collaboration. I also received financial support by the Bavarian Academic Forum (BayWISS) – Doctoral Consortium “Health Research”, which enabled me to participate in various conferences and visit other research centres. For this I am really grateful, as these experiences were an integral part of my education. I furthermore want to acknowledge my mentors Sebastian and Dr. Tobias Renkawitz for their examination of this work, the committee of the defence and Jack for proofreading. Last but definitely not least I want to thank my mother Angelika, brother Martin, Sophie, Hektor, Loki and all my friends and flatmates for their love and support through the highs and lows. You made this journey amazing.

Contents

Declaration of Authorship	iii
Abstract	vi
Acknowledgements	ix
1 Introduction	38
2 Anatomy and functionality of the shoulder complex	43
3 Musculoskeletal modelling within the AnyBody™ Modeling System	51
3.1 The shoulder model of the AnyBody™ Modeling System	51
3.2 Recruitment of muscles within the AnyBody™ Modeling System . .	53
4 Evaluation of musculoskeletal modelling parameters of the shoulder complex during humeral abduction above 90°	55
4.1 Introduction	55
4.2 Materials and Methods	56
4.2.1 Experimental setup	56
4.2.2 Musculoskeletal modelling	57
Torus obstacle method for the deltoid wrapping (T)	58
Three element Hill muscle model (H) and strength scaling (S)	59
Motion capture driven clavicular protraction/elevation (CL) .	60
Force-dependent kinematics of the GH joint (FDK)	60
Alteration of scapula/clavicle rhythm (RHY)	60
Simulation	61
Validation of model activity vs. EMG	61
4.3 Results	63
4.4 Discussion	67

4.5	Conclusion	69
5	Modelling of the torus obstacle method as wrapping approach for the del- toid muscle group and investigation of muscle model parameters	70
5.1	Introduction	70
5.2	Materials and Methods	73
5.2.1	Torus modelling	73
5.2.2	Moment arm evaluation	75
5.2.3	Force transmission	76
5.2.4	Parameter evaluation of the Hill model	77
5.2.5	Recruitment criterion	79
5.3	Results	80
5.3.1	Moment arm evaluation	80
5.3.2	Force transmission	84
5.3.3	Parameter evaluation of the Hill model	89
5.3.4	Recruitment criterion	91
5.4	Discussion	95
5.4.1	Torus modelling	95
5.4.2	Moment arm evaluation	96
5.4.3	Force transmission	97
5.4.4	Parameter evaluation of the Hill model	99
5.4.5	Recruitment criterion	100
5.5	Conclusion	101
6	Clinical application: Biceps tendon transfer	102
6.1	Introduction	102
6.2	Materials & Methods	105
6.3	Results	107
6.4	Discussion	115
6.5	Conclusion	117
7	The effect of tears of the m. supraspinatus on the forces and muscle acti- vation pattern of the shoulder complex	118
7.1	Introduction	118
7.2	Materials and Methods	122
7.2.1	Experimental setup	122

7.2.2	Musculoskeletal computation of intact models and a simulated tear of the m. supraspinatus	124
7.2.3	Electromyographic comparison of healthy and pathological subjects	127
7.3	Results	129
7.3.1	Musculoskeletal computation of intact models and a simulated tear of the supraspinatus: Healthy subjects group with intact vs. pathological models	129
7.3.2	Forces and muscle activities of intact models and pathological models of the healthy vs. the pathological group	139
7.3.3	EMG comparison between the healthy vs. the pathological group	147
7.4	Discussion	155
7.4.1	Musculoskeletal simulation of intact models and simulated tears of the m. supraspinatus	155
	Comparison between intact and pathological models of the healthy group	155
	Comparison between intact models of the healthy group and pathological models of the patient group	156
7.4.2	EMG comparison between healthy subjects and patients with a tear of the m. supraspinatus	157
7.5	Conclusion	159
8	Conclusion	160
A	Supplementary material to chapter 5	177
A.1	Activity of the deltoids and GH joint reaction force of the ellipsoid model	177
A.2	Lateral and posterior momentarm comparison	179
A.3	Moments transmitted onto the humerus from the tori	181
A.4	Muscle activities and joint reaction force of the torus model with $p = 3$ and all forces / moments transmitted	183
B	Supplementary material to chapter 6	185
B.0.1	Joint reaction forces and moments on the elbow joint for the flexion, pronation and pouring motion	186

B.0.2	Joint reaction forces on the glenohumeral joint for the flexion, pronation and pouring motion	190
C	Supplementary material to chapter 7	193
C.0.1	Muscle activities of intact models and pathological models of the healthy subject group	194
	Neutral position	194
	Neutral position with 5N in hand	197
	Internal rotation	200
	External rotation	203
	External rotation with 5N in hand	206
C.0.2	Forces acting on the glenoid of intact models and pathological models of the healthy subject group	210
	Neutral position	210
	Neutral position with 5N in hand	212
	Internal rotation	214
	External rotation	216
	External rotation with 5N in hand	218
C.0.3	Numeric comparison of forces and muscle activities of intact models and pathological models of the healthy subject group	220
	Neutral position	220
	Neutral position with 5N in hand	221
	Internal rotation	222
	External rotation	223
	External rotation with 5N in hand	224
C.0.4	Kinematics of the humerus of healthy and pathological subjects	225
	Neutral position	225
	Neutral position with 5 N in hand	226
	Internal rotation	227
	External rotation	228
	External rotation with 5N in hand	229
C.0.5	Muscle activities of intact models and pathological models of the healthy vs. the pathological group	231
	Neutral position	231
	Neutral position with 5N in hand	234

	Internal rotation	237
	External rotation	240
	External rotation with 5N in hand	243
C.0.6	Forces acting on the glenoid of intact models and pathological models of the healthy vs. the pathological group	247
	Neutral position	247
	Neutral position with 5N in hand	249
	Internal rotation	251
	External rotation	253
	External rotation with 5N in hand	255
	Numeric comparison of forces and muscle activities of intact models and pathological models of the healthy vs. the pathological group	257
	Neutral position	257
	Neutral position with 5N in hand	258
	Internal rotation	259
	External rotation	260
	External rotation with 5N in hand	261
C.0.7	EMG comparison between the healthy vs. the pathological group	263
	Neutral position	263
	Neutral position 5N in hand	268
	Internal rotation	273
	External rotation	278
	External rotation 5N in hand	283
C.0.8	Median differences in the EMG between the healthy and pathological group	288
	Neutral position	288
	Neutral position 5N in hand	289
	Internal rotation	290
	External rotation	291
	External rotation 5N in hand	292

List of Figures

2.1	The joints and bones of the shoulder complex. (Adapted from Neumann, 2002 Figure 5-1.)	44
2.2	Range of motion of the shoulder complex (Adapted from Schünke, Schulte, and Schumacher, 2007).	45
2.3	The main muscles involved in the shoulder, posterior view. (Adapted from Henry Gray: Anatomy of the Human Body 1918, IV. Myology, 7. The Fascia and Muscles of the Upper Extremity. a. The Muscles Connecting the Upper Extremity, Fig. 409).	46
2.4	The main muscles involved in the shoulder, anterior view. (Adapted from Henry Gray: Anatomy of the Human Body 1918, IV. Myology, 7. The Fascia and Muscles of the Upper Extremity. a. The Muscles Connecting the Upper Extremity, Fig. 410).	47
2.5	The main muscles involved in the shoulder, top: rotator cuff muscles posterior view, bottom: rotator cuff muscles anterior view. (Adapted from Henry Gray: Anatomy of the Human Body 1918, IV. Myology, 7. The Fascia and Muscles of the Upper Extremity. a. The Muscles Connecting the Upper Extremity, Fig. 411 & 412).	48
3.1	Graphical representation of the AMS shoulder model (AMMR version V 2.2.2) from the posterior view.	52
4.1	Optical motion capture and EMG sensor placement on a test subject .	57
4.2	Preliminary implementation of the tori as an alternative wrapping for the deltoids	58
4.3	Principle of operation of the 3 element muscle model according to Hill. (Adapted from Delp et al., 1990 & O'Neill et al., 2013)	59

4.4	Resultant GH joint reaction force of the 16 combinations in %BW over the abduction angle of the humerus. Grey depicts the reference force data (Retrieved 15. May, 2018 from http://www.OrthoLoad.com , files: s1r_210206_1_42, s2r_040408_1_2, s2r_270306_1_86s3l_190308_1_48, s4r_140207_1_70, s5r_131108_1_40, s8r_161208_1_17, s8r_161208_1_31) and the continuous line the unchanged Basic model	64
4.5	Activity of considered muscle groups over the abduction angle. Continuous line: Mean EMG of all subjects. Grey area: standard deviation of EMG of all subjects. Dashed line: Mean activity of the Basic models of the considered muscle groups. Dash-dot line: Mean activity of the H-CL-T-S3 parameter combination.	66
5.1	Deltoid muscle elements of the model of the AMMR v.7.2 with anterior elements highlighted in red. Left: Abduction at 90° , Right: Abduction at 120°	72
5.2	Model with the translated tori in default position at 0° abduction (left) and muscle pathing at 120° abduction, tori are graphically omitted (right)	74
5.3	Torus obstacles of the deltoid within the AMS. On the left is the model in default position at 0° of abduction. On the right is the model at 120° abduction, where the position of the tori translate on the long axis of the humerus with a fixed distance to the acromion (blue coordinate system) as the humeral head moves under the scapula (green coordinate system)	75
5.4	Moment arms during glenohumeral abduction in the range 20 – 120° of the anterior deltoid elements. Grey: moment arms from a cadaver study by Ackland et al., 2008 Black: anterior deltoid moment arms of the via point model, 6 associated model elements. Lines are labelled from 1-6 from the most anterior to the most lateral element. Orange: anterior deltoid moment arms of the ellipsoid model, 4 associated model elements. Lines are labelled from 1-4 from the most anterior to the most lateral element. Blue: anterior deltoid moment arms of the torus model, 4 associated model elements. Lines are labelled from 1-4 from the most anterior to the most lateral element.	81

5.5	Moment arms during glenohumeral abduction in the range 20 – 120°. Each part of the deltoid (anterior, lateral, posterior) is represented by 4 model elements (black lines), with an increasing numeration from 1-12 from the most anterior to the most posterior element. Grey depicts the moment arms from a cadaver study (Ackland et al., 2008)	83
5.6	Activity of the anterior, lateral and posterior deltoid groups during abduction between 30-120° of the EMG mean (blue) and it's standard deviation (blue envelope), the mean of the NOFM model (purple), the FXZ model (yellow) and the ALLFM configuration (red) with p = 5 .	85
5.7	Resultant GH joint reaction force in %BW over the abduction angle of the humerus. Grey depicts an envelope of the in-vivo data (Retrieved 15. May, 2018 from http://www.OrthoLoad.com , files: s1r_210206_1_42, s2r_040408_1_2, s2r_270306_1_86, s3l_190308_1_48, s4r_140207_1_70, s5r_131108_1_40, s8r_161208_1_17, s8r_161208_1_31) in comparison to the NOFM (purple), FXZ (yellow) and ALLFM approaches in force transmission	86
5.8	Forces transmitted from the anterior, lateral and posterior tori carrier elements onto the humerus from the ALLFM model (see 5.2.3) during abduction of the humerus in the range 30-120°. X,Y and Z components are expressed in the humerus coordinate frame (Figure 5.3, green coordinate system).	88
5.9	Resultant GH joint reaction force over abduction angle of single alterations of the Hill model. Single parameters are set to 50% of their initial value. Parameters are explained in detail in Table 5.1. Grey depicts the in-vivo force data (Retrieved 15. May, 2018 from www.OrthoLoad.com , files: s1r_210206_1_42, s2r_040408_1_2, s2r_270306_1_86, s3l_190308_1_48, s4r_140207_1_70, s5r_131108_1_40, s8r_161208_1_17, s8r_161208_1_31). 89	
5.10	Resultant GH joint reaction force over abduction angle of single alterations of the Hill model, single parameters set to 200% of their initial value. Parameters are explained in detail in Table 5.1. Grey depicts the in-vivo force data(Retrieved 15. May, 2018 from www.OrthoLoad.com , files: s1r_210206_1_42, s2r_040408_1_2, s2r_270306_1_86, s3l_190308_1_48, s4r_140207_1_70, s5r_131108_1_40, s8r_161208_1_17, s8r_161208_1_31). 90	

5.11	Activity of the m. supraspinatus muscle during humeral abduction in the range 30-120° of four model configurations: polynomial recruitment criterion with power $p=3$ (green) and $p=5$ (purple). Dashed lines are with a force applied to the palm of 20 N	91
5.12	Activity of the anterior, lateral and posterior deltoid groups during abduction between 30-120° of the EMG mean (blue), the mean of the ALLFM model with $p = 5$ (purple) and the ellipsoid model with $p = 5$ (orange). Standard deviations are provided by the corresponding shaded areas	93
5.13	Resultant GH joint reaction force in %BW over the abduction angle of the humerus. Grey depicts an envelope of the in-vivo data from literature (Retrieved 15. May, 2018 from http://www.OrthoLoad.com , files: s1r_210206_1_42, s2r_040408_1_2, s2r_270306_1_86, s3l_190308_1_48, s4r_140207_1_70, s5r_131108_1_40, s8r_161208_1_17, s8r_161208_1_31) in comparison to the torus model with $p=5$ and the ellipsoid model with $p=5$	94
6.1	Different origins of the biceps caput longum a) original model (ORG) b) tendon insertion on the bicipital groove at the humeral head (HH) c) tendon insertion on the coracoid at the origin of the caput breve (CB)	105
6.2	IS force in the GH joint over the EL flexion angle during flexion for the ORG, HH, CB and OFF model	108
6.3	IS force in the GH joint over the EL pronation angle during pronation for the ORG, HH, CB and OFF model	109
6.4	IS force in the GH joint over the EL pronation angle during the pouring motion for the ORG, HH, CB and OFF model	110
6.5	Representation of the force direction acting on the glenoid, where the arrows indicate the largest shift from the ORG model to the surgical models for flexion (magenta), pronation (green) and pouring (red) . .	111
6.6	PA force in the EL joint over the EL flexion angle during the flexion motion for the ORG, HH, CB and OFF model	112
6.7	PA force in the EL joint over the EL pronation angle during the pronation motion for the ORG, HH, CB and OFF model	113
6.8	PA force in the EL joint over the EL pronation angle during the pouring motion for the ORG, HH, CB and OFF model	114

7.1	EMG sensor placement of the 14 contemplated muscles of interest on a healthy test subject.	123
7.2	Scapula segment with the simulated glenoid (blue dots) and the coordinate system in which the forces acting on the glenoid are expressed. The Y direction of the coordinate system is referred to from inferior to superior, the Z anterior to posterior and the negative X direction as compression force.	126
7.3	EMG computation steps of the middle deltoid of one subject during neutral position (5 N) trial. Top: raw EMG signal (blue). Second: wavelet de-noised signal (cyan), RMS of the rloess smoothed wavelet signal (orange). Third: RMS interpolated over abduction angle from MoCap model (blue) and computed for 5° increments (red dot). Fourth: normalized signal (blue) and 5° increments (red dots) to the 85° position.	128
7.4	Activities of the m. supraspinatus computed by the models of the healthy control group over the abduction angle in 5° increments. Activities are from the neutral position, internal rotation and external rotation trials without weight.	130
7.5	Activities of the m. supraspinatus computed by the models of the healthy control group over the abduction angle in 5° increments. Activities are from the neutral position, internal rotation and external rotation trials with 5 N load in hand.	131
7.6	Computed muscle activities of the anterior, posterior and lateral deltoids over the abduction angle in 5° increments during the internal rotation trial with 5 N load in hand. Blue depicts the activities of the intact model and red the modelled tear of the m. supraspinatus Blue depicts the activities of the intact model and red the modelled tear of the m. supraspinatus of the healthy subject cohort.	133
7.7	Computed muscle activities of infraspinatus, subscapularis and teres minor over the abduction angle in 5° increments during the internal rotation trial with 5 N load in hand. Blue depicts the activities of the intact model and red the modelled tear of the m. supraspinatus of the healthy subject cohort.	134

7.8	Computed muscle activities of the biceps, triceps and pectoralis major over the abduction angle in 5° increments during the internal rotation trial with 5 N load in hand. Blue depicts the activities of the intact model and red the modelled tear of the m. supraspinatus of the healthy subject cohort.	135
7.9	Projected median GH joint reaction force of all models onto the glenoid of intact and pathological models of the healthy subject cohort during the internal rotation trial with 5 N load in hand. Intact/healthy models (blue) and pathological models (red) with their starting value at 25° abduction and the progression up to 85° abduction.	137
7.10	Compression force, inferior-superior force and anterior-posterior force of intact (blue) and pathological (red) models of the healthy subject cohort during the internal rotation trial with 5 N load in hand over the abduction angle in 5° increments.	138
7.11	Flexion and external rotation angle over abduction of the healthy cohort (blue) and pathological cohort (red) during the internal rotation trial with 5 N load in hand.	140
7.12	Computed muscle activities of the anterior, posterior and lateral deltoids over the abduction angle in 5° increments during the internal rotation trial with 5 N load in hand. Blue depicts the activities of the intact model of the healthy subject group and red the modelled tear of the m. supraspinatus of the patient group.	141
7.13	Computed muscle activities of the infraspinatus, subscapularis and teres minor over the abduction angle in 5° increments during the internal rotation trial with 5 N load in hand. Blue depicts the activities of the intact model of the healthy subject group and red the modelled tear of the m. supraspinatus of the patient group.	142
7.14	Computed muscle activities of the biceps, triceps and pectoralis major over the abduction angle in 5° increments during the internal rotation trial with 5 N load in hand. Blue depicts the activities of the intact model of the healthy subject group and red the modelled tear of the m. supraspinatus of the patient group.	143

7.15	Projected median GH joint reaction force of all models onto the glenoid of intact models of the healthy subject cohort and pathological models of the patient group during the internal rotation trial with 5 N load in hand. Intact models of the healthy control (blue) and pathological models of the patient group (red) with their starting value at 25° abduction and the progression up to 85° abduction.	145
7.16	Compression force, inferior-superior force and anterior-posterior force of intact models of the healthy control (blue) and pathological models of the patient group (red) during the internal rotation trial with 5 N load in hand over the abduction angle in 5° increments.	146
7.17	EMG muscle activities normalized to the 85° position of the neutral position trial with 5 N load in hand of the trapezius pars descendens, trapezius pars transversa and trapezius pars ascendens over the abduction angle in 5° increments during the internal rotation trial with 5 N load in hand. Blue depicts the EMG activities of the healthy subject group and red of the patient group.	149
7.18	EMG muscle activities normalized to the 85° position of the neutral position trial with 5 N load in hand of the anterior deltoid, lateral deltoid and posterior deltoid over the abduction angle in 5° increments during the internal rotation trial with 5 N load in hand. Blue depicts the EMG activities of the healthy subject group and red of the patient group.	150
7.19	EMG muscle activities normalized to the 85° position of the neutral position trial with 5 N load in hand of the infraspinatus, serratus anterior and latissimus over the abduction angle in 5° increments during the internal rotation trial with 5 N load in hand. Blue depicts the EMG activities of the healthy subject group and red of the patient group.	151
7.20	EMG muscle activities normalized to the 85° position of the neutral position trial with 5 N load in hand of the biceps, triceps and rhomboideus minor over the abduction angle in 5° increments during the internal rotation trial with 5 N load in hand. Blue depicts the EMG activities of the healthy subject group and red of the patient group.	152

7.21	EMG muscle activities normalized to the 85° position of the neutral position trial with 5 N load in hand of the rhomboideus major and pectoralis major over the abduction angle in 5° increments during the internal rotation trial with 5 N load in hand. Blue depicts the EMG activities of the healthy subject group and red of the patient group. .	153
A.1	Resultant GHJF in the range of 20 – 120° humeral abduction. The grey shaded area is an envelope of the in-vivo data obtained by Bergmann et al. The orange line is the average calculated GHJF from the motion capture models with ellipsoid wrapping and $p = 5$, with the orange shaded area representing the standard deviation.	177
A.2	Activity of the anterior, lateral and posterior deltoid groups during abduction between 30-120° of the EMG mean (blue) and the ellipsoid model with $p = 5$ (orange). Standard deviations are provided by the corresponding shaded areas	178
A.3	Moment arms during glenohumeral abduction in the range 20 – 120° of the lateral deltoid elements. Grey: moment arms from a cadaver study by Ackland et al., 2008 Black: lateral deltoid moment arms of the via point model, 4 associated model elements. Orange: lateral deltoid moment arms of the ellipsoid model, 4 associated model elements. Blue: lateral deltoid moment arms of the torus model, 4 associated model elements.	179
A.4	Moment arms during glenohumeral abduction in the range 20 – 120° of the posterior deltoid elements. Grey: moment arms from a cadaver study by Ackland et al., 2008 Black: posterior deltoid moment arms of the via point model, 2 associated model elements. Orange: posterior deltoid moment arms of the ellipsoid model, 4 associated model elements. Blue: posterior deltoid moment arms of the torus model, 4 associated model elements.	180
A.5	Moments transmitted from the anterior, lateral and posterior tori carrier elements onto the humerus from the ALLFM model (see 5.2.3) during abduction of the humerus in the range 30-120°. X,Y and Z components are expressed in the humerus coordinate frame (Figure 5.3, green coordinate system).	181

A.6	Activity of the anterior, lateral and posterior deltoid groups during abduction between 30-120° of the EMG mean (blue), the ellipsoid (orange) and the torus model (purple) with $p = 3$	183
A.7	Resultant GH joint reaction force in %BW over the abduction angle of the humerus. Grey depicts an envelope of the in-vivo data (Retrieved 15. May, 2018 from http://www.OrthoLoad.com , files: s1r_210206_1_42, s2r_040408_1_2, s2r_270306_1_86, s3l_190308_1_48, s4r_140207_1_70, s5r_131108_1_40, s8r_161208_1_17, s8r_161208_1_31) in comparison to the the ellipsoid (orange) and the torus model (purple) with $p = 3$	184
B.1	Forces and moments acting on the EL joint over the EL flexion angle during flexion for the ORG, HH, CB and OFF model	186
B.2	Forces and moments acting on the EL joint over the EL pronation angle during pronation for the ORG, HH, CB and OFF model	187
B.3	Forces and moments acting on the EL joint over the EL pronation angle during the pouring motion for the ORG, HH, CB and OFF model	188
B.4	Forces in the GH joint over the EL flexion angle during flexion for the ORG, HH, CB and OFF model	190
B.5	Forces in the GH joint over the EL pronation angle during pronation for the ORG, HH, CB and OFF model	191
B.6	Forces in the GH joint over the EL pronation angle during the pouring motion for the ORG, HH, CB and OFF model	192
C.1	Computed muscle activities of the anterior, posterior and lateral deltoids over the abduction angle in 5° increments during the neutral position trial. Blue depicts the activities of the intact model and red the modelled tear of the m. supraspinatus. Blue depicts the activities of the intact model and red the modelled tear of the m. supraspinatus of the healthy subject cohort.	194
C.2	Computed muscle activities of infraspinatus, subscapularis and teres minor over the abduction angle in 5° increments during the neutral position trial with 5 N load in hand. Blue depicts the activities of the intact model and red the modelled tear of the m. supraspinatus of the healthy subject cohort.	195

C.3	Computed muscle activities of the biceps, triceps and pectoralis major over the abduction angle in 5° increments during the neutral position trial. Blue depicts the activities of the intact model and red the modelled tear of the m. supraspinatus of the healthy subject cohort. . . .	196
C.4	Computed muscle activities of the anterior, posterior and lateral deltoids over the abduction angle in 5° increments during the neutral position trial with 5 N load in hand. Blue depicts the activities of the intact model and red the modelled tear of the m. supraspinatus. Blue depicts the activities of the intact model and red the modelled tear of the m. supraspinatus of the healthy subject cohort.	197
C.5	Computed muscle activities of infraspinatus, subscapularis and teres minor over the abduction angle in 5° increments during the neutral position trial with 5 N load in hand. Blue depicts the activities of the intact model and red the modelled tear of the m. supraspinatus of the healthy subject cohort.	198
C.6	Computed muscle activities of the biceps, triceps and pectoralis major over the abduction angle in 5° increments during the neutral position trial with 5 N load in hand. Blue depicts the activities of the intact model and red the modelled tear of the m. supraspinatus of the healthy subject cohort.	199
C.7	Computed muscle activities of the anterior, posterior and lateral deltoids over the abduction angle in 5° increments during the internal rotation trial. Blue depicts the activities of the intact model and red the modelled tear of the m. supraspinatus. Blue depicts the activities of the intact model and red the modelled tear of the m. supraspinatus of the healthy subject cohort.	200
C.8	Computed muscle activities of infraspinatus, subscapularis and teres minor over the abduction angle in 5° increments during the internal rotation trial. Blue depicts the activities of the intact model and red the modelled tear of the m. supraspinatus of the healthy subject cohort.	201
C.9	Computed muscle activities of the biceps, triceps and pectoralis major over the abduction angle in 5° increments during the internal rotation trial. Blue depicts the activities of the intact model and red the modelled tear of the m. supraspinatus of the healthy subject cohort.	202

C.10	Computed muscle activities of the anterior, posterior and lateral deltoids over the abduction angle in 5° increments during the external rotation trial. Blue depicts the activities of the intact model and red the modelled tear of the m. supraspinatus. Blue depicts the activities of the intact model and red the modelled tear of the m. supraspinatus of the healthy subject cohort.	203
C.11	Computed muscle activities of infraspinatus, subscapularis and teres minor over the abduction angle in 5° increments during the external rotation trial. Blue depicts the activities of the intact model and red the modelled tear of the m. supraspinatus of the healthy subject cohort.	204
C.12	Computed muscle activities of the biceps, triceps and pectoralis major over the abduction angle in 5° increments during the external rotation trial. Blue depicts the activities of the intact model and red the modelled tear of the m. supraspinatus of the healthy subject cohort.	205
C.13	Computed muscle activities of the anterior, posterior and lateral deltoids over the abduction angle in 5° increments during the external rotation trial with 5 N load in hand. Blue depicts the activities of the intact model and red the modelled tear of the m. supraspinatus. Blue depicts the activities of the intact model and red the modelled tear of the m. supraspinatus of the healthy subject cohort.	206
C.14	Computed muscle activities of infraspinatus, subscapularis and teres minor over the abduction angle in 5° increments during the external rotation trial with 5 N load in hand. Blue depicts the activities of the intact model and red the modelled tear of the m. supraspinatus of the healthy subject cohort.	207
C.15	Computed muscle activities of the biceps, triceps and pectoralis major over the abduction angle in 5° increments during the external rotation trial with 5 N load in hand. Blue depicts the activities of the intact model and red the modelled tear of the m. supraspinatus of the healthy subject cohort.	208
C.16	Compression force, inferior-superior force and anterior-posterior force of intact (blue) and pathological (red) models of the healthy subject cohort during the neutral position trial over the abduction angle in 5° increments.	210

C.17	Projected median GH joint reaction force of all models onto the glenoid of intact and pathological models of the healthy subject cohort during the neutral position trial. Intact/healthy models (blue) and pathological models (red) with their starting value at 25° abduction and the progression up to 85° abduction.	211
C.18	Compression force, inferior-superior force and anterior-posterior force of intact (blue) and pathological (red) models of the healthy subject cohort during the neutral position trial with 5 N load in hand over the abduction angle in 5° increments.	212
C.19	Projected median GH joint reaction force of all models onto the glenoid of intact and pathological models of the healthy subject cohort during the neutral position trial with 5 N load in hand. Intact/healthy models (blue) and pathological models (red) with their starting value at 25° abduction and the progression up to 85° abduction.	213
C.20	Compression force, inferior-superior force and anterior-posterior force of intact (blue) and pathological (red) models of the healthy subject cohort during the internal rotation trial over the abduction angle in 5° increments.	214
C.21	Projected median GH joint reaction force of all models onto the glenoid of intact and pathological models of the healthy subject cohort during the internal rotation trial. Intact/healthy models (blue) and pathological models (red) with their starting value at 25° abduction and the progression up to 85° abduction.	215
C.22	Compression force, inferior-superior force and anterior-posterior force of intact (blue) and pathological (red) models of the healthy subject cohort during the external rotation trial over the abduction angle in 5° increments.	216
C.23	Projected median GH joint reaction force of all models onto the glenoid of intact and pathological models of the healthy subject cohort during the external rotation trial. Intact/healthy models (blue) and pathological models (red) with their starting value at 25° abduction and the progression up to 85° abduction.	217

C.24	Compression force, inferior-superior force and anterior-posterior force of intact (blue) and pathological (red) models of the healthy subject cohort during the external rotation trial with 5 N load in hand over the abduction angle in 5° increments.	218
C.25	Projected median GH joint reaction force of all models onto the glenoid of intact and pathological models of the healthy subject cohort during the external rotation trial with 5 N in hand. Intact/healthy models (blue) and pathological models (red) with their starting value at 25° abduction and the progression up to 85° abduction.	219
C.26	Flexion and external rotation angle over abduction of the healthy cohort (blue) and pathological cohort (red) during the neutral position trial.	225
C.27	Flexion and external rotation angle over abduction of the healthy cohort (blue) and pathological cohort (red) during the neutral position trial with 5 N load in hand.	226
C.28	Flexion and external rotation angle over abduction of the healthy cohort (blue) and pathological cohort (red) during the internal rotation trial.	227
C.29	Flexion and external rotation angle over abduction of the healthy cohort (blue) and pathological cohort (red) during the external rotation trial.	228
C.30	Flexion and external rotation angle over abduction of the healthy cohort (blue) and pathological cohort (red) during the external rotation trial with 5 N load in hand.	229
C.31	Computed muscle activities of the anterior, posterior and lateral deltoids over the abduction angle in 5° increments during the neutral position trial. Blue depicts the activities of the intact model of the healthy subject group and red the modelled tear of the m. supraspinatus of the patient group.	231
C.32	Computed muscle activities of the infraspinatus, subscapularis and teres minor over the abduction angle in 5° increments during the neutral position trial. Blue depicts the activities of the intact model of the healthy subject group and red the modelled tear of the m. supraspinatus of the patient group.	232

C.33	Computed muscle activities of the biceps, triceps and pectoralis major over the abduction angle in 5° increments during the neutral position trial. Blue depicts the activities of the intact model of the healthy subject group and red the modelled tear of the m. supraspinatus of the patient group.	233
C.34	Computed muscle activities of the anterior, posterior and lateral deltoids over the abduction angle in 5° increments during the neutral position trial with 5 N load in hand. Blue depicts the activities of the intact model of the healthy subject group and red the modelled tear of the m. supraspinatus of the patient group.	234
C.35	Computed muscle activities of the infraspinatus, subscapularis and teres minor over the abduction angle in 5° increments during the neutral position trial with 5 N load in hand. Blue depicts the activities of the intact model of the healthy subject group and red the modelled tear of the m. supraspinatus of the patient group.	235
C.36	Computed muscle activities of the biceps, triceps and pectoralis major over the abduction angle in 5° increments during the neutral position trial with 5 N load in hand. Blue depicts the activities of the intact model of the healthy subject group and red the modelled tear of the m. supraspinatus of the patient group.	236
C.37	Computed muscle activities of the anterior, posterior and lateral deltoids over the abduction angle in 5° increments during the internal rotation trial. Blue depicts the activities of the intact model of the healthy subject group and red the modelled tear of the m. supraspinatus of the patient group.	237
C.38	Computed muscle activities of the infraspinatus, subscapularis and teres minor over the abduction angle in 5° increments during the internal rotation trial. Blue depicts the activities of the intact model of the healthy subject group and red the modelled tear of the m. supraspinatus of the patient group.	238
C.39	Computed muscle activities of the biceps, triceps and pectoralis major over the abduction angle in 5° increments during the internal rotation trial. Blue depicts the activities of the intact model of the healthy subject group and red the modelled tear of the m. supraspinatus of the patient group.	239

C.40	Computed muscle activities of the anterior, posterior and lateral deltoids over the abduction angle in 5° increments during the external rotation trial. Blue depicts the activities of the intact model of the healthy subject group and red the modelled tear of the m. supraspinatus of the patient group.	240
C.41	Computed muscle activities of the infraspinatus, subscapularis and teres minor over the abduction angle in 5° increments during the external rotation trial. Blue depicts the activities of the intact model of the healthy subject group and red the modelled tear of the m. supraspinatus of the patient group.	241
C.42	Computed muscle activities of the biceps, triceps and pectoralis major over the abduction angle in 5° increments during the external rotation trial. Blue depicts the activities of the intact model of the healthy subject group and red the modelled tear of the m. supraspinatus of the patient group.	242
C.43	Computed muscle activities of the anterior, posterior and lateral deltoids over the abduction angle in 5° increments during the external rotation trial with 5 N load in hand. Blue depicts the activities of the intact model of the healthy subject group and red the modelled tear of the m. supraspinatus of the patient group.	243
C.44	Computed muscle activities of the infraspinatus, subscapularis and teres minor over the abduction angle in 5° increments during the external rotation trial with 5 N load in hand. Blue depicts the activities of the intact model of the healthy subject group and red the modelled tear of the m. supraspinatus of the patient group.	244
C.45	Computed muscle activities of the biceps, triceps and pectoralis major over the abduction angle in 5° increments during the external rotation trial with 5 N load in hand. Blue depicts the activities of the intact model of the healthy subject group and red the modelled tear of the m. supraspinatus of the patient group.	245
C.46	Compression force, inferior-superior force and anterior-posterior force of intact models of the healthy control (blue) and pathological models of the patient group (red) during the neutral position trial over the abduction angle in 5° increments.	247

C.47	Projected median GH joint reaction force of all models onto the glenoid of intact models of the healthy subject cohort and pathological models of the patient group during the neutral position trial. Intact models of the healthy control (blue) and pathological models of the patient group (red) with their starting value at 25° abduction and the progression up to 85° abduction.	248
C.48	Compression force, inferior-superior force and anterior-posterior force of intact models of the healthy control (blue) and pathological models of the patient group (red) during the neutral position trial with 5 N load in hand over the abduction angle in 5° increments.	249
C.49	Projected median GH joint reaction force of all models onto the glenoid of intact models of the healthy subject cohort and pathological models of the patient group during the neutral position trial with 5 N load in hand. Intact models of the healthy control (blue) and pathological models of the patient group (red) with their starting value at 25° abduction and the progression up to 85° abduction.	250
C.50	Compression force, inferior-superior force and anterior-posterior force of intact models of the healthy control (blue) and pathological models of the patient group (red) during the internal rotation trial over the abduction angle in 5° increments.	251
C.51	Projected median GH joint reaction force of all models onto the glenoid of intact models of the healthy subject cohort and pathological models of the patient group during the internal rotation trial. Intact models of the healthy control (blue) and pathological models of the patient group (red) with their starting value at 25° abduction and the progression up to 85° abduction.	252
C.52	Compression force, inferior-superior force and anterior-posterior force of intact models of the healthy control (blue) and pathological models of the patient group (red) during the external rotation trial over the abduction angle in 5° increments.	253

C.53	Projected median GH joint reaction force of all models onto the glenoid of intact models of the healthy subject cohort and pathological models of the patient group during the external rotation trial. Intact models of the healthy control (blue) and pathological models of the patient group (red) with their starting value at 25° abduction and the progression up to 85° abduction.	254
C.54	Compression force, inferior-superior force and anterior-posterior force of intact models of the healthy control (blue) and pathological models of the patient group (red) during the external rotation trial with 5 N load in hand over the abduction angle in 5° increments.	255
C.55	Projected median GH joint reaction force of all models onto the glenoid of intact models of the healthy subject cohort and pathological models of the patient group during the external rotation trial with 5 N load in hand. Intact models of the healthy control (blue) and pathological models of the patient group (red) with their starting value at 25° abduction and the progression up to 85° abduction.	256
C.56	EMG muscle activities normalized to the 85° position of the neutral position trial with 5 N load in hand of the trapezius pars descendens, trapezius pars transversa and trapezius pars ascendens over the abduction angle in 5° increments during the neutral position trial. Blue depicts the EMG activities of the healthy subject group and red of the patient group.	263
C.57	EMG muscle activities normalized to the 85° position of the neutral position trial with 5 N load in hand of the anterior deltoid, lateral deltoid and posterior deltoid over the abduction angle in 5° increments during the neutral position trial. Blue depicts the EMG activities of the healthy subject group and red of the patient group.	264
C.58	EMG muscle activities normalized to the 85° position of the neutral position trial with 5 N load in hand of the infraspinatus, serratus anterior and latissimus over the abduction angle in 5° increments during the neutral position trial. Blue depicts the EMG activities of the healthy subject group and red of the patient group.	265

C.59 EMG muscle activities normalized to the 85° position of the neutral position trial with 5 N load in hand of the biceps, triceps and rhomboideus minor over the abduction angle in 5° increments during the neutral position trial. Blue depicts the EMG activities of the healthy subject group and red of the patient group.	266
C.60 EMG muscle activities normalized to the 85° position of the neutral position trial with 5 N load in hand of the rhomboideus major and pectoralis major over the abduction angle in 5° increments during the neutral position trial. Blue depicts the EMG activities of the healthy subject group and red of the patient group.	267
C.61 EMG muscle activities normalized to the 85° position of the neutral position trial with 5 N load in hand of the trapezius pars descendens, trapezius pars transversa and trapezius pars ascendens over the abduction angle in 5° increments during the neutral position trial with 5 N load in hand. Blue depicts the EMG activities of the healthy subject group and red of the patient group.	268
C.62 EMG muscle activities normalized to the 85° position of the neutral position trial with 5 N load in hand of the anterior deltoid, lateral deltoid and posterior deltoid over the abduction angle in 5° increments during the neutral position trial with 5 N load in hand. Blue depicts the EMG activities of the healthy subject group and red of the patient group.	269
C.63 EMG muscle activities normalized to the 85° position of the neutral position trial with 5 N load in hand of the infraspinatus, serratus anterior and latissimus over the abduction angle in 5° increments during the neutral position trial with 5 N load in hand. Blue depicts the EMG activities of the healthy subject group and red of the patient group.	270
C.64 EMG muscle activities normalized to the 85° position of the neutral position trial with 5 N load in hand of the biceps, triceps and rhomboideus minor over the abduction angle in 5° increments during the neutral position trial with 5 N load in hand. Blue depicts the EMG activities of the healthy subject group and red of the patient group.	271

C.65	EMG muscle activities normalized to the 85° position of the neutral position trial with 5 N load in hand of the rhomboideus major and pectoralis major over the abduction angle in 5° increments during the neutral position trial with 5 N load in hand. Blue depicts the EMG activities of the healthy subject group and red of the patient group. .	272
C.66	EMG muscle activities normalized to the 85° position of the neutral position trial with 5 N load in hand of the trapezius pars descendens, trapezius pars transversa and trapezius pars ascendens over the abduction angle in 5° increments during the internal rotation trial. Blue depicts the EMG activities of the healthy subject group and red of the patient group.	273
C.67	EMG muscle activities normalized to the 85° position of the neutral position trial with 5 N load in hand of the anterior deltoid, lateral deltoid and posterior deltoid over the abduction angle in 5° increments during the internal rotation trial. Blue depicts the EMG activities of the healthy subject group and red of the patient group.	274
C.68	EMG muscle activities normalized to the 85° position of the neutral position trial with 5 N load in hand of the infraspinatus, serratus anterior and latissimus over the abduction angle in 5° increments during the internal rotation trial. Blue depicts the EMG activities of the healthy subject group and red of the patient group.	275
C.69	EMG muscle activities normalized to the 85° position of the neutral position trial with 5 N load in hand of the biceps, triceps and rhomboideus minor over the abduction angle in 5° increments during the internal rotation trial. Blue depicts the EMG activities of the healthy subject group and red of the patient group.	276
C.70	EMG muscle activities normalized to the 85° position of the neutral position trial with 5 N load in hand of the rhomboideus major and pectoralis major over the abduction angle in 5° increments during the internal rotation trial. Blue depicts the EMG activities of the healthy subject group and red of the patient group.	277

C.71 EMG muscle activities normalized to the 85° position of the neutral position trial with 5 N load in hand of the trapezius pars descendens, trapezius pars transversa and trapezius pars ascendens over the abduction angle in 5° increments during the external rotation trial. Blue depicts the EMG activities of the healthy subject group and red of the patient group.	278
C.72 EMG muscle activities normalized to the 85° position of the neutral position trial with 5 N load in hand of the anterior deltoid, lateral deltoid and posterior deltoid over the abduction angle in 5° increments during the external rotation trial. Blue depicts the EMG activities of the healthy subject group and red of the patient group.	279
C.73 EMG muscle activities normalized to the 85° position of the neutral position trial with 5 N load in hand of the infraspinatus, serratus anterior and latissimus over the abduction angle in 5° increments during the external rotation trial. Blue depicts the EMG activities of the healthy subject group and red of the patient group.	280
C.74 EMG muscle activities normalized to the 85° position of the neutral position trial with 5 N load in hand of the biceps, triceps and rhomboideus minor over the abduction angle in 5° increments during the external rotation trial. Blue depicts the EMG activities of the healthy subject group and red of the patient group.	281
C.75 EMG muscle activities normalized to the 85° position of the neutral position trial with 5 N load in hand of the rhomboideus major and pectoralis major over the abduction angle in 5° increments during the external rotation trial. Blue depicts the EMG activities of the healthy subject group and red of the patient group.	282
C.76 EMG muscle activities normalized to the 85° position of the neutral position trial with 5 N load in hand of the trapezius pars descendens, trapezius pars transversa and trapezius pars ascendens over the abduction angle in 5° increments during the external rotation trial with 5 N load in hand. Blue depicts the EMG activities of the healthy subject group and red of the patient group.	283

C.77	EMG muscle activities normalized to the 85° position of the neutral position trial with 5 N load in hand of the anterior deltoid, lateral deltoid and posterior deltoid over the abduction angle in 5° increments during the external rotation trial with 5 N load in hand. Blue depicts the EMG activities of the healthy subject group and red of the patient group.	284
C.78	EMG muscle activities normalized to the 85° position of the neutral position trial with 5 N load in hand of the infraspinatus, serratus anterior and latissimus over the abduction angle in 5° increments during the external rotation trial with 5 N load in hand. Blue depicts the EMG activities of the healthy subject group and red of the patient group. .	285
C.79	EMG muscle activities normalized to the 85° position of the neutral position trial with 5 N load in hand of the biceps, triceps and rhomboideus minor over the abduction angle in 5° increments during the external rotation trial with 5 N load in hand. Blue depicts the EMG activities of the healthy subject group and red of the patient group. .	286
C.80	EMG muscle activities normalized to the 85° position of the neutral position trial with 5 N load in hand of the rhomboideus major and pectoralis major over the abduction angle in 5° increments during the external rotation trial with 5 N load in hand. Blue depicts the EMG activities of the healthy subject group and red of the patient group. .	287

List of Tables

2.1	Muscles involved in the shoulder complex with their anatomical insertions, origins and functionality (Adapted from Schünke, Schulte, and Schumacher, 2007).	50
4.1	Overview of the abbreviations of the altered/included model configurations	62
4.2	Pearson correlations r between EMG and model activities in the range 30-140° of the contemplated combinations ordered from lowest to highest mean r for the seven contemplated muscle groups. Abbreviations for the cases are provided in Table 4.1.	63
5.1	Overview of the parameters used in the Hill model of the AMS and their description (Adapted from the reference manual of the AMS)	78
5.2	RMSE between each muscle element and the associated reference data in mm. Each row is sorted from the anterior to posterior element of the respective muscle group.	82
6.1	Overview of the three investigated motions with regard to the kinematics of the humerus and elbow	106
6.2	Maximum deviation of the surgical models in comparison to the ORG insertion point of the LBT during each motion task	107
7.1	Contemplated muscles and their respective EMG sensor number of the experimental setup (see Figure 7.1 for a graphical representation).	123

7.2	Differences in median values of muscle activities and GH joint reaction forces between intact and pathological models of the healthy subject cohort during the internal rotation trial with 5 N load in hand in 5° increments. Asterisks indicate the significance level. AD = anterior deltoid, LD = lateral deltoid, PD = posterior deltoid, INF = infraspinatus, SS = subscapularis, BIC = biceps, TRI = triceps, TM = teres minor, PM = pectoralis major, CF = compression force, ISF = inferior-superior force, APF = anterior-posterior force	136
7.3	Differences in median values of muscle activities, GH joint reaction forces and kinematics between intact models of the healthy subject cohort and pathological models of the patient group during the internal rotation trial with 5 N load in hand in 5° increments. Asterisks indicate the significance level. AD = anterior deltoid, LD = lateral deltoid, PD = posterior deltoid, INF = infraspinatus, SS = subscapularis, BIC = biceps, TRI = triceps, TM = teres minor, PM = pectoralis major, CF = compression force, ISF = inferior-superior force, APF = anterior-posterior force, FLX = Flexion angle, ER = external rotation angle	144
7.4	Differences in median values of EMG activities normalized to the 85° position of the neutral position trial with 5 N load in hand between the healthy subject cohort and patient group during the internal rotation trial with 5 N load in hand in 5° increments. Asterisks indicate the significance level. TD = trapezius descendens, TT = trapezius transversa, TA = trapezius ascendens, AD = anterior deltoid, LD = lateral deltoid, PD = posterior deltoid, INF = infraspinatus, SER = serratus anterior, LAT = latissimus, BIC = biceps, TRI = triceps, RMA = rhomboideus major, RMI = rhomboideus minor, PEC = pectoralis major	154

C.1	Differences in median values of muscle activities, GH joint reaction forces and kinematics between intact and pathological models of the healthy subject cohort during the neutral position trial in 5° increments. Asterisks indicate the significance level. AD = anterior deltoid, LD = lateral deltoid, PD = posterior deltoid, INF = infraspinatus, SS = subscapularis, BIC = biceps, TRI = triceps, TM = teres minor, PM = pectoralis major, CF = compression force, ISF = inferior-superior force, APF = anterior-posterior force, FLX = Flexion angle, ER = external rotation angle	220
C.2	Differences in median values of muscle activities, GH joint reaction forces and kinematics between intact and pathological models of the healthy subject cohort during the neutral position trial with 5 N load in hand in 5° increments. Asterisks indicate the significance level. AD = anterior deltoid, LD = lateral deltoid, PD = posterior deltoid, INF = infraspinatus, SS = subscapularis, BIC = biceps, TRI = triceps, TM = teres minor, PM = pectoralis major, CF = compression force, ISF = inferior-superior force, APF = anterior-posterior force, FLX = Flexion angle, ER = external rotation angle	221
C.3	Differences in median values of muscle activities, GH joint reaction forces and kinematics between intact and pathological models of the healthy subject cohort during the internal rotation trial in 5° increments. Asterisks indicate the significance level. AD = anterior deltoid, LD = lateral deltoid, PD = posterior deltoid, INF = infraspinatus, SS = subscapularis, BIC = biceps, TRI = triceps, TM = teres minor, PM = pectoralis major, CF = compression force, ISF = inferior-superior force, APF = anterior-posterior force, FLX = Flexion angle, ER = external rotation angle	222

C.4	Differences in median values of muscle activities, GH joint reaction forces and kinematics between intact and pathological models of the healthy subject cohort during the external rotation trial in 5° increments. Asterisks indicate the significance level. AD = anterior deltoid, LD = lateral deltoid, PD = posterior deltoid, INF = infraspinatus, SS = subscapularis, BIC = biceps, TRI = triceps, TM = teres minor, PM = pectoralis major, CF = compression force, ISF = inferior-superior force, APF = anterior-posterior force, FLX = Flexion angle, ER = external rotation angle	223
C.5	Differences in median values of muscle activities, GH joint reaction forces and kinematics between intact and pathological models of the healthy subject cohort during the external rotation trial with 5 N load in hand in 5° increments. Asterisks indicate the significance level. AD = anterior deltoid, LD = lateral deltoid, PD = posterior deltoid, INF = infraspinatus, SS = subscapularis, BIC = biceps, TRI = triceps, TM = teres minor, PM = pectoralis major, CF = compression force, ISF = inferior-superior force, APF = anterior-posterior force, FLX = Flexion angle, ER = external rotation angle	224
C.6	Differences in median values of muscle activities, GH joint reaction forces and kinematics between intact models of the healthy subject cohort and pathological models of the patient group during the internal rotation trial with 5 N load in hand in 5° increments. Asterisks indicate the significance level. AD = anterior deltoid, LD = lateral deltoid, PD = posterior deltoid, INF = infraspinatus, SS = subscapularis, BIC = biceps, TRI = triceps, TM = teres minor, PM = pectoralis major, CF = compression force, ISF = inferior-superior force, APF = anterior-posterior force, FLX = Flexion angle, ER = external rotation angle	257

C.7	Differences in median values of muscle activities, GH joint reaction forces and kinematics between intact models of the healthy subject cohort and pathological models of the patient group during the neutral position trial with 5 N load in hand in 5° increments. Asterisks indicate the significance level. AD = anterior deltoid, LD = lateral deltoid, PD = posterior deltoid, INF = infraspinatus, SS = subscapularis, BIC = biceps, TRI = triceps, TM = teres minor, PM = pectoralis major, CF = compression force, ISF = inferior-superior force, APF = anterior-posterior force, FLX = Flexion angle, ER = external rotation angle	258
C.8	Differences in median values of muscle activities, GH joint reaction forces and kinematics between intact models of the healthy subject cohort and pathological models of the patient group during the internal rotation trial in 5° increments. Asterisks indicate the significance level. AD = anterior deltoid, LD = lateral deltoid, PD = posterior deltoid, INF = infraspinatus, SS = subscapularis, BIC = biceps, TRI = triceps, TM = teres minor, PM = pectoralis major, CF = compression force, ISF = inferior-superior force, APF = anterior-posterior force, FLX = Flexion angle, ER = external rotation angle	259
C.9	Differences in median values of muscle activities, GH joint reaction forces and kinematics between intact models of the healthy subject cohort and pathological models of the patient group during the external rotation trials in 5° increments. Asterisks indicate the significance level. AD = anterior deltoid, LD = lateral deltoid, PD = posterior deltoid, INF = infraspinatus, SS = subscapularis, BIC = biceps, TRI = triceps, TM = teres minor, PM = pectoralis major, CF = compression force, ISF = inferior-superior force, APF = anterior-posterior force, FLX = Flexion angle, ER = external rotation angle	260

C.10	Differences in median values of muscle activities, GH joint reaction forces and kinematics between intact models of the healthy subject cohort and pathological models of the patient group during the external rotation trial with 5 N load in hand in 5° increments. Asterisks indicate the significance level. AD = anterior deltoid, LD = lateral deltoid, PD = posterior deltoid, INF = infraspinatus, SS = subscapularis, BIC = biceps, TRI = triceps, TM = teres minor, PM = pectoralis major, CF = compression force, ISF = inferior-superior force, APF = anterior-posterior force, FLX = Flexion angle, ER = external rotation angle	261
C.11	Differences in median values of EMG activities normalized to the 85° position of the neutral position trial with 5 N load in hand between the healthy subject cohort and patient group during the neutral position trial in 5° increments. Asterisks indicate the significance level. TD = trapezius descendens, TT = trapezius transversa, TA = trapezius ascendens, AD = anterior deltoid, LD = lateral deltoid, PD = posterior deltoid, INF = infraspinatus, SER = serratus anterior, LAT = latissimus, BIC = biceps, TRI = triceps, RMA = rhomboideus major, RMI = rhomboideus minor, PEC = pectoralis major	288
C.12	Differences in median values of EMG activities normalized to the 85° position of the neutral position trial with 5 N load in hand between the healthy subject cohort and patient group during the neutral position trial with 5 N load in hand in 5° increments. Asterisks indicate the significance level. TD = trapezius descendens, TT = trapezius transversa, TA = trapezius ascendens, AD = anterior deltoid, LD = lateral deltoid, PD = posterior deltoid, INF = infraspinatus, SER = serratus anterior, LAT = latissimus, BIC = biceps, TRI = triceps, RMA = rhomboideus major, RMI = rhomboideus minor, PEC = pectoralis major	289

C.13 Differences in median values of EMG activities normalized to the 85° position of the neutral position trial with 5 N load in hand between the healthy subject cohort and patient group during the internal rotation trial in 5° increments. Asterisks indicate the significance level. TD = trapezius descendens, TT = trapezius transversa, TA = trapezius ascendens, AD = anterior deltoid, LD = lateral deltoid, PD = posterior deltoid, INF = infraspinatus, SER = serratus anterior, LAT = latissimus, BIC = biceps, TRI = triceps, RMA = rhomboideus major, RMI = rhomboideus minor, PEC = pectoralis major	290
C.14 Differences in median values of EMG activities normalized to the 85° position of the neutral position trial with 5 N load in hand between the healthy subject cohort and patient group during the external rotation trial in 5° increments. Asterisks indicate the significance level. TD = trapezius descendens, TT = trapezius transversa, TA = trapezius ascendens, AD = anterior deltoid, LD = lateral deltoid, PD = posterior deltoid, INF = infraspinatus, SER = serratus anterior, LAT = latissimus, BIC = biceps, TRI = triceps, RMA = rhomboideus major, RMI = rhomboideus minor, PEC = pectoralis major	291
C.15 Differences in median values of EMG activities normalized to the 85° position of the neutral position trial with 5 N load in hand between the healthy subject cohort and patient group during the external rotation trial with 5 N load in hand in 5° increments. Asterisks indicate the significance level. TD = trapezius descendens, TT = trapezius transversa, TA = trapezius ascendens, AD = anterior deltoid, LD = lateral deltoid, PD = posterior deltoid, INF = infraspinatus, SER = serratus anterior, LAT = latissimus, BIC = biceps, TRI = triceps, RMA = rhomboideus major, RMI = rhomboideus minor, PEC = pectoralis major	292

List of Abbreviations

AC	A cr o mioclavicular
ALLFM	A ll forces and m oments transmitted from carrier segments to the humerus
AMMR	A nyBody M anaged M odeling R epository
AMS	A nyBody M odeling S ystem
BM	B ase m odel
BW	B ody w eight
CB	long biceps tendon inserted at the c aput b reve
CL	Motion capture driven c lavicular protraction & elevation
DOF	D egree o f freedom
EL	E lbow
EMG	E lectrom y ography
FDK	F orce- d ependent k inematics
FXZ	Only forces in X (compression) and Z (anterior-posterior) direction are transmitted
GH	G lenohumeral
H	H ill muscle model
HH	long biceps tendon inserted at the bicipital groove on the h umeral h ead
IS	I nferior- s uperior
LBT	L ong b iceps tendon

ML	M edial-l a lteral
MoCap	M otion cap ture
MRI	M agnetic resonance i maging
MVC	M aximum v oluntary c ontraction
NOFM	N o forces and m oments are transmitted from the three carrier segments
OFF	long biceps tendon disabled and turned off
ORG	long biceps tendon in its original state
PA	P osterior- a nterior
PEEK	P oly e ther e ther k etone
RHY	Alteration of scapular/clavicle rhythm
RMS	R oot m ean square
RMSE	R oot m ean square e rror
ROM	R ange of m otion
S	S trength scaling
SC	S ernoclavicular
SLAP	S uperior labrum from a nterior to p osterior
ST	S capulo t horacic
T	T orus obstacle method for deltoid wrapping

List of Symbols

r	Pearson correlation coefficient
p	Power of the polynomial muscle recruitment criterion
M	Moment arm derived from the tendon excursion method
N	Newton
Nm	Newton meter
∂l	Change in length of the tendon during a given amount of joint rotation
$\partial \theta$	Change in rotation angle during a given amount of joint rotation

Dedicated to Angelika & Martin.

Chapter 1

Introduction

Disorders of the musculoskeletal system ranked as one of the major contributing factors for the inability to work (Meyer, Wenzel, and Schenkel, 2018). This fact is an immense burden on the affected individuals, healthcare and social welfare systems where the indirect costs are predominant (Woolf and Pfleger, 2003). Musculoskeletal disorders in general cover a variety of pathologies, and one specific area with a high impact is the shoulder complex, as it affects millions of people world wide. The reported incidence of shoulder complaints e.g. in the Netherlands is estimated at 11.2/1000 patients/year (van der Windt et al., 1995). The prevalence of shoulder pain has been found to be as high as 15.4% in men and 24.9% in women who reported weekly episodes of pain (Pribicevic, 2012) which is comparable to 20% and 20.7% reported by similar studies (Pope et al., 1997; Yamamoto et al., 2010). Up to 70% of these painful conditions can be attributed to injuries or degeneration of the muscles and tendons of the rotator cuff (Chard et al., 1991). Investigations of the prevalence of rotator cuff tears have identified age, history of trauma and use of the dominant arm as key risk factors for developing a pathology (Yamamoto et al., 2010; Minagawa et al., 2013). Yamamoto et al., 2010 tested the population of a village (n=683) employing physical examination and ultrasonography for determining the prevalence of rotator cuff tears. They reported a 20.7% positive rate in the tested subjects, whereas 36% of these subjects were symptomatic, while 16.9% of the subjects without symptoms also tested positive for rotator cuff tears. Minagawa et al., 2013 did a similar study and found a prevalence of 22.1% in the general population, with the asymptomatic tear being twice as common as a symptomatic tear. However, these asymptomatic tears can progress to become symptomatic and painful while limiting the range of motion (Mall et al., 2010; Moosmayer et al., 2013).

A co-morbidity of rotator cuff tears is often instabilities of the long biceps tendon anchor, tears of the labrum, or long biceps instabilities (Hawi et al., 2017). If conservative treatments of shoulder diseases with a long biceps tendon pathology and cuff tears fail, operative techniques are considered in order to relieve pain and regain strength and function (Boileau et al., 2002). While restoring the functionality of the rotator cuff is the main focus, the long biceps tendon is often cut to relieve pain (Walch et al., 2005). From a clinical point of view, there are a couple of ways to proceed after releasing the long biceps tendon from the glenoid rim (Voss et al., 2017). Several varying techniques and constructs are available to perform a long biceps tendon tenodesis, including an array of intra-articular, suprapectoral, and subpectoral fixation methods of the bisected tendon (Schoch, Geyer, and Drews, 2017) in order to restore function.

When multiple surgical techniques are being used simultaneously, there is no consensus as to which method is preferable and how they affect the biomechanics of the shoulder-arm complex. Analysing the mechanical changes within the shoulder-arm complex of the aforementioned techniques could provide insights about post surgical muscle function and joint stability.

Considering the muscles comprising the group of the rotator cuff, the most commonly affected one is the m. supraspinatus (Moor et al., 2014). The m. supraspinatus has two main purposes, that of stabilising the humeral head on the glenoid in combination with the other muscles making up the rotator cuff and to abduct the humerus in conjunction with the deltoids and to a lesser extent, other muscles spanning the glenohumeral joint. If an isolated tear occurs without ruptures of other muscles of the rotator cuff and remains untreated, the tear size does not necessarily progress and can heal without surgical treatment (Fucentese et al., 2012). In order to diagnose a tear of the m. supraspinatus, several tools are typically used in clinical practice. Sonography (Mack et al., 1985; Crass, Craig, and Feinberg, 1988; Wiener and Seitz Jr, 1993; Moppes, Veldkamp, and Roorda, 1995) and magnetic resonance imaging (Quinn et al., 1995; Ferri et al., 2005) show high sensitivity and specificity for identifying this pathology. The full-can and empty-can tests are used for initial testing to identify a tear of the m. supraspinatus, where the empty can test is more painful for some patients (Itoi et al., 1999; Timmons et al., 2016).

In addition to these techniques, studies have been conducted which utilise electromyography to assess muscle activation patterns of patients with rotator cuff tears (Witte et al., 2012; Witte et al., 2014a; Witte et al., 2014b; Kai et al., 2015; Sakaki et al., 2015). In conjunction to this, rehabilitation exercises have been analysed via electromyography in order to identify activation levels of the rotator cuff and m. supraspinatus in healthy subjects to a certain extent (Edwards et al., 2017). Another research focus is on how the m. supraspinatus and the deltoids are recruited during the empty and full can test (Reinold et al., 2007a). Ekstrom and Osborn, 2004 provides an overview of studies conducting electromyographic measurements of the m. supraspinatus which compare the empty and full can test and found no significant difference between the tests. Patients also reported pain during the internal rotation or the empty can test. Furthermore, electromyography has been shown to play an important role in the detection of myopathy (Fuglsang-Frederiksen, 2006).

With millions of people affected by this particular pathology, a large field of research has been dedicated to improvement of diagnostics, surgery, clinical outcome and a general better understanding of the involved biomechanics. Cadaver studies in the clinical field are being used for detailed examination; for e.g. strength of the rotator cuff muscles (Keating et al., 1993) or effects on the biomechanics of the glenohumeral joint (Soslowky, Malicky, and Blasier, 1997; Oh et al., 2011). Where cadaver studies excel in investigating resulting changes in morphology (e.g. Sakurai et al., 1998) and effects on the involved structures of the shoulder, they cannot fully describe muscle activation patterns and therefore the forces acting on the joints. Simulation based approaches however offer the opportunity to compute effects of shoulder disorders during activities of daily living and their effects on the biomechanics of the shoulder-arm complex. In particular musculoskeletal models allow for a subject specific calculation of muscles activities, their resulting forces and consequently joint reaction forces without the need for in-vivo measurements. Several musculoskeletal models of the upper limb and shoulder region have been developed (van der Helm; Charlton and Johnson, 2006; Favre, Snedeker, and Gerber, 2009) or adapted (Sins et al., 2015) over the years and are used in a variety of applications. Detailed overviews of existing models and their use are provided by Prinold et al., 2013 and Bolsterlee, Veeger, Dirkjan H E J, and Chadwick, 2013.

As tears of the rotator cuff are the dominant disorder within the shoulder complex, several simulation studies have focused on various aspects of the rotator cuff. These include the assessment of muscle transfers of latissimus dorsi, teres major or a combination of these two to compensate for inoperable massive rotator cuff tears in a simulation environment (Magermans et al., 2004a; Magermans et al., 2004b) or the simulated effects of full tears of the rotator cuff on the risk of impingement in hand-bike and handrim wheelchair propulsion (Drongelen et al., 2013). Leschinger et al., 2019 simulated a rotator cuff repair with a variation in insertion of the virtual muscle and the change in joint reaction force. Hölscher et al., 2016a used a musculoskeletal model to analyse the effects of various combinations of rotator cuff tears on the glenohumeral joint reaction force.

While these models see a variety of use to answer and describe clinical issues from a biomechanical perspective, they are still under constant improvement. One major issue is the discrepancy of simulated joint reaction forces in musculoskeletal models which use an inverse dynamics approach to in vivo measured force data in humeral abduction above 90° (Bergmann et al., 2011). An increase in magnitude of the resultant glenohumeral joint reaction force occurs in patients with instrumented implants during humeral abduction above 90°, which is also indicated by a high activity of the muscles spanning the shoulder joint from electromyographic measurements (Wickham et al., 2010). Musculoskeletal models using an inverse dynamics approach show lower activities and a decline in joint reaction force above 90° humeral abduction. Nikooyan et al., 2010 used these in vivo measurements for validation purposes of the Delft shoulder model (van der Helm, 1994a; van der Helm, 1994b; Nikooyan et al., 2011). Other than these valuable (but scarce) in vivo force measurements, electromyography is also utilized to validate musculoskeletal models by comparing the measured amplitude to predicted model activities (Groot et al., 2004; Morrow, Kaufman, and An, 2010; Nikooyan et al., 2010; Nikooyan et al., 2011). A study which utilised electromyographic signals to drive a musculoskeletal model which also incorporated patients with the instrumented implants was conducted by Nikooyan et al., 2012. They surmised that muscle co-contraction e.g. from the m. latissimus dorsi causes the increase in glenohumeral joint reaction force above 90° abduction. However, Sins et al., 2015 reported increasing reaction forces and showed the contrast to existing models in force behaviour during abduction above 90° where several changes were implemented.

Since they used an inverse dynamics approach, in theory no co-contraction should be involved as a computational implementation of this phenomenon is not included in this type of model.

Where various predictive models of the shoulder complex exist, a core modelling parameter seems to be missing as most of them fail to compute the joint reaction force accurately.

The combination of musculoskeletal models and electromyographic measurements are typically utilised in the two ways, that of either validating a model or using patient specific electromyographic signals as an input. A third option would also be of interest, whether a model can predict a change in muscle activation patterns which can point towards a targeted use of electromyography as a tool for diagnosis.

Combining the afore mentioned clinical relevance of tears of the m. supraspinatus, electromyographic measurements and biomechanics derived from musculoskeletal simulations leads to the outline and aim of this thesis, which addresses several research questions:

1. Investigation and improvement of an existing model of the shoulder complex:
Is there an alternative explanation for the rising muscle activities and glenohumeral joint reaction force above 90° abduction? (Chapter 4 & Chapter 5)
2. Computation of several operative techniques of a biceps tendon transfer:
Is one technique closer to the healthy state of the shoulder-arm complex from a biomechanical point of view? (Chapter 6)
3. Simulation of a full tear of the m. supraspinatus with a focus on muscle activation pattern and glenohumeral joint reaction force:
Can a generic musculoskeletal model predict changes in the muscle recruitment of pathologies accurately? (Chapter 7)

This thesis is structured to answer these research questions with a clear outline and is hereby divided in sections with their own introductions, methods, results, discussions and conclusions. Chapters 2 & 3 provide an overview over the anatomy of the shoulder complex and the utilised musculoskeletal simulation program which incorporates the basis for this presented work.

Chapter 2

Anatomy and functionality of the shoulder complex

In the following section, the anatomy of the shoulder complex and the functionality of the involved joints and muscles are described. The selection of the joints, degrees of freedom (DOF) and muscles hereby reflects the components important in conjunction with the musculoskeletal modelling aspects incorporated in this work and are thus simplified to a certain extend.

The shoulder comprises four body segments: the humerus, the scapula, the clavicle and the thorax (summarized as one segment). These segments are linked by four joints (Figure 2.1):

- Acromioclavicular (AC) joint : Connects the scapula at the acromion with the distal end of the clavicle.
- Glenohumeral (GH) joint : Connects the humeral head to the glenoid cavity of the scapula.
- Scapulothoracic (ST) joint : The ST joint is not a true joint, as it does not connect two bones with each other but slides over the ribs of the thorax.
- Sternoclavicular (SC) joint : Links the entire complex of the shoulder segments to the thorax, where the proximal end of the clavicle connects to the sternum.

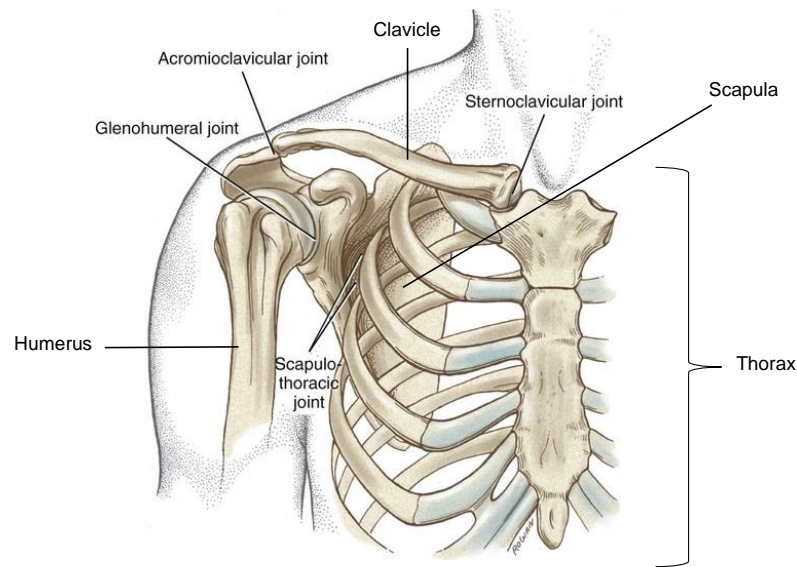


FIGURE 2.1: The joints and bones of the shoulder complex. (Adapted from Neumann, 2002 Figure 5-1.)

There are six DOF's possible with respect to the GH joint. The clavicle is able to conduct axial rotation, pronation and elevation at the SC joint, and the distal end subsequently translates and moves the scapula via the AC joint. The scapula itself glides over the ribs of the thorax (ST joint). The humerus connects at the distal end of the scapula (the glenoid), which provides the entire complex with 3 translational DOF's at the GH joint. The conjunction of the humerus to the scapula itself incorporates 3 rotational DOF's. These DOF's are not entirely independent, as at higher abduction angles of the humerus the humeral head would impinge at the acromion of the scapula. To circumvent this, the clavicle and scapula rotate upward simultaneously in order to open up the joint. This interplay of humerus, scapula and clavicle is called the scapulohumeral or glenohumeral rhythm (simplified as shoulder rhythm). The interplay of the involved structures results in a large range of motion (ROM) of the shoulder complex, which is depicted in Figure 2.2. A detailed description of shoulder functionality is provided by Veege and Helm], 2007.

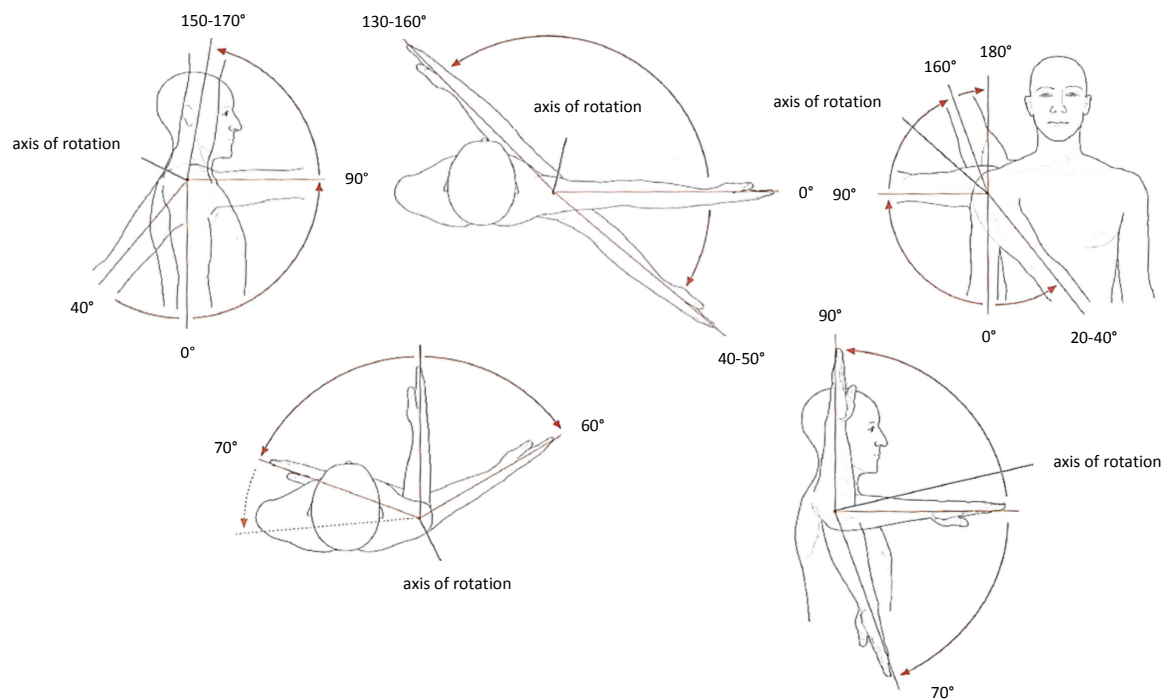


FIGURE 2.2: Range of motion of the shoulder complex (Adapted from Schünke, Schulte, and Schumacher, 2007).

A graphical guide to the anatomy of the involved muscles spanning the shoulder complex is illustrated in Figures 2.3, 2.4 & 2.5, where a detailed guide of muscle insertions, origins and functionality is provided in Table 2.1.

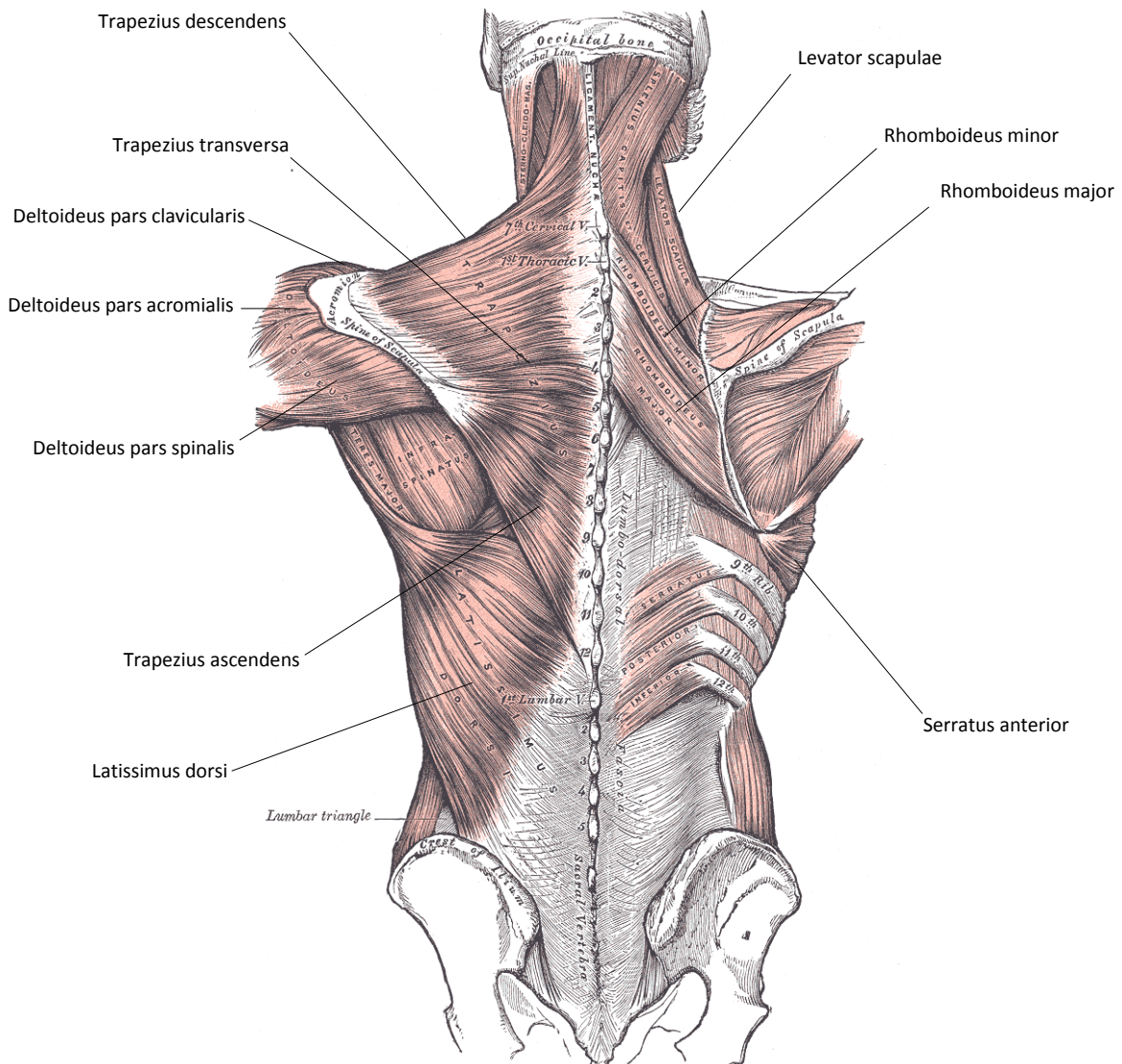
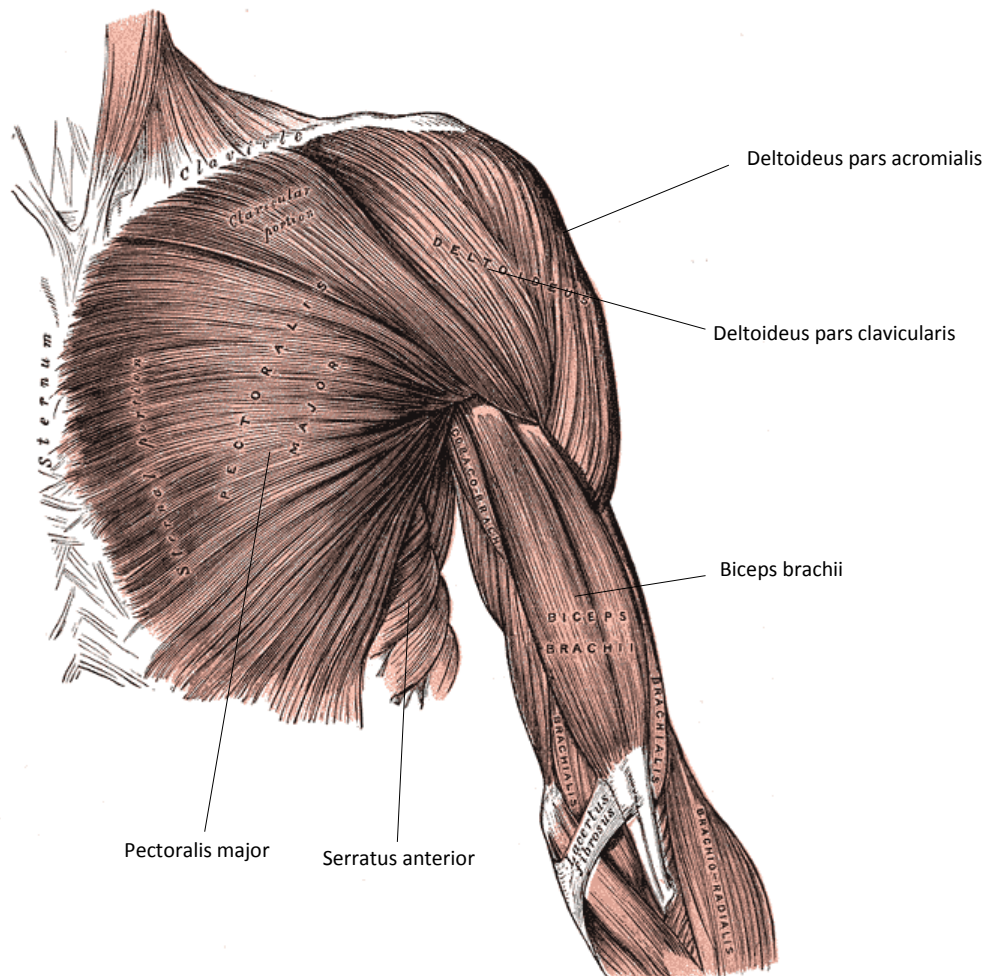


FIGURE 2.3: The main muscles involved in the shoulder, posterior view. (Adapted from Henry Gray: Anatomy of the Human Body 1918, IV. Myology, 7. The Fascia and Muscles of the Upper Extremity. a. The Muscles Connecting the Upper Extremity, Fig. 409).



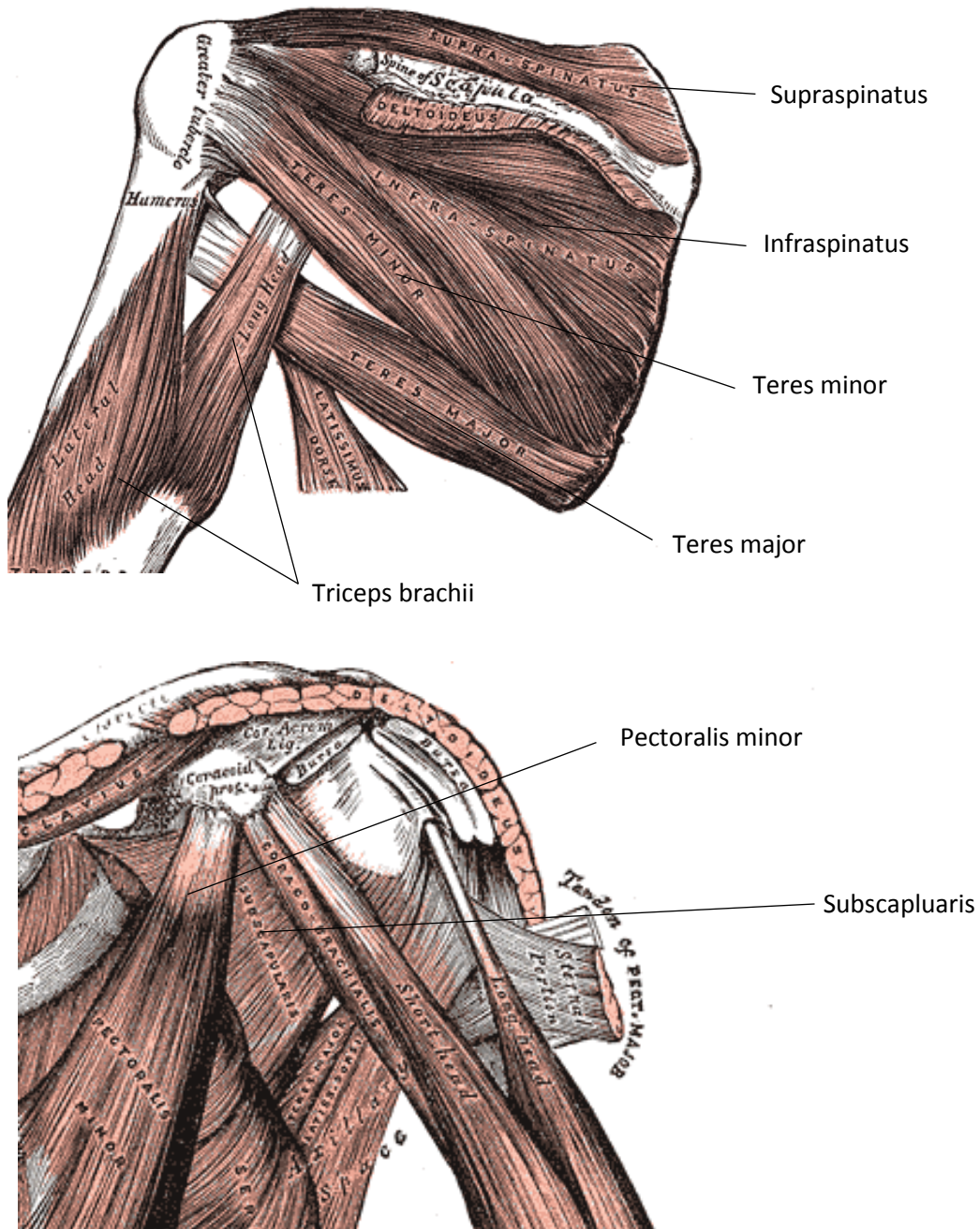


FIGURE 2.5: The main muscles involved in the shoulder, top: rotator cuff muscles posterior view, bottom: rotator cuff muscles anterior view. (Adapted from Henry Gray: Anatomy of the Human Body 1918, IV. Myology, 7. The Fascia and Muscles of the Upper Extremity. a. The Muscles Connecting the Upper Extremity, Fig. 411 & 412).

Muscle	Origin	Insertion	Function
Biceps brachii (Figure 2.4)	Caput longum: Tuberculum supraglenoidale (Scapula) Caput breve: Proc. coracoideus (Scapula)	Tuberositas radii (Radius), Lacertus fibrosus (Ulna)	Elbow joint: Flexion, Supination Shoulder joint: Abduction and inward rotation (Caput longum) , Anteversion (Caput longum and Caput breve)
Deltoides pars acromialis (Figure 2.3 & 2.4)	Acromion (Scapula)	Tuberositas deltoidea (Humerus)	Abduction of the humerus
Deltoides pars clavicularis (Figure 2.3 & 2.4)	Clavicle	Tuberositas deltoidea (Humerus)	Anteversion, inward rotation, abduction
Deltoides pars spinalis (Figure 2.4)	Spina scapulae (Scapula)	Tuberositas deltoidea (Humerus)	Retroversion, outward rotation, abduction
Infraspinatus (Figure 2.5)	Fossa infraspinata (Scapula)	Tuberculum majus (Humerus)	External rotation
Latissimus dorsi (Figure 2.3)	Pars vertebralis: - procc. spinosi of 7. - 12 . thoracic vertebrae - above fascia thoracolumbalis from spinous process of the lumbar vertebrae and os sacrum (facies dorsalis ossis sacri) Pars iliaca: rear third of the crista iliaca Pars costalis: 9 . - 12. rib Pars scapularis: angulus inferior	Crista tuberculi minoris (Humerus)	Inward rotation, adduction, retroversion
Levator scapulae (Figure 2.3)	Procc. transversi 1.-4. cervical vertebrae	Angulus superior (Scapula)	pulls Scapula cranial-medial, bends the neck
Pectoralis major (Figure 2.4)	Medial half of clavicle, sternum, 2.-6. rib cartilage, lamina anterior of rectus sheath (Thorax)	Crista tuberculi majoris (Humerus)	Adduction and internal rotation, Anteversion

Muscle	Origin	Insertion	Function
Pectoralis minor (Figure 2.5)	3-5. rib (Thorax)	Proc. coracoideus (Scapula)	Drawing down of the scapula
Rhomboideus major (Figure 2.3)	Procc. spinosi 1-4. thoracic vertebrae (Thorax)	Margo medialis (Scapula)	Fixation of scapula, pulls Scapula cranial-medial
Rhomboideus minor (Figure 2.3)	Procc. spinosi 6. and 7. cervical vertebrae	Margo medialis (Scapula)	Fixation of scapula, pulls Scapula cranial-medial
Serratus anterior (Figure 2.3 & 2.4)	1.-9. rib (Thorax)	Scapula pars superior, intermedia, inferior	Translation of scapula lateral-ventral, rotation of scapula lateral-ventral
Subscapularis (Figure 2.5)	Fossa subscapularis (Scapula)	Tuberculum minus (Humerus)	Internal rotation
Supraspinatus (Figure 2.5)	Fossa supraspinata (Scapula)	Tuberculum majus (Humerus)	Abduction
Teres major (Figure 2.5)	Angulus inferior (Scapula)	Crista tuberculi minoris (Humerus)	Inward rotation, adduction, retroversion
Teres minor (Figure 2.5)	Margo lateralis (Scapula)	Tuberculum majus (Humerus)	External rotation, weak abduction
Trapezius pars ascendens (Figure 2.3)	Procc. spinosi 5.-12. thoracic vertebrae	Spina scapulae (Scapula)	Pulling scapula caudal-medial
Trapezius pars descendens (Figure 2.3)	Os occipitale, procc spinosi of all cervical vertebrae	Lateral third of clavicle (Clavicle)	Pulls scapula diagonal upwards and rotates it outward
Trapezius pars transversa (Figure 2.3)	Procc. spinosi 1.-4. thoracic vertebrae	Acromion (Scapula)	Shifts scapula to medial
Triceps brachii (Figure 2.5)	Caput longum: Tuberculum infraglenoidale (Scapula) Caput mediale: back of humerus, distal of sulcus n. radialis, septum intermusculare mediale Caput laterale: back of humerus, proximal of sulcus n. radialis, septum intermusculare laterale	Tuberositas radii (Radius), Lacertus fibrosus (Ulna)	Elbow joint: Extension Shoulder joint: Retroversion and adduction (Caput longum)

TABLE 2.1: Muscles involved in the shoulder complex with their anatomical insertions, origins and functionality (Adapted from Schünke, Schulte, and Schumacher, 2007).

Chapter 3

Musculoskeletal modelling within the AnyBody™ Modeling System

3.1 The shoulder model of the AnyBody™ Modeling System

The AnyBody™ Modeling System (AMS) has been selected for all the musculoskeletal modelling and simulation aspects of this work, as the AMS has demonstrated a good comparability between predicted joint loadings to in-vivo loads (e.g. Marra et al., 2015).

The shoulder sub-model within the AMS is based on the van der Helm model (van der Helm, 1994b), where specific parameters regarding e.g. insertion, origin, muscle fibre length and cross-sectional area are implemented from multiple sources and can be found in the AMS documentation. For the various computational studies conducted within the framework of this thesis, two iterations of the AMS are utilised. This originates from improvements of the utilised shoulder model, which were implemented by other research groups and were published during the duration of this work. These are the AMS V.7.1.0 with the shoulder model of the AnyBody managed modelling repository (AMMR) V. 2.2.0 and the AMS V.7.2.0 with the AMMR version V 2.2.2.. A notable difference between these two shoulder models is the improvement of the deltoid muscle group, where muscle insertion and origin points, strength of the elements and the wrapping were changed by Strzelczak et al., 2018.

Clavicular protraction, elevation, axial rotation, scapula protraction and elevation are computed as a function of the humerus motion and based on a linear regression model by J.H. de Groot and R. Brand (Groot and Brand, 2001). The third degree of freedom of the scapula is defined by a surface contact on an ellipsoid, which is approximating the thorax and prevents the scapula from penetrating the ribcage. The dependent kinematics of the humerus, scapula and clavicle are referred to as shoulder rhythm. Furthermore, the modelled GH joint includes a mechanism which ensures that the force within the GH joint is always kept within the glenoid cavity. The model incorporates 104 single muscle elements in order to represent the various muscles of the shoulder complex (Figure 3.1).

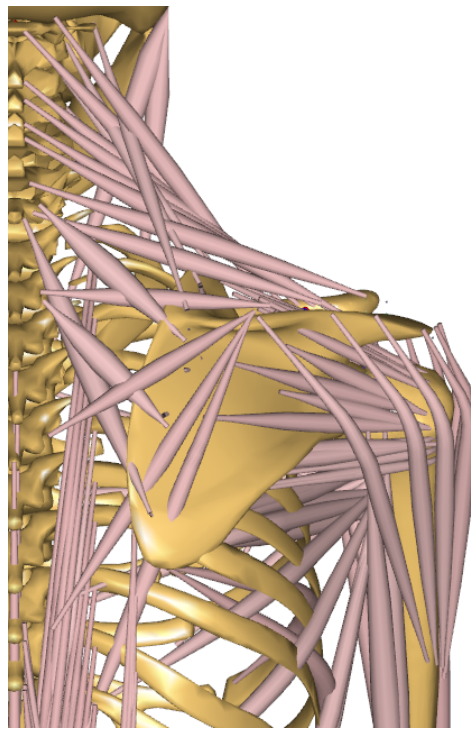


FIGURE 3.1: Graphical representation of the AMS shoulder model (AMMR version V 2.2.2) from the posterior view.

The AMS offers several features which are utilised in this thesis. It allows for the input of motion capture marker trajectories, where the kinematics of the segments are computed by a kinematically over-determinate optimization approach (Andersen et al., 2010). The involved body segments are scaled by these markers, where the distribution of the subject specific body weight follows a length-mass-fat scaling law (Rasmussen et al., 2005). In order to model test subjects which participate in motion capture experiments, the initial segment length, body height, body weight and marker trajectories are required as input parameters. For the computation of a large number of models e.g. to evaluate changes within the model or to compute multiple trials of different subjects, an external Python script is utilised (Lund, Rasmussen, and Andersen, 2019).

3.2 Recruitment of muscles within the AnyBodyTM Modeling System

The computational approach used by the AMS is hereby based on the principles of inverse dynamics. With the kinematics as known input, the system computes the required muscle forces which are necessary to bring the segment masses, external loads and inertia effects into dynamic equilibrium. Since the musculoskeletal system is highly redundant by nature in terms of multiple muscles and elements spanning a given joint, a muscle recruitment criterion is needed to distribute the loads onto multiple muscle elements within a simulation.

The following section describes the mathematical principles of how the AMS solves this redundancy. It is taken from Damsgaard et al., 2006 with small adaptations, where the AMS was originally developed by the authors of this paper.

The solution of the muscle recruitment problem in the inverse dynamics approach is generally formulated as an optimization problem on the form

$$\underset{\mathbf{f}}{\text{Minimize}} \quad G(\mathbf{f}^{(M)}) \quad (3.1)$$

$$\text{Subject to } \mathbf{C}\mathbf{f} = \mathbf{d}, \quad (3.2)$$

$$0 \leq f_i^{(M)} \leq N_i, i \in \{1, \dots, n^{(M)}\}, \quad (3.3)$$

where G is the objective function, i.e., the assumed criterion of the recruitment strategy of the central nervous system, stated in terms of the muscle forces, $\mathbf{f}^{(M)}$. G is minimized with respect to all unknown forces in the problem, $\mathbf{f} = [\mathbf{f}^{(M)T} \mathbf{f}^{(R)T}]^T$, i.e., muscle forces, $\mathbf{f}^{(M)}$, and joint reactions, $\mathbf{f}^{(R)}$. Eq. 3.2 is the dynamic equilibrium equations, which enter as constraints into the optimization. \mathbf{C} is the coefficient-matrix for the unknown forces and the right-hand side, \mathbf{d} , contains all known applied loads and inertia forces. The non-negativity constraints on the muscle forces, Equation 3.3, state that muscles can only pull, not push, and the upper bounds limit their capability, i.e., N_i is the strength of the muscle. The most popular form of the objective function, G , is the polynomial criteria.

$$G(\mathbf{f}^{(M)}) = \sum_{i=1}^{n^{(M)}} \left(\frac{f_i^{(M)}}{N_i} \right)^p. \quad (3.4)$$

G is stated with a variable power, p , and a normalizing function for each muscle, N_i . The normalized muscle force is often referred to as the muscle activity.

While these equations provide the underlying mathematics of the muscle recruitment within the AMS, Equation 3.4 is of special interest for this thesis as the power p of the objective function is altered in Chapter 5.

Chapter 4

Evaluation of musculoskeletal modelling parameters of the shoulder complex during humeral abduction above 90°

The following chapter has been published in a similar form in the Journal of Biomechanics under Aurbach et al., 2020b.

4.1 Introduction

One of the aims of this thesis is to simulate a full thickness tear of the m. supraspinatus and its biomechanical impact on muscle recruitment and joint reaction forces. Where one of the main purposes of the m. supraspinatus is to aid in the abduction of the humerus, it is important to incorporate a model which has the ability to predict the muscle activities and acting forces accordingly. As stated as the first research question in chapter 1, the issue of discrepancy between in-vivo measured GH joint reaction forces as compared to computed forces by a musculoskeletal simulation program is addressed in this section. While musculoskeletal models using an inverse dynamics approach achieve reasonable results for e.g. the knee joint (Marra et al., 2015), they seem to underperform with regard to the shoulder joint. Nikooyan et al., 2012 showed that with EMG as input for a model, joint reaction forces increase, and they traced it back to several muscles stabilizing the shoulder by co-contraction.

Predictive models utilising an inverse dynamics approach on the other hand do not incorporate this co-contraction mechanism as of yet. Sins et al., 2015 provide an overview of GH joint reaction forces over the humeral abduction angle of various models and highlight this issue. In their adaption of the AMS shoulder model to an implant they simultaneously computed joint reaction forces with an increasing trend above 90° of abduction. Changes they applied in the modelling environment are notably a mechanism which allows the humeral head to translate and the incorporation of the AMS internal Hill muscle model. So it seems that an inverse dynamics approach can actually produce this force behaviour without regarding muscle co-contraction in its underlying computation. Ambrósio et al., 2011 tested three different models of the upper limb region and also reported a rising trend in joint reaction force up to 100° abduction, where they also applied a Hill muscle model. However, an assessment of single parameters is missing, as these models present the combination of a variety of implemented features simultaneously. Thus, the aim of this work is to evaluate the influence of kinematic, kinetic and muscle model parameters of the AMS shoulder model in order to achieve realistic muscle activation and GH joint forces up to 140° humeral abduction. The selected parameters are based on experience from testing the existing model and literature which elaborated several mechanisms that affect the GH joint reaction force (Sins et al., 2015; Flores-Hernandez et al., 2019).

4.2 Materials and Methods

4.2.1 Experimental setup

Ten male test subjects ($weight = 81.7 \pm 16.2kg$, $height = 1.79 \pm 0.07m$, $age = 32.3 \pm 7.9years$) were measured during abduction of the humerus in order to provide reference data. The subjects were verbally instructed to conduct the test motion in the coronal plane with their palm facing medial and no weight in hand. The kinematics were recorded with a motion capture system (Vicon®, Vicon Motion Systems Ltd., UK) with markers placed on the pelvis, thorax, humerus and clavicle. The EMG activities of the m. deltoideus pars clavicularis/ acromialis/ spinalis, m. trapezius pars ascendens/ transversa/ descendens and the m. infraspinatus were captured by surface electromyographic (EMG) sensors (Delsys Trigno IM, Delsys® Inc., MA, US.) with a sampling frequency of 1.1 kHz.

4.2. Materials and Methods

Previous to electrode placement, the location site was cleaned with an alcoholic solution in order to minimize influences on the acquired signal due to dead skin cells or salt. These were placed according to recommendations in literature (Barbero, Merletti, and Rainoldi, 2012; Criswell and Cram, 2011), where the location of the markers and EMG sensors is exemplified in Figure 4.1. Maximum voluntary contraction (MVC) measurements were taken for the normalization of the EMG data according to Konrad (Konrad, 2006). Each test subject performed three abduction trials.

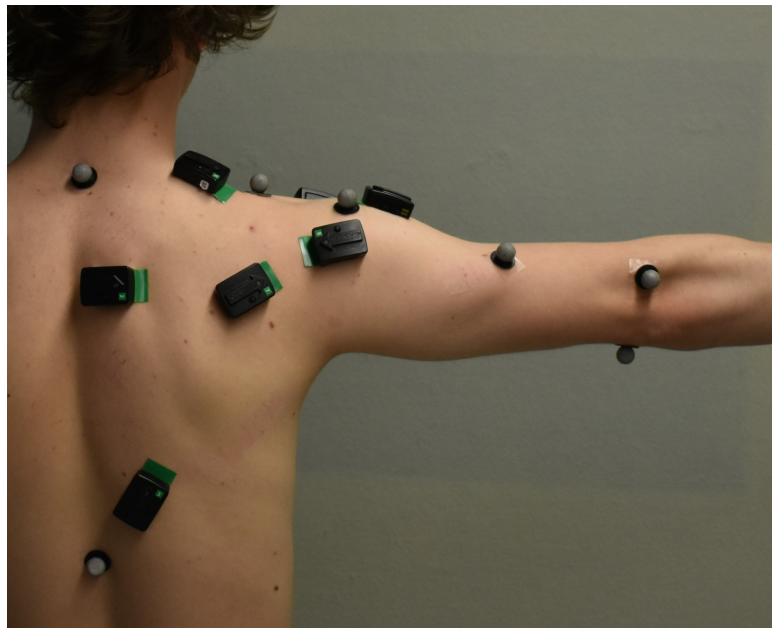


FIGURE 4.1: Optical motion capture and EMG sensor placement on a test subject

4.2.2 Musculoskeletal modelling

For the assessment of which alterations affect the GH reaction force and the muscle recruitment of the model, several changes were applied to this base model (BM):

Torus obstacle method for the deltoid wrapping (T)

The deltoid muscle group in total is divided into 12 modelled muscle elements, where each of the anterior, lateral and posterior deltoid is associated with 4 of these representatives. In order to keep them from sliding over the humeral head during motion, each of the muscles is passing through a fixed point located outside of the humeral head. However, this results in a non-physiological wrapping and muscle pathing, which affects the moment arms of the deltoid and thus its recruitment pattern. In order to provide a more physiologically wrapping around the humeral head, the via points were replaced with toroid structures (tori) where the muscle element is pathing through the inner tube (Havelková, 2016) (see Figure 4.2). The tori are modelled with an outer radius of 28 mm which is based upon the radius of the humeral head (Wataru et al., 2005). They are oriented with a 45° inclination to the longitudinal axis of the humerus. The axis of revolution of the most lateral torus at a default position of 0° humeral abduction, external rotation and flexion is in the coronal plane. The anterior and posterior tori are rotated in 10° increments to point with their axis of revolution towards the thorax (see Figure 4.2). Like the via points they move with the humeral head, but due to their curvature they result in a different elongation of the muscle elements. This implementation is done preliminary for the assessment of this sub study. An updated version with a detailed description of forces, moment arms and kinematics of the torus obstacle method is conducted in chapter 5.

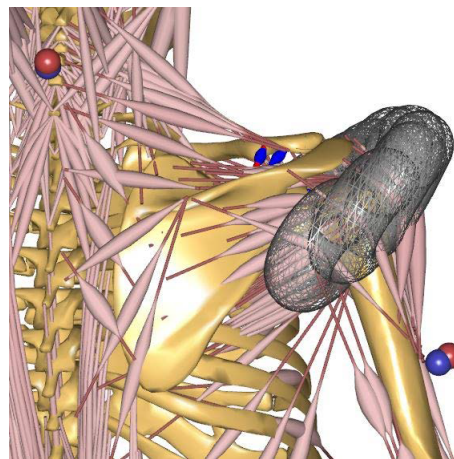


FIGURE 4.2: Preliminary implementation of the tori as an alternative wrapping for the deltoids

Three element Hill muscle model (H) and strength scaling (S)

With the shoulder complex having a large range of motion, the muscle elements exhibit a considerable change in length. Thus, the Hill muscle model (Hill, 1938) from the AMMR is used. This results in a varying strength of the muscle element depending on its length, which changes the muscle recruitment and introduces passive forces. Figure 4.3 (A) depicts the schematic representation of a Hill muscle element, where blue is the stiffness of the tendon and is called the serial elastic element, orange the stiffness of the muscle fibres or parallel elastic element and red (CE) is the contractile element, which is responsible for active force production. The fibre penetration angle is taken into account under the angle α . Figure 4.3 (B) depicts the tendon force which is exerted by an elongation of the element. Figure 4.3 (C) shows the force output of the muscle belly, where red highlights the variation of the strength of the CE element if its elongated or contracted with regard to its optimal fibre length and by a larger elongation the passive force of the parallel elastic element. The tendon slack length of the muscle elements used in the Hill model are scaled with a set of predefined positions by the AMMR with regard to the individual anthropometrics of the test subjects, whereas the other variables of the Hill model are constants provided by the AMMR.

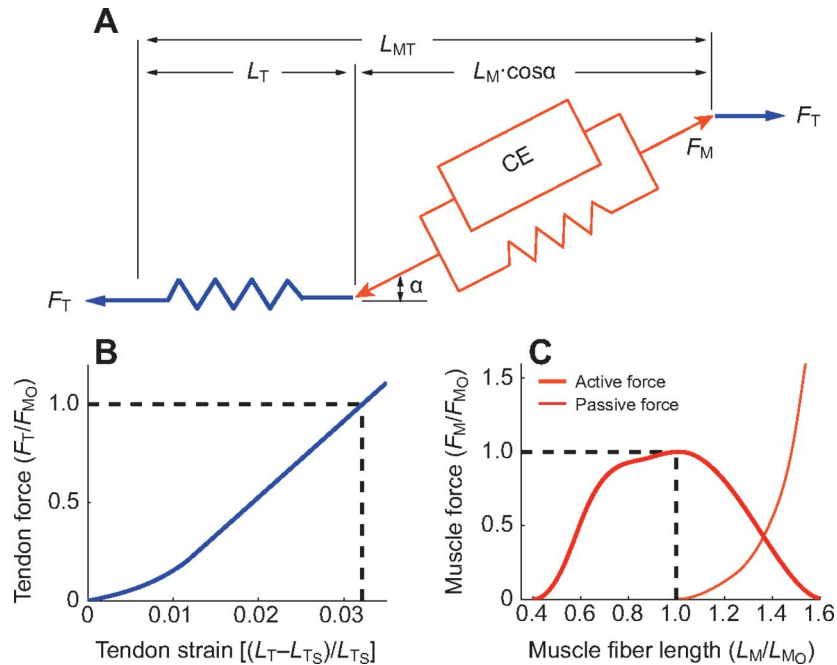


FIGURE 4.3: Principle of operation of the 3 element muscle model according to Hill. (Adapted from Delp et al., 1990 & O'Neill et al., 2013)

Utilisation of the Hill model required to take strength scaling into account which was altered by a factor of two (S2) and three (S3) in order to assess whether it has an influence on the force behaviour. The scaling is applied to the maximum force the muscle elements can produce, which simultaneously scales the resistant force of the passive stiffness elements. The factors were derived from previous testing on which scaling factors provide reasonable amplitudes in muscle activity with regard to literature (Wickham et al., 2010).

Motion capture driven clavicular protraction/elevation (CL)

The kinematics of clavicle and scapula are computed by the shoulder rhythm, which does not account for subject individual kinematics. An initial testing of the motion capture models has indicated a discrepancy between the marker placed on the AC joint (see Figure 2.1) from the measurements to the position derived from the shoulder rhythm. To account for subject individual motion, the DOF's of the clavicular protraction and elevation are replaced with the kinematics from this motion capture marker.

Force-dependent kinematics of the GH joint (FDK)

During an active state of the muscles spanning over the GH joint, the humeral head translates in the proximo-distal and anterior-posterior direction (Graichen et al., 2000; Massimini et al., 2012). This is implemented using force dependant kinematics (Skipper Andersen et al., 2017), which is a local forward dynamics approach. Spring forces representing the stiffness of the capsule act against the forces within the joint allowing for a translation of the humerus segment depending on the computed muscle forces from the inverse dynamics optimization. The spring stiffness is adjusted to fit the translation according to literature (Massimini et al., 2012), with a maximum of 6.0 mm in anterior-posterior and 2.5 mm in inferior-superior direction.

Alteration of scapula/clavicle rhythm (RHY)

The current rhythm for the scapula and clavicle is driven via a linear relationship with regard to the humeral elevation angle. An alternative rhythm was implemented where the kinematics follow a non-linear set of equations (Ludewig et al., 2009). The impact of a variation of the scapulothoracic rhythm on the GH joint reaction force was furthermore highlighted by Flores-Hernandez et al., 2019.

Simulation

From the six modifications T, H, S, CL, FDK and RHY, 16 different combinations are considered. For each combination, 30 trials from the experimental setup have been calculated within the AMS, resulting in 480 models. The AMS V.7.1.0. is used for the study, where the shoulder is based on the model version from the AMMR V 2.0.0.. Automatization, scaling and marker optimization are utilised as described in chapter 3.

Validation of model activity vs. EMG

The root mean square (RMS) of all EMG signals is calculated with a window size of 100 ms and the offset of the baseline is subtracted from each channel from the raw data. The signals are normalised to the MVC trials. In order to provide an inter-subject comparability, the abduction angle from the model was taken to replace the time dependency. The RMS values are distributed equally between 30-140° using a polynomial interpolation. For validation, a linear relationship between EMG activity and muscle force is assumed (Ringelberg, 1985) and a Pearson correlation coefficient r is calculated between model activity and EMG. The mean resultant GH joint reaction force of each parameter combination is computed by interpolation over the abduction angle and each subject's force is normalized to its bodyweight (BW). The resultant GH joint reaction force is then compared in a qualitative manner to the in-vivo data provided by OrthoLoad (2008, Retrieved 15. May, 2018 from <http://www.OrthoLoad.com>, files: s1r_210206_1_42, s2r_040408_1_2, s2r_270306_1_86s, 3l_190308_1_48, s4r_140207_1_70, s5r_131108_1_40, s8r_161208_1_17, s8r_161208_1_31).

Table 4.1 provides a short overview of the implemented alterations in order to facilitate the results and discussion.

Abbreviation	Model configuration
Basic (BM)	Unchanged model from the AMMR V.2.2.0.
T	Torus wrapping of the deltoids
H	Utilisation of the Hill muscle model
S	Strength scaling in combination with H
CL	Clavicle driven via motion capture marker
FDK	Translation of the humerus enabled
RHY	Non-linear shoulder rhythm

TABLE 4.1: Overview of the abbreviations of the altered/included model configurations

4.3 Results

From the 30 trials, 19 converged within the standard kinematic error tolerance of the AMMR after the marker based motion optimization for all parameter combinations, which did not include the marker on the clavicle. 27 trials converged for all models, which used the clavicle marker. Overall, 368 out of 480 models were calculated. Table 4.2 shows the results of the parameter study with regard to r between EMG data and model prediction. Model alterations T, RHY, FDK and CL showed higher r values for some muscle groups, but exhibited a lower r than the BM. A notable divergence from the BM is observable once the three element Hill type muscle model is implemented, where r increases approximately 0.6 from a negative to a positive correlation. A combination of alterations H and CL has an increased correlation by 0.35 due to a better agreement of the trapezoidal muscles. The combination of H-CL-T-S3 incorporates the highest correlation of 0.87 ± 0.09 .

Case	Trap. desc.	Trap. trans.	Trap. asc.	Delt. clav.	Delt. acr.	Delt. spin.	Infra	Mean+std
T	-0.93	-0.95	0.08	0.52	-0.67	-0.30	-0.65	-0.41 \pm 0.51
RHY	-0.90	-0.35	0.21	-0.08	-0.66	-0.27	-0.68	-0.39 \pm 0.36
FDK	-0.89	-0.96	0.17	0.68	-0.63	-0.26	-0.60	-0.36 \pm 0.55
CL	-0.88	-0.44	0.08	0.70	-0.67	-0.33	-0.67	-0.32 \pm 0.50
Basic	-0.86	-0.74	0.33	0.26	-0.52	-0.09	-0.45	-0.30 \pm 0.44
H-S2	-0.09	-0.76	0.75	0.56	0.33	0.64	0.64	0.30 \pm 0.50
H	0.41	-0.79	0.70	0.52	0.22	0.56	0.56	0.31 \pm 0.47
H-S3	-0.09	-0.74	0.77	0.56	0.42	0.71	0.68	0.33 \pm 0.51
H-T-S3	0.01	-0.79	0.77	0.52	0.46	0.72	0.72	0.34 \pm 0.52
H-CL-T-S3-RHY	0.97	0.49	0.66	0.83	0.39	0.65	0.83	0.69 \pm 0.19
H-CL	0.97	0.94	0.83	0.82	0.50	0.74	0.87	0.81 \pm 0.15
H-CL-T	0.97	0.94	0.83	0.83	0.54	0.76	0.91	0.83 \pm 0.13
H-CL-T-S2	0.96	0.95	0.84	0.84	0.60	0.80	0.92	0.84 \pm 0.11
H-CL-S3	0.97	0.96	0.85	0.84	0.65	0.84	0.91	0.86 \pm 0.10
H-CL-T-S3-FDK	0.97	0.94	0.86	0.86	0.65	0.84	0.93	0.86 \pm 0.10
H-CL-T-S3	0.97	0.95	0.85	0.86	0.67	0.84	0.94	0.87 \pm 0.09

TABLE 4.2: Pearson correlations r between EMG and model activities in the range 30-140° of the contemplated combinations ordered from lowest to highest mean r for the seven contemplated muscle groups.

Abbreviations for the cases are provided in Table 4.1.

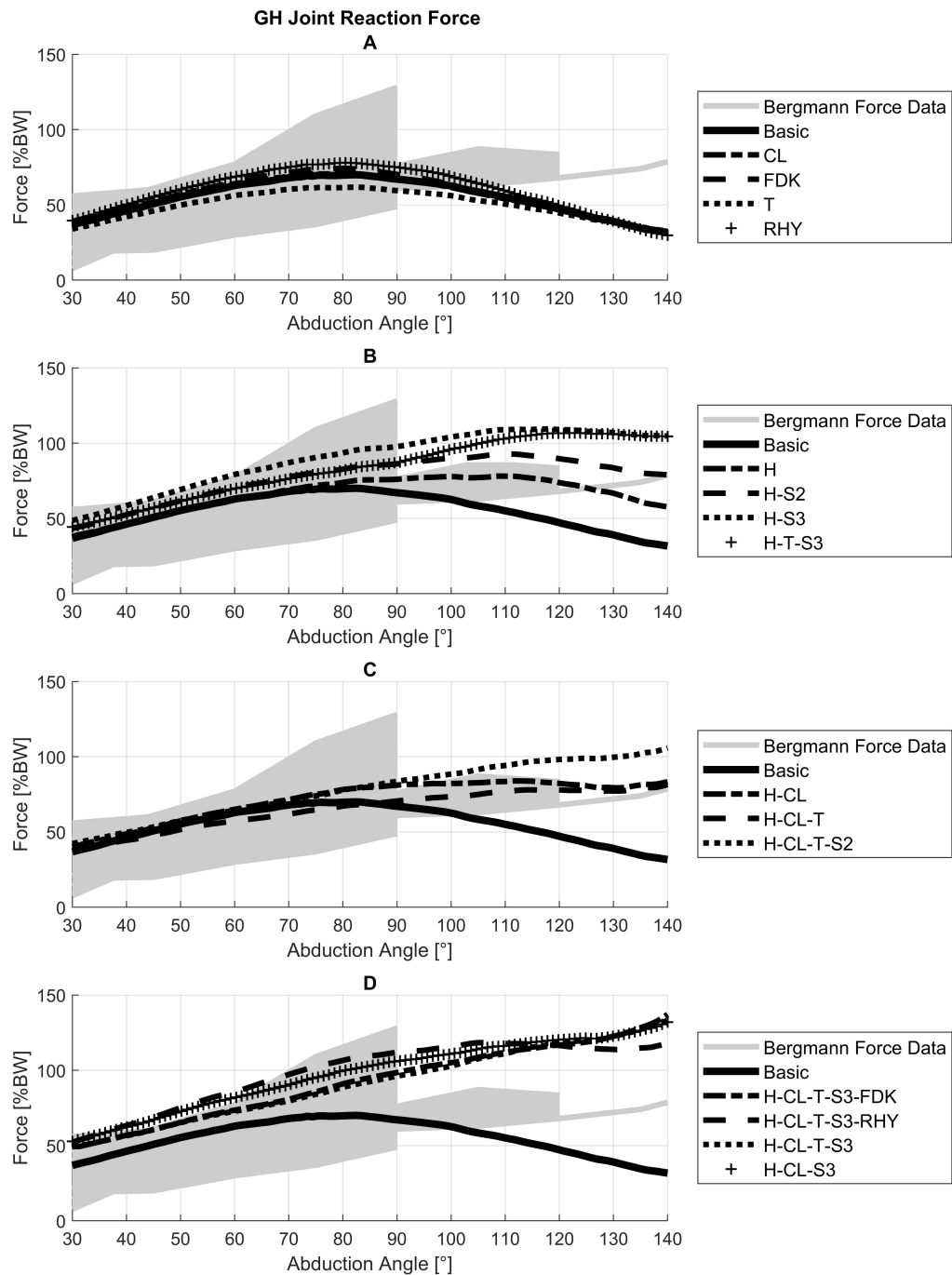


FIGURE 4.4: Resultant GH joint reaction force of the 16 combinations in %BW over the abduction angle of the humerus. Grey depicts the reference force data (Retrieved 15. May, 2018 from <http://www.OrthoLoad.com>, files: s1r_210206_1_42, s2r_040408_1_2, s2r_270306_1_86s3l_190308_1_48, s4r_140207_1_70, s5r_131108_1_40, s8r_161208_1_17, s8r_161208_1_31) and the continuous line the unchanged Basic model

4.3. Results

A similar trend is notable for the resulting GH joint reaction force, with the CL, FDK, T and RHY alterations having almost no influence on the trend of the resultant force (Figure 4.4 (A)). Like the BM, their corresponding peaks are attained between 80-90° abduction. With implementation of the Hill model and a variation in muscle strength, the force reaches its maximum between 110-120° abduction and remains on an overall higher level (Figure 4.4 (B)). The addition of the CL alteration to the Hill model changes the shape of the force progression, which exhibits a drop between 120-130° and a rising trend afterwards (Figure 4.4 (C)). Including the strength scaling S3, the force has an overall higher level of 6-18% BW in comparison to the BM, but keeps rising continuously until 140° of abduction up to 112-140% BW (Figure 4.4 (D)). Figure 4.5 shows the muscle activities of the BM in comparison to the H-CL-T-S3, which represents the highest Pearson correlation. Whereas in the BM all the muscle activities have their maximum between 70-90° abduction and their minimum at 140°, the corresponding EMG activities keep rising constantly. The H-CL-T-S3 model follows the trend of the EMG data for the trapezius muscles. For the deltoids however, the activity reaches its maximum between 100 and 110° with a decline afterwards.

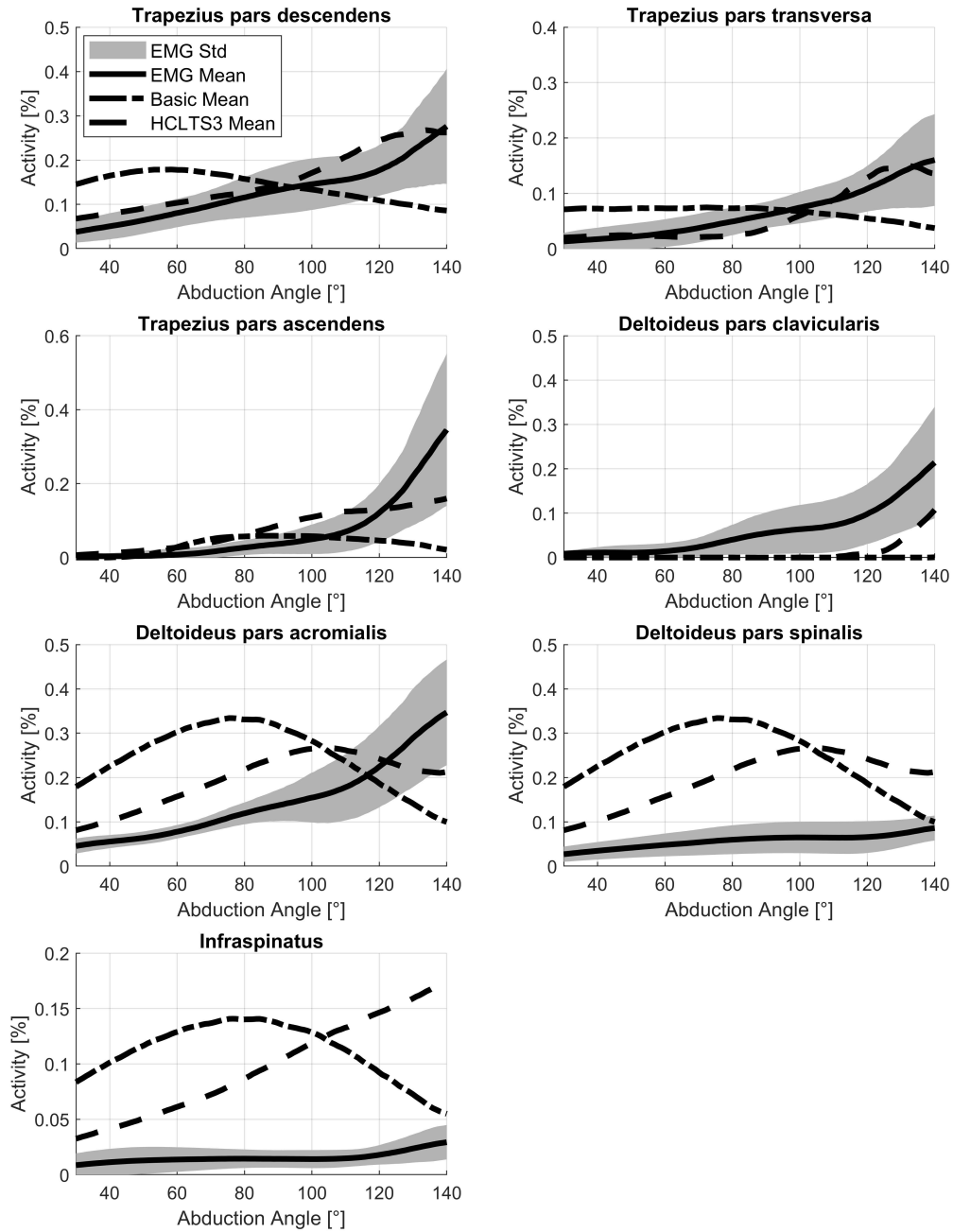


FIGURE 4.5: Activity of considered muscle groups over the abduction angle. Continuous line: Mean EMG of all subjects. Grey area: standard deviation of EMG of all subjects. Dashed line: Mean activity of the Basic models of the considered muscle groups. Dash-dot line: Mean activity of the H-CL-T-S3 parameter combination.

4.4 Discussion

With the aim to identify critical parameters for modelling the shoulder during abduction angles $>90^\circ$, utilization of the Hill type muscle model showed the most pronounced effect on the resultant GH joint reaction force.

Comparing EMG and model muscle activity has several issues. Among those are shifting of the muscle belly under the sensor (Barbero, Merletti, and Rainoldi, 2012)- and potential crosstalk (Rajaratnam, 2014; Solomonow et al., 1994). A common approach is to assess muscle ON/OFF times (Lund et al., 2012). However, the focus of this study is on the behaviour of the model above 90° shoulder abduction. Therefore, a Pearson r between EMG and model activity was chosen as parameter of interest to evaluate the trends of the recruitment (Nikooyan et al., 2011).

Where implementation of the T, CL, FDK and RHY mechanisms yielded effects on the muscle recruitment pattern (see Table 4.2) and the single components of the joint reaction force, the trend of the resultant force within the GH joint was maintained. Table 4.2 and Figure 4.5 indicate a discrepancy between the measured and simulated muscle activities of the deltoid parts. While the anterior deltoid shows almost no activation within the model during abduction, the posterior part carries the major part of the load. This depends on the muscle wrapping and hence the different moment arms, where the model of the AMMR v.7.1.0 which was used in this study was improved by Strzelczak et al., 2018 as stated in section 3.1. A detailed examination of the influences of these changes on model behaviour is conducted in section 5.

While the activity of the deltoids showed the lowest Pearson r in the H-CL-T-S3, the curve progression appears to be in better agreement with literature (Wickham et al., 2010) than with the experimental EMG. This is most likely due to noise domination and an overall low activity level as no additional weights were applied.

The scaling of the strength (S) in combination with the Hill model was conducted for two reasons, to take a scaling of the passive forces into account and a large discrepancy of the muscle activities predicted by the model in comparison to literature (Wickham et al., 2010). This discrepancy however originated from the deltoid model of the AMMR v 7.1.0. and is not apparent in the studies conducted in section 5. Upscaling the strength of the muscle elements by a factor of three is most likely not physiologically reasonable. An alternative approach to manipulate the passive forces is the alteration of how strong these activate depending on the elongation of the muscle elements. A closer investigation of the parameters of the Hill model and their effect on the GH joint reaction force is provided in chapter 5.

Using a motion capture marker (CL) to replace the clavicle elevation and protraction of the shoulder rhythm has improved the Pearson correlations in combination with the Hill model. However, the previously described calibration sequence which determines the optimal fibre and tendon length of the virtual muscle elements use the hard coded rhythm. This results in a mismatch between assumed optimal positions during the calibration and subject individual kinematics of the shoulder rhythm.

While all the implemented changes deserve a continuative investigation on a more detailed level, they do not influence the resultant joint reaction force, with exception for the utilisation of the Hill model.

The biggest improvement in the correlation of the muscle activities and the trend behaviour of the joint reaction force emerged with the utilization of the Hill model. The shoulder joint exhibits one of the largest ranges of motion within the human body, hence antagonistic muscles e.g. the m. latissimus dorsi stretch above a threshold where the passive non-linear stiffness is activated. These forces act against the protagonist muscles like the deltoids, which have to exert a higher force to compensate for the passive stiffness from the antagonistic muscle groups. Additionally, with the strength of each muscle element depending on its elongation, the solver distributes the forces to muscles with less mechanically advantageous moment arms when the strength of a more suitable muscle declines. Both effects contribute to an increase of the GH joint reaction force above 90° abduction.

4.5. Conclusion

Where Nikooyan et al. showed that the latissimus dorsi activation as co-contractor causes rising GH joint reaction forces after 90° abduction in their utilized model (Nikooyan et al., 2012), it is not active in the model used in this study. This indicates that the effect of the Hill model on the GH joint reaction force might be at least a complementary explanation for the force behaviour after 90° abduction.

Ambrósio et al., 2011 have also shown this force behaviour and compared three models to each other, where all used the Hill model and traced it back to the complexity of one of their models.

To the best of my knowledge, the mechanical properties of the Hill model have not been described as possible explanation for the force behaviour in the GH joint as of yet. Furthermore, the implemented changes FDK, RHY, CL and T all have a direct influence on the elongation of the muscle elements and thus the active and passive elements of the Hill muscle model. Where the major outcome of this study indicated that the Hill model is a physiologically reasonable explanation for the rising trend in resultant GH joint force above 90° abduction, these parameters should also be considered for investigation in future work.

4.5 Conclusion

Under the premise of muscle activities and forces within the GH joint rising after 90° of humeral abduction, it is proposed that the Hill type muscle model might be essential for accurately modelling the shoulder above 90° abduction as it yields two effects:

1. The passive stiffness of the three element Hill type model introduces an additional set of forces into the equilibrium equations.
2. With a change in strength in dependency of the elongation of each muscle element, the solver distributes the load to muscles with less mechanically advantageous moment arms.

However, parameters of the Hill model are highly subject specific and taken into focus for future research. The dependence of the strength-length relation of the muscle elements furthermore demand a strong emphasize of accurate modelling of muscle trajectories during dynamic movements.

Chapter 5

Modelling of the torus obstacle method as wrapping approach for the deltoid muscle group and investigation of muscle model parameters

Parts of the following chapter have been published in a similar form in the Journal of Biomechanics under Aurbach et al., 2020a.

5.1 Introduction

The forces acting on the glenohumeral joint are of major interest for assessing pathologies (Hölscher et al., 2016b), instabilities (Soslowky, Malicky, and Blasier, 1997) and potential risks for secondary injury (Vidt et al., 2018) as they incorporate the cumulative forces resulting from the musculoskeletal sub-system spanning the shoulder complex. The research questions 2. and 3. stated in chapter 1 (regarding the simulation of a biceps tendon transposition and the change in muscle recruitment with a tear of the m. supraspinatus) both need an adequate model for assessing force behaviour in the GH joint.

Based on chapter 4, two issues emerged which need to be addressed in order to achieve an improvement in model behaviour:

1. There is a discrepancy in activation of the virtual muscle elements associated with the anterior, lateral and posterior deltoid with regard to EMG measurements (see Figure 4.5). The muscle group of the deltoids is the main protagonist during humeral abduction in terms of activity and strength, thus contributing strongly to the forces acting on the shoulder joint. An opposite activation from anterior to posterior part subsequently alters the effective direction of the forces acting on the glenoid. This makes drawing conclusions with regard to loading of the joint questionable.
2. The Hill model has a major influence on the muscle activation and resulting glenohumeral joint reaction force. As the underlying mathematical implementation consists of several parameters, it is of interest how sensitive these are.

With regard to point 1, major improvements to the deltoid model of the AMS v.7.1.0 were implemented by Strzelczak et al., 2018 in order to solve some of the issues associated with the modelled deltoids, which are introduced in the AMS v.7.2.0.. The type of the muscle elements was changed from via points to a wrapping on ellipsoid objects. Additionally, the origin and insertion points of the muscle elements were changed to a more even distribution and the initial strength from the AMS v.7.1.0 was redistributed, resulting in stronger lateral deltoid elements and weaker posterior ones.

However, the implemented ellipsoid obstacles bring up the issue that in abduction angles $>90^\circ$, the muscle elements lose contact to the obstacles, which leads to the elements representing a straight line from their origin to insertion point. This results in the muscle elements of the anterior deltoid sliding under the lateral muscle elements, which is exemplified in Figure 5.1. Furthermore, by losing contact to their respective obstacle, the muscle elements cease to transmit forces onto the bony structures.

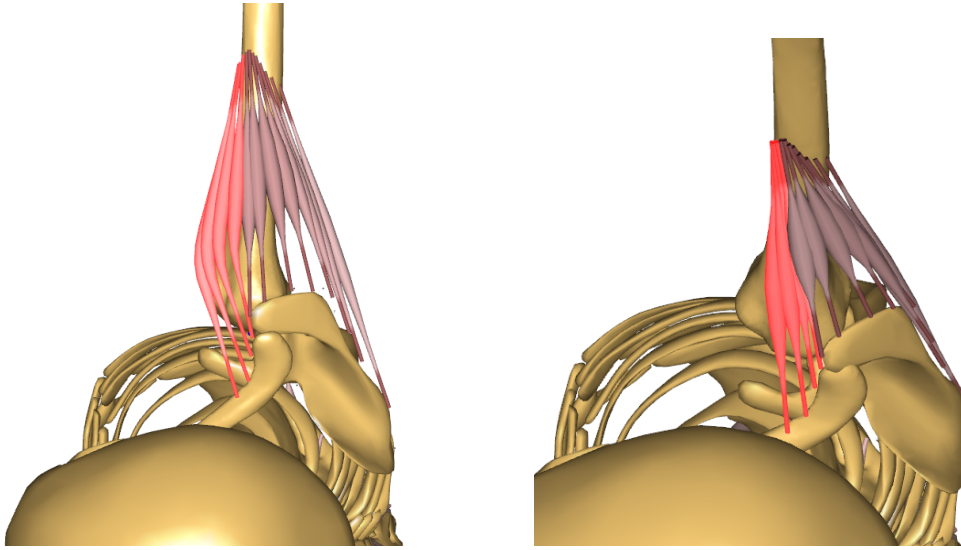


FIGURE 5.1: Deltoid muscle elements of the model of the AMMR v.7.2 with anterior elements highlighted in red. Left: Abduction at 90° , Right: Abduction at 120°

A wrapping surface more suited to cover the entire range of motion of the shoulder complex is the torus obstacle method (Havelková, 2016; Havelková and Krňoul, 2018, Špička and Havelková, 2018), where the muscle elements are guided through the inner tube of the tori. While preliminary implementation for initial testing was conducted in chapter 4, adequate kinematics for these virtual obstacles need to be implemented as they have to respect the interplay of scapular, clavicle and humerus motion. Thus, a large part of this section focuses on a designated modelling of the torus obstacle approach by implementing dedicated drivers for this type of obstacle and to incorporate improvements of the deltoid muscle model from Strzelczak et al., 2018.

5.2 Materials and Methods

5.2.1 Torus modelling

The AMS v.7.2.0. is used for modelling of the shoulder complex, where the shoulder model from the AMMR Version v.2.2.2. is providing the basis. The origin and insertion points of the 12 virtual muscle elements representing the deltoid are taken from the ellipsoid based wrapping approach by Strzelczak et al., 2018. In order to provide the size of the tori for each virtual muscle element, an MRI based approach is employed to extract the wrapping geometry which is based on the method from Kam et al. Man, 2017. This study uses subject specific MRI scans of the shoulder as input for the semi-automatic process of the model development.

The 12 insertion and origin points from the generic model of the AMS are taken and fitted onto the segments extracted from the MRI scan. The insertion and origin point of each muscle and the centre point of the humeral head describe a plane, which is used to cut the deltoid muscle volume from the MRI. From each cut, the central line is extracted and the position and the minor radius of each torus is calculated via an optimization algorithm to fit the curvature of the central line. The optimization provides the minor radius for each torus and the initial contact point between the virtual muscle element and the torus. The MRI measurements and the computation to fit the tori according to MRI images is hereby conducted by the project partners and co-authors of the publication Aurbach et al., 2020a.

Figure 5.2 depicts the tori of each deltoid muscle element of the model, where on the left the positioning at a default orientation of 0° humeral abduction is shown. The right side shows the pathing of the muscles at 120° abduction. The major radius is set to 50 mm and the centre positioned on a straight line from the humeral head through the initial contact point on the transversal plane. This allows the muscle elements conditional sliding on the inner tube of the tori while still being separate from the neighbouring muscle element.

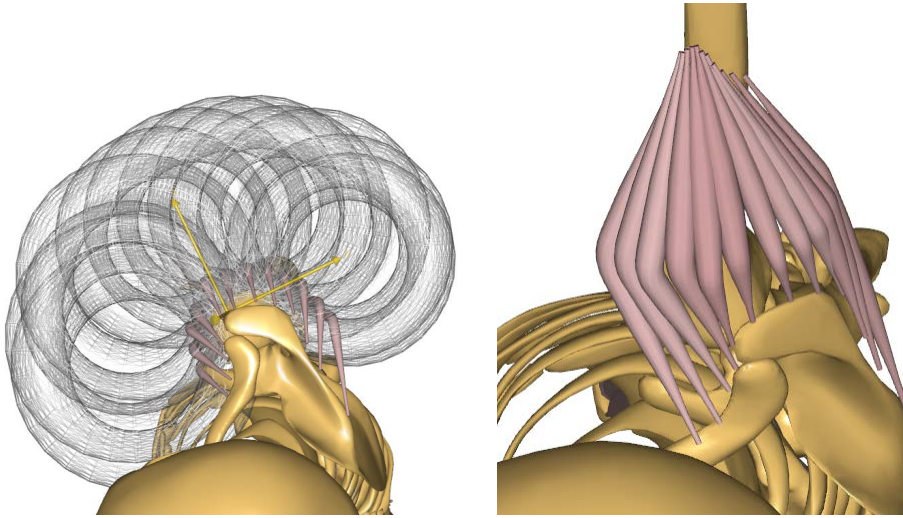


FIGURE 5.2: Model with the translated tori in default position at 0° abduction (left) and muscle pathing at 120° abduction, tori are graphically omitted (right)

In order to provide a continuous wrapping during motion, these positions are manually adjusted. Several kinematic couplings are implemented in order to determine the trajectories of the tori during abduction, which are described in the following passage. The anterior-posterior and medial-lateral translation of each torus is fixed to the humerus segment, as the humerus is exhibiting a larger range of motion than the clavicle or scapula. Initial testing showed that a kinematic coupling of e.g., the tori of the posterior deltoid to the scapula resulted in an physiologically unrealistic muscle path. For the inferior-superior translation along the longitudinal axis of the humerus, the tori are restrained at their initial distance with regard to the acromion. This enables the tori to translate with respect to the longitudinal axis of the humerus, see Fig 5.3 and prevents the tori from penetrating the scapula, as the humerus moves under the acromion during elevation.

The tori are oriented with their axis of revolution being parallel to the long axis of the humerus and rotate with the humerus in the flexion and abduction plane. For the rotation around the longitudinal axis, the tori rotate with the coordinate frame of the thorax to maintain independence from humeral external/internal rotation. With a fixed rotation of the tori around the humerus axis, the tori would penetrate the thorax during external/internal rotation of the upper arm resulting in physiologically unreasonable trajectories.

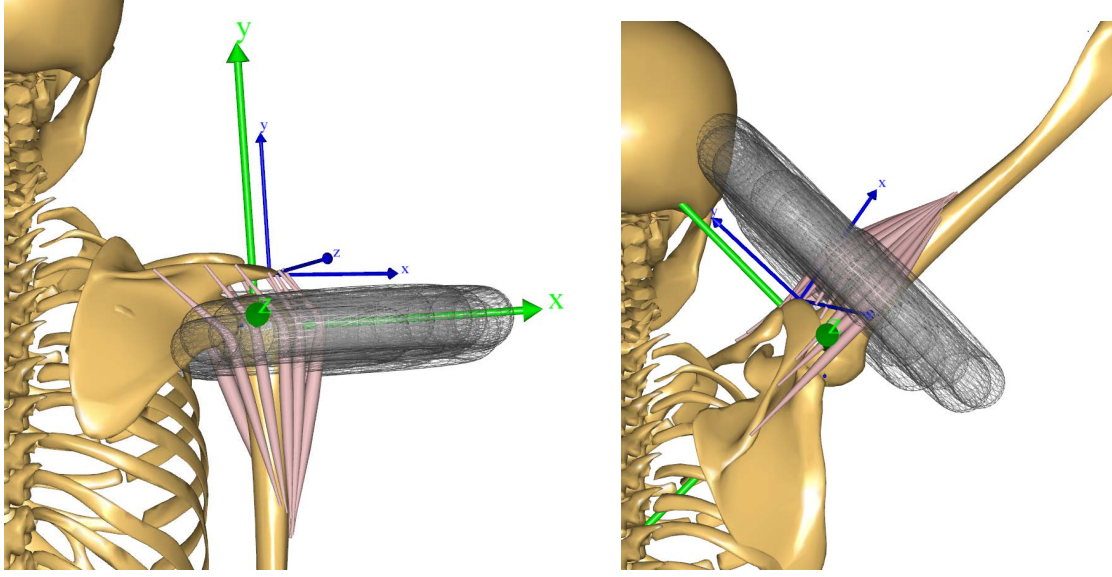


FIGURE 5.3: Torus obstacles of the deltoid within the AMS. On the left is the model in default position at 0° of abduction. On the right is the model at 120° abduction, where the position of the tori translate on the long axis of the humerus with a fixed distance to the acromion (blue coordinate system) as the humeral head moves under the scapula (green coordinate system)

5.2.2 Moment arm evaluation

One of the most important parameters of a modelled muscle element is its moment arm, as it is a key factor for load distribution and resulting joint force (Nussbaum, Chaffin, and Rechten, 1995; Raikova and Prilutsky, 2001). Furthermore, the solver of the AMS distributes the load to muscle elements with a favourable moment arm. The moment arms of the 12 muscle elements representing the deltoid are calculated with the tendon excursion method (An et al., 1984), it "determines the moment arm of muscle-tendon forces as the ratio between tendon displacement observed during a given amount of joint rotation and the corresponding joint rotation angle" Hashizume et al., 2016, which is described by the equation

$$M = \frac{\partial l}{\partial \theta} \quad (5.1)$$

In order to evaluate the three different deltoid models, the moment arms are calculated for the via point model, the ellipsoid wrapping and the torus approach first described in section 5.2.1.

Three different models are computed for each wrapping approach. External rotation and flexion angles of the humerus are set to 0° and a constant velocity of $10 \frac{\circ}{s}$ of humeral abduction in the range of $20 - 120^\circ$ is applied. These results are compared with a cadaver study conducted by Ackland et al., 2008.

5.2.3 Force transmission

Where section 5.2.1 describes the driver scheme and orientation of the torus obstacles, the transmission of the forces exerted on and by the tori need further explanation. With a virtual muscle element having contact with a wrapping obstacle, it can exert forces onto this object. Each torus of the 4 muscle elements associated with the anterior, lateral and posterior deltoid group is placed on a virtual massless carrier segments which moves as described in 5.2.1 according to the kinematics of the humerus. These carrier segments are kinetically coupled to the centre of the humeral head. Three configurations of the torus model are tested:

1. No forces and moments are transmitted from the three carrier segments (NOFM)
2. Only forces in X (compression) and Z (anterior-posterior) direction (FXZ) are transmitted onto the humeral head (see Figure 5.3, green coordinate system)
3. All forces and moments exerted by the tori onto the carrier segments are transmitted onto the humeral head (ALLFM)

The behaviour of the deltoid muscle activity and glenohumeral joint reaction force of the three configurations is evaluated with the same methodology of chapter 4 by comparing the activities to the measured EMG and the GH joint reaction force to the in vivo data from Bergmann, 2008. The AMMR v.2.2.0. is used for this study and the Hill model is employed. Parameters are evaluated in the range of $30-120^\circ$ humeral abduction. The models from chapter 4 which did not converge during the kinematic optimization were reworked, resulting in 30 functional models. Except for using the Hill model, none of the evaluated alterations to the model of chapter 4 were implemented.

5.2.4 Parameter evaluation of the Hill model

The study on the effect of various modelling parameters on the GH joint reaction force of chapter 4 showed that the only applied parameter which had an influence on the trend of the force after 90° is the utilization of the three element Hill model.

The Hill model is a simplification of physiological properties originating from the muscle structure and involved cell behaviour and types (Hill, 1938). Where there are several different expressions of the Hill model (Arslan et al., 2019) the standard Hill model uses three major components in order to describe the force a muscle element can exert. Table 5.1 describes all parameters and their constants implemented in the AMS in detail.

Several studies and models of the shoulder complex have incorporated the Hill model (e.g. Ambrósio et al., 2011; Sins et al., 2015), but a detail evaluation of critical parameters is missing.

It is of interest, which of the involved parameters of the Hill model are sensitive to alterations.

A parameter study using the torus model described in section 5.2.1 with the configuration of transmitting all forces and moments (ALLFM) (see 5.2.3) is conducted, where each parameter of the Hill model of the AMMR V 2.2.2 is individually altered to 50% and to 200% of its original value, where the other parameters are maintained.

Chapter 5. Modelling of the torus obstacle method as wrapping approach for the deltoid muscle group and investigation of muscle model parameters

Parameter	Description
F0	The nominal strength, i.e., the maximal isometric muscle force.
Lt0	Nominal tendon length.
Fcfast	Relative amount of fast fibers ($0 \leq F_{cfast} \leq 1$).
Lf0	Muscle fiber length. In muscle models with length-varying strength, this is the optimal fiber length. Zero or negative lengths are ignored.
Vol0	Volume of the muscle fibers, which is used during muscle recruitment. Zero or negative volumes are ignored.
Gamma0	Nominal pennation angle.
Epsilon0	Nominal tendon strain, i.e., the strain at the isometric muscle force in the serial elastic element.
Jt	Shape constant for the tendon (serial elastic) element force relationship.
Jpe	Shape constant for the parallel elastic element force relationship.
K1	Normalized maximum contraction velocity. The maximum velocity, called V0, is basically K1 times Lf0 (for K2=0).
K2	Contribution to normalized maximum velocity for fast fibers. K2 adds to V0's component from K1; K2's contribution to V0 is K2 times Lfbar times Fcfast.
PEFactor	Relative stiffness parameter for the parallel elastic element. PEFactor times Lfbar is the fiber length at which the parallel elastic elements produce a force of F0.

TABLE 5.1: Overview of the parameters used in the Hill model of the AMS and their description (Adapted from the reference manual of the AMS)

Motion is conducted from a standing position from an initial position of 0° humerus flexion, 4° abduction and 20° internal rotation with a constant abduction velocity up to 120° abduction. F_0 is not altered, as it is the same as in the simple muscle model and originates from specific cadaver studies where the shoulder model is build upon.

The default human model with 75 kg and 1.75 m is used with the shoulder rhythm of the AMS and the resulting GH joint reaction force compared to the in vivo data.

5.2.5 Recruitment criterion

One of the aims of this thesis is the simulation of a tear of the m. supraspinatus and how the recruitment of the other muscles changes accordingly once it is omitted. The m. supraspinatus carries out the roles of a stabilizer and abductor (Wuelker et al., 1994a; see for an overview Gasbarro, Bondow, and Debski, 2017), which is reflected in studies measuring its EMG activity (Wickham et al., 2010; Reinold et al., 2007b). However, the inverse dynamic model shows a lower activity of the muscle group during abduction than is reported in literature from EMG measurements. Within the model the majority of the load is distributed onto the deltoid muscle group as its is stronger and has a more mechanically advantageous moment arm. An approach to distribute the load more evenly between the muscle groups is to increase the power of the polynomial recruitment criterion (see Equation 3.4). A higher polynomial power of the recruitment criterion penalties muscles with a high activation, thus damping the main actors and shifting the load to a more even distribution. In order to assess a change of an alteration of the recruitment criterion of the solver, a study is conducted with the torus model (ALLFM), where the Hill model is used with the shoulder rhythm during abduction of the humerus with 0° external rotation, 0° flexion and a constant velocity in humeral abduction from 30° to 120° . The model is computed in 4 different configurations:

1. Model with polynomial recruitment criterion of $p=3$
2. Model with polynomial recruitment criterion of $p=5$
3. Model with polynomial recruitment criterion of $p=3$, 20 N virtual load in hand
4. Model with polynomial recruitment criterion of $p=5$, 20 N virtual load in hand

A virtual load acting in the direction of gravity is applied to the palm of the latter two models in order to make the activity of the m. surpaspinatus comparable to literature (Wickham et al., 2010). A second study is conducted on model behaviour with a polynomial power of the recruitment criterion of 5 by utilizing the motion capture and EMG data from the reworked trials described in section 5.2.3. 30 subject specific motion capture models are calculated for the evaluation of the deltoid activity and the resultant GH joint reaction force each for the torus model in the ALLFM configuration and the ellipsoid model, resulting in 60 models.

5.3 Results

In the following section the results of the various studies on model alterations are described.

5.3.1 Moment arm evaluation

Figure 5.4 shows the computed moment arms of the muscle elements representing the anterior deltoid from the study conducted in section 5.2.2 and the data from a cadaver study conducted by Ackland et al., 2008 (grey) using the tendon excursion method. The reference data has a moment arm of 8 mm at 20° abduction with regard to the GH joint, which increases up to 30 mm at 120° abduction. The black graphs depict the moment arms from the via point model, where 6 of the 12 model elements are associated in this model with the anterior deltoid. They show a linear trend with an initially negative moment arm exhibited by all elements. The moment arms of all three models become more positive from the anterior to more lateral elements. The moment arms of the ellipsoid model has the steepest increase over the entire ROM, with an initial linear behaviour, but show an increased curvature from the most anterior to the most lateral element. The moment arms of the torus model start with the steepest increase but flatten out at 40° in their inclination. At 120° degree abduction, the ellipsoid model tends to over estimate the moment arms (32.5 to 38.4 mm) in comparison to the reference data from literature (30.7 mm), where the torus model underestimates the moment arm (22.7 to 25.6 mm). The highest deviation from the reference data at 120° abduction is yielded by the via point model (6.0 to 22.4 mm).

5.3. Results

At 105°, the most lateral anterior element of the ellipsoid model (Ellipsoid 4) is in decline in comparison to the other elements. The results for the lateral and posterior elements of all wrapping approaches are provided in Appendix A.

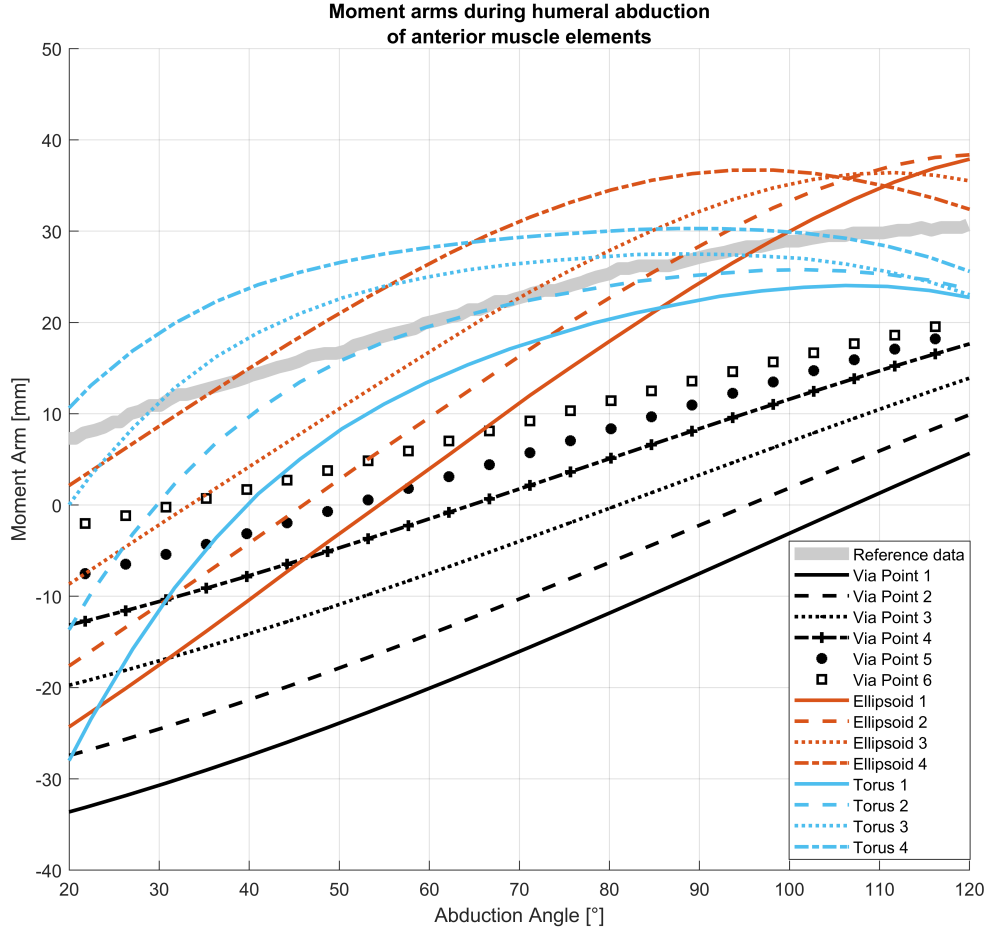


FIGURE 5.4: Moment arms during glenohumeral abduction in the range 20 – 120° of the anterior deltoid elements. Grey: moment arms from a cadaver study by Ackland et al., 2008 Black: anterior deltoid moment arms of the via point model, 6 associated model elements. Lines are labelled from 1-6 from the most anterior to the most lateral element. Orange: anterior deltoid moment arms of the ellipsoid model, 4 associated model elements. Lines are labelled from 1-4 from the most anterior to the most lateral element. Blue: anterior deltoid moment arms of the torus model, 4 associated model elements. Lines are labelled from 1-4 from the most anterior to the most lateral element.

Anterior, lateral and posterior moment arms of the torus wrapping are shown in Figure 5.5. Curve progression between the four anterior elements of the deltoid during abduction is in accordance with the reference data. The two elements of the lateral part orientated towards anterior side fit the reference data in slope behaviour, whereas the two elements oriented to the posterior side exhibit a decreasing trend from $20^\circ - 120^\circ$. The best agreement with regard to the reference data of the lateral deltoid is provided by element 6. The elements representing the posterior deltoid encapsulate the reference data. Nevertheless, they show an opposite trend in the slope property where the reference data is increasing but a decrease is found in the simulation data.

Table 5.2 shows the root means square error (RMSE) of Figure 5.5 between the associated muscle elements of each group of the deltoids and the reference data. The lowest RMSE for the anterior, lateral and posterior group are 3.9, 1.7 and 5.8 mm, respectively. The largest deviations occur on the outer elements of each muscle group with 12.6, 10.4 and 20.5 mm.

Muscle group	RMSE [mm]			
Anterior Deltoid	12.6	6.2	3.9	6.4
Lateral Deltoid	1.7	3.0	7.0	10.4
Posterior Deltoid	20.5	12.9	5.8	11.7

TABLE 5.2: RMSE between each muscle element and the associated reference data in mm. Each row is sorted from the anterior to posterior element of the respective muscle group.

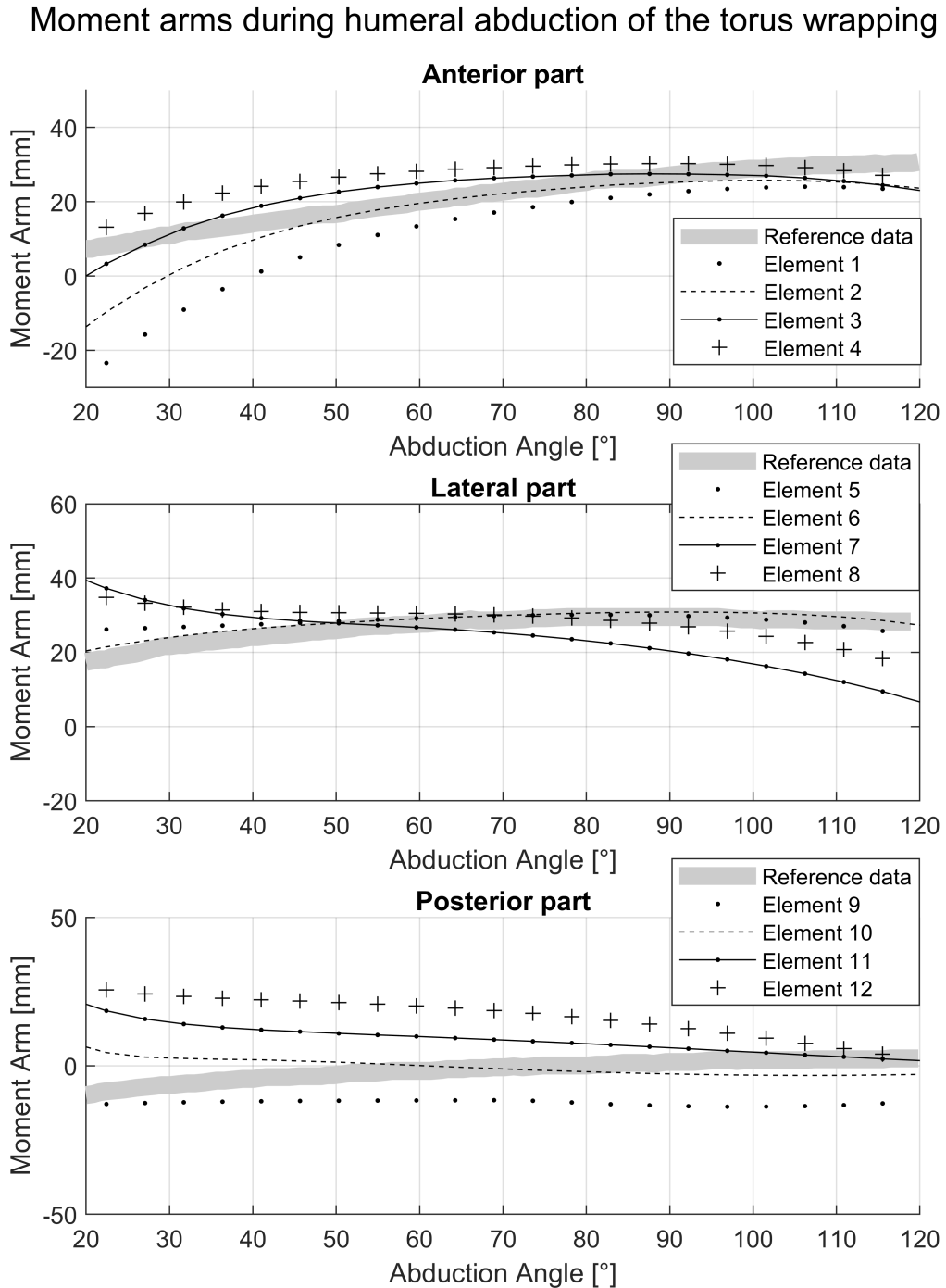


FIGURE 5.5: Moment arms during glenohumeral abduction in the range 20 – 120°. Each part of the deltoid (anterior, lateral, posterior) is represented by 4 model elements (black lines), with an increasing numeration from 1-12 from the most anterior to the most posterior element. Grey depicts the moment arms from a cadaver study (Ackland et al., 2008)

5.3.2 Force transmission

The effects of the three different configurations in force transmission (5.2.3) on the activation of the anterior, lateral and posterior deltoid are depicted in Figure 5.6. For the anterior activities, the Pearson correlation r is at 0.33 for the configuration of no forces and moments (NOFM) transmitted from the virtual carrier segment to the humerus with regard to the mean EMG of the 30 abduction trials. The correlation becomes negative with $r = -0.16$ while transmitting only the X and Z components of the force (FXZ). The highest level of agreement with the EMG data $r = 0.93$ for the case of transmitting all forces and moments (ALLFM). The mean EMG activity of the anterior deltoid has a steady increase up to 100° abduction, with a steeper inclination in the range 100-120° of humeral abduction.

The activity of the ALLFM model shows a steadily increasing trend up to 120° of abduction, with an activity of 25.2 % where the EMG is at 18.9%. The NOFM model peaks at 90° abduction with 21% activity and declines to 18.9% activity at 120°. At 60° abduction, the FXZ model reaches its peak with 18.3% activity and declines to 16% at 120°. For the lateral activities, the correlation values between the model activity and the EMG activity are 0.05 (NOFM), 0.59 (FXZ) and 0.81 (ALLFM). The EMG activity is constantly increasing in the interval 30-120° abduction from 7.0% to 32.5%.

The NOFM model starts at the highest activity level of all models with, peaks at 60° with 21.7% and declines to 18.9% at 120°. The FXZ model peaks at 80° abduction with 22% and declines like the NOFM model. The ALLFM model is at 11.9% activity at 30° and has two peaks. One at 71° abduction with 19.2%, where it declines to 90° of abduction and rises afterwards up to 20.6% at 120°.

For the posterior muscle activity, the EMG shows a lower activation than the anterior or lateral part with a maximum of 9.3% at 95° abduction. The correlation values r between posterior EMG and models are -0.94, 0.13 and 0.73. Where the ALLFM model exhibits an increase up to 20% activity level at 120° abduction, the NOFM and FXZ models have a opposite trend with regard to the EMG data with no activity at 70° abduction.

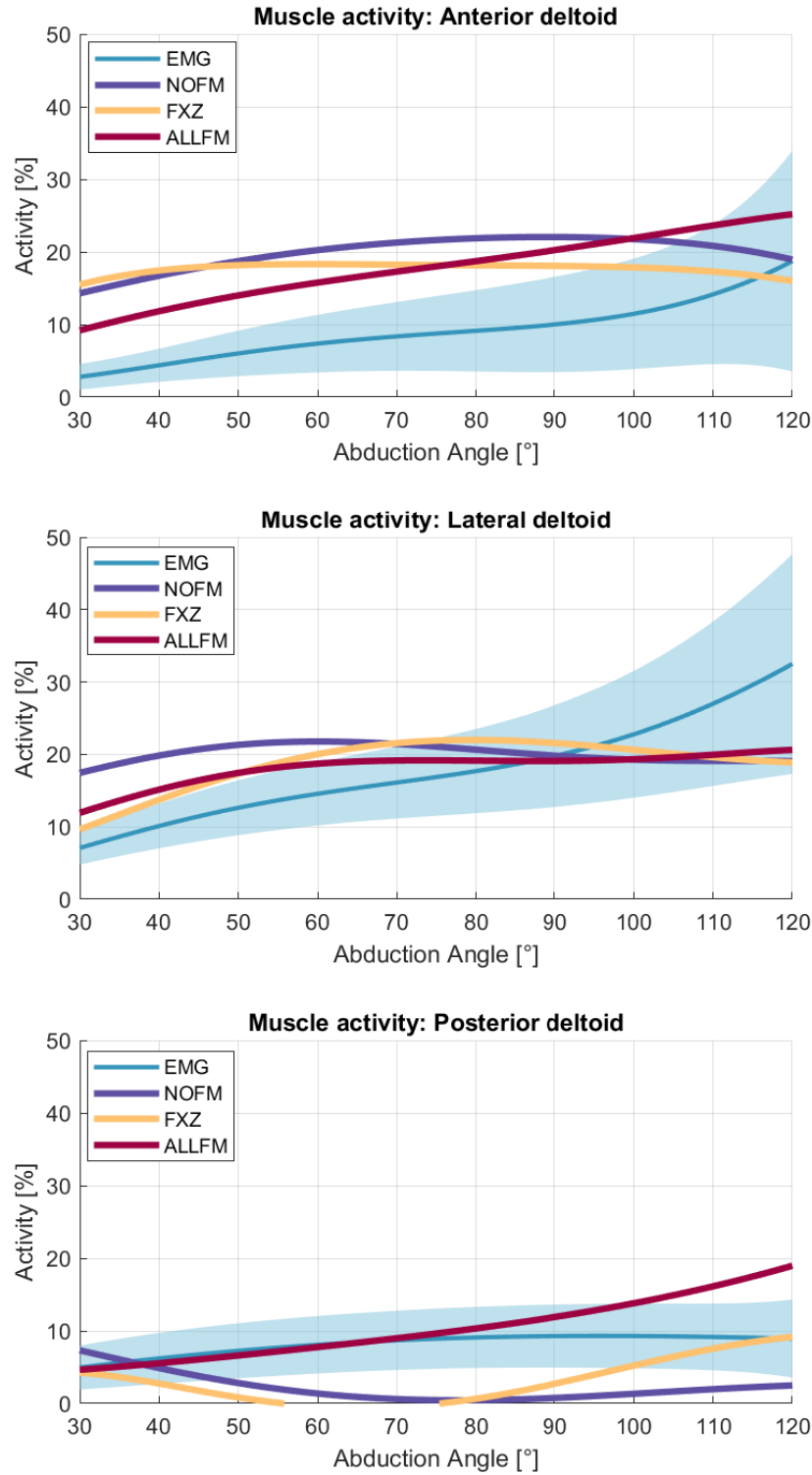


FIGURE 5.6: Activity of the anterior, lateral and posterior deltoid groups during abduction between 30-120° of the EMG mean (blue) and it's standard deviation (blue envelope), the mean of the NOFM model (purple), the FXZ model (yellow) and the ALLFM configuration (red) with $p = 5$

The computed resultant GH joint reaction force of the various force transmission configurations are depicted in Figure 5.7. Grey is the in-vivo forces in analogy to chapter 4. Where the resultant forces of all model configurations are inside the envelope of the reference data at 30° humeral abduction, they are lower at 120° abduction. At 120°, the two subjects that were able to reach this abduction angle exhibited a measured GH joint reaction force between 68 %BW and 83.4%BW, where the average of the ALLFM models is at 55.9%BW. The FXZ reaches a resultant force of 38.9%BW and the NOFM of 46.3%BW.



FIGURE 5.7: Resultant GH joint reaction force in %BW over the abduction angle of the humerus. Grey depicts an envelope of the in-vivo data (Retrieved 15. May, 2018 from <http://www.OrthoLoad.com>, files: s1r_210206_1_42, s2r_040408_1_2, s2r_270306_1_86, s3l_190308_1_48, s4r_140207_1_70, s5r_131108_1_40, s8r_161208_1_17, s8r_161208_1_31) in comparison to the NOFM (purple), FXZ (yellow) and ALLFM approaches in force transmission

5.3. Results

From the ALLFM model configuration, the average forces exerted by the anterior, lateral and posterior virtual carrier segments on which the associated tori are placed are provided in Figure 5.8, where the X,Y and Z directions correspond to the coordinate frame of the humerus segment (Figure 5.3, green coordinate system).

The lowest exerted force from all three carrier elements applied onto the humerus is the component acting in its longitudinal (Y) direction. The components exerting the highest forces of each carrier segment correspond to the deltoid activation pattern of the anterior, lateral and posterior part depicted in Figure 5.6. The anterior carrier element has the highest force contribution in the Z or anterior-posterior direction, which increases starting at 23 N to 70 N over the entire range of abduction.

The lateral carrier element mainly applies a force in the negative X direction of the humerus with a maximum force exerted of -41 N at 40° abduction and a declining trend afterwards. The main force exerted by the posterior carrier element acts in the negative Z direction in opposition to the anterior force, where the trend is increasing and is at its peak at -23 N at 120° abduction. The associated moments can be found in Appendix A.

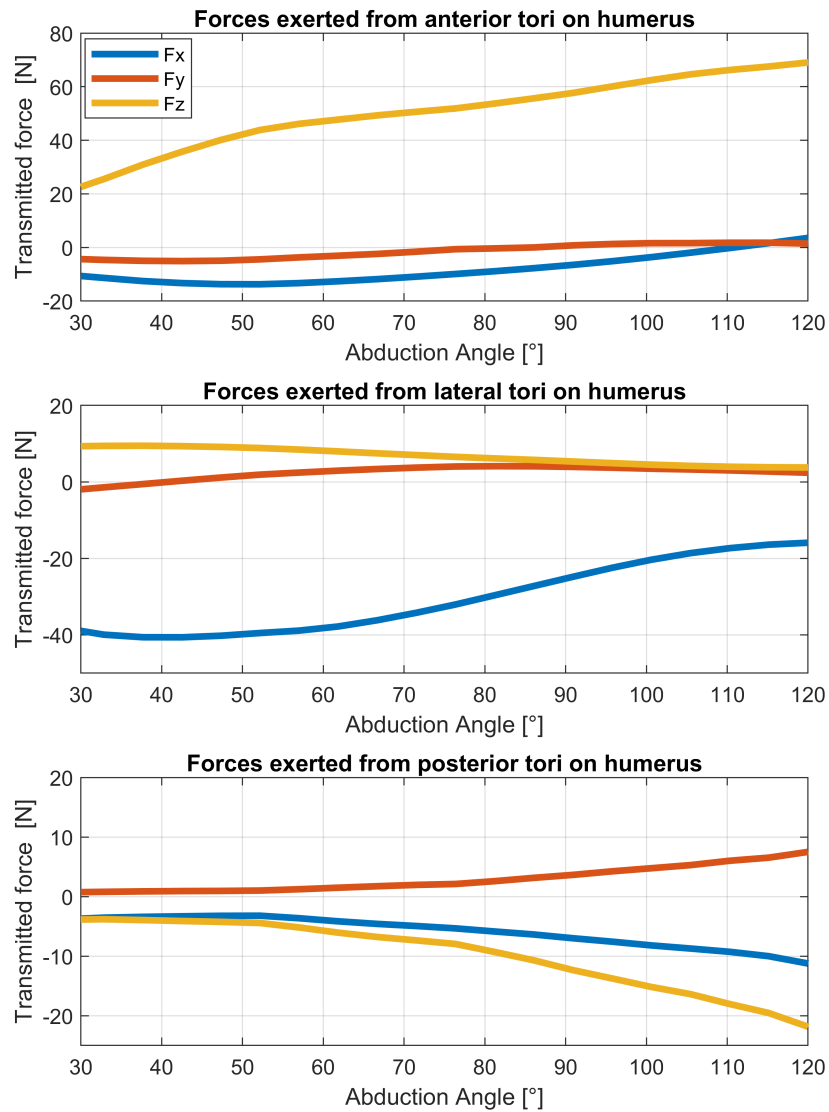


FIGURE 5.8: Forces transmitted from the anterior, lateral and posterior tori carrier elements onto the humerus from the ALLFM model (see 5.2.3) during abduction of the humerus in the range 30-120°. X,Y and Z components are expressed in the humerus coordinate frame (Figure 5.3, green coordinate system).

5.3.3 Parameter evaluation of the Hill model

Only three parameters were sensitive to a decrease of 50% of their (see Figure 5.9) or an increase to 200% of their initial value (see Figure 5.10) in their impact on the resultant GH joint reaction force:

1. The relative stiffness parameter of the muscle fibres (PE)
2. The muscle fibre length (LF0)
3. The shape constant for the parallel elastic element (Jp)

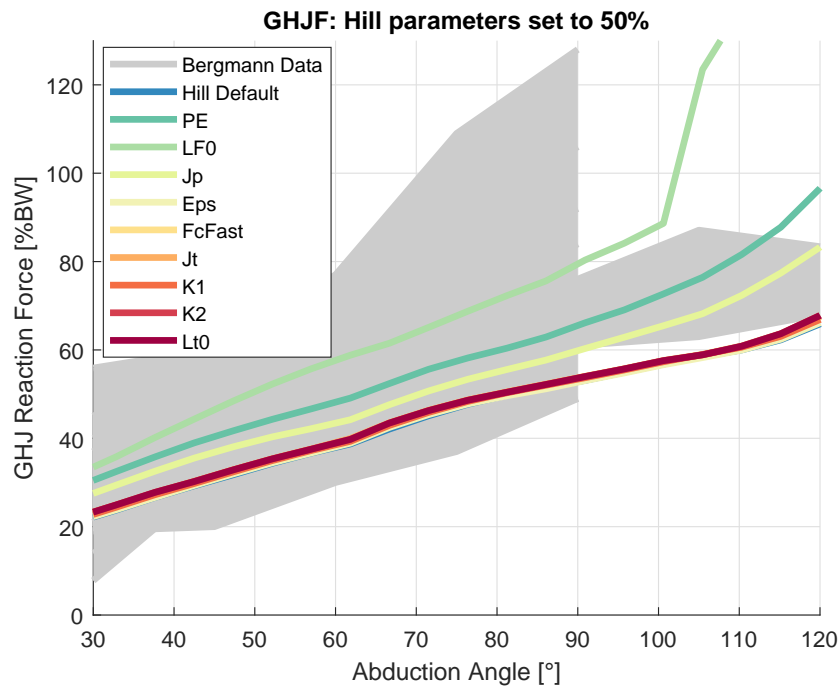


FIGURE 5.9: Resultant GH joint reaction force over abduction angle of single alterations of the Hill model. Single parameters are set to 50% of their initial value. Parameters are explained in detail in Table 5.1. Grey depicts the in-vivo force data (Retrieved 15. May, 2018 from www.OrthoLoad.com, files: s1r_210206_1_42, s2r_040408_1_2, s2r_270306_1_86, s3l_190308_1_48, s4r_140207_1_70, s5r_131108_1_40, s8r_161208_1_17, s8r_161208_1_31).

While the default model using the torus wrapping with the ALLFM configuration is at 67%BW at 120° humeral abduction, the model with Jp set to 50% of its initial value reaches 83%BW. Decreasing PE by 50% results in a force at 120° of 97%BW and a change to LF0 causes muscle overload and an overestimation of the force after 100° abduction, with a force of 137%BW at 120°. These model configuration also lead to initially increased forces at 30° abduction and a steeper inclination in their trend (Figure 5.9).

Where decreasing single parameters causes increased resultant GH joint reaction forces, setting them to 200% of their initial value leads to a slight decrease at 120°. Up to 100° abduction, there is no mentionable difference in resultant GH joint reaction force with regard to the default model.

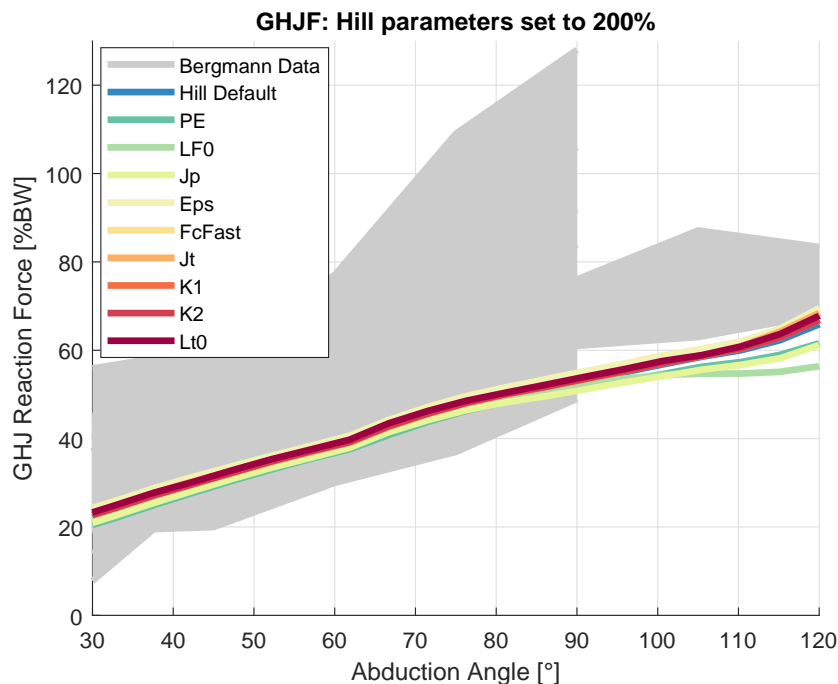


FIGURE 5.10: Resultant GH joint reaction force over abduction angle of single alterations of the Hill model, single parameters set to 200% of their initial value. Parameters are explained in detail in Table 5.1. Grey depicts the in-vivo force data(Retrieved 15. May, 2018 from www.OrthoLoad.com, files: s1r_210206_1_42, s2r_040408_1_2, s2r_270306_1_86, s3l_190308_1_48, s4r_140207_1_70, s5r_131108_1_40, s8r_161208_1_17, s8r_161208_1_31).

5.3.4 Recruitment criterion

Figure 5.11 depicts the activity of the m. supraspinatus muscle over the humeral abduction angle with a change in the power of the polynomial recruitment criterion and an applied weight to the palm of 20 N. The standard criterion inhibits a power of $p = 3$, where the activity of the m. supraspinatus is at 6.5% at 30° abduction and reaches its maximum at 57° abduction with 9.4% activity. With the applied force in the hand, its maximum activity is at 22.0% at the same abduction angle. Using an increased power of $p = 5$ results in a higher activation of the m. supraspinatus with 8.5% at 30° and its maximum being reached at 72° abduction with 13.2% activity. The maximum activation with 20 N load in hand is at 30.9% activity.

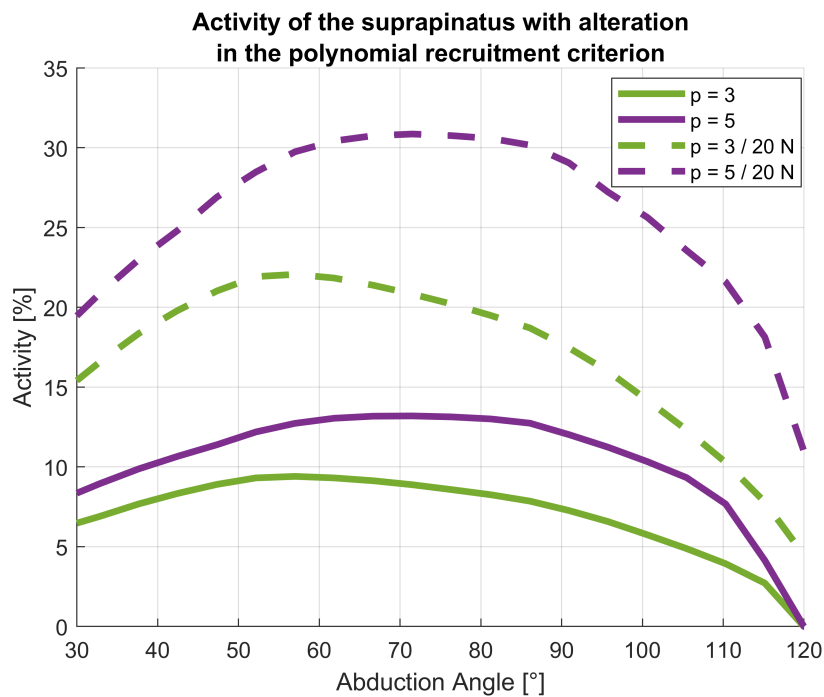


FIGURE 5.11: Activity of the m. supraspinatus muscle during humeral abduction in the range 30-120° of four model configurations: polynomial recruitment criterion with power $p=3$ (green) and $p=5$ (purple). Dashed lines are with a force applied to the palm of 20 N

Figure 5.12 provides a comparison of the activities of the anterior, lateral and posterior deltoid of the torus model (ALLFM) with a polynomial recruitment criterion of 5 (purple), the ellipsoid model with $p=5$ (orange) and the respective EMG activities (blue). For the muscle activity of the anterior deltoid, the mean activity of the ellipsoid model has a correlation of $r = 0.97$ with regard to the EMG activity and the torus model $r = 0.99$. Where the anterior deltoid EMG activity at 30° abduction is at 3%, the torus and ellipsoid model with $p=5$ both yield 9.7%.

At 120° abduction, the EMG inhibits an activity of 19.1%, the ellipsoid model 27.5% and the torus model 30.4%. Both models overestimate the activity of the anterior deltoid in comparison to the EMG activity. The lateral activities of both models have a similar trend up to 80° abduction, after which both models underestimate the EMG where the ellipsoid model declines to 11.4% at 120° and the torus model to 20.3% with the EMG activity of the lateral deltoid is at 34.8%. Correlation coefficients for the ellipsoid and torus model are 0.03 and 0.87, respectively.

For the lateral component, both models behave similar in trend and activity level up to 90° abduction, where the torus model shows higher forces at 120° abduction than the ellipsoid model and EMG with 21.6%. The correlation for the ellipsoid model is at 0.84, while the torus model yields an r of 0.91.

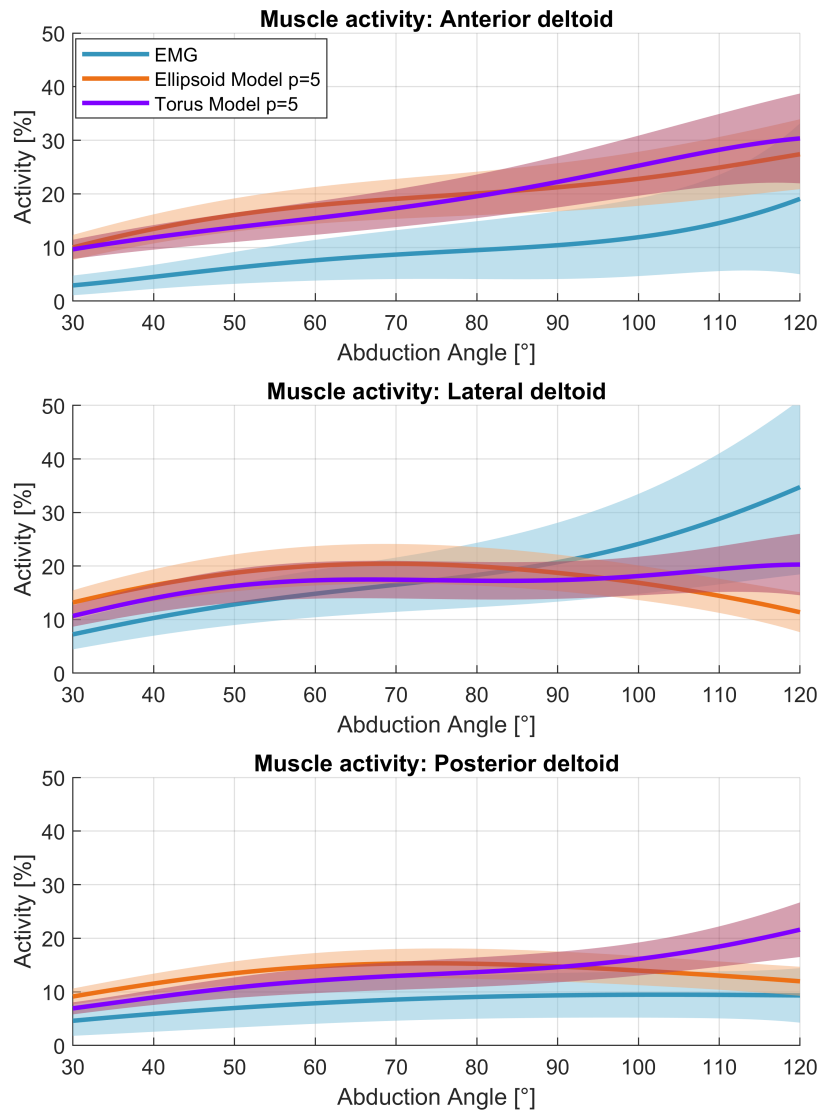


FIGURE 5.12: Activity of the anterior, lateral and posterior deltoid groups during abduction between 30-120° of the EMG mean (blue), the mean of the ALLFM model with $p = 5$ (purple) and the ellipsoid model with $p = 5$ (orange). Standard deviations are provided by the corresponding shaded areas

A comparison of the resultant GH joint reaction force of the torus and ellipsoid model to the in-vivo Bergman data is provided in Figure 5.13. The resultant forces are similar up to 80° abduction in progression and magnitude. After 80° the ellipsoid model declines to 49.7%BW. The torus model exhibits a rising trend in force which is in agreement to the in-vivo data, with 74.1%BW at 120° humeral abduction.

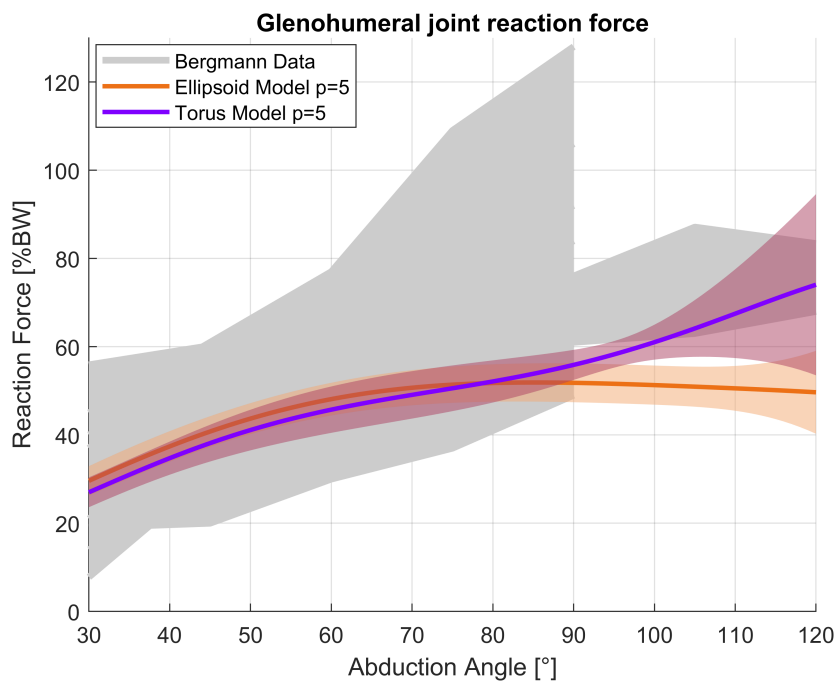


FIGURE 5.13: Resultant GH joint reaction force in %BW over the abduction angle of the humerus. Grey depicts an envelope of the in-vivo data from literature (Retrieved 15. May, 2018 from <http://www.OrthoLoad.com>, files: s1r_210206_1_42, s2r_040408_1_2, s2r_270306_1_86, s3l_190308_1_48, s4r_140207_1_70, s5r_131108_1_40, s8r_161208_1_17, s8r_161208_1_31) in comparison to the torus model with p=5 and the ellipsoid model with p=5

5.4 Discussion

The aim of chapter 5 was to improve and analyse the muscle activities of the deltoid group and the resultant GH joint reaction force with comparison to experimentally derived muscle activities and in-vivo force measurements from literature. The torus approach as a wrapping method for the deltoid muscle group yields several advantages. It prevents an overlapping of the different muscle elements over the entire range of motion (see Figure 5.2-right) and furthermore, with a continuous muscle-obstacle contact, the forces (Figure 5.8) and moments (Figure A.5) resulting from the muscle elements onto the obstacles are continuously exerted onto the humerus, which results in higher forces than the ellipsoid model Figure 5.13. This is in better agreement with the data from Bergmann, 2008.

Limitations and issues of comparing computed muscle activities to EMG measurements are discussed in section 4.4 and apply to all following sub-studies which utilize EMG as a validation method. All computed deltoid activities from the ellipsoid and torus model show a better agreement to the EMG than the via point model (see chapter 4.3).

5.4.1 Torus modelling

The two major limitations of this work are the use of data sets from different anatomical studies and the manual adjustment from the MRI based initial positions of the tori. Several parameters e.g. muscle cross-sectional area, insertion origin points of the deltoids and bone geometries are not from the same subject as the MRI scan. This has a direct influence on the workflow from the MRI fitting, as the cutting planes are calculated from the anatomical data of the original model. This discrepancy influences the initial positions of the tori derived from the MRI which results in crossing existing obstacles of other muscle groups of the AnyBodyTM model e.g. a sphere in the humeral head. Due to this reason, they are reworked manually to prevent this issue.

A better approach for future consideration and to eliminate the limitations of this work is to conduct a cadaver study which should not only take into account the subject specific anatomy, but also the curvature and orientation of the deltoid muscle fibres during all rotational degrees of freedom of the humerus. This would allow for a mathematical description of the tori in dependency of humeral elevation.

While the force data from the in vivo measurements shows a rising trend in GH joint reaction force which is also achieved by the torus model, it must be noted that a quantitative comparison is not feasible. The data from literature is not only from a different subject group, but it is also done with individuals after a total shoulder arthroplasty, whom potentially have a different muscle recruitment and pretension of the muscles in comparison to healthy subjects.

However, the focus of this study is on the feasibility of the torus wrapping of the deltoids in general to be considered for future studies, as their structure has the benefit of approximating the curvature of the deltoid similar to an ellipsoid wrapping but offers a better guidance such as a via point approach and a continuous force transmission.

5.4.2 Moment arm evaluation

Figure 5.4 highlights the issue of the via point model with regard to its moment arm in the abduction plane. Where the moment arm of the anterior deltoid from the cadaver study (Ackland et al., 2008) is positive and keeps increasing over the contemplated abduction range, all moment arms of the virtual deltoid elements of the via point model start of negative and are lower in amplitude. This leads to a dissonant activation (see chapter 4.3) as the solver does not regard these elements for the load distribution during abduction. The ellipsoid and torus model behave similar in curve progression, which is largely dependent on the change in muscle element origin/insertion and redistribution of the strength (see section 5.1). Due to the curvature of the ellipsoid and torus objects, the moment arms become non-linear in nature, which is in accordance with the cadaver study.

With the use of the tendon excursion method (Equation 5.1), the moment arms are computed from the incremental change in length. As the tori restrict the muscle elements as they bend around the inner tube, the moment arms become smaller with regard to the ellipsoid model. When the muscle elements lose contact to the obstacles in the ellipsoid model, they exhibit their maximum shortening capacity as they are represented by a straight line from insertion to origin. The relative change of the most anterior element hereby exceeds the more lateral placed elements, resulting in an intersection of the moment arms (see Figure 5.4).

Figure 5.5 shows a change in the slope of the moment arms from the anterior to the posterior side. This occurs, as the motion of the humerus during abduction is perpendicular to the thorax, not the scapula plane which results in a stronger curvature of the muscle elements on the anterior part (see Figure 5.2-right).

5.4.3 Force transmission

Where the ellipsoid and torus model behave similar in their moment arms in comparison to the via point model, the major difference in higher degrees of abduction is the force transmission provided by the tori. The NOFM and FXZ force transmission configurations showed larger disagreements with regard to deltoid activity and resultant GH joint reaction force than the ALLFM configuration (Figure 5.6), which is reflected in their lower Pearson correlations and the rusting amplitude of the GH joint reaction force (Figure 5.7).

While at 120° abduction the activities of the anterior deltoid fit the EMG closer in amplitude for the NOFM and FXZ configuration, the curvature over the entire examined range of abduction exhibits the opposite trend. The force transmission configurations need to be evaluated from a physiological point of view. The forces exerted by the wrapping objects onto the segments are reflecting a muscle pressing on its underlying bony structure when it contracts.

Where the NOFM model neglects these forces and moments entirely, some forces should be expected in reality. With the FXZ model a force transmission is assumed which only acts perpendicular to the long axis of the humerus, only regarding a compressive force but neglecting frictional forces from the deltoid.

While the ALLFM model showed the highest correlation with regard to the EMG, the activities of the anterior and posterior deltoid are overestimated especially in abduction angles >90°. It stands to reason, whether it is physiologically reasonable that the virtual torus objects can transmit moments onto the humerus and also whether the magnitude of these forces are reasonable, as they are up to 70 N in the anterior carrier segment at 120° abduction (Figure 5.8).

Another issue to be raised is the point of attack of these forces and moments. As the coordinate frames of the virtual anterior, lateral and posterior carrier segments are aligned with the coordinate frame placed in the centre of the humeral head in an initial position of 0° abduction, they are moving on the longitudinal axis of the humerus head in order to prevent a penetration of the segments due to the kinematics of the shoulder rhythm (see section 5.4.1).

However, the forces and moments are transmitted onto the reference point in the humeral head. Furthermore, the model assumes a force transmission from the anterior, lateral and posterior deltoid onto the humerus segment. A force transmission from the posterior deltoid onto the scapula or from the anterior deltoid onto the clavicle are also possible configurations. It is not clear, how these forces are distributed in-vivo. Future work should investigate the pressure distribution onto the segments with a cadaver study including a pressure measuring foil in order to assess the point of attack and magnitude of these forces and provide a validation to the computed forces from the tori carrier segments.

The GH joint reaction force aggregates the kinetics from all muscle elements spanning over the shoulder joint. While it is largely dependent on the deltoid activation, which consequently changes the recruitment of the other involved muscles and thus the forces, it can only conditionally provide a measure of validation for looking at changes to one isolated muscle group.

For the purpose of this thesis, it is opted for the ALLFM configuration and the torus approach, as they yielded the best agreement to the EMG and in vivo force data.

5.4.4 Parameter evaluation of the Hill model

From the parameter study on the variables of the Hill model, three properties showed a sensitivity in a decrease to 50% of their initial value or increase to 200% with regard to the resultant GH joint reaction force:

1. The relative stiffness parameter of the muscle fibres (PE)
2. The muscle fibre length (LF0)
3. The shape constant for the parallel elastic element (Jp)

The aim of this particular study was to identify possible crucial parameters which could be optimized.

The muscle fibre length defined in the Hill muscle model is equal to the optimal muscle fibre length at which the virtual muscle element can exert its maximum active force (see Figure 4.3). Decreasing the muscle fibre length impacts the ratio between its initial value and its relative change in length, which results in the muscle elements operating at a lower strength level as this curve gets compressed. Muscle elements with a mechanically less efficient moment arm but less relative shortening are regarded more in this case as compared to the original state of the Hill model. This results in higher joint reaction forces.

The length of the muscle belly can be derived for example from MRI (Juul-Kristensen et al., 2000) or cadaver studies. As it is a geometrical property and can be measured in-vivo or be extracted from cadaver studies. It is unlikely that the properties set in the default model differ or show a variance of 50% or 200% of their already implemented length.

The PE and Jp constants are more questionable. Scovil and Ronsky, 2006 have shown a large variance in reported parameters from literature and conducted a similar approach by variation of the Hill parameters of $\pm 50\%$ for walking and running models with a focus on the lower limb region.

A limitation of testing these parameters is the application to all muscle elements simultaneously.

However, the Hill model with regard to shoulder muscles seems stable in its current configuration and is thus used in its current form in chapters 6 & 7.

5.4.5 Recruitment criterion

EMG measurements of the m. supraspinatus show a high activity during abduction in the coronal plane during normal abduction (Wickham et al., 2010) and internal/external rotation (Reinold et al., 2007c; Kai et al., 2015).

Wickham et al., 2010 have measured the activity of the surpaspinatus of test subjects conducting humeral abduction up to 165° while holding a light dumbbell with the average weight of 2.5 ± 0.65 kg. Peak m. supraspinatus activity is reached at 88° of abduction with an approximate 57 %MVC value.

The modelled muscle activities depicted in Figure 5.11 underestimate this peak, where the model using a polynomial recruitment with the power of 5 is in better agreement as it reaches a maximum of 30.9% activity at 72° of abduction. Where with a recruitment criterion of $p = 3$ the deltoids carry the majority of the load as they are stronger and have a better moment arm, an increased muscle synergy is forced by a higher power. This results in a higher activation of muscle elements inhibiting a less favourable moment arm, which causes increased forces on the GH joint. This relationship can be seen by comparing Figure 5.7 and Figure 5.13. The resultant GH joint reaction force of the models using the ALLFM configuration differ in amplitude at 120°, where a recruitment criterion with the power of 5 results in an average 74.1%BW which is between the two forces of the in-vivo force study (68%BW and 83.4%BW).

Andersen, 2018 has described the effects of a change in the power of the muscle recruitment during gait with a focus on the knee joint, where he investigated powers of 2, 3 and 4 for the polynomial recruitment criterion. Where in his study the differences on force behaviour and force production of the involved muscles were small, they have a more severe effect on the shoulder joint. This might be due to a severe decomposition of the muscles in the shoulder model, where Holmberg and Klarbring, 2012 have shown that higher decomposition influences muscle recruitment when a polynomial criterion is utilised.

Overall the muscle activities did not exhibit notable fast activation or deactivation by using a higher order criterion and show a continuous trend, which is ultimately reflected in a continuous progression of the GH joint reaction force.

5.5 Conclusion

This model is assigned to assess m. supraspinatus tears, which take mostly effect during abduction. The results from the validation shows a behaviour of the model suitable for abduction tasks in the range between $20 - 120^\circ$ by using the torus model with the ALLFM configuration, the Hill model and a polynomial recruitment criterion with the power of 5.

Overall there are four mechanisms identified which cause an increase in the resultant GH joint reaction force and improves model behaviour with regard to EMG measurements:

1. The passive forces arising from the muscle stiffness described by the Hill model
2. A change in recruitment induced by the Hill model where the strength of an elements is dependent on its elongation
3. Reaction forces of muscle elements onto surfaces/obstacles which are transmitted to the body segments
4. Increased muscle synergism causes muscle elements being recruited more which have a less mechanically efficient moment arm, thus increasing joint reaction forces

Chapter 6

Clinical application: Biceps tendon transfer

Parts of the introduction and discussion of this chapter were created in collaboration with the project partner PD Dr. med. Carsten Englert.

6.1 Introduction

Instabilities of the long biceps tendon anchor, tears of the labrum or long biceps instabilities appear often as co-morbidity of rotator cuff tears (Baumgarten, Chang, and Foley, 2019). Very early stages of instability of the long biceps tendon (LBT) in the bicipital groove can be related to histopathological changes Gkait et al., 2018 and result finally in macroscopically luxation or rupture of the tendon. From a mechanical point of view, the co-morbidity of LBT and SLAP (superior labral tear from anterior to posterior) pathologies of rotator cuff tears has a direct influence on the forces acting on the glenoid. These changes are highly depending on the expansion and origin of the weakened rotator cuff (Boileau et al., 2002). In a m. supraspinatus tear, the shoulder reaction force is deviated cranial anteriorly and cause an overload of the LBT and the upper ventral third of the glenoid rim. Prolonged mechanical repetitive disuse is a well-known factor for the development of pathological processes leading to degenerative SLAP lesions of the shoulder joint. The onset of small biomechanical changes can eventually progress to pathologic symptoms such as subacromial impingement or in cuff tear arthropathy.

If conservative treatments of shoulder diseases with an LBT pathology and cuff tears fail, operative techniques can be considered to relieve pain and regain strength and

function (Boileau et al., 2002). Whereas the rotator cuff is the main issue, the long biceps tendon is often cut to release pain (Walch et al., 2005). From a clinical point of view, there are several ways to proceed after releasing the LBT from the glenoid rim (Voss et al., 2017; Voss et al., 2016; Voss, Imhoff, and Dyrna, 2018). Multiple varying techniques and constructs are available to perform an LBT tenodesis, including an array of intra-articular, suprapectoral and subpectoral fixation methods of the cut end of the LBT (Schoch, Geyer, and Drews, 2017). Some surgeons prefer an open subpectoral fixation of the LBT. This procedure is comparable to an arthroscopic manoeuvre in terms of speed (Forsythe et al., 2020). Fixation of the LBT can be accomplished using various materials and various designs for example titan, PEEK or Polyamide materials with an all suture anchor, suture loaded anchor or interference screws.

From a surgeons perspective, it is still controversial to suture the LBT inferior to the bicipital groove to the pectoral tendon, short biceps tendon or at the top of the bicipital groove. In SLAP lesions of the LBT pathologies systematic reviews and meta-analysis show similar functional outcome scores for various techniques (Hurley et al., 2018). In combined pathologies with single superior rotator cuff tears, the biceps tenodesis in combination with rotator cuff repair results in a better outcome than cuff repair with tenotomy. The multitude of applied operational techniques with only minor obvious clinical differences suggest that there is no obvious, superior surgical technique which is reflected in short term clinical investigations (Baumgarten, Chang, and Foley, 2019; Gowd, Beck, and Waterman, 2020; Kerschbaum et al., 2019; Na et al., 2019). Clinical investigations of a LBT surgery have often follow up periods from 6 months to five years, but the biomechanical impact of transposition surgery involving the LBT will be lifelong.

A method to acquire joint forces and moments in order to investigate such procedures or pathologies from a mechanical point of view is by a computational approach. A study with a focus on shoulder injuries conducted by Hölscher computed the acting force on the glenoid by simulation of different tears of the rotator cuff in order to assess instabilities during simulated activities of daily living with repetitive mechanical use. Another application is the simulation of muscle transfers of latissimus dorsi, teres major or a combination of these two to compensate for inoperable massive rotator cuff tears in a simulation environment (Magermans et al., 2004a; Magermans et al., 2004b).

With the presented clinical issue and the utilization of a musculoskeletal model, the second research question introduced in chapter 1 is investigated, whether one surgical technique is superior from a biomechanical point of view.

6.2 Materials & Methods

For this study, the model of the shoulder complex from the AMMR v.2.2.0 beta in conjunction with the shoulder rhythm and the Hill model is employed. Both legs and the left arm are omitted. The default human model with a height of 1.75 m and 75 kg is used for this study.

In order to simulate different surgical techniques of a biceps tendon transplantation, four model configuration are applied. To assess the behaviour of a healthy shoulder and EL complex with regard to joint reaction forces and moments, the unchanged model (ORG) is computed. Hence, the biceps caput longum originating from the scapula and spanning over the humeral head (Figure 6.1 a). A cut of the long biceps tendon with a new insertion on the humeral head is remodelled with an origin 15 mm anterior and 20 mm lateral in the bicipital groove on the humeral head (HH) (Figure 6.1 b). For a transplantation to the tendon of the short biceps, the caput longum is inserted in superposition to the caput breve and originating on the coracoid (CB) (Figure 6.1 c). A complete cut of the caput longum at the tendon without reinsertion is modelled by setting the strength of the virtual muscle element to zero (OFF) and disabling the passive elements of the Hill model. This results in the muscle element not being regarded by the muscle recruitment solver of the software for the biceps caput longum.

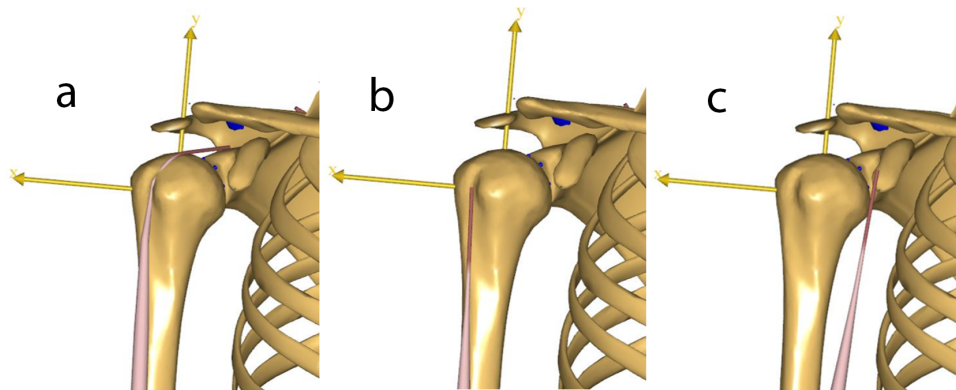


FIGURE 6.1: Different origins of the biceps caput longum a) original model (ORG) b) tendon insertion on the bicipital groove at the humeral head (HH) c) tendon insertion on the coracoid at the origin of the caput breve (CB)

For each of these four configurations, three kinematic tasks are simulated, which incorporate main functionalities of the biceps caput longum: EL flexion, EL pronation and a combination of humeral abduction, rotation and EL pronation in order to approximate a pouring motion. Each task is simulated starting from an initial position moving with constant velocity to an end position, which can be found in Table 6.1.

Motion	Initial position of the model		End position of the model	
	Humerus	Elbow	Humerus	Elbow
EL flexion	10° flexion	5° flexion	10° flexion	125° flexion
	5° abduction	-90° pronation	5° abduction	-90° pronation
	-5° external rotation		-5° external rotation	
EL pronation	10° flexion	90° flexion	10° flexion	90° flexion
	20° abduction	-90° pronation	20° abduction	90° pronation
	-2° external rotation		-2° external rotation	
Pouring	65° flexion	25° flexion	65° flexion	25° flexion
	20° abduction	10° pronation	38° abduction	70° pronation
	-2° external rotation		-32° external rotation	

TABLE 6.1: Overview of the three investigated motions with regard to the kinematics of the humerus and elbow

Each model is provided with a virtual force of 20 N in the palm acting in the direction of the gravity in order to simulate a load bearing case with medium weight. The motion tasks are calculated with the ORG, HH, CB and OFF model configuration. For assessing the impact on the GH joint of the different surgical techniques, the medial-lateral (ML), inferior-superior (IS) and posterior-anterior (PA) forces acting on the glenoid are analysed. For the EL joint, the contemplated forces are the ML component, the proximo-distal (PD) force and the PA force. Furthermore, the acting axial (A) and lateral (L) moment are investigated.

6.3 Results

The different insertion points of the LBT with ORG, HH, CB, and OFF, change the moment arm of the biceps caput longum. This results in a variation of the muscle recruitment of the modelling system, which effects the resulting forces within the GH and EL joint. A comprehensive overview of the results can be found in the appendix. In the following forces with a potential clinical relevance are discussed.

Table 6.2 provides the maximum deviation of the surgical models in comparison to the ORG insertion point of the LBT during each motion task. The OFF model shows the largest deviations from the ORG model for EL flexion and EL pronation. During the pouring motion, the CB model yields the largest divergences in shoulder and EL forces and moments. The HH model exhibits for all three motions the smallest differences to the ORG model.

Model	Δ GH	Δ GH	Δ GH	Δ EL	Δ EL	Δ EL	Δ EL	Δ EL
	MLF[N]	ISF[N]	PAF[N]	MLF[N]	PDF[N]	PAF[N]	AM[Nm]	LM[Nm]
Flexion								
HH	49	26	10	7	19	21	0.2	0.4
CB	51	28	10	18	53	60	0.8	1.4
OFF	50	27	10	19	56	65	0.8	1.5
Pronation								
HH	43	25	15	2	1	9	0.2	0.2
CB	45	25	11	17	8	22	0.9	0.4
OFF	43	25	15	16	18	54	1.5	1.1
Pouring								
HH	6	21	2	3	6	6	0.3	0.4
CB	23	22	17	20	42	41	1.0	1.2
OFF	7	20	2	4	10	11	0.4	0.6

TABLE 6.2: Maximum deviation of the surgical models in comparison to the ORG insertion point of the LBT during each motion task

Figure 6.2 depicts the IS joint reaction force acting on the glenoid for the three contemplated movements. During EL flexion, all surgical models are similar in force magnitude to the ORG model up to 45° with a divergence <5% to the intact model. The differences increase to 30% higher forces at 125° EL flexion from 150 N to 191 N, where all surgical models behave the same in force progression and magnitude.

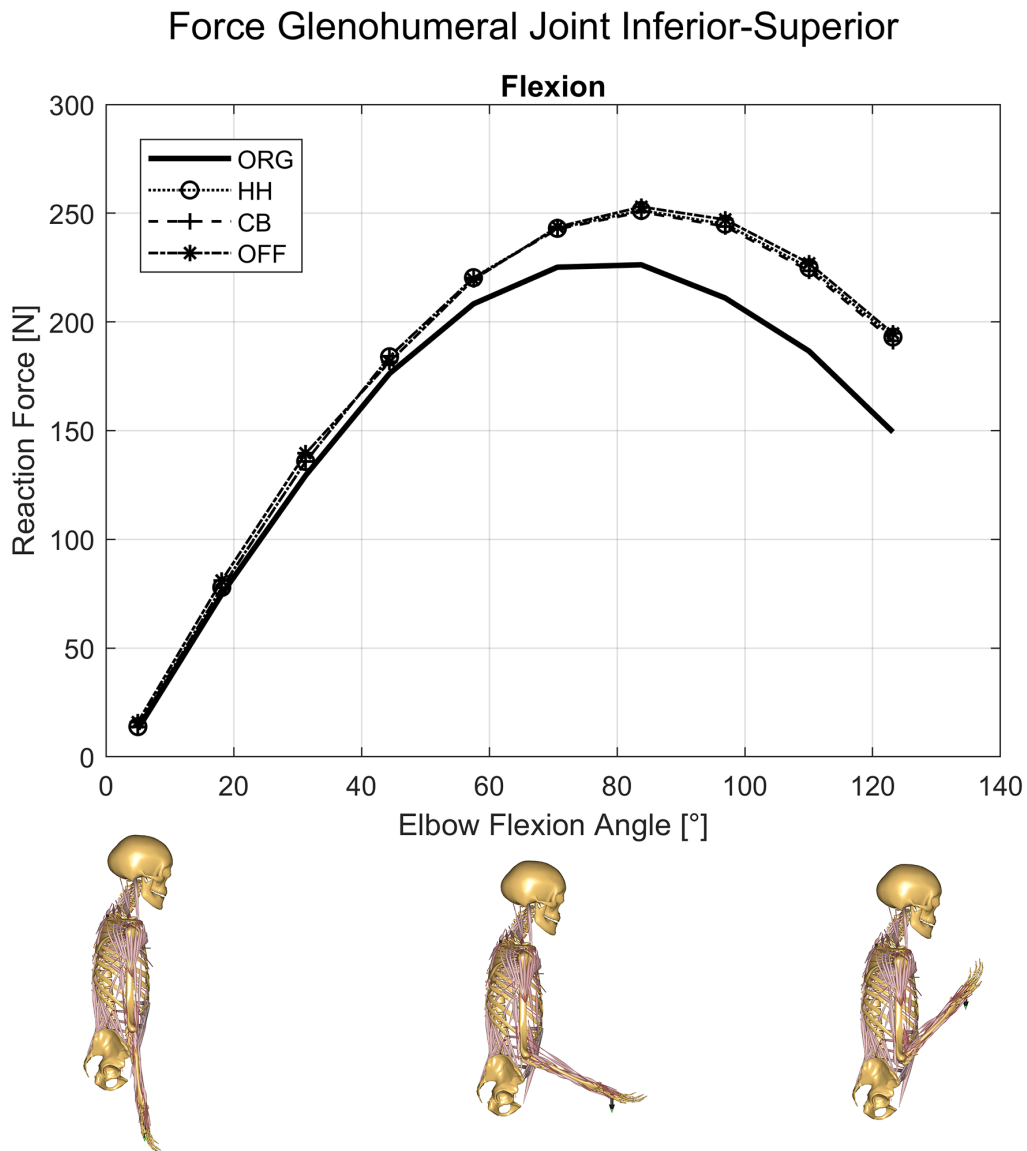


FIGURE 6.2: IS force in the GH joint over the EL flexion angle during flexion for the ORG, HH, CB and OFF model

6.3. Results

During pronation of the EL (Figure 6.3), the reaction forces in the IS direction of the surgical models have the largest deviation from the ORG model at -90° pronation with a divergence of 17% higher forces from 250 N to 290 N. The deviation becomes less than 5% in the range of $60-90^\circ$ pronation.

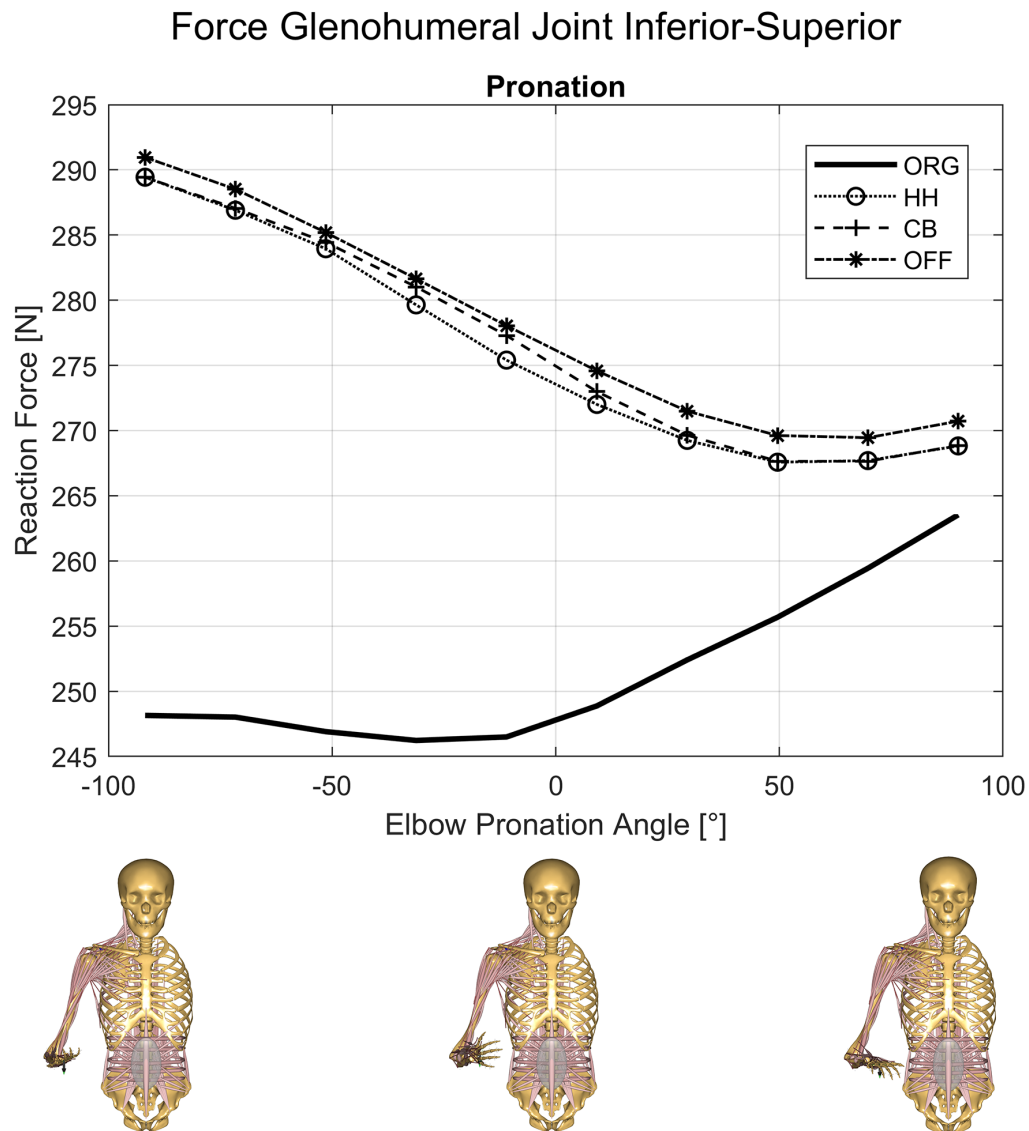


FIGURE 6.3: IS force in the GH joint over the EL pronation angle during pronation for the ORG, HH, CB and OFF model

For the combined motion of approximating a pouring movement involving GH abduction, external rotation and EL pronation (Figure 6.4), the divergence of the CB model is at the beginning of the movement at 8% to the ORG model, whereas the HH and OFF model show deviations of 2%.

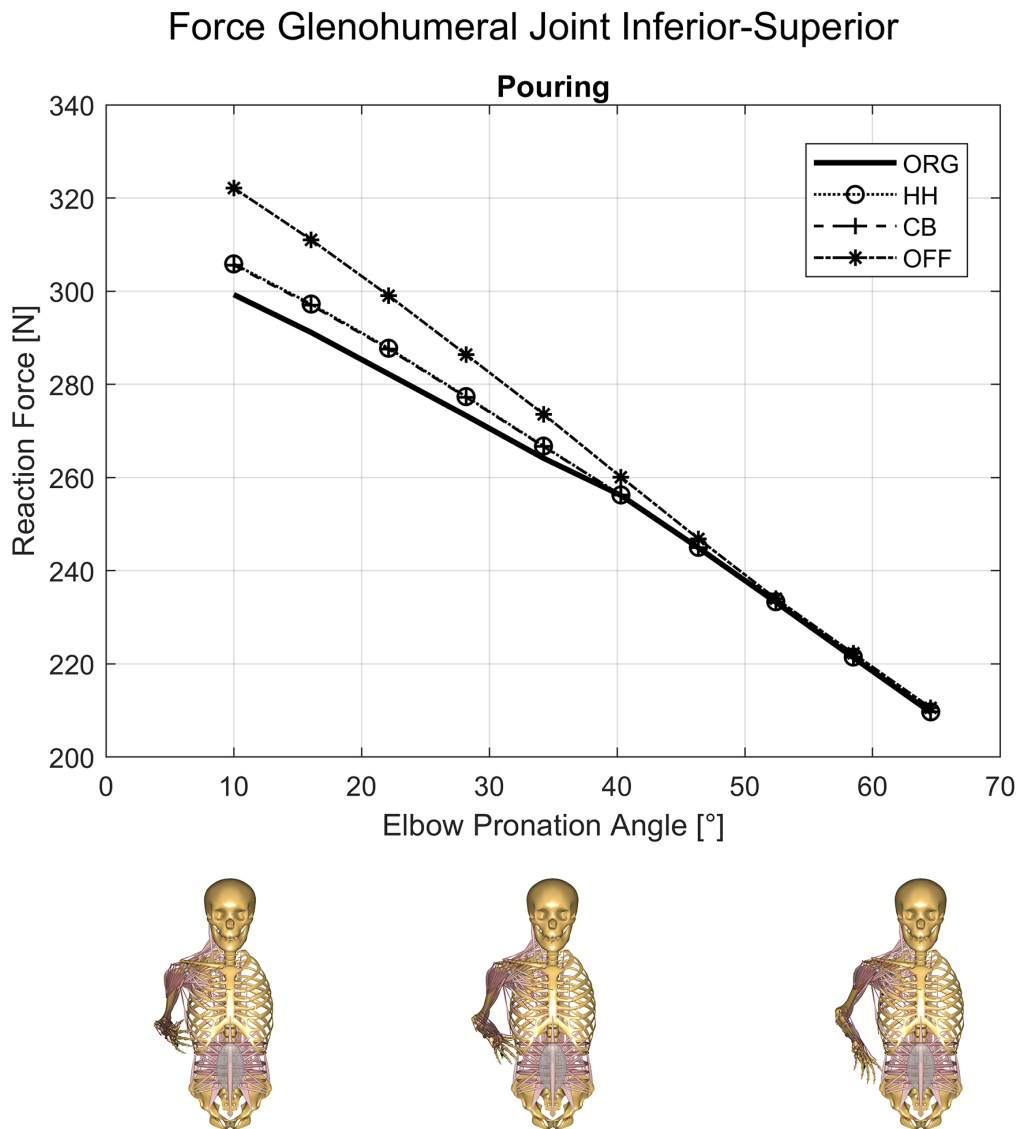


FIGURE 6.4: IS force in the GH joint over the EL pronation angle during the pouring motion for the ORG, HH, CB and OFF model

Figure 6.5 shows the GH joint reaction force originating from the centre of the humeral head projected onto the glenoid plane. Depicted is the largest shift from the ORG model to the surgical models during each motion. This corresponds with Figure 6.3, where at 125° flexion, the joint reaction force of the ORG model is oriented towards the centre of the glenoid. It shifts towards the edge of the virtual glenoid capsule with the increased IS force (magenta arrow). The same can be observed for the models at -90° pronation (green arrow). Only a minor shift occurred for the models during the pouring motion (red arrow).

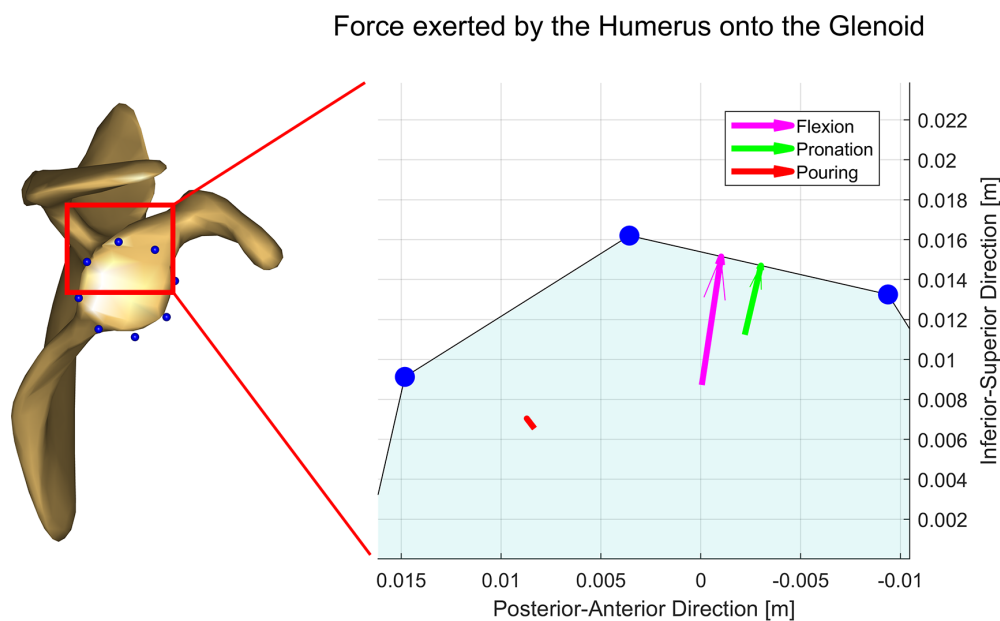


FIGURE 6.5: Representation of the force direction acting on the glenoid, where the arrows indicate the largest shift from the ORG model to the surgical models for flexion (magenta), pronation (green) and pouring (red)

Figure 6.6 depicts the PA force acting on the EL joint during the flexion of the EL. The HH model is closely following the ORG model up to 110° flexion, with a deviation at maximum flexion of 18 N to the ORG model and an opposite trend in force progression. The CB model follows the trend of the ORG model up to 80° flexion, with an opposite trend of an increasing PA force afterwards. The maximum deviation is at the end of the movement with 55 N. The AP force of the OFF model deviates from the ORG model at 70° EL flexion similar to the CB with a peak deviation of 62 N at the largest angle.

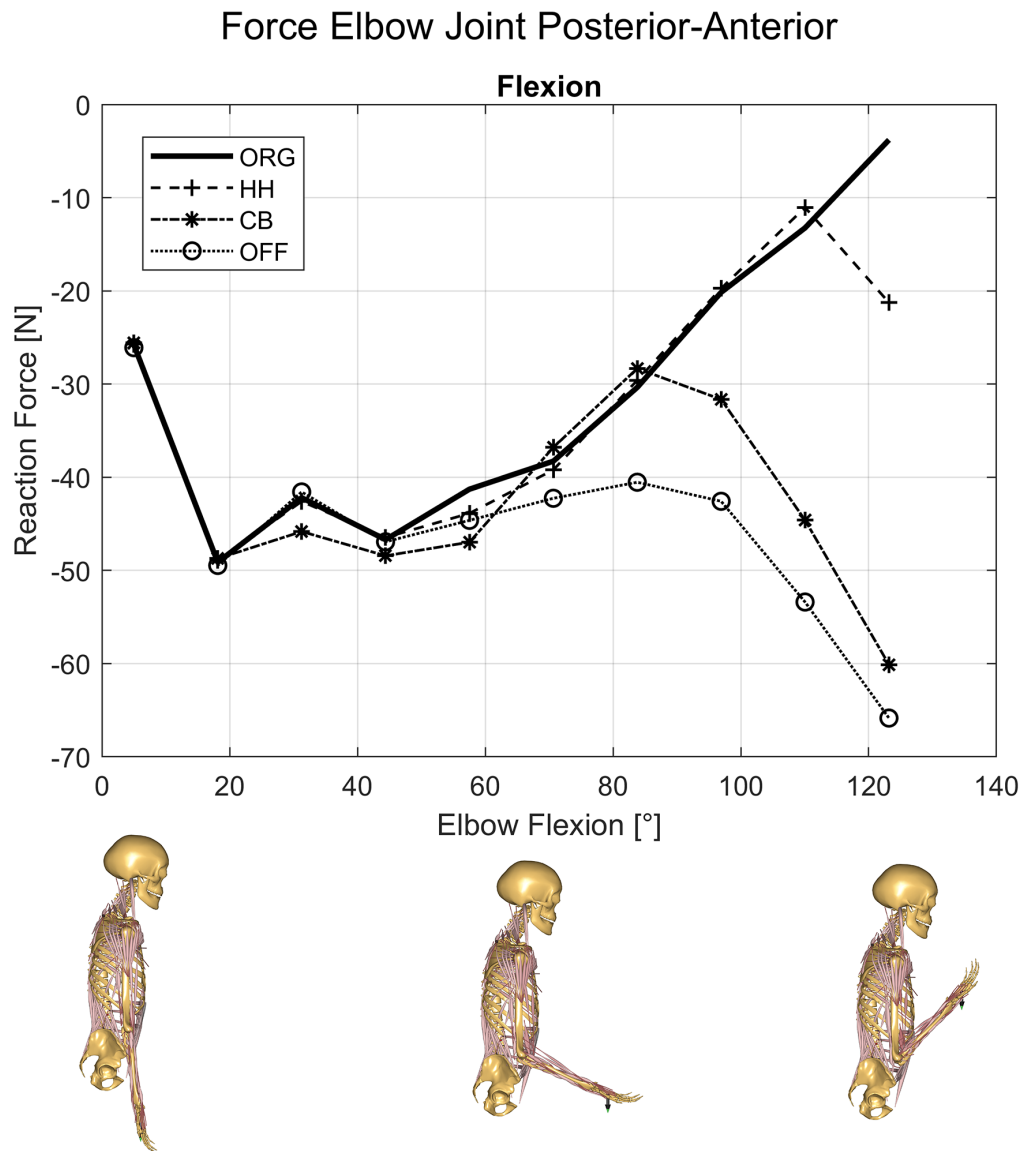


FIGURE 6.6: PA force in the EL joint over the EL flexion angle during the flexion motion for the ORG, HH, CB and OFF model

During pronation (Figure 6.7), the OFF model exhibits the largest divergence from the ORG model in the range between -90° to -10° , with a peak of 52 N higher PA force at -50° . The HH model follows the trend of the ORG model closely, while the CB model shows minor deviations.

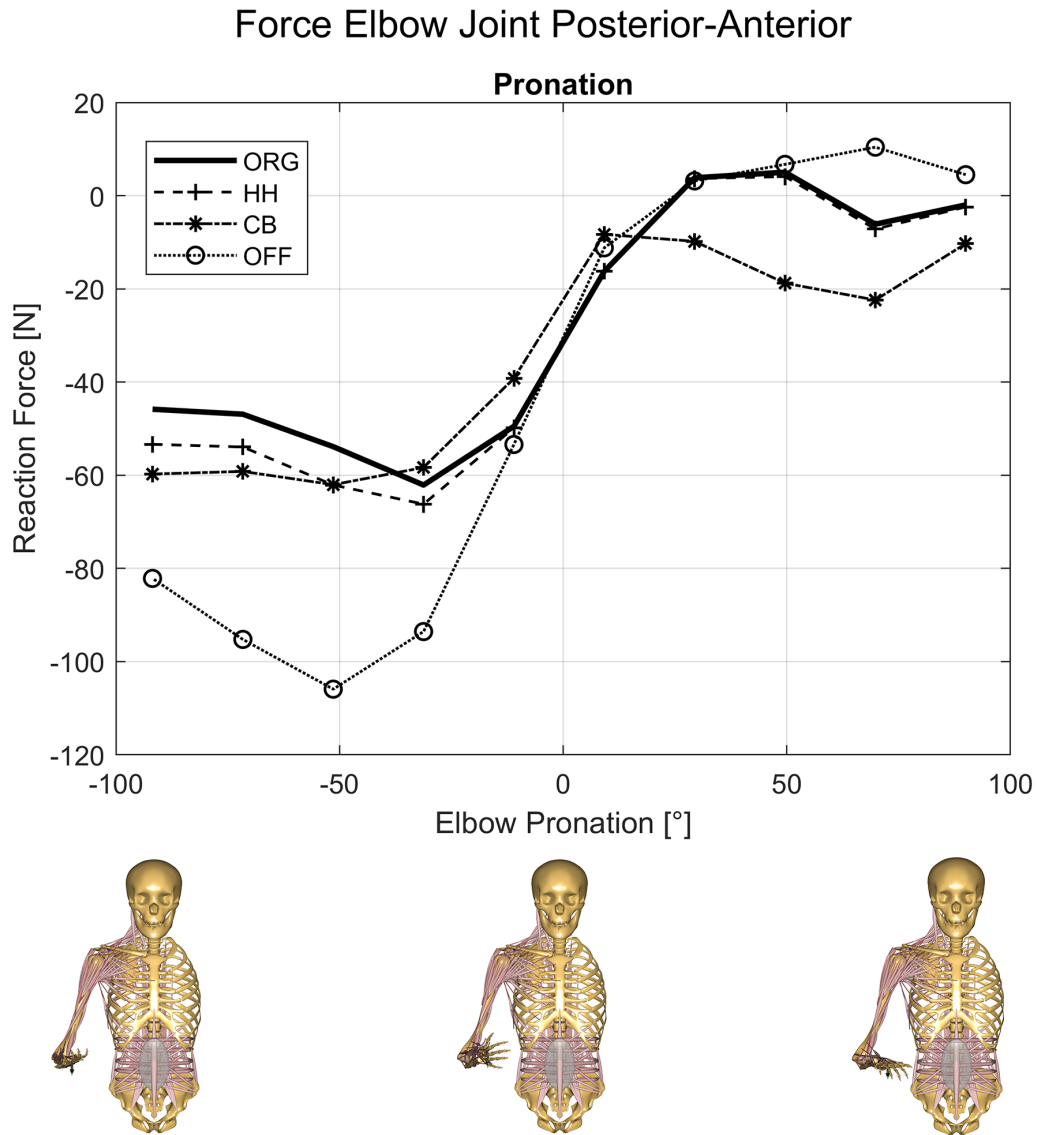


FIGURE 6.7: PA force in the EL joint over the EL pronation angle during the pronation motion for the ORG, HH, CB and OFF model

For the pouring motion (Figure 6.8), the HH and OFF model follow the trend of the intact model, while the CB model starts with a deviation at the beginning of the motion, peaks at 40 N difference at 40° EL pronation and 25 N at the end of the motion.

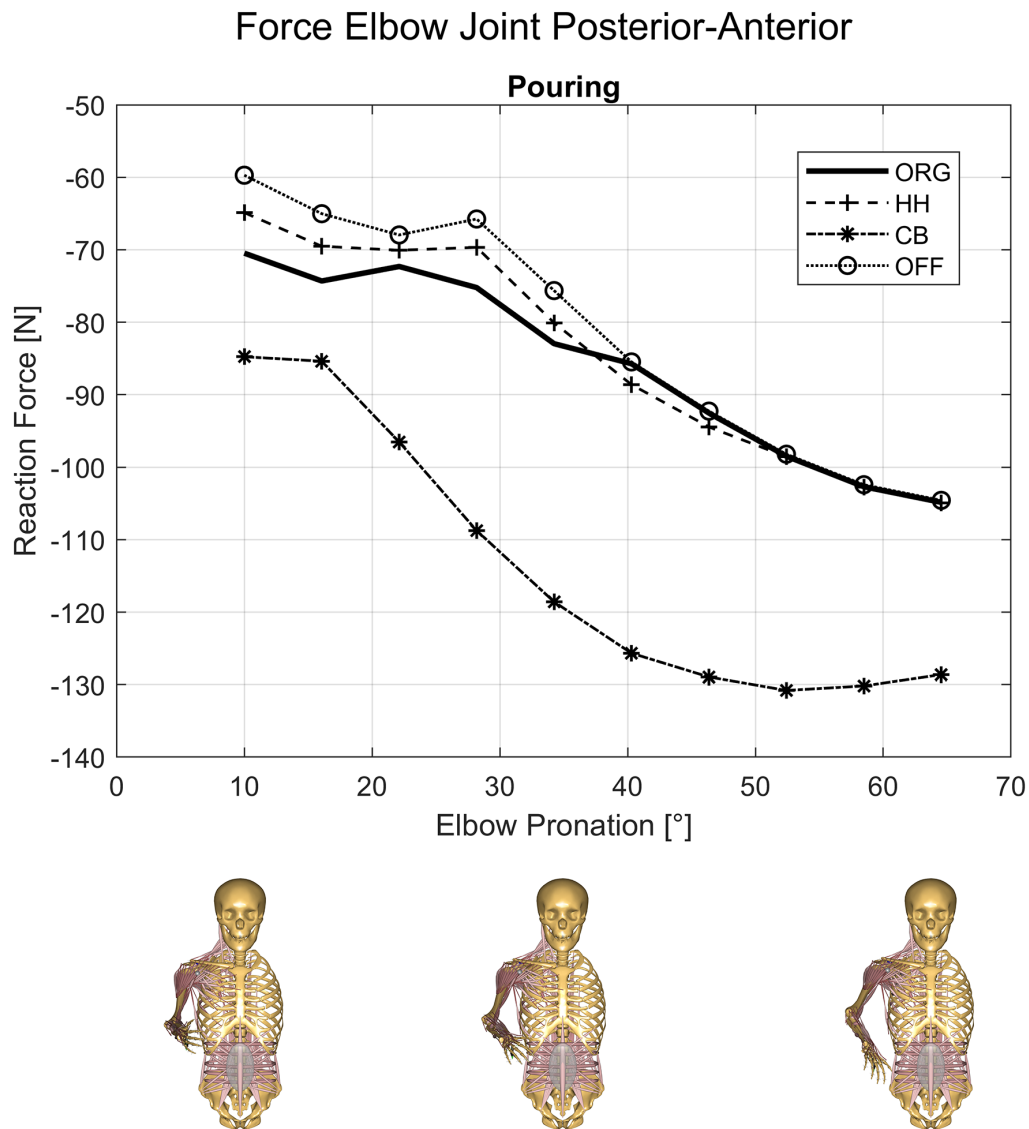


FIGURE 6.8: PA force in the EL joint over the EL pronation angle during the pouring motion for the ORG, HH, CB and OFF model

6.4 Discussion

The results from the computational study suggest that a tenodesis of the LBT at the bicipital groove is showing the least divergence in forces and moments with regard to an intact biceps, as the direction of the moment arm of the LBT is preserved. This would be in line with an assessment of Scapinelli et al., 1999, which concluded the reinsertion of the LBT at the bicipital groove as the method of choice. The LBT is spanning over the GH and the EL joints. Surgery to the LBT, which changes the mechanics and muscle recruitment results in an impact to the joint reaction force to the GH as well as the EL joint.

The GH joint reaction forces show almost no difference between the modelled pathologies. All diverge from the original model configuration in the IS direction, as with all modelled surgical techniques, the biceps tendon is no longer spanning over the humeral head. This computed result is contradictory to an experimental study from Soslowky, Malicky, and Blasier, 1997, where they hypothesized that there would be no depression of the humeral head from the biceps tendon, which is contradictory to other studies which describe a depression of the humeral head from the biceps (Halder et al., 2001; Warner and McMahon, 1995) However, these studies all argue for the caput longum being a major stabilizer next to the m. supraspinatus and m. infraspinatus. This agrees with this study as higher shear forces implicate less stability.

The higher forces occurring in the IS direction of the analysed procedures (Figure 6.5) can be interpreted as an increased pressure of the humeral head onto the glenoid cavity. This is an indication of a more unstable configuration of the shoulder for all surgical techniques as shear forces increase while the compression component decreases. In higher abduction angles of the humerus, which is exemplified by the pouring motion, more muscles in the shoulder act together in order to conduct the given motion. Thus, the influence of the biceps becomes less prevalent and only results in minor changes of the contact between humerus and glenoid. This indicates that the shoulder is less stable during motion where the biceps caput longum is the main active muscle.

Considering the forces acting on the EL joint, the difference in the contemplated surgical techniques becomes more distinct as less muscles are spanning the EL joint with the biceps caput longum being one of the strongest. Where both the OFF and CB model show considerable deviations from the ORG model in flexion, pronation and the pouring motion, the HH model always follows closest in trend and magnitude to the ORG model for all forces and moments (see Table 6.2 & B). While the line of action of the biceps caput longum is almost the same with the HH technique in comparison to the ORG model, omitting the biceps or placing the origin on the coracoid results in a different pulling direction. This is most prevalent in the PA force direction of the EL joint, where higher shear forces on the joint occur. However, to the best of my knowledge, no study reported long-term issues in the elbow joint after a tenodesis to the coracoid. In contrary, Gumina et al., 2011 reported good outcomes and restored functionality in long term behaviour after reinsertion of the LBT at the coracoid. This might be due to the simplification of the biceps caput longum spanning in a straight line from origin to insertion to the coracoid for a tendodesis at this point. In reality the moment arm is most likely oriented more lateral, thus producing less shear forces in the elbow joint. Inserting the tendon origin of the LBT on the origin point of the caput breve has the limitation that two lines of action are superimposed. This is a limitation as the model does not account for muscle bulging and might not reflect the in-vivo moment arm accurately. In the in-vivo case, the muscle volumes would push each other apart, resulting in two different lines of action and thus muscle recruitment of the system. This in turn affects the calculated joint reaction forces. Another limitation is that the model does not regard a difference in pretension of the virtual muscle elements, which might occur after a tenodesis influencing the muscular recruitment pattern.

The modelled outcome of the tenotomy, which exhibited the largest shear forces on the EL joint supports the assessment, that instabilities in the elbow occur in patients with a released or untreated tear of the biceps caput longum (Mariani et al., 1988). This is due to the increased activity of the biceps caput breve and no stabilization of the caput longum, which would generate a torque in the opposite direction.

While musculoskeletal models yield the possibility to allow insights into the acting forces on the joints, absolute values should be treated with care as these models are still under development and are constant subject of optimization. However, the assertion that inserting the origin of the LBT at the bicipital groove will produce forces and moments within the EL joint more similar to that of a healthy case should hold true as the moment arm is oriented in the same direction. From a mechanical point of view, this surgical technique thus could be superior.

6.5 Conclusion

The outcome of this study with regard to the second research question addressed in chapter 1 indicates, that a reinsertion of the LBT at the bicipital groove is closest to the case of an intact LBT from a biomechanical point of view and superior to a release of the tendon or a reinsertion at the coracoid. In SLAP lesions and rotator cuff tears preserving the LBT entirely might be beneficial as it provides stability for the GH joint in movements where the biceps is the main active muscle.

Chapter 7

The effect of tears of the m. supraspinatus on the forces and muscle activation pattern of the shoulder complex

Chapters 4 and 5 are focused on modelling parameters, alterations and validation of a musculoskeletal model of the shoulder complex with a focus on humeral abduction. The following chapter uses the presented essential modelling aspects of chapter 5 as it's basis for the computation of a tear of the m. supraspinatus.

7.1 Introduction

As stated in chapter 1, lesions of the rotator cuff and especially the m. supraspinatus are musculoskeletal disorders which affect millions of people world wide. With the risk of the development of these pathologies growing due to age (Yamamoto et al., 2010; Minagawa et al., 2013) and the increasing global life expectancy (World Health Organization, 2016), these conditions will likely become even more prevalent.

The importance and mechanical role of the m. supraspinatus in abduction motions has been described as an abductor (Howell et al., 1986) and humeral head compressor (Wuelker et al., 1994b).

Wuelker et al., 1994b conducted a cadaver study and applied forces with hydrodynamic cylinders to the rotator cuff and deltoid muscles and concluded that the m. supraspinatus creates mainly a compression force and produces less torque than the deltoids.

What cadaver studies using mechanically applied forces to simulate muscles do not account for however is the active force a muscle can produce depending on its elongation. While it is difficult to acquire the necessary parameters for an accurate modelling of the force-length relation (Rassier, MacIntosh, and Herzog, 1999), chapters 4 and 5 have demonstrated the importance of respecting these properties for assessing shoulder force behaviour and muscle activation.

Using the assumption that a model is adequately incorporating the most necessary muscle parameters and kinematics of the involved bony structures, the musculoskeletal simulation approach might provide better insights for some research questions opposed to a cadaver study.

Steenbrink et al., 2009 simulated among other rotator cuff tear combinations an isolated tear of the m. supraspinatus which exhibited a posterior-superior point of attack of the resultant force vector on the glenoid. The study analysed a static position (79° elevation plane, 46° elevation, 31° external rotation, 90° elbow flexion) and concluded, that a tear of the m. supraspinatus does not necessarily introduce instability of the joint but increases deltoid loading. As a modelling basis they used the Delft shoulder model. Vidt et al., 2018 simulated a tear of the m. supraspinatus with the shoulder model from the OpenSim software and simulated patient specific pull and axilla wash tasks and concluded, that a tear of the m. supraspinatus causes lower peak forces with a smaller component of the compressive force. Steenbrink et al., 2010 have shown experimentally (EMG) and numerically, that the deltoid compensates for a loss of m. supraspinatus and m. infraspinatus while adductor muscles activate in order to stabilize the joint. However, their study highlighted a high variability of patients applying different combinations of adductor 'out-of-phase' contractions.

Common clinical initial tests for a tear of the m. supraspinatus that involve kinematics of patients are the full can and empty can test, which are conventionally conducted in the scapula plane. At 90° humeral abduction in the scapula plane, the patient exerts an upward force against resistance provided by the clinician, where weakness or pain are indicators of a rotator cuff tear. Conducting these tests in the coronal plane have shown to exhibit equal or better results in terms of sensitivity (Gillooly, Chidambaram, and Mok, 2010).

EMG based studies of these tests argue for a better selectivity of the full can test with the humerus rotated externally. These are based on the middle m. deltoideus and m. subscapularis exhibiting less activity, so the m. supraspinatus is exerted more in isolation (Lee et al., 2014). Furthermore, the m. supraspinatus seems to exhibit comparable levels of activation in both internal (empty can) and external (full can) rotation (Reinold et al., 2007a), and the empty can test causes more pain to the patients (Itoi et al., 1999; Timmons et al., 2016).

Hölscher et al., 2016b have analysed static positions, with the AMS and the via point deltoid model, which reflect the full and empty can test and compared the forces acting on the glenoid between intact models and simulated tears of various rotator cuff muscles. In agreement with the aforementioned studies, forces acting on the glenoid tended to point towards the edges of the glenoid indicating less stability.

To the best of my knowledge, a detailed description of muscle activities and potential changes in recruitment during a large ROM has not been conducted yet.

To the best of my knowledge, a simulation of kinematics reflecting the empty and full can test between healthy and pathological models in conjunction with EMG measurements of a wider ROM has not been done yet.

The aim of this section is to compute a change in muscle recruitment between a healthy control group and a patient group with tears of the m. supraspinatus during motions which is reflect by the empty and full can test during abduction in the coronal plane.

By combining the ability of musculoskeletal models to reflect muscle activation patterns to a certain degree could allow for models pointing towards new regions of interest. A change in the computed recruitment might be comparable to a change in EMG measurements taken from patients with a tear of the m. supraspinatus in comparison to a healthy control group. For this purpose, this study uses experimentally derived input for the updated model of chapter 5.

Additionally, an alternative approach for EMG normalization without conducting MVC measurements is explored within the framework of this study due to two reasons which occurred during a pre-study:

1. MVC measurements might cause pain to patients with symptomatic rotator cuff tears and might cause them to exert a lower force than otherwise expected
2. MVC measurements are extremely time consuming which potentially limits their use in clinical practice

7.2 Materials and Methods

7.2.1 Experimental setup

For assessing the effects of a tear of the m. supraspinatus with regard to changes in muscle recruitment and forces acting on the GH joint, a healthy cohort and a pathological cohort are compared to each other. The benchmark cohort consists of 19 healthy volunteers ($weight = 67.9 \pm 12.0\text{kg}$, $height = 1.74 \pm 0.08\text{m}$, $age = 24.4 \pm 8.5\text{years}$). The pathological group is recruited by a clinician and contains 8 patients ($weight = 83.3 \pm 13.6\text{kg}$, $height = 1.75 \pm 0.05\text{m}$, $age = 57.9 \pm 14.7\text{years}$) with attested tears of the m. supraspinatus muscle.

Each subject performed 6 different humeral abduction tasks in the coronal plane up to their respective maximum range of motion:

1. **Neutral position:** Humeral abduction from a default position with the palm of the hand oriented medial
2. **Neutral position (5 N):** Humeral abduction from a default position with the palm of the hand oriented medial with holding a dumbbell of 0.5 kg \approx 5 N
3. **Internal rotation:** Humeral abduction with internal rotation of the humerus, palm oriented lateral with the elbow joint axis vertical to the coronal plane
4. **Internal rotation (5 N):** Humeral abduction with internal rotation of the humerus, palm oriented lateral with the elbow joint axis vertical to the coronal plane with holding a dumbbell of 0.5 kg \approx 5 N
5. **External rotation:** Humeral abduction with external rotation of the humerus, palm oriented anterior with the elbow joint axis in the coronal plane
6. **External rotation (5 N):** Humeral abduction with external rotation of the humerus, palm oriented anterior with the elbow joint axis in the coronal plane with holding a dumbbell of 0.5 kg \approx 5 N

7.2. Materials and Methods

Subjects were instructed verbally and visually by an operator mimicking the movement in front of them to conduct the required motion accordingly. The kinematics were measured analogous to the study conducted in section 4.2.1. The electromyographic activities of 14 muscles were recorded with surface EMG sensors (Delsys Trigno IM, Delsys® Inc., MA, US.) during the six motion tasks. The recorded muscles and their location is provided by Table 7.1 and Figure 7.1.

Muscle Sensor No.	Trapezius pars descendens 1	Trapezius pars transversa 2	Trapezius pars ascendens 3
Muscle Sensor No.	Deltoideus pars clavicularis 4	Deltoideus pars acromialis 5	Deltoideus pars spinalis 6
Muscle Sensor No.	Infraspinatus 7	Serratus anterior 8	Latissimus dorsi 9
Muscle Sensor No.	Biceps brachii 10	Triceps brachii 11	Rhomboideus minor 12
Muscle Sensor No.	Rhomboideus major 13	Pectoralis major 14	

TABLE 7.1: Contemplated muscles and their respective EMG sensor number of the experimental setup (see Figure 7.1 for a graphical representation).

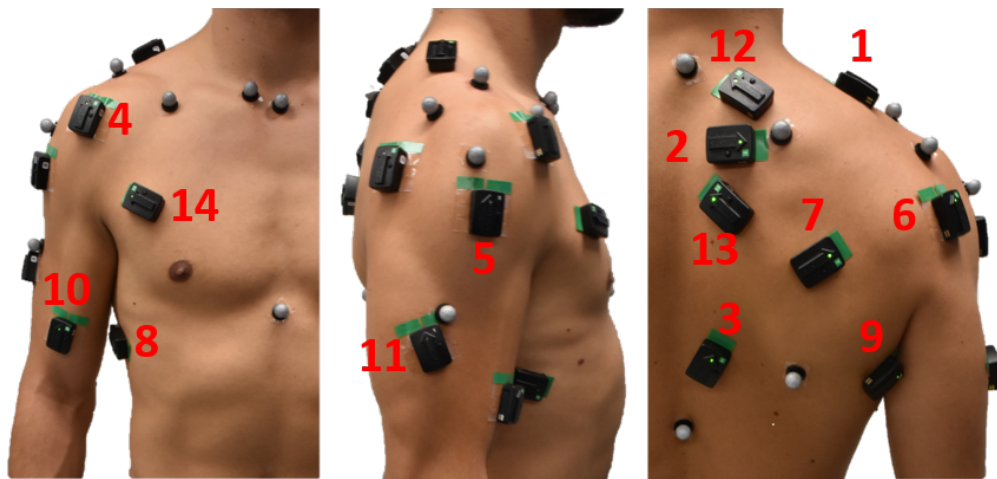


FIGURE 7.1: EMG sensor placement of the 14 contemplated muscles of interest on a healthy test subject.

EMG sensors are placed according to Barbero, Merletti, and Rainoldi, 2012 and Criswell and Cram, 2011. In contrast to the EMG data sets computed in chapter 4 and chapter 5, it is refrained from conducting MVC measurements in order to be considerate with potential pain of the pathological subjects and to satisfy the requirement of a minimal system which is suitable for a fast assessment.

The experiments were conducted by student assistants after a detailed briefing.

7.2.2 Musculoskeletal computation of intact models and a simulated tear of the m. supraspinatus

The model configuration with the implemented tori (ALLFM) and a polynomial power of 5 for the muscle recruitment is used for all the subjects from the benchmark and pathological cohort (see chapter 5). In order to simulate a tear of the m. supraspinatus and to assess changes of the recruitment pattern and joint reaction forces, the computation is divided in three subgroups:

1. Intact models of the healthy group: These models provide a baseline on how the muscle recruitment and resulting joint reaction forces behave in a healthy cohort with an intact model.
2. Pathological models of the healthy group: By exclusion of the m. supraspinatus but with the exact same underlying kinematics, this model group shows the difference in muscle activation and joint reaction forces if all other parameters of the model are kept the same.
3. Pathological models of the pathological group: The models of the pathological group take into account a tear of the m. supraspinatus and potential alterations in the kinematics conducted by the patients.

Pathological models are simulated by exclusion of the six virtual muscle elements of the m. supraspinatus muscle group. Models are scaled to the respective anthropometrics and weight of the measured subjects, segment motion optimized by the marker trajectories and an external python script controls the input parameters and automatization (see chapter 3). Simulations are computed with the kinematic input of the six motion capture trials. The subgroup of the intact and pathological models of the healthy group hereby inhibit the same kinematics and differ only in the exclusion of the m. supraspinatus within the simulation.

Muscle activities and GH joint reaction forces are compared with the intact and pathological models of the healthy group and the intact models of the healthy group to the pathological models of the pathological group in the abduction range 25-85° and computed in 5° increments. For the comparison between the healthy and pathological models, 18 muscle groups are considered: *anterior deltoid, lateral deltoid, posterior deltoid, infraspinatus, subscapularis, teres major, teres minor, trapezius descendens, trapezius transversus, trapezius ascendens, serratus anterior, latissimus dorsi, biceps brachii, triceps brachii, pectoralis major, pectoralis minor, rhomboideus major, rhomboideus minor*.

The three components of the joint reaction force acting on the glenoid are compared independently and a resultant shift of the force vector is visualized by projection on the glenoid interface. The forces are expressed within a fixed coordinate frame moving with the scapula which is depicted in Figure 7.2, where the Y direction of the coordinate system is referred to from inferior to superior, the Z anterior to posterior and the negative X direction as compression force.

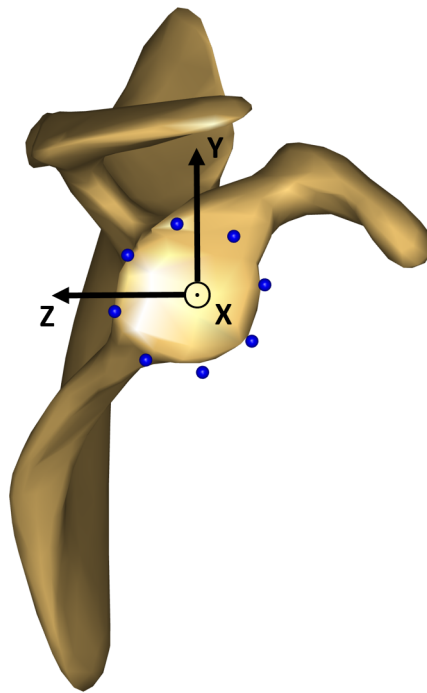


FIGURE 7.2: Scapula segment with the simulated glenoid (blue dots) and the coordinate system in which the forces acting on the glenoid are expressed. The Y direction of the coordinate system is referred to from inferior to superior, the Z anterior to posterior and the negative X direction as compression force.

As each muscle group is represented by several elements within the model, an envelope is created where for each step in the computation the maximum muscle activity of the grouped muscle elements is computed. The discretization of the musculoskeletal computation is set to 50 for the time dependent motion capture trials. Each parameter of interest is interpolated with a cubic spline over the respective abduction angle. The parameters are resampled over a uniform abduction vector in the range of 25-85° with 5° increments.

As the sample size of the pathological group is small and an initial testing for normal distribution of the parameters of interest was found to be negative, the Mann–Whitney U test (Wilcoxon rank-sum test) is taken as statistical tool for the comparison between the healthy and pathological group by providing the level of significance. The differences in the median and the Mann–Whitney U test are computed between all parameters of interest (muscle activities and joint reaction forces) for each 5° increment of the intact versus the pathological models of the healthy group and the intact models of the healthy group versus the pathological models of the pathological group. For the latter case, the difference in humeral flexion and external rotation is also computed as the kinematics are from two different groups and might differ.

7.2.3 Electromyographic comparison of healthy and pathological subjects

The mean from each EMG sensor in every trial is subtracted in order to compensate for the sensor offset. In order to de-noise the EMG signal, a wavelet approach is used. As a mother wavelet, the Daubechies 7 (db7) with a 4-level decomposition is chosen (Mahaphonchaikul et al., 2010; Phinyomark, Limsakul, and Phukpattaranont, 2011), where the level of interest is the D3 (Wang et al., 2014). The RMS of each de-noised signal is computed with a window size of 500ms as the movements are conducted with a low angular velocity of the humerus. As the measurement from the EMG sensors and the motion capture data are synchronized, they share the same relative time axis but with different sample frequencies (0.2 and 1.1 kHz, respectively). For each trial, the RMS is interpolated with a cubic spline over its respective time and computed over the time axis of the associated model and smoothed with the rloess method. A second interpolation is conducted analogous to section 7.2.2 where the model time dependent RMS signals are computed over the angle of abduction in 5° increments from 25-85°. Each of these filtered and interpolated signals is normalized to its magnitude at the 85° position of the neutral position trial with load in hand. Figure 7.3 illustrates the different steps in computation of the respective EMG signals. The same method of the model based approach (see section 7.2.2) for the analysis and comparison of the two groups is applied to the processed EMG signals, where the differences between the medians and the Mann–Whitney U test of the healthy and the pathological subjects are computed.

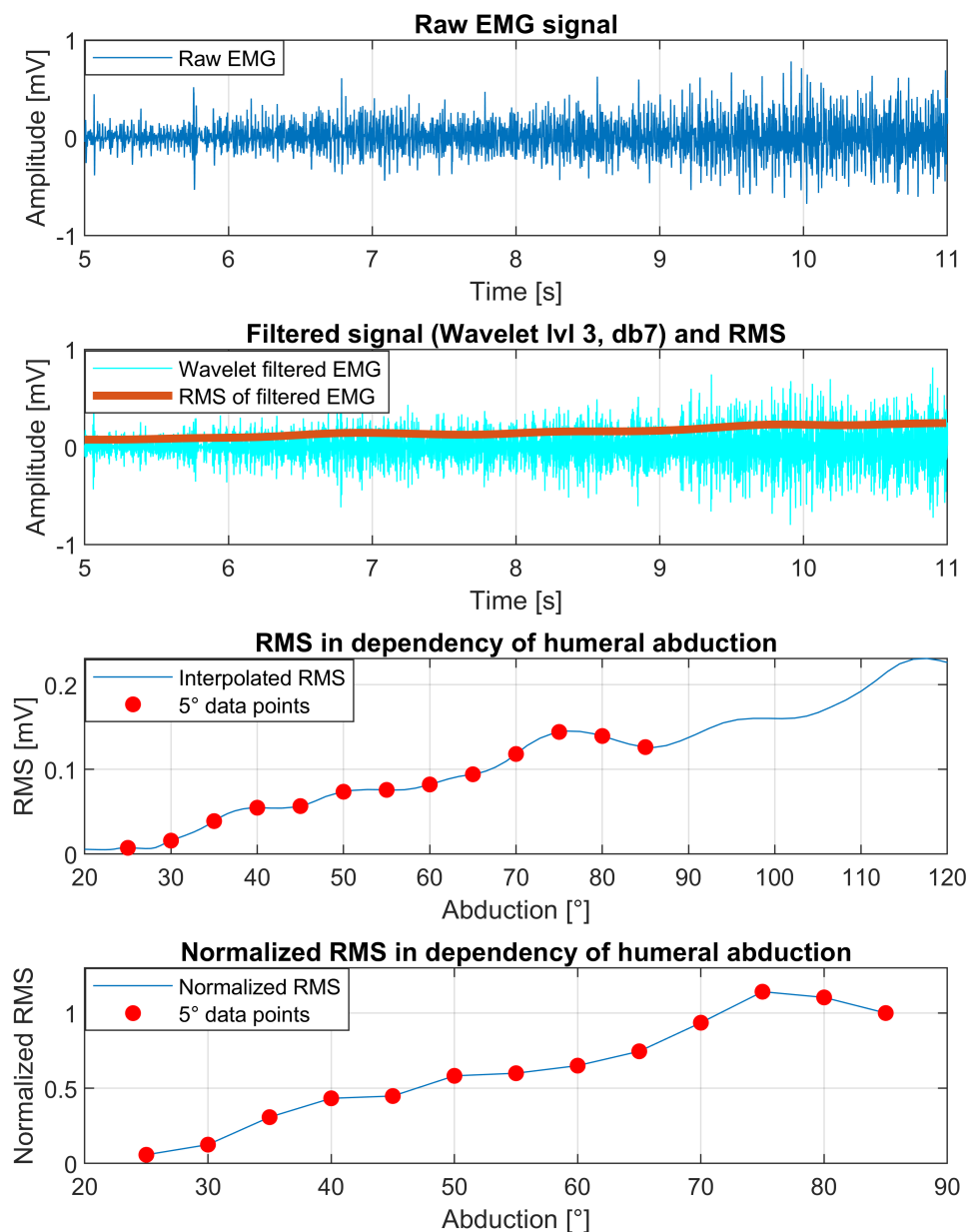


FIGURE 7.3: EMG computation steps of the middle deltoid of one subject during neutral position (5 N) trial. Top: raw EMG signal (blue). Second: wavelet de-noised signal (cyan), RMS of the loess smoothed wavelet signal (orange). Third: RMS interpolated over abduction angle from MoCap model (blue) and computed for 5° increments (red dot). Fourth: normalized signal (blue) and 5° increments (red dots) to the 85° position.

7.3 Results

The main results from the modelled effects of a tear of the m. supraspinatus and the EMG based analysis are presented in this section, but only a selection of the major findings is provided in detail. All computed parameters are provided in appendix C.

7.3.1 Musculoskeletal computation of intact models and a simulated tear of the supraspinatus: Healthy subjects group with intact vs. pathological models

From the 20 different data sets for each motion, the kinematic marker based optimization converged for 19 trials in the neutral position, 18 trials in the neutral position with 5 N, 19 trials for internal rotation, 18 trials for internal rotation with weight, 19 trials of the external rotation and 19 trials for the external rotation with weight. Disabling the m. supraspinatus did not cause model failure, thus the number of compared intact models to pathological ones is the same and yields the same kinematics.

Figures 7.4 & 7.5 show the simulated activity of the m. supraspinatus of the intact models of the healthy subject group. The peak median activities for the trials without a simulated weight range between 8-9% activity. The median of trials with an applied load peak at 13% activity. Where the peak median forces behave similar between the 6 different trials, the behaviour over the abduction angle differs between the neutrals position, internal and external rotation trials. A large variance is found for the m. supraspinatus activity over all angles.

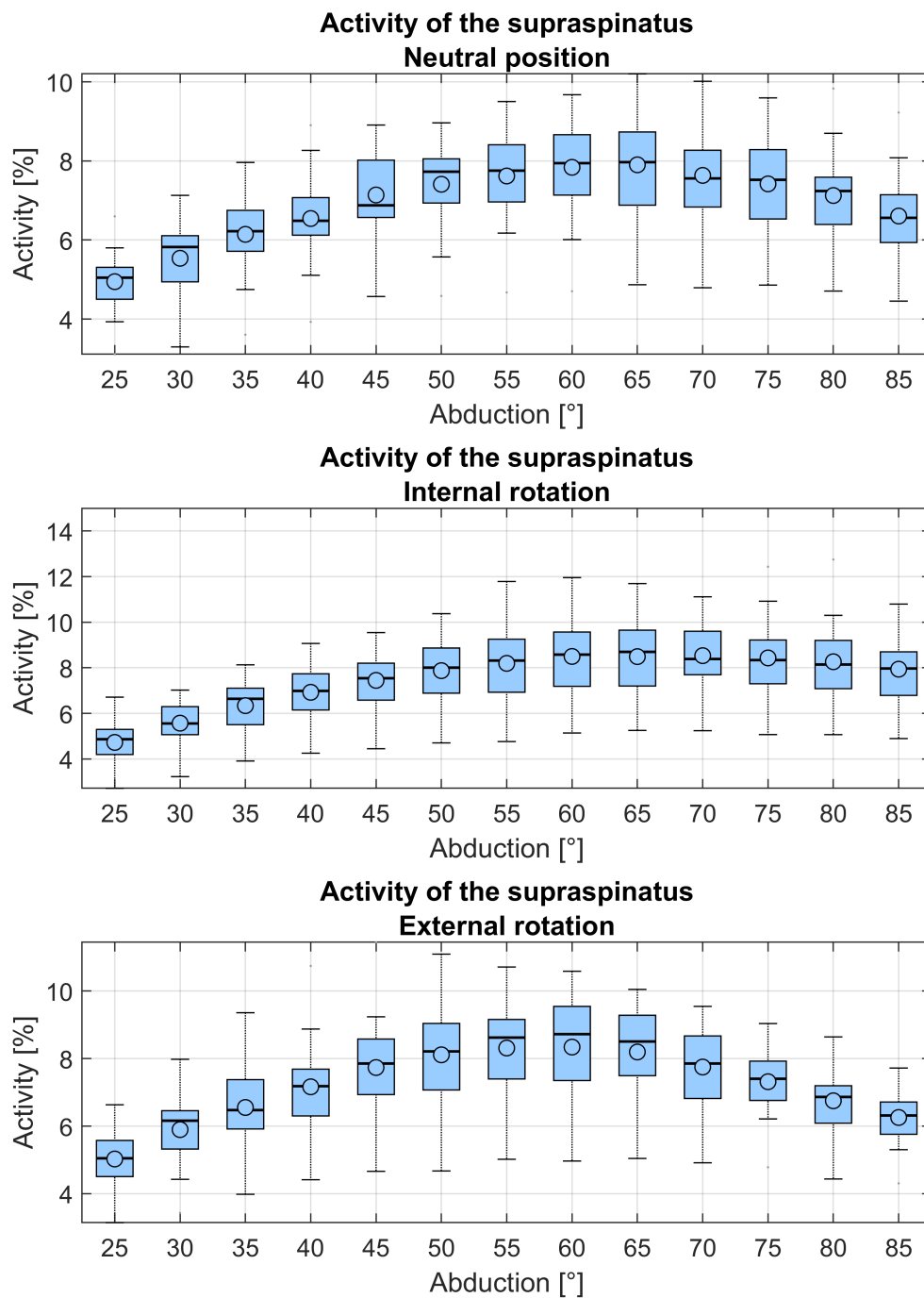


FIGURE 7.4: Activities of the m. supraspinatus computed by the models of the healthy control group over the abduction angle in 5° increments. Activities are from the neutral position, internal rotation and external rotation trials without weight.

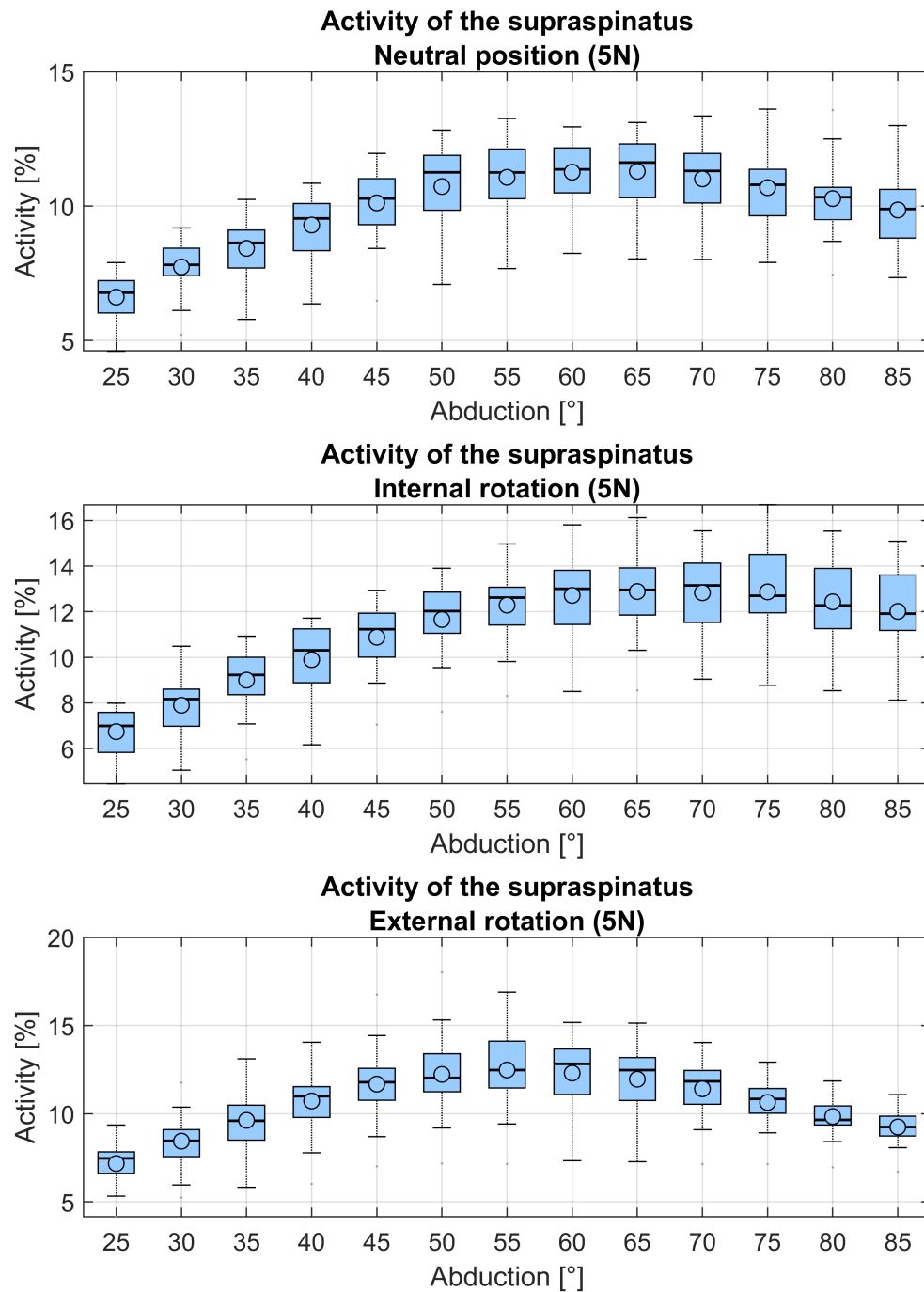


FIGURE 7.5: Activities of the m. supraspinatus computed by the models of the healthy control group over the abduction angle in 5° increments. Activities are from the neutral position, internal rotation and external rotation trials with 5 N load in hand.

The comparison between intact models and a simulated tear of the m. supraspinatus did not show any differences in the activation of trapezius descendens / transversa / ascendens, serratus anterior, latissimus, rhomboideus minor / major, teres major and pectoralis minor elements. Teres major, latissimus, pectoralis minor and rhomboideus minor elements did not exhibit a consistent or notable activation in all trials, where some outliers occurred.

The evaluated parameters for the case of an internal rotation with an applied load of 5 N in hand are depicted in detail in this section, as they exemplify the most notable differences on the muscle recruitment and thus GH joint reaction force.

Figures 7.6, 7.7 and 7.8 depict the muscle activities over the 5° humeral abduction increments of the intact and pathological models of the internal rotation trial with a load of 5 N. As with the activity of the m. supraspinatus, a large distribution in the muscle activities occurs in all trials between different subjects.

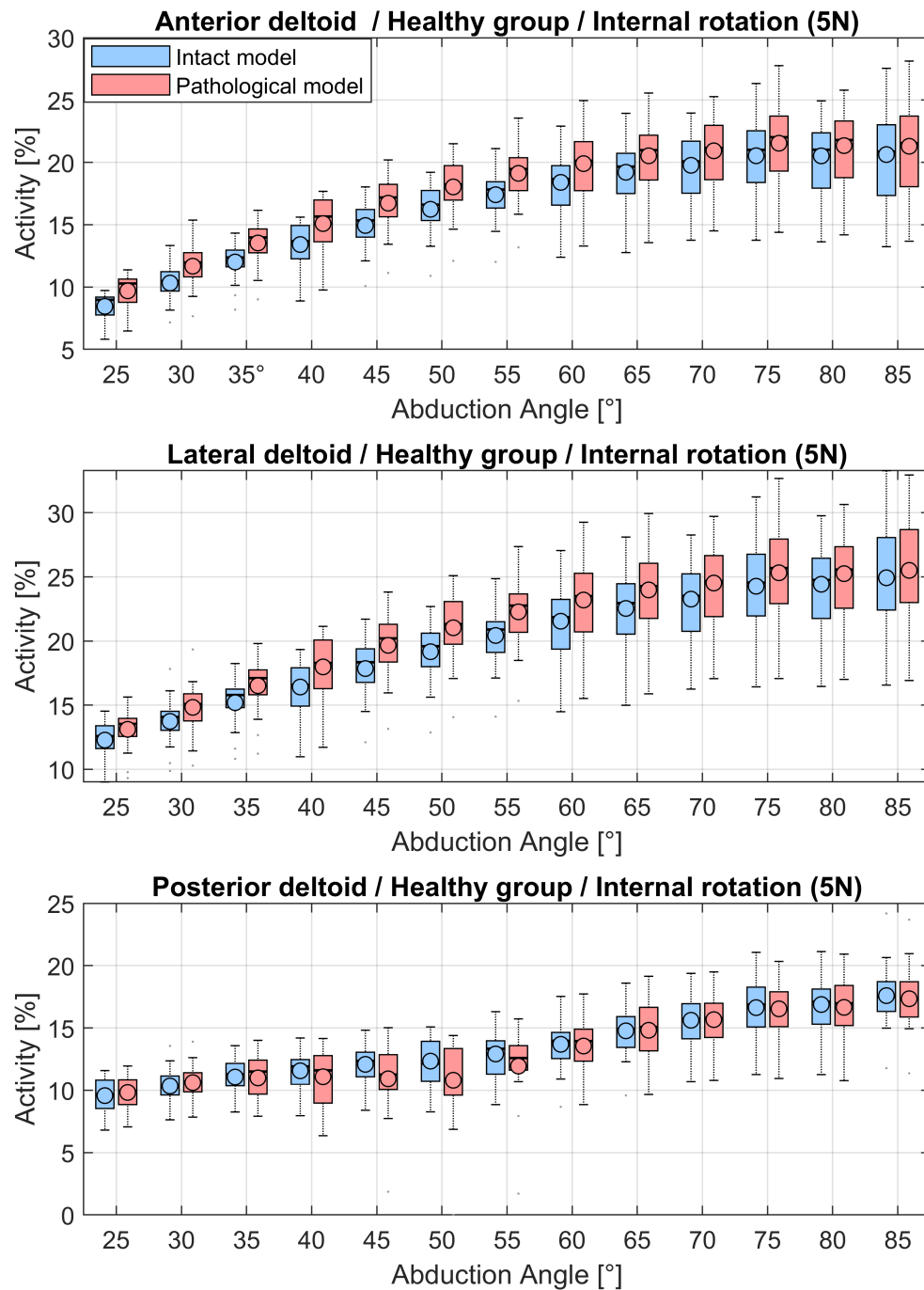


FIGURE 7.6: Computed muscle activities of the anterior, posterior and lateral deltoids over the abduction angle in 5° increments during the internal rotation trial with 5 N load in hand. Blue depicts the activities of the intact model and red the modelled tear of the m. supraspinatus. Blue depicts the activities of the intact model and red the modelled tear of the m. supraspinatus of the healthy subject cohort.

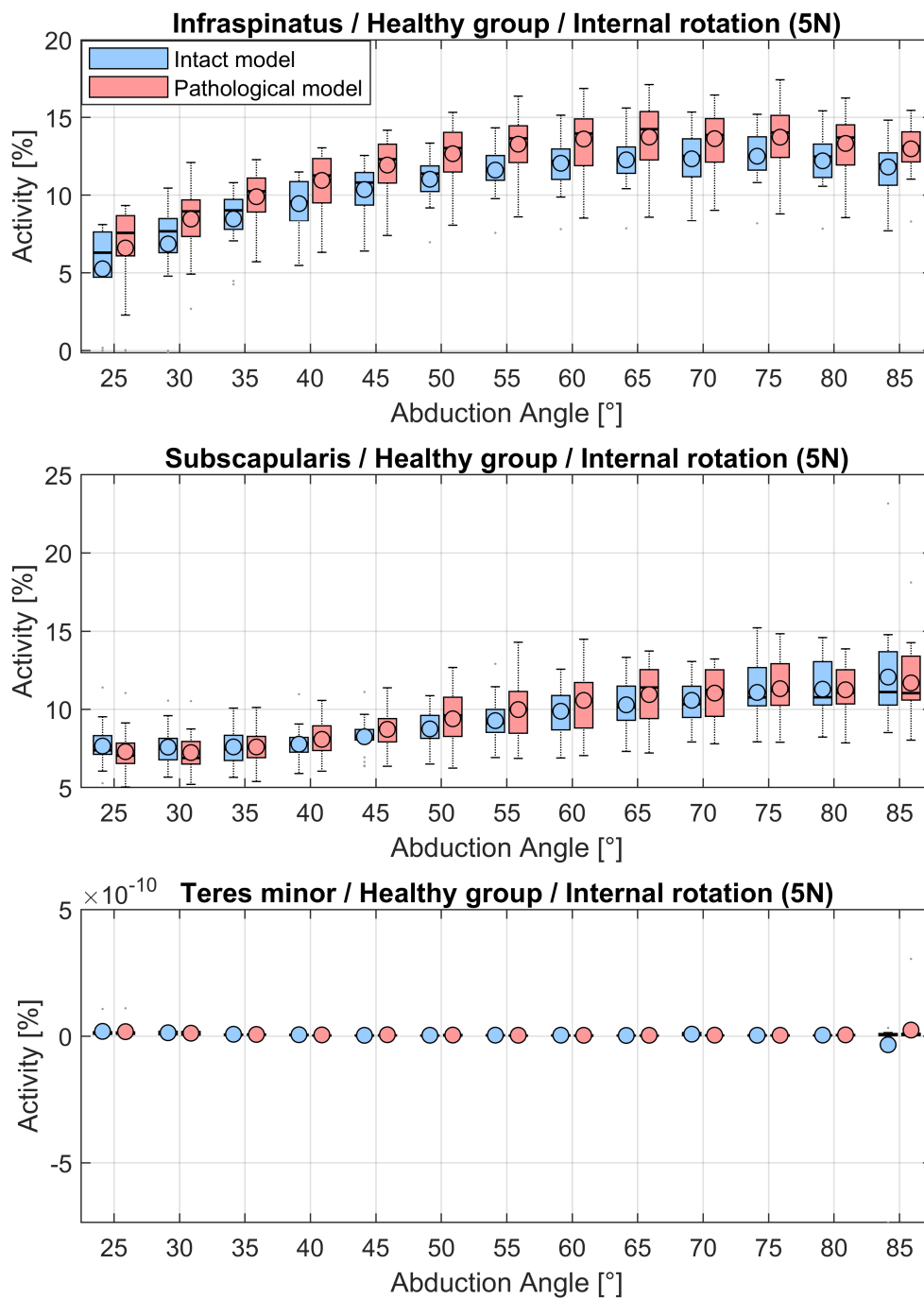


FIGURE 7.7: Computed muscle activities of infraspinatus, subscapularis and teres minor over the abduction angle in 5° increments during the internal rotation trial with 5 N load in hand. Blue depicts the activities of the intact model and red the modelled tear of the m. supraspinatus of the healthy subject cohort.

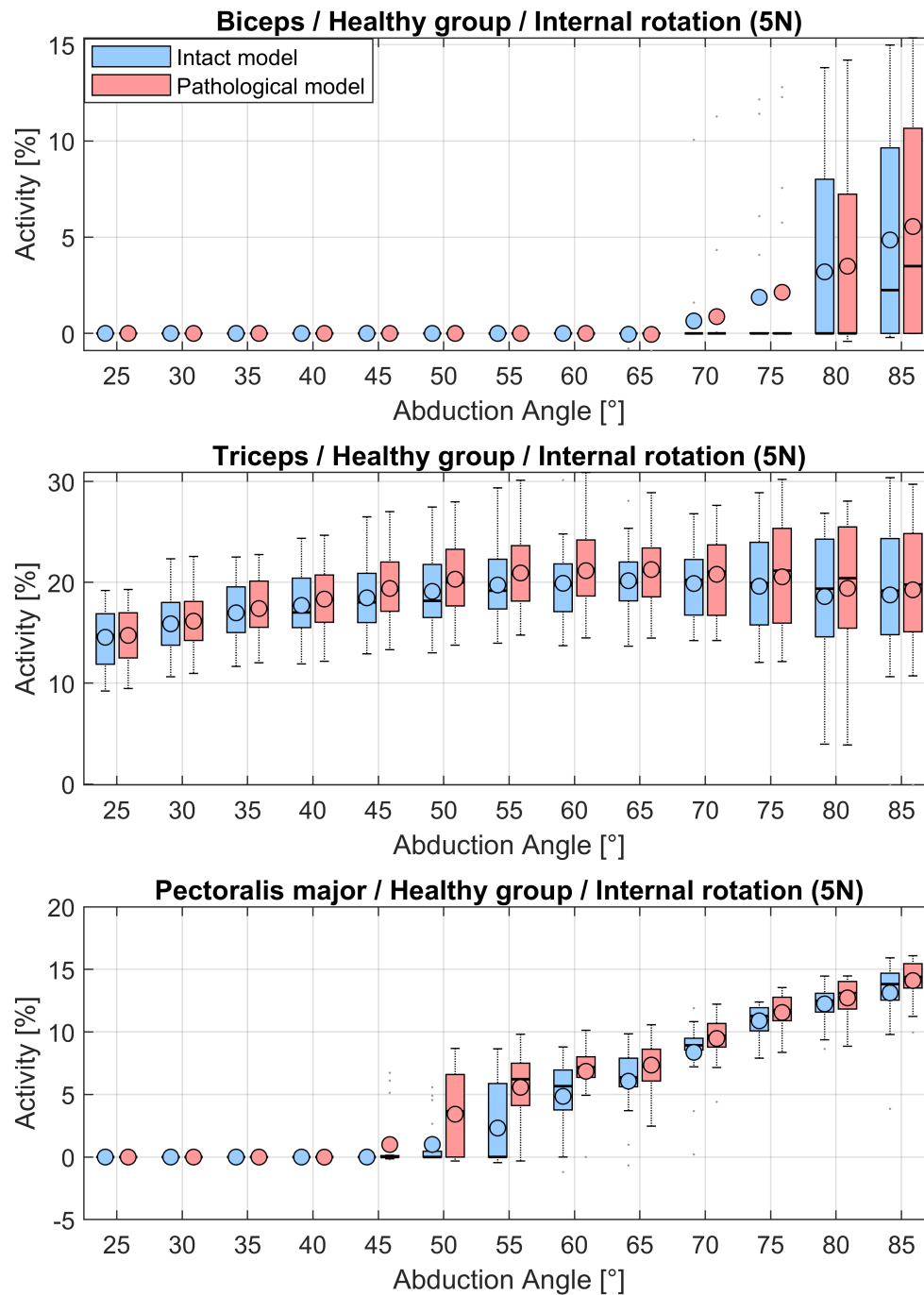


FIGURE 7.8: Computed muscle activities of the biceps, triceps and pectoralis major over the abduction angle in 5° increments during the internal rotation trial with 5 N load in hand. Blue depicts the activities of the intact model and red the modelled tear of the m. supraspinatus of the healthy subject cohort.

Table 7.2 provides the differences in the median of the intact vs. the pathological models of the healthy subject group for the case of the internal rotation with a load of 5 N for the contemplated muscle activities and the three components of the GH joint reaction force. Positive values denote an increase of the pathological models with regard to the intact models. Statistical significant differences between the groups at 5° intervals are denoted with one, two or three asterisks corresponding to $p \leq 0.05$, $p \leq 0.01$ and $p \leq 0.001$. Where the subscapularis (SS) and the posterior deltoid (PD) show a decrease for the contemplated trial, the other muscle activities exhibit increased values. Considering all trials, the anterior deltoid (AD), lateral deltoid (LD) and the infraspinatus (INF) inhibit the most significant differences in their respective medians. While the activities tend to increase in the pathological models, the differences tend to be under 2% activity except for some outliers in the pectoralis major (PM) and are considered to be not significant.

Abduction [°]	AD [%]	LD [%]	PD [%]	INF [%]	SS [%]	BIC [%]	TRI [%]	TM [%]	PM [%]	CF [%BW]	ISF [%BW]	APF [%BW]
25	1.3**	1.0	0.3	1.3	-0.3	0.0	0.1	0.0	0.0	-3.2**	0.5	1.5**
30	1.5*	1.0*	0.4	1.3*	-0.6	0.0	0.3	0.0	0.0	-3.3**	0.5	2.4***
35	1.6**	1.3*	0.2	1.2*	0.1	0.0	0.4	0.0	0.0	-3.9**	-0.2	3.1***
40	2.0*	1.7*	-0.3	1.7**	0.3	0.0	1.3	0.0	0.0	-3.8**	0.8	3.2***
45	1.8*	1.9*	-1.1	1.5**	0.6	0.0	1.2	0.0	0.0	-5.5***	0.9	3.4***
50	1.6*	1.7*	-1.2	1.6**	0.9	0.0	1.8	0.0	3.7*	-4.1**	0.3	3.7***
55	1.6*	1.9*	-0.7	2.0*	0.9	0.0	1.7	0.0	6.2*	-5.3*	-0.1	4.1***
60	1.5	1.6	0.0	1.8*	0.6	0.0	1.6	0.0	1.5	-4.0	-1.2	6.0***
65	1.3	1.3	0.2	2.0*	1.3	0.0	1.1	0.0	0.9	-4.4	-0.2	5.4***
70	1.1	1.1	0.1	1.3*	0.9	0.0	0.8	0.0	0.8	-5.4	-0.2	5.1**
75	1.0	1.1	-0.3	1.5	0.4	0.0	1.2	0.0	0.5	-4.8	-0.5	4.1*
80	0.8	0.8	-0.1	1.2*	0.3	0.0	1.0	0.0	0.6	-4.6	1.2	3.3*
85	0.7	0.7	-0.1	1.2*	-0.1	1.2	0.6	0.0	0.6	-6.2	0.5	3.1

TABLE 7.2: Differences in median values of muscle activities and GH joint reaction forces between intact and pathological models of the healthy subject cohort during the internal rotation trial with 5 N load in hand in 5° increments. Asterisks indicate the significance level. AD = anterior deltoid, LD = lateral deltoid, PD = posterior deltoid, INF = infraspinatus, SS = subscapularis, BIC = biceps, TRI = triceps, TM = teres minor, PM = pectoralis major, CF = compression force, ISF = inferior-superior force, APF = anterior-posterior force

7.3. Results

A comparison of the resultant GH joint reaction forces shows no significant difference in the superior-inferior direction on the glenoid for all computed trials. The compression force (CF) and anterior-posterior force (APF) between intact and pathological models have the most distinguished differences. For all models where the m. suprapinatus element is excluded, the respective compression force decreases while the force component pointing in the anterior direction in the glenoid increases (Figure 7.10). This results in a shift in the trajectory of the resultant force vector originating from the centre of the humeral head (Figure 7.9) with an increase in the superior and anterior direction when projected on the glenoid. This effect occurs in all computed trials, where it is more severe in the two trials with an internal rotation of the humerus mimicking the empty can test. For all computed abduction trials and configurations, the reaction force always follows a path anterior/superior section of the glenoid. Internal or external rotation did not affect the general direction.

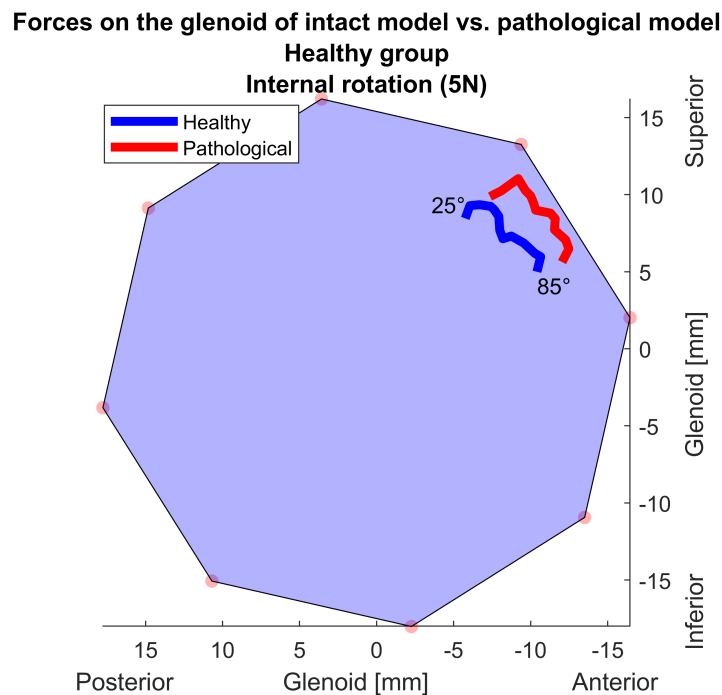


FIGURE 7.9: Projected median GH joint reaction force of all models onto the glenoid of intact and pathological models of the healthy subject cohort during the internal rotation trial with 5 N load in hand. Intact/healthy models (blue) and pathological models (red) with their starting value at 25° abduction and the progression up to 85° abduction.

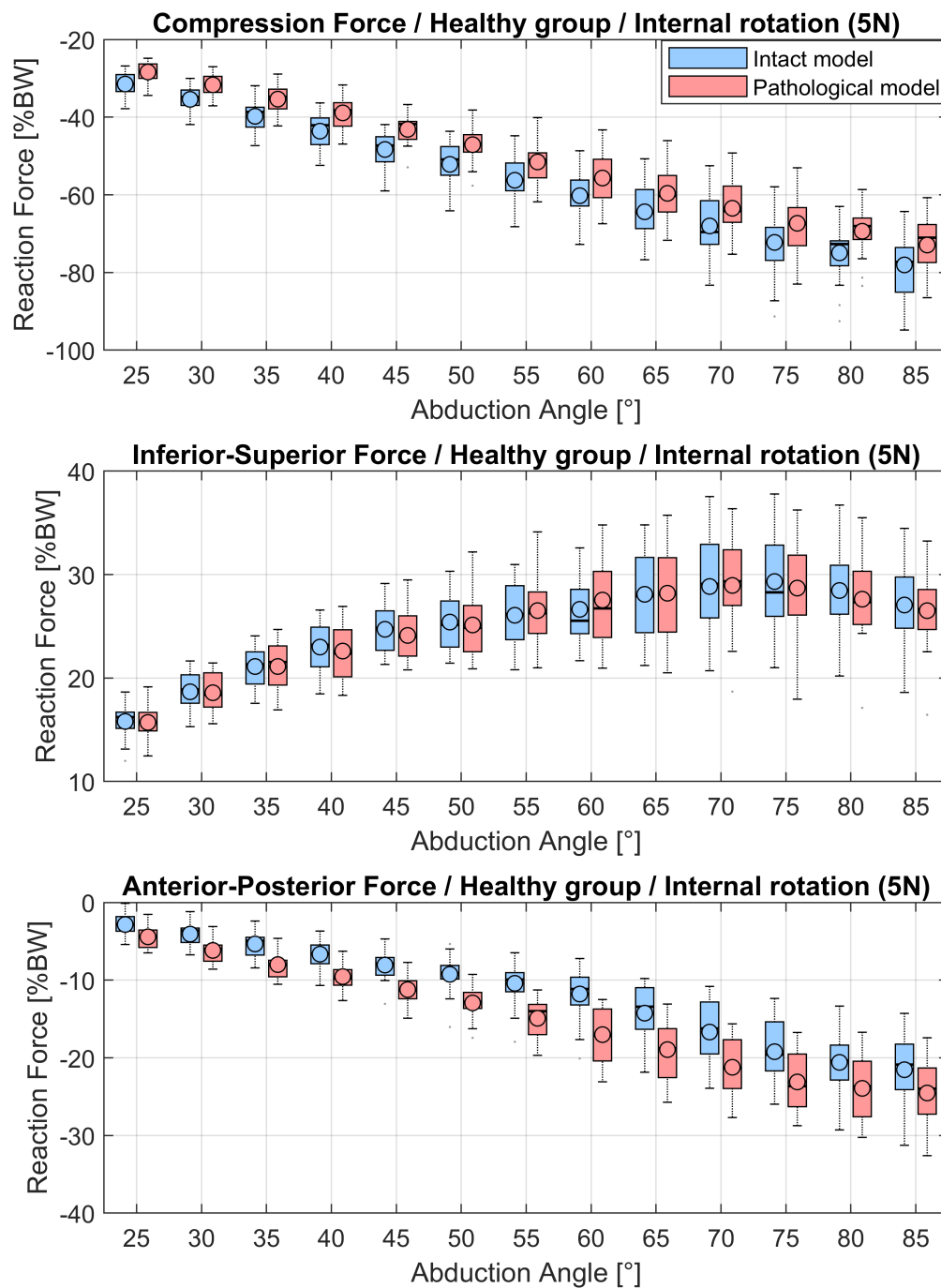


FIGURE 7.10: Compression force, inferior-superior force and anterior-posterior force of intact (blue) and pathological (red) models of the healthy subject cohort during the internal rotation trial with 5 N load in hand over the abduction angle in 5° increments.

7.3.2 Forces and muscle activities of intact models and pathological models of the healthy vs. the pathological group

Due to pain and the resulting inability to conduct the required motions adequately, several trials could not be conducted by the patient group. From the 8 different data sets for each motion of the pathological group, the kinematic marker based optimization converged for 8 trials in the neutral position, 8 trials in the neutral position with 5 N load in hand, 7 trials for internal rotation, 7 trials for internal rotation with load, 8 trials of the external rotation and 7 trials for the external rotation with an applied force.

During the motion of the neutral trials with and without weight, no significant differences occurred in the kinematics of the flexion and external rotation, with the largest deviation of -11.1° at 35° abduction during the neutral position with applied load. Differences in the flexion angle over all trials remained under 10° and were not significant. A significant difference in external rotation angle is found in the internal rotation trial, where the pathological subjects trended to conduct less internal rotation. For the external rotation trials, the pathological subjects also tended to conduct less external rotation than the healthy control group.

Figures 7.12, 7.13, and 7.14 depict the contemplated muscle activities of the intact models of the healthy group and the pathological models of the pathological group. During all trials, the medians of the simulated muscle activities are significantly higher in the pathological models of the pathological group, except for the subscapularis (see Table 7.3). The median differences in muscle activities are hereby higher than in the comparison of intact and pathological models of the healthy group which share the same kinematics (see section 7.3.1).

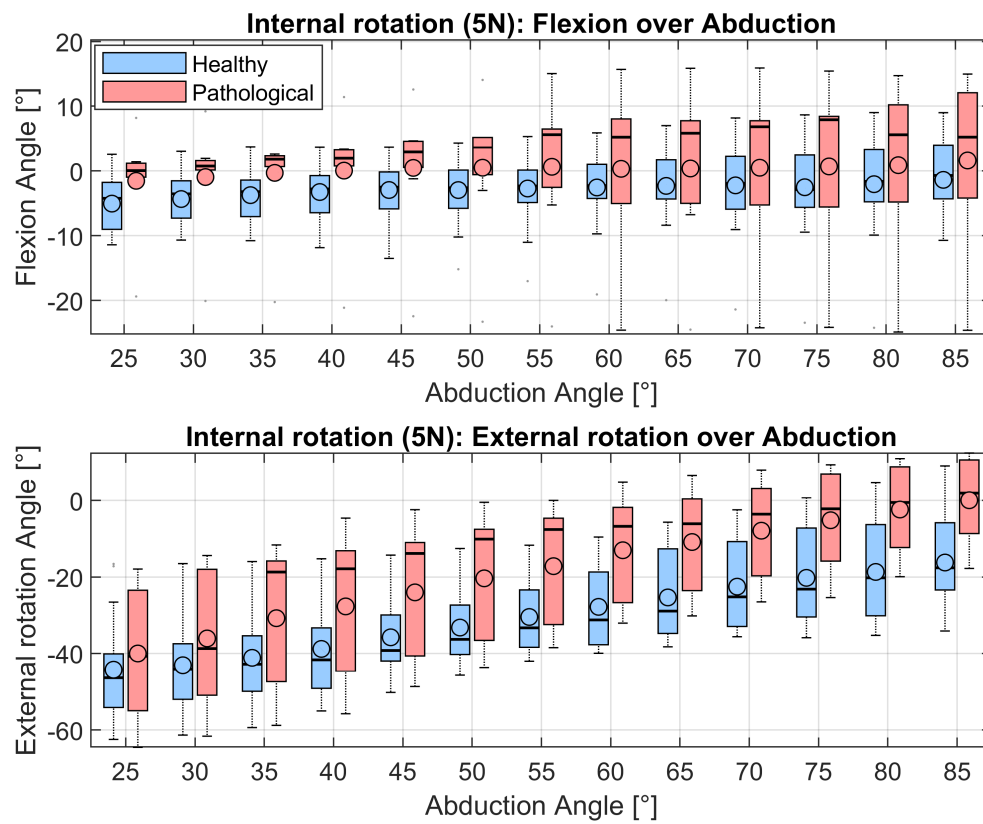


FIGURE 7.11: Flexion and external rotation angle over abduction of the healthy cohort (blue) and pathological cohort (red) during the internal rotation trial with 5 N load in hand.

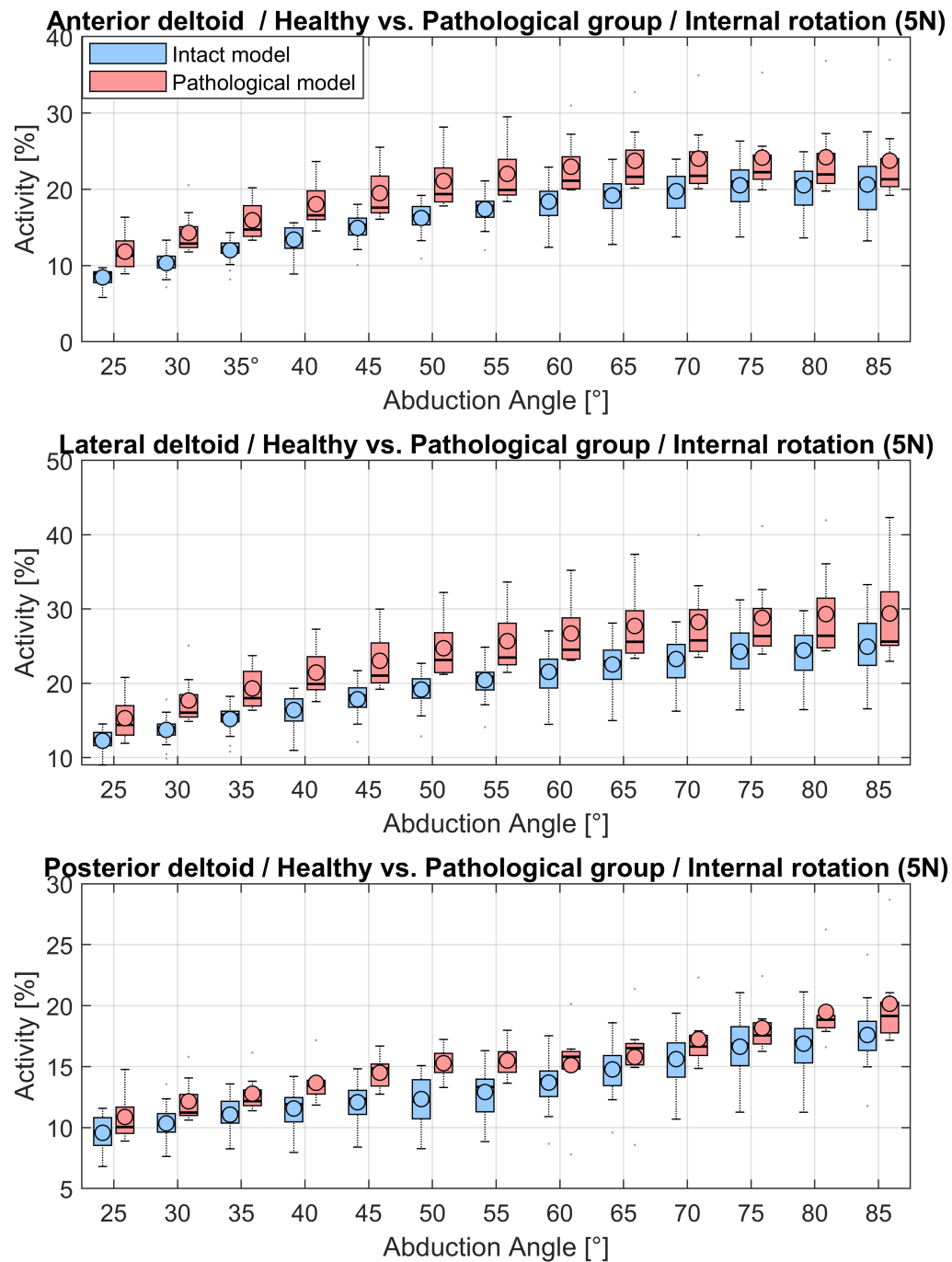


FIGURE 7.12: Computed muscle activities of the anterior, posterior and lateral deltoids over the abduction angle in 5° increments during the internal rotation trial with 5 N load in hand. Blue depicts the activities of the intact model of the healthy subject group and red the modelled tear of the m. supraspinatus of the patient group.

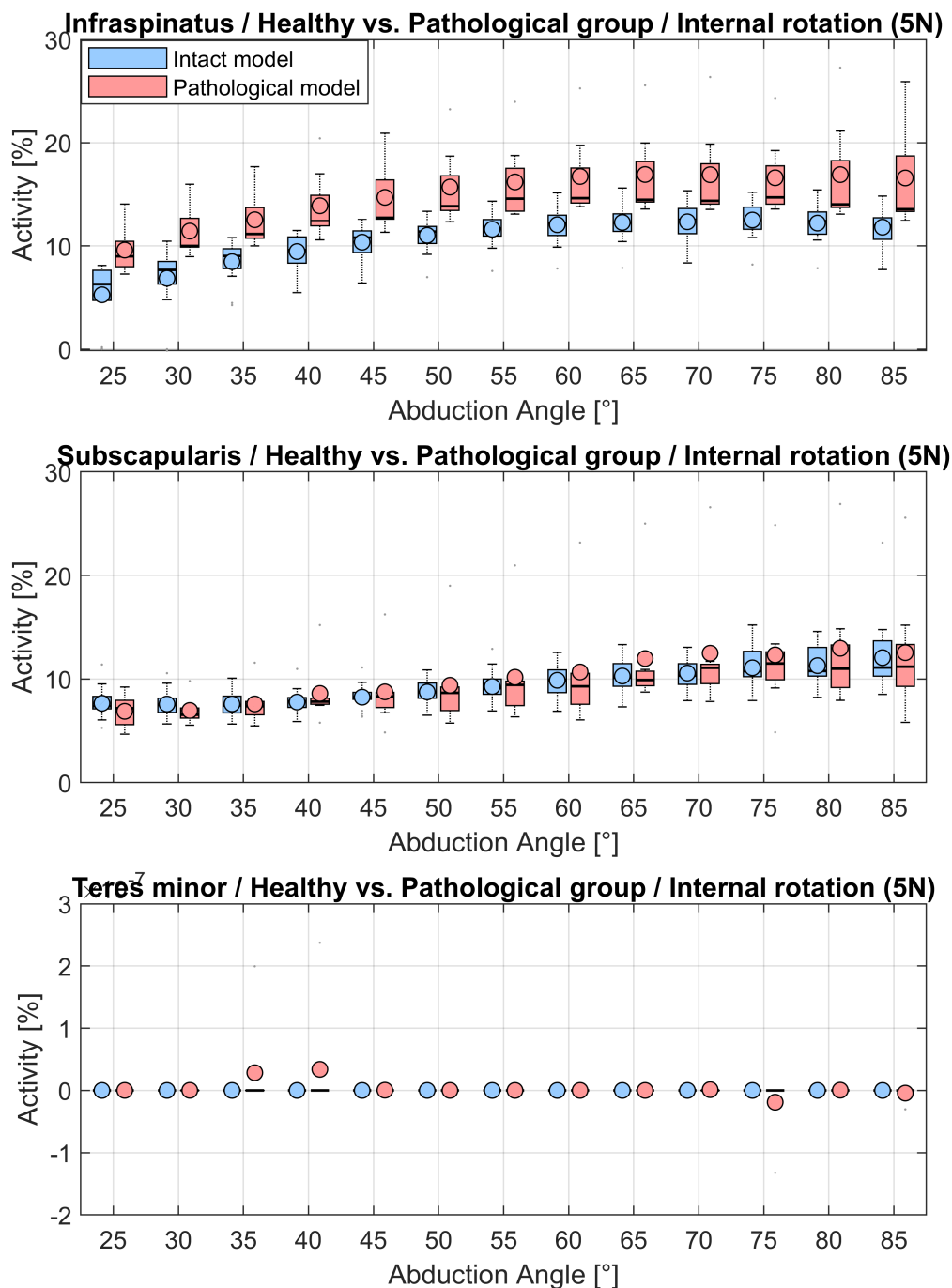


FIGURE 7.13: Computed muscle activities of the infraspinatus, subscapularis and teres minor over the abduction angle in 5° increments during the internal rotation trial with 5 N load in hand. Blue depicts the activities of the intact model of the healthy subject group and red the modelled tear of the m. supraspinatus of the patient group.

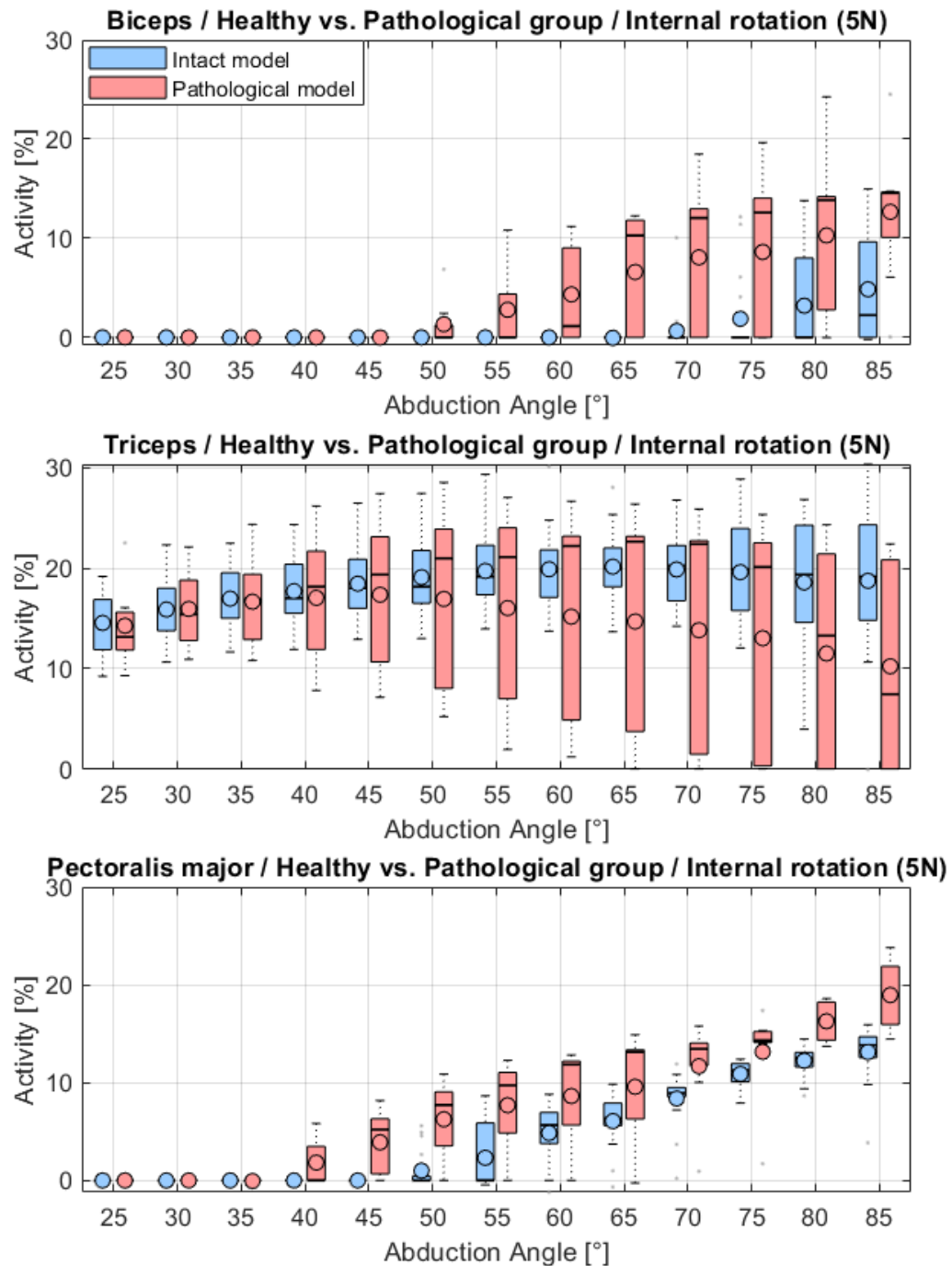


FIGURE 7.14: Computed muscle activities of the biceps, triceps and pectoralis major over the abduction angle in 5° increments during the internal rotation trial with 5 N load in hand. Blue depicts the activities of the intact model of the healthy subject group and red the modelled tear of the m. supraspinatus of the patient group.

Chapter 7. The effect of tears of the m. supraspinatus on the forces and muscle activation pattern of the shoulder complex

Abduction [°]	AD [%]	LD [%]	PD [%]	INF [%]	SS [%]	BIC [%]	TRI [%]	TM [%]	PM [%]	CF [%BW]	ISF [%BW]	APF [%BW]	FLX [°]	ER [°]
25	2.3**	1.8*	0.4	2.7***	-0.2	0.0	-1.6	0.0	0.0	-7.1**	3.5	-0.2	-4.3*	-5.6
30	2.4***	2.0***	1.0*	2.3***	-0.9	0.0	-0.6	0.0	0.0	-7.9**	3.1	0.5	-4.3	-5.4
35	2.4***	2.2***	0.9*	2.1***	-0.1	0.0	-0.1	0.0	0.0	-7.3***	3.7	0.6	-5.0	-24.1
40	2.9***	3.3**	1.5*	2.9***	0.0	0.0	1.1	0.0	0.0	-6.9**	4.5*	0.2	-4.8*	-23.8
45	2.3**	2.7**	2.5**	1.9***	0.1	0.0	1.4	0.0	5.2*	-8.6***	4.0*	0.2	-5.4*	-25.4
50	2.8***	3.5***	3.1**	2.5***	-0.1	0.0	2.8	0.0	7.7*	-9.2**	2.4	0.1	-6.2	-26.2
55	2.1**	2.6**	2.0**	2.9***	0.3	0.0	1.9	0.0	9.7*	-11.7***	1.5	0.4	-7.9	-25.7*
60	2.5**	2.7**	1.8	2.4***	-0.6	1.1	2.5	0.0	6.2	-13.6**	0.2	-0.4	-7.5	-24.5*
65	2.0**	2.6*	1.6	2.2***	-0.2	10.3	2.7	0.0	6.8	-13.2***	1.7	-0.3	-8.0	-22.8*
70	1.7*	2.3	0.9	1.8**	0.8	12.0	2.2	0.0	4.5**	-15.4**	2.2	-1.7	-8.7	-21.6*
75	1.2	1.8	0.7	2.2**	0.7	12.6	0.2	0.0	3.1**	-15.5**	0.8	-3.5	-10.8	-21.0*
80	0.9	1.6	1.7	1.5**	0.2	13.9	-6.1	0.0	4.0***	-11.6***	3.3*	-4.1	-7.2	-19.7*
85	0.4	0.7	1.7	1.6**	0.1	12.3	-11.7	0.0	5.0***	-13.0***	2.8	-3.2	-5.9	-19.5*

TABLE 7.3: Differences in median values of muscle activities, GH joint reaction forces and kinematics between intact models of the healthy subject cohort and pathological models of the patient group during the internal rotation trial with 5 N load in hand in 5° increments. Asterisks indicate the significance level. AD = anterior deltoid, LD = lateral deltoid, PD = posterior deltoid, INF = infraspinatus, SS = subscapularis, BIC = biceps, TRI = triceps, TM = teres minor, PM = pectoralis major, CF = compression force, ISF = inferior-superior force, APF = anterior-posterior force, FLX = Flexion angle, ER = external rotation angle

In terms of the resultant joint reaction force acting on the glenoid, a significant difference is found in the compression force where the median of the pathological group is up to 15.5%BW lower during the internal rotation with applied load. A similar trend is observable in the internal rotation trial without load, where the compression force is significantly lower up to 60° abduction. A significant difference in the trials of the neutral humerus position is found in the compression force up to 35° and an increase of the anterior posterior force component towards the anterior side up to 45°. During the trial of the neutral position with load, these two force components show a significant difference in their medians up to 40°. The differences in the external rotation trials become less noticeable and yields no significant difference in the reaction forces for the trial without load, and only partial significant differences in the external rotation trial with load. The trends are the same as with the other trials, where the median compressive force decreases while the anterior posterior component increases towards the anterior direction.

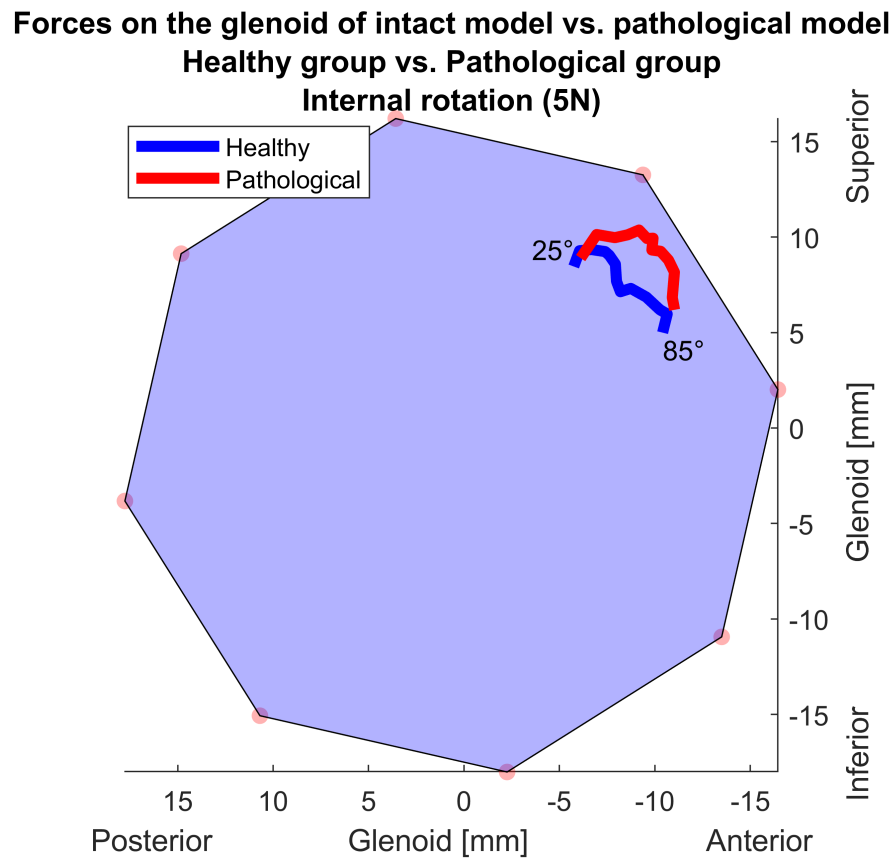


FIGURE 7.15: Projected median GH joint reaction force of all models onto the glenoid of intact models of the healthy subject cohort and pathological models of the patient group during the internal rotation trial with 5 N load in hand. Intact models of the healthy control (blue) and pathological models of the patient group (red) with their starting value at 25° abduction and the progression up to 85° abduction.

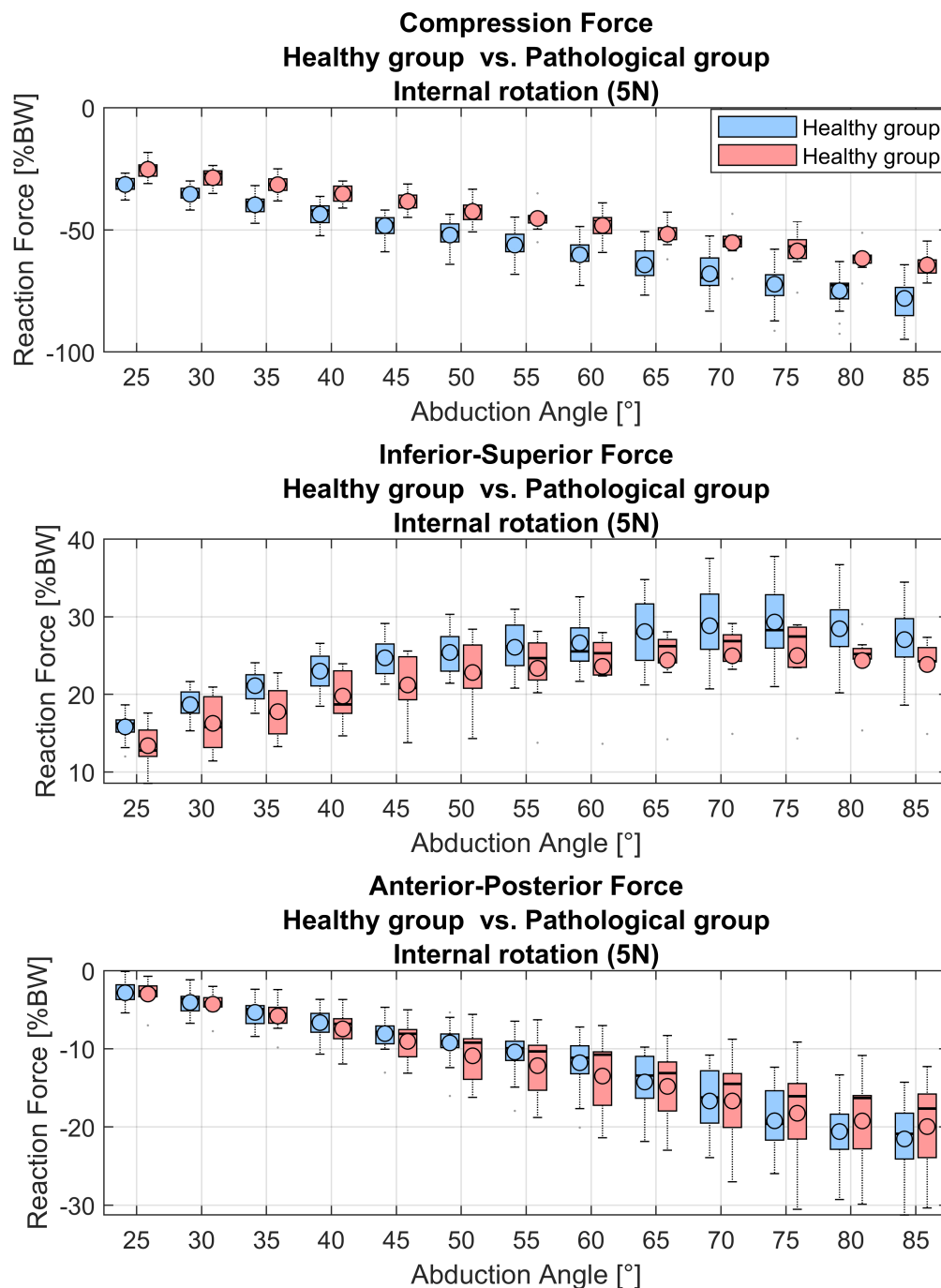


FIGURE 7.16: Compression force, inferior-superior force and anterior-posterior force of intact models of the healthy control (blue) and pathological models of the patient group (red) during the internal rotation trial with 5 N load in hand over the abduction angle in 5° increments.

7.3.3 EMG comparison between the healthy vs. the pathological group

With 14 involved EMG sensors, loosening of the electrodes during the experiments was a major issue. Each EMG signal of each trial was examined in retrospect and every trial excluded where one sensor had lost contact and did not show an EMG signal.

After exclusion of the corrupted trials, from the healthy group 18 trials were used for the neutral position, 18 trials for the neutral position with 5 N load, 14 for the internal rotation, 14 for the internal rotation with 5 N load, 17 for the external rotation and 17 for the external rotation with 5 N load.

From the 8 different data sets for each trial of the pathological group, the kinematic marker based optimization converged for 7 trials in the neutral position, 7 trials in the neutral position with 5 N, 5 trials for internal rotation, 6 trials for internal rotation with weight, 6 trials of the external rotation and 5 trials for the external rotation with weight.

Figures 7.17- 7.21 show the comparison between the EMG of the healthy to the pathological subject group normalized to the 85° position of their respective neutral position trials with applied load. Table 7.4 provides the differences in the medians of the EMG between the healthy and pathological subjects for the internal rotation trial with 5 N load in hand. The resulting activities of all subjects and computed differences for the other trials is provided in C.0.7 and C.0.8.

The comparison of the medians between the healthy and the pathological group is inconclusive. Where most of the muscles evaluated during the 5° abduction increments showed no significant differences, the results depict large variances between the subjects. Significant differences in median values occurred during the trial in the neutral position in the processed EMG signals of the muscle groups of the anterior deltoid (AD) in the ranges 25-50° abduction, the triceps (TRI) in the 75-85° abduction and rhomboideus major (RMA) in the range 40-50°. In the neutral position with load in hand, only the rhomboideus minor showed a significant difference in the 25-45° abduction range. During internal rotation, only the rhomboideus major showed a significant difference in the abduction range 40-85°.

The internal rotation with weight showed more significant differences with the trapezius transversus (TT) in the range 35-85°, the trapezius ascendens (TA) in the range 45-50°, the AD between 35-55° posterior deltoid (PD) at 35° and the rhomboideus major in the range of 25-70°. The external rotation trial did not have significant differences in the respective medians. During the external rotation trial with weight, significant differences were found for the TA in 70-85°, latissimus (LAT) 70-85° and the biceps (BIC) at 85° abduction.

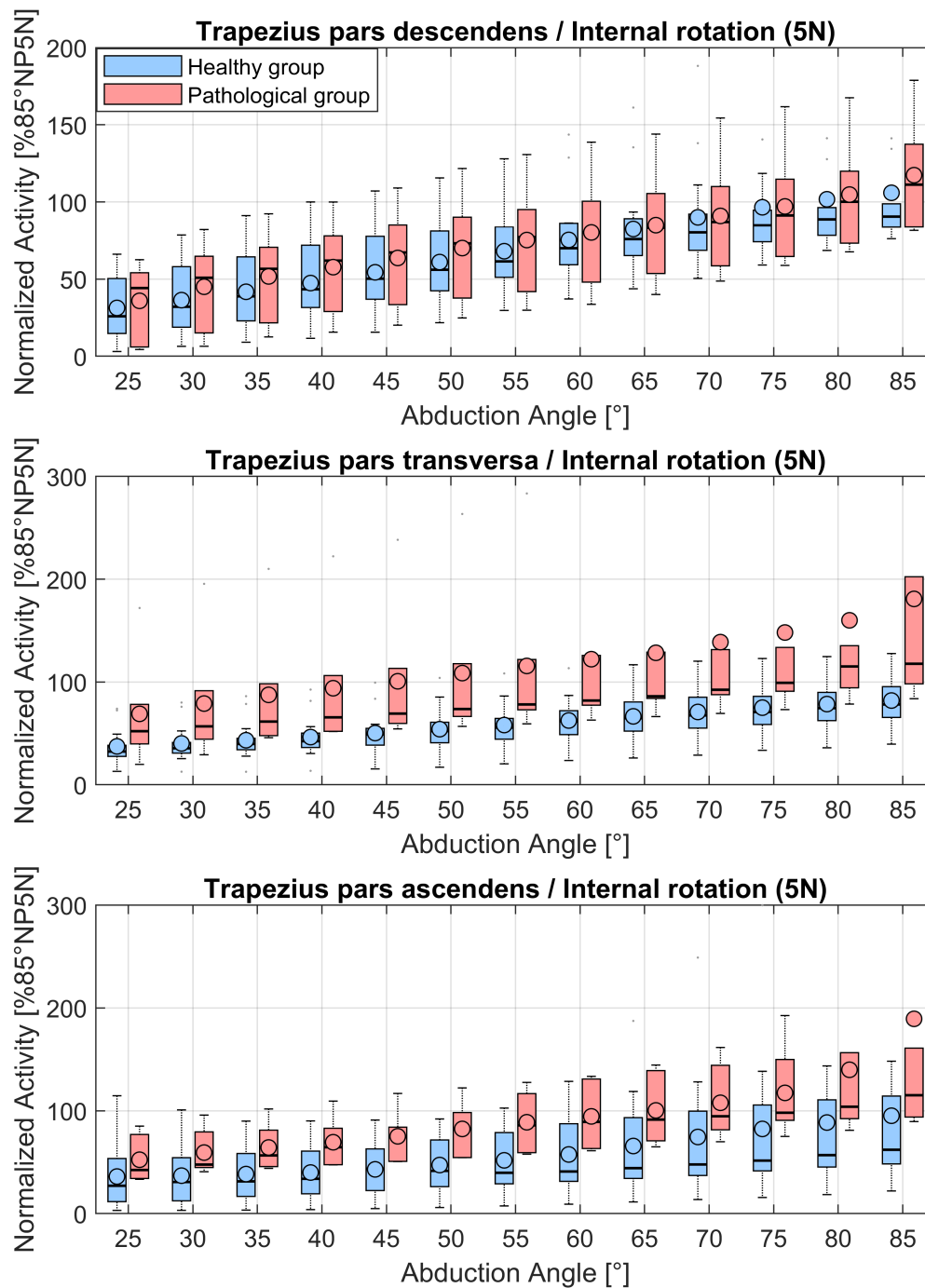


FIGURE 7.17: EMG muscle activities normalized to the 85° position of the neutral position trial with 5 N load in hand of the trapezius pars descendens, trapezius pars transversa and trapezius pars ascendens over the abduction angle in 5° increments during the internal rotation trial with 5 N load in hand. Blue depicts the EMG activities of the healthy subject group and red of the patient group.

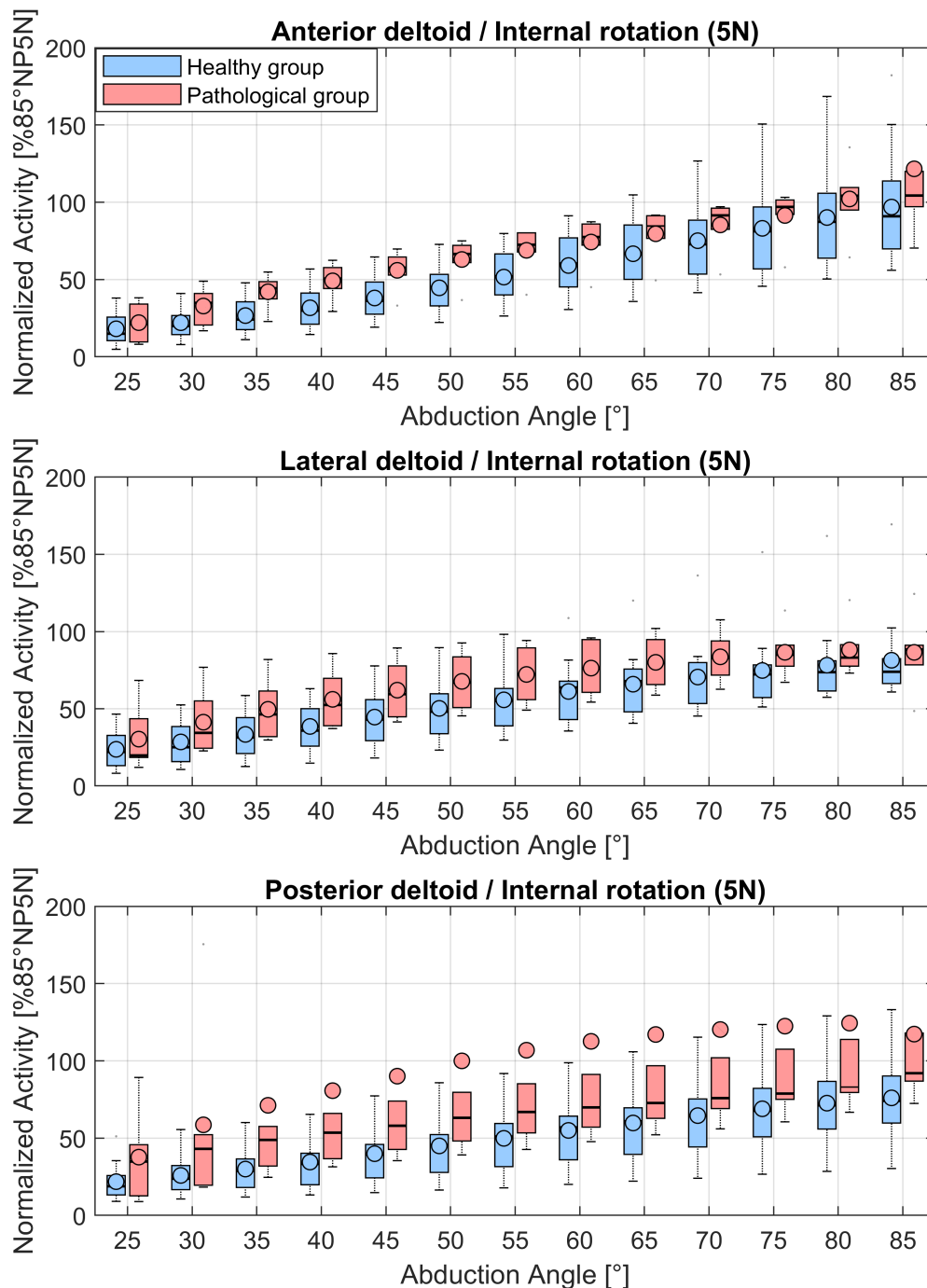


FIGURE 7.18: EMG muscle activities normalized to the 85° position of the neutral position trial with 5 N load in hand of the anterior deltoid, lateral deltoid and posterior deltoid over the abduction angle in 5° increments during the internal rotation trial with 5 N load in hand. Blue depicts the EMG activities of the healthy subject group and red of the patient group.

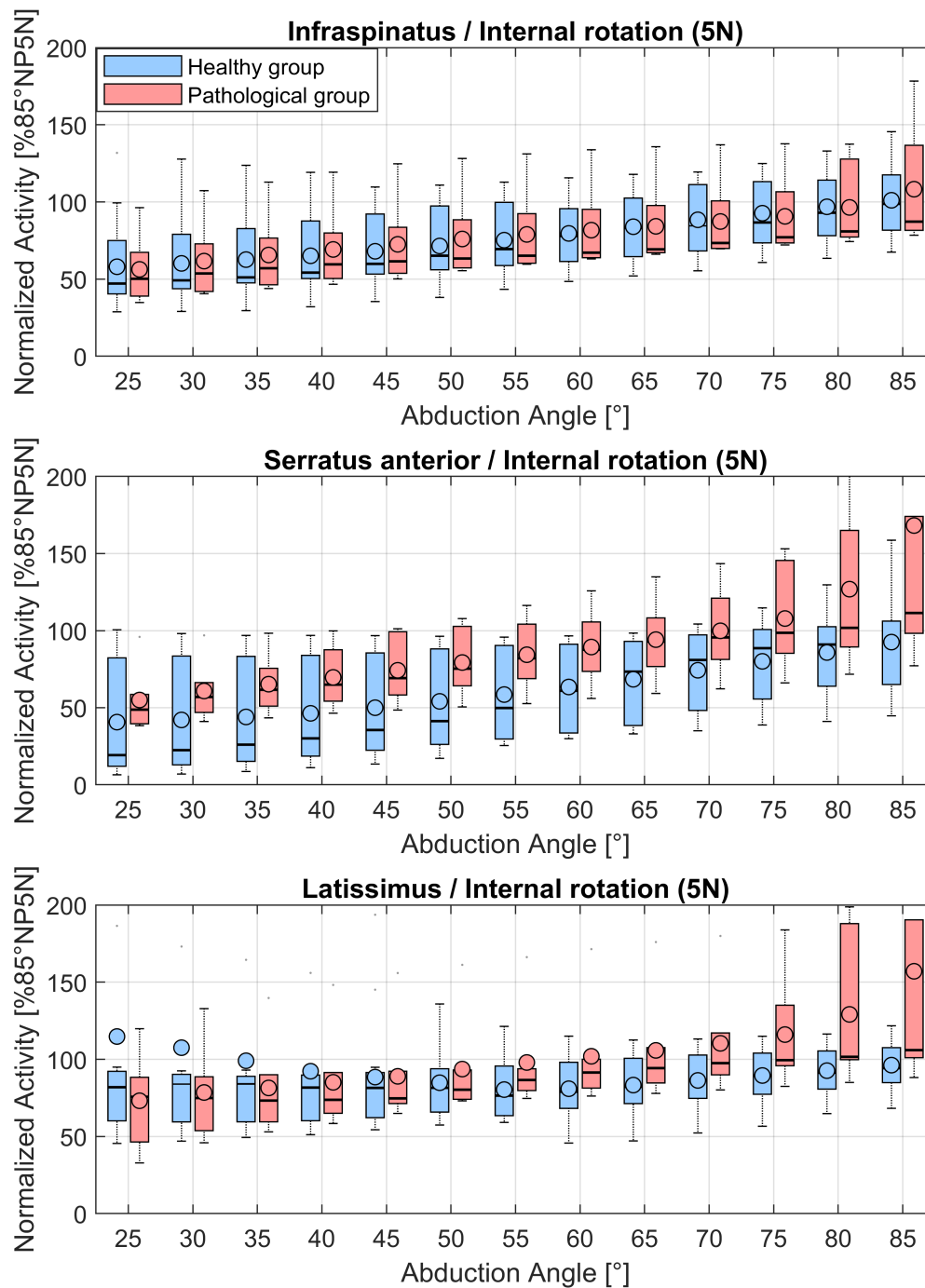


FIGURE 7.19: EMG muscle activities normalized to the 85° position of the neutral position trial with 5 N load in hand of the infraspinatus, serratus anterior and latissimus over the abduction angle in 5° increments during the internal rotation trial with 5 N load in hand. Blue depicts the EMG activities of the healthy subject group and red of the patient group.

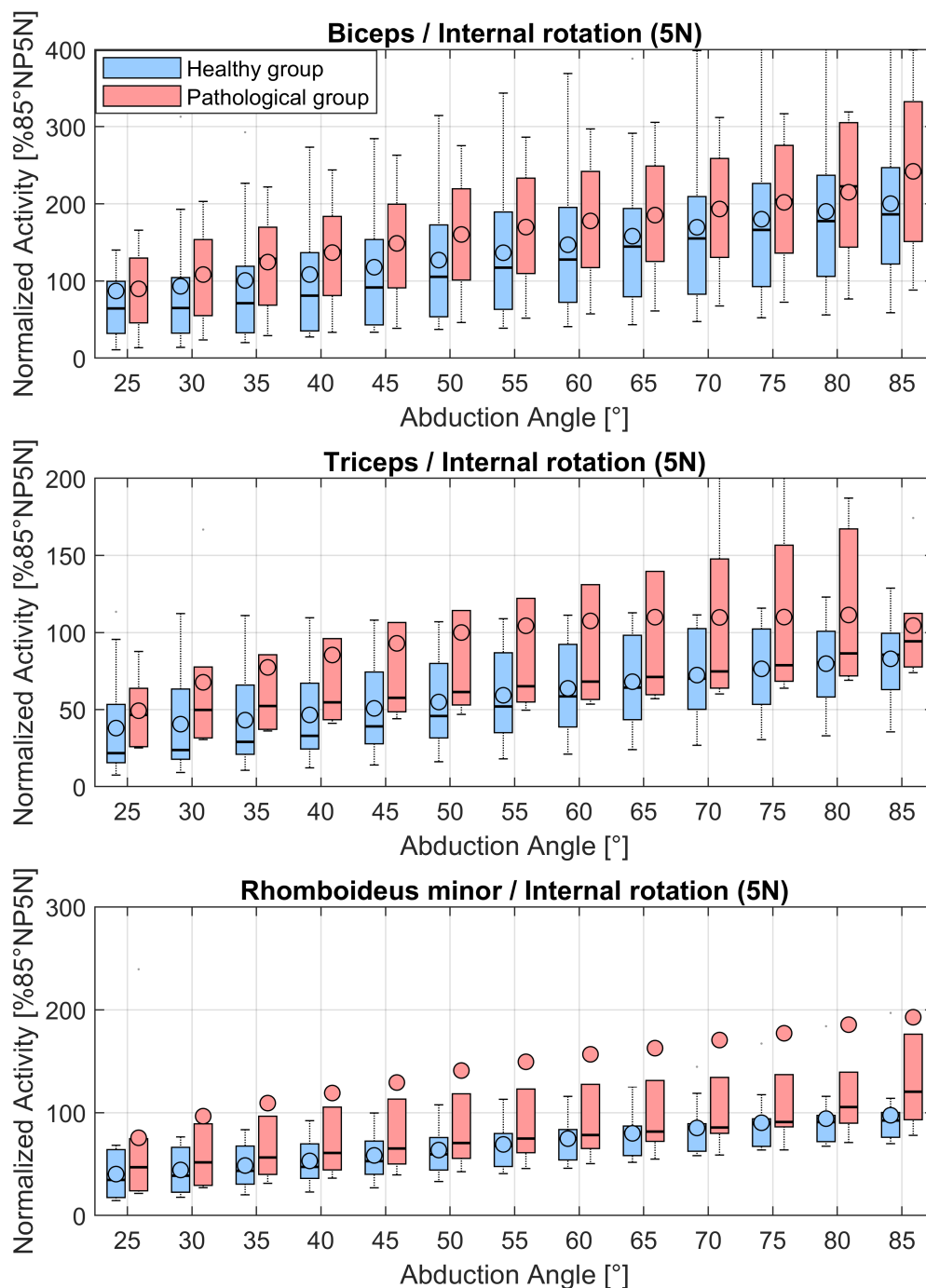


FIGURE 7.20: EMG muscle activities normalized to the 85° position of the neutral position trial with 5 N load in hand of the biceps, triceps and rhomboideus minor over the abduction angle in 5° increments during the internal rotation trial with 5 N load in hand. Blue depicts the EMG activities of the healthy subject group and red of the patient group.

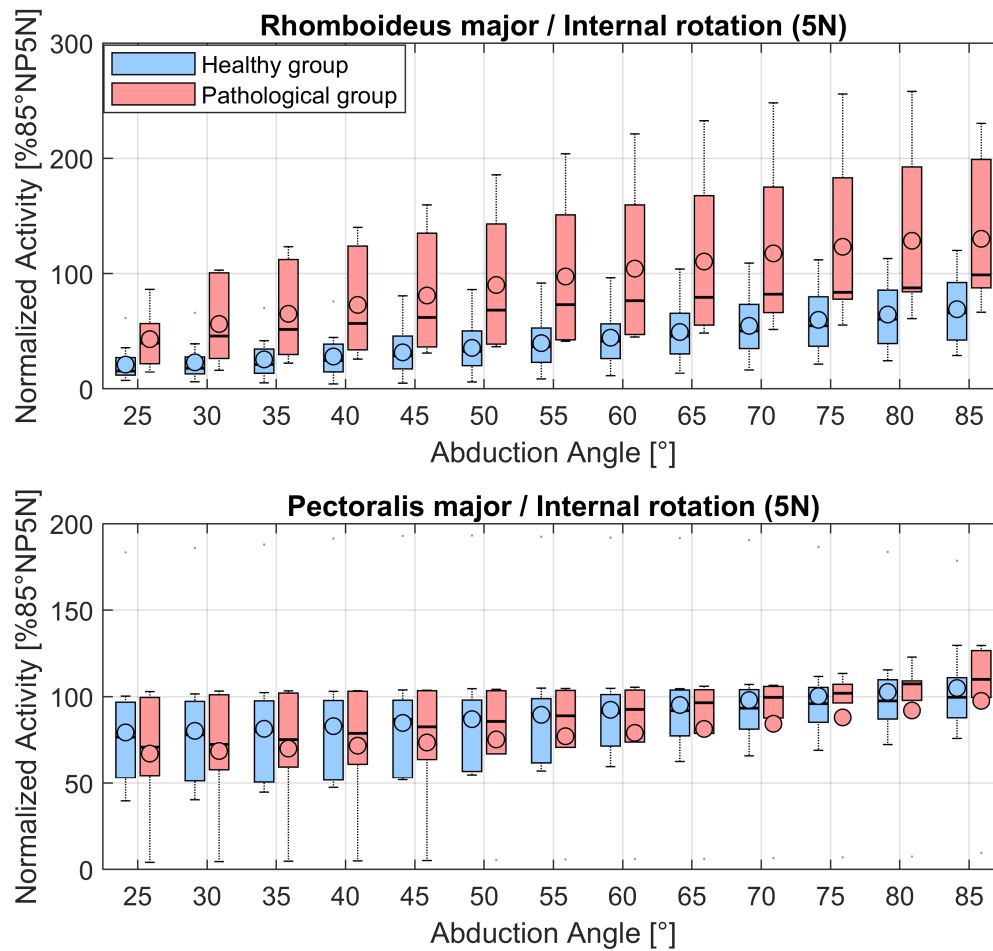


FIGURE 7.21: EMG muscle activities normalized to the 85° position of the neutral position trial with 5 N load in hand of the rhomboideus major and pectoralis major over the abduction angle in 5° increments during the internal rotation trial with 5 N load in hand. Blue depicts the EMG activities of the healthy subject group and red of the patient group.

Chapter 7. The effect of tears of the m. supraspinatus on the forces and muscle activation pattern of the shoulder complex

Abduction [°]	TD [%85°]	TT [%85°]	TA [%85°]	AD [%85°]	LD [%85°]	PD [%85°]	INF [%85°]	SER [%85°]	LAT [%85°]	BIC [%85°]	TRI [%85°]	RMA [%85°]	RMI [%85°]	PEC [%85°]
25	18.3	19.8	15.3	6.3	-2.3	16.0	3.1	29.5	-6.2	27.6	24.8	24.2*	12.3	-5.8
30	18.8	21.3	16.9	15.0	9.3	19.3	4.5	34.5	-8.6	42.4	26.0	27.9*	13.0	-5.5
35	17.8	21.8**	25.2	20.2*	14.9	20.1*	6.0	35.6	-10.5	57.6	23.3	30.4*	13.0	-4.7
40	18.6	23.2**	30.7	20.7*	16.6	20.2	5.4	34.9	-7.9	58.3	21.8	32.2*	13.6	-4.6
45	17.0	20.2**	30.7*	21.4*	16.4	18.5	1.6	33.7	-6.8	58.4	18.5	33.3*	12.3	-4.3
50	17.1	21.5*	40.7*	21.4*	18.9	17.6	-1.8	34.0	-1.2	54.3	15.6	35.9*	11.0	-2.8
55	15.7	22.5*	46.1	20.4*	17.2	15.9	-4.3	32.2	10.1	51.6	13.1	36.6*	7.1	-0.6
60	10.3	20.1*	48.2	17.2	12.4	12.9	-10.8	26.6	12.4	48.8	9.6	35.1*	3.8	2.0
65	7.4	21.3*	47.2	17.6	11.7	11.9	-13.9	19.6	12.1	41.0	6.9	33.7*	0.9	4.6
70	6.7	24.9*	46.9	18.7	12.7	11.5	-10.7	14.6	11.0	40.3	4.7	31.9*	-0.6	6.3
75	6.4	28.5*	46.5	15.8	12.7	11.1	-9.6	10	10.1	39.0	2.9	29.0	1.9	6.0
80	11.4	40.6*	47.0	16.9	9.4	12.2	-12.1	10.8	10.2	45.1	5.9	27.2	14.6	9.9
85	20.7	39.6*	53.0	13.4	14.4	17.9	-11.5	18.6	11.7	54.3	8.7	33.0*	28.0	10.4

TABLE 7.4: Differences in median values of EMG activities normalized to the 85° position of the neutral position trial with 5 N load in hand between the healthy subject cohort and patient group during the internal rotation trial with 5 N load in hand in 5° increments. Asterisks indicate the significance level. TD = trapezius descendens, TT = trapezius transversa, TA = trapezius ascendens, AD = anterior deltoid, LD = lateral deltoid, PD = posterior deltoid, INF = infraspinatus, SER = serratus anterior, LAT = latissimus, BIC = biceps, TRI = triceps, RMA = rhomboideus major, RMI = rhomboideus minor, PEC = pectoralis major

7.4 Discussion

Where the model has been validated up to 120° abduction in chapter 5, four of the eight patients could not abduct their arm higher than 90° due to pain. The evaluation of all parameters of interest is thus limited in the range 25-85° as all subjects could achieve this abduction angle.

7.4.1 Musculoskeletal simulation of intact models and simulated tears of the m. supraspinatus

Comparison between intact and pathological models of the healthy group

The evaluation of simulated tears of the m. supraspinatus from the intact and pathological models of the same subject group highlight the change in recruitment when the underlying kinematics are exactly the same and the only difference is the exclusion of the six virtual muscle elements.

As the m. supraspinatus spans only over the GH joint, all muscles which connect the scapula to the thorax did not show any difference in their respective activation. Where in general all muscle elements spanning over the GH joint showed increased activation, the anterior deltoid, lateral deltoid and infraspinatus showed a significant increase in their activation (see Table 7.2, Figures 7.6, 7.7, 7.8 & Appendix C).

However, changes in terms of absolute difference in activation magnitude are small. Sections 5.3.4 and 5.4.5 of chapter 5 argue for a higher order polynomial criterion of Equation 3.4 to increase muscle synergism and activate the m. supraspinatus elements more, which is in better agreement to literature (e.g. Wickham et al., 2010). By omitting the m. supraspinatus group from the pathological models, the higher order criterion results in a more even distribution of the load the other muscles need to compensate for. Not using the higher order criterion would cause less activation of the m. supraspinatus and also cause lower activity increase in other muscles, but might distinguish the main compensatory muscles better.

GH joint reaction forces for all trials showed a decrease in compression force and an increase in the anterior direction on the glenoid, with the resultant force pointing more towards the edges. This is in line with findings by Steenbrink et al., 2009, Vidt et al., 2018 and Hölscher et al., 2016b. Even when all muscles spanning the shoulder joint showed no significant increase, the cumulative differences are noticeable in the components of the joint reactions forces. In the inferior-superior direction of the glenoid, the joint reaction forces were less noticeable than in the posterior-anterior or compression direction. This is due to the moment arm of the m. supraspinatus. With a lower compression force however, the inferior-superior and posterior-anterior components have a larger impact on the resultant force direction.

The largest differences in the trajectory of the resultant GH joint reaction force on the glenoid occurred during both internal rotation trials with and without weight in the anterior and superior direction. This could be interpreted as the humeral head translating more towards the acromion and narrowing the space between them, thus compressing the muscles and tendons. It would be in line with patients experiencing more pain during internal then in external rotation (Itoi et al., 1999; Timmons et al., 2016).

Comparison between intact models of the healthy group and pathological models of the patient group

Comparing the intact models of the healthy subject group to the pathological models of the patient group show similar results of the force trajectories projected on the glenoid for all trials, with significant lower compression forces and an increase in the anterior direction on the glenoid. During the external rotation trial without weight, no significant differences were found in the computed forces in all direction.

However, there are significant differences in the muscle recruitment for all computed trials in the anterior deltoid, lateral deltoid, infraspinatus, biceps, pectoralis major and teres minor, which are four to five times higher then in the comparison between the intact and pathological models of the healthy group. While the computed activations between the healthy and pathological group are significantly different for all trials, the computed joint reaction forces become less distinguishable.

The parameter which is variable between the compared groups is the kinematics of the humerus. Patients tended to conduct less external rotation during the trials. While differences between the groups are not necessarily significant, a deviation is found non the less. If the underlying modelling is assumed to be correct, this leads to the potential conclusion that patients try to change their kinematics in a minor way in order to achieve a different recruitment of the muscles spanning the GH joint which results in a better stability of the humeral head.

7.4.2 EMG comparison between healthy subjects and patients with a tear of the m. supraspinatus

Two major limitations of the EMG study need to be addressed. For one, the cohort of the patients with 8 subjects where some of the trials were not usable is rather small. Furthermore, the approach of a sub-maximal normalization to the 85° position of the neutral position trial with 5 N load in hand makes the results more difficult to interpret and to set in comparison to the modelled muscle activities.

A steep incline from 5-85° abduction indicates muscles with an increasing activation during the abduction motion (e.g. the deltoids in Figure 7.18), where a lower inclination points to muscles with a low activation (e.g. latissimus dorsi in Figure 7.19)

The conjunction of differences in model activities and EMG activities in this context should be a indicator to muscle regions where a difference according to the model can be expected.

It has to be noted, that sensors placed on the rhomboid region are most likely capturing activities of the trapezius region as only surface EMG is used in this study and the rhomboids are in a deeper muscles layer.

Significant differences in activation pattern in the EMG signals were found in the trapezius pars transversa and ascendens, anterior and posterior deltoid and rhomboideus major for the internal rotation trial with 5 N load in hand.

For the neutral position trial without weight, anterior and lateral deltoid, triceps and rhomboideus major showed significant differences in the medians between the two groups. For the external rotation trial e.g. the latissimus and trapezius pars ascendens exhibited significant differences in abduction angles >70°.

These EMG activation patterns are not in agreement with the predicted changes in model activity. As the sensors placed on the rhomboids are actually capturing the activity of the trapezius, and trapezius and rhomboid sensors showed significant activation patterns, the experimental outcome agrees rather with results described by Steenbrink et al., 2010. They argued for contraction of the adductors of patients in order to achieve stability where in the model e.g. the latissimus is not active. Furthermore, a significant change in the sensors placed on the trapezius muscle regions indicates an alteration of the shoulder rhythm in patients as this muscle region is responsible for scapula kinematics. The utilised models all use the same underlying shoulder rhythm, which is not taking kinematic changes due to pain or alternative compensation schemes from the central nervous system in the form of co-contraction into account.

The discrepancy would argue that the model in its current state cannot depict symptomatic cases of tears of the m. supraspinatus accurately, as they seem to show changes in muscle regions which are either activated as co-contractors or affect the scapula kinematics.

This would indicate, that a group of patients with a tear of the m. supraspinatus follows a different activation pattern.

The modelled results might be valid for asymptomatic cases where the kinematics behave the same in a healthy and pathological population.

If the model is to be trusted however, the changes in activation are distributed evenly to the surrounding muscle elements and changes in magnitude of the activity are small, which might be undetectable by EMG measurements due to a large variance that already occurs in the healthy population (see Wickham et al., 2010).

7.5 Conclusion

From the EMG measurements it is concluded, that symptomatic patients with a tear of the m. supraspinatus might have changed kinematics and use different muscles in order to stabilize the joint which is not incorporated in the used model. The hypotheses that a generic model could predict alterations in muscle recruitment is not confirmed with this study, but that patient specific kinematics of the scapula are needed to improve the prediction. The model however could describe changes in the joint reaction forces acting on the glenoid for asymptomatic cases. This could lead to a better understanding of early stages and development of co-morbidities of a tear of the m. supraspinatus. Furthermore, the model would predict that asymptomatic cases of a tear of the m. supraspinatus are likely not detectable by the means of EMG measurements during abduction in the coronal plane.

Chapter 8

Conclusion

The purpose of this thesis is to investigate the three research questions stated in chapter 1:

1. Investigation and improvement of an existing model of the shoulder complex:
Is there an alternative explanation for the rising muscle activities and glenohumeral joint reaction force above 90° abduction? (Chapter 4 & Chapter 5)
2. Computation of several operative techniques of a biceps tendon transfer:
Is one technique closer to the healthy state of the shoulder-arm complex from a biomechanical point of view? (Chapter 6)
3. Simulation of a full tear of the m. supraspinatus with a focus on muscle activation pattern and glenohumeral joint reaction force:
Can a musculoskeletal model predict changes in the muscle recruitment of pathologies accurately? (Chapter 7)

To conclude this thesis, the answers to these three questions and the main points this work elaborates on are stated as

1. The mechanical properties of the three element Hill model are a key modelling parameter and a physiologically reasonable explanation for force behaviour in the glenohumeral joint above 90° humeral abduction. To the best of my knowledge, this strong emphasize on the Hill model for the force behaviour in the shoulder has not been described yet.
2. From a biomechanical perspective, the reinsertion technique of the biceps caput longum at the bicipital groove is the simulated closest to the healthy state with regard to forces and moments acting on the elbow if the tendon can not be reinserted at its original position. This is due to the preservation of its moment arm with regard to the elbow. This technique seems superior to other reinsertion techniques from a mechanical perspective.
3. A generic model can not predict muscle recruitment changes of patients with a symptomatic tear of the m. supraspinatus. Patient specific kinematics of the scapular seem necessary. The model however could be beneficial to explore early stages or asymptomatic cases.

Bibliography

- Ackland, David C. et al. (2008). "Moment arms of the muscles crossing the anatomical shoulder". In: *Journal of anatomy* 213.4, pp. 383–390. DOI: 10.1111/j.1469-7580.2008.00965.x.
- Ambrósio, Jorge et al. (2011). "Multibody biomechanical models of the upper limb". In: *Procedia IUTAM* 2. IUTAM Symposium on Human Body Dynamics, pp. 4–17. ISSN: 2210-9838. DOI: <https://doi.org/10.1016/j.piutam.2011.04.002>. URL: <http://www.sciencedirect.com/science/article/pii/S2210983811000034>.
- An, K. N. et al. (1984). "Determination of muscle orientations and moment arms". In: *Journal of biomechanical engineering* 106.3, pp. 280–282. ISSN: 0148-0731. DOI: 10.1115/1.3138494.
- Andersen, M. S. et al. (2010). "A computationally efficient optimisation-based method for parameter identification of kinematically determinate and over-determinate biomechanical systems". In: *Computer methods in biomechanics and biomedical engineering* 13.2, pp. 171–183. DOI: 10.1080/10255840903067080.
- Andersen, Michael Skipper (2018). "How sensitive are predicted muscle and knee contact forces to normalization factors and polynomial order in the muscle recruitment criterion formulation?" In: *International Biomechanics* 5.1, pp. 88–103. DOI: 10.1080/23335432.2018.1514278. eprint: <https://doi.org/10.1080/23335432.2018.1514278>. URL: <https://doi.org/10.1080/23335432.2018.1514278>.
- Arslan, Yunus Ziya et al. (2019). "11 - Exoskeletons, Exomusculatures, Exosuits: Dynamic Modeling and Simulation". In: *Biomechatronics*. Ed. by Marko B. Popovic. Academic Press, pp. 305–331. ISBN: 978-0-12-812939-5. DOI: <https://doi.org/10.1016/B978-0-12-812939-5.00011-2>. URL: <http://www.sciencedirect.com/science/article/pii/B9780128129395000112>.
- Aurbach, M. et al. (2020a). "Torus obstacle method as a wrapping approach of the deltoid muscle group for humeral abduction in musculoskeletal simulation". In: *Journal of Biomechanics*, p. 109864. ISSN: 0021-9290. DOI: <https://doi.org/10.1016/j.jbiomech.2020.109864>.

- 1016/j.jbiomech.2020.109864. URL: <http://www.sciencedirect.com/science/article/pii/S0021929020302876>.
- Aurbach, Maximilian et al. (2020b). "Evaluation of musculoskeletal modelling parameters of the shoulder complex during humeral abduction above 90°". In: *Journal of Biomechanics* 106, p. 109817. ISSN: 0021-9290. DOI: <https://doi.org/10.1016/j.jbiomech.2020.109817>. URL: <http://www.sciencedirect.com/science/article/pii/S0021929020302372>.
- Barbero, Marco, Roberto Merletti, and Alberto Rainoldi (2012). *Atlas of Muscle Innervation Zones: Understanding Surface Electromyography and Its Applications*. Milano: Springer. ISBN: 9788847024625. DOI: 10.1007/978-88-470-2463-2. URL: <http://site.ebrary.com/lib/alltitles/docDetail.action?docID=10595021>.
- Baumgarten, Keith M., Peter S. Chang, and Elaine K. Foley (2019). "Patient-determined outcomes after arthroscopic rotator cuff repair with and without biceps tenodesis utilizing the PITT technique". In: *Journal of shoulder and elbow surgery* 28.6, pp. 1049–1055. ISSN: 1058-2746. DOI: 10.1016/j.jse.2019.01.024.
- Bergmann, G. (2008). *Charité Universitaetsmedizin Berlin "OrthoLoad"*. Ed. by Orthoload.
- Bergmann, G. et al. (2011). "In vivo gleno-humeral joint loads during forward flexion and abduction". In: *Journal of Biomechanics* 44.8, pp. 1543–1552. ISSN: 00219290. DOI: 10.1016/j.jbiomech.2011.02.142.
- Boileau, Pascal et al. (2002). "Arthroscopic biceps tenodesis: a new technique using bioabsorbable interference screw fixation". In: *Arthroscopy : the journal of arthroscopic & related surgery : official publication of the Arthroscopy Association of North America and the International Arthroscopy Association* 18.9, 1002–1012. ISSN: 0749-8063. DOI: 10.1053/j.jars.2002.36488. URL: <https://doi.org/10.1053/j.jars.2002.36488>.
- Bolsterlee, Bart, Veeger, Dirkjan H E J, and Edward K. Chadwick (2013). "Clinical applications of musculoskeletal modelling for the shoulder and upper limb". In: *Medical & biological engineering & computing* 51.9, pp. 953–963. DOI: 10.1007/s11517-013-1099-5.
- Chard, M. D. et al. (1991). "Shoulder disorders in the elderly: A community survey". In: *Arthritis & Rheumatism* 34.6, pp. 766–769. DOI: 10.1002/art.1780340619. eprint: <https://onlinelibrary.wiley.com/doi/pdf/10.1002/art.1780340619>. URL: <https://onlinelibrary.wiley.com/doi/abs/10.1002/art.1780340619>.
- Charlton, I. W. and G. R. Johnson (2006). "A model for the prediction of the forces at the glenohumeral joint". In: *Proceedings of the Institution of Mechanical Engineers*.

- Part H, Journal of engineering in medicine* 220.8, pp. 801–812. ISSN: 0954-4119. DOI: 10.1243/09544119JEIM147.
- Crass, Jeffrey R, Edward V Craig, and Samuel B Feinberg (1988). “Ultrasonography of rotator cuff tears: a review of 500 diagnostic studies”. In: *Journal of Clinical Ultrasound* 16.5, pp. 313–327.
- Criswell, Eleanor and Jeffrey R. Cram, eds. (2011). *Cram’s introduction to surface electromyography*. 2. ed. Sudbury, MA: Jones and Bartlett. ISBN: 9780763732745.
- Damsgaard, Michael et al. (2006). “Analysis of musculoskeletal systems in the Any-Body Modeling System”. In: *Simulation Modelling Practice and Theory* 14.8, pp. 1100–1111.
- Delp, S. L. et al. (1990). “An interactive graphics-based model of the lower extremity to study orthopaedic surgical procedures”. In: *IEEE transactions on bio-medical engineering* 37.8, pp. 757–767. ISSN: 0018-9294. DOI: 10.1109/10.102791.
- Drongelen, Stefan [van et al. (2013). “The influence of simulated rotator cuff tears on the risk for impingement in handbike and handrim wheelchair propulsion”. In: *Clinical Biomechanics* 28.5, pp. 495 –501. ISSN: 0268-0033. DOI: <https://doi.org/10.1016/j.clinbiomech.2013.04.007>. URL: <http://www.sciencedirect.com/science/article/pii/S0268003313000909>.
- Edwards, Peter K et al. (2017). “A systematic review of electromyography studies in normal shoulders to inform postoperative rehabilitation following rotator cuff repair”. In: *journal of orthopaedic & sports physical therapy* 47.12, pp. 931–944.
- Ekstrom, Richard A. and Roy W. Osborn (2004). “Chapter 15 - Muscle Length Testing and Electromyographic Data for Manual Strength Testing and Exercises for the Shoulder”. In: *Physical Therapy of the Shoulder (Fourth Edition)*. Ed. by Robert A. Donatelli. Fourth Edition. Saint Louis: Churchill Livingstone, pp. 435 –463. ISBN: 978-0-443-06614-6. DOI: <https://doi.org/10.1016/B978-044306614-6.50017-X>. URL: <http://www.sciencedirect.com/science/article/pii/B978044306614650017X>.
- Favre, Philippe, Jess G. Snedeker, and Christian Gerber (2009). “Numerical modelling of the shoulder for clinical applications”. In: *Philosophical transactions. Series A, Mathematical, physical, and engineering sciences* 367.1895, pp. 2095–2118. ISSN: 1364-503X. DOI: 10.1098/rsta.2008.0282.
- Ferri, Melanie et al. (2005). “Sonography of full-thickness supraspinatus tears: comparison of patient positioning technique with surgical correlation”. In: *American Journal of Roentgenology* 184.1, pp. 180–184.

- Flores-Hernandez, Cesar et al. (2019). "Scapulothoracic rhythm affects glenohumeral joint force". In: *JSES Open Access* 3.2, pp. 77 –82. ISSN: 2468-6026. DOI: <https://doi.org/10.1016/j.jses.2019.03.004>. URL: <http://www.sciencedirect.com/science/article/pii/S2468602619300129>.
- Forsythe, Brian et al. (2020). "Arthroscopic Suprapectoral and Open Subpectoral Biceps Tenodeses Produce Similar Outcomes: A Randomized Prospective Analysis". In: *Arthroscopy : the journal of arthroscopic & related surgery : official publication of the Arthroscopy Association of North America and the International Arthroscopy Association* 36.1, pp. 23–32. ISSN: 0749-8063. DOI: 10.1016/j.arthro.2019.07.009.
- Fucentese, Sandro et al. (2012). "Evolution of nonoperatively treated symptomatic isolated full-thickness supraspinatus tears." In: *The Journal of bone and joint surgery. American volume* 94 9, pp. 801–8.
- Fuglsang-Frederiksen, Anders (2006). "The role of different EMG methods in evaluating myopathy". In: *Clinical Neurophysiology* 117.6, pp. 1173–1189. ISSN: 13882457. DOI: 10.1016/j.clinph.2005.12.018.
- Gasbarro, Gregory, Benjamin Bondow, and Richard Debski (2017). "Clinical anatomy and stabilizers of the glenohumeral joint". In: *Annals of Joint* 2.10. URL: <http://aoj.amegroups.com/article/view/3864>.
- Gillooly, John Joseph, Ramiah Chidambaram, and Daniel Mok (2010). "The lateral Jobe test: A more reliable method of diagnosing rotator cuff tears". In: *International journal of shoulder surgery* 4.2, pp. 41–43. ISSN: 0973-6042. DOI: 10.4103/0973-6042.70822.
- Glaits, Sergio A. et al. (2018). "Regional histologic differences in the long head of the biceps tendon following subpectoral biceps tenodesis in patients with rotator cuff tears and SLAP lesions". In: *Knee surgery, sports traumatology, arthroscopy : official journal of the ESSKA* 26.8, pp. 2481–2489. ISSN: 0942-2056. DOI: 10.1007/s00167-018-4839-0.
- Gowd, Anirudh K., Edward C. Beck, and Brian R. Waterman (2020). "Editorial Commentary: Aim High or Go Low? Outcomes Are Equivalent for Arthroscopic Suprapectoral and Mini-open Subpectoral Biceps Tenodesis". In: *Arthroscopy: The Journal of Arthroscopic & Related Surgery* 36.1, pp. 33 –35. ISSN: 0749-8063. DOI: <https://doi.org/10.1016/j.arthro.2019.08.022>. URL: <http://www.sciencedirect.com/science/article/pii/S0749806319307224>.

- Graichen, Heiko et al. (2000). "Glenohumeral translation during active and passive elevation of the shoulder — a 3D open-MRI study". In: *Journal of Biomechanics* 33.5, pp. 609–613. ISSN: 00219290. DOI: 10.1016/S0021-9290(99)00209-2.
- Groot, J. H. de and R. Brand (2001). "A three-dimensional regression model of the shoulder rhythm". In: *Clinical biomechanics (Bristol, Avon)* 16.9, pp. 735–743. ISSN: 0268-0033. DOI: 10.1016/S0268-0033(01)00065-1.
- Groot, Jurriaan H. de et al. (2004). "Isometric shoulder muscle activation patterns for 3-D planar forces: a methodology for musculo-skeletal model validation". In: *Clinical biomechanics (Bristol, Avon)* 19.8, pp. 790–800. ISSN: 0268-0033. DOI: 10.1016/j.clinbiomech.2004.05.013.
- Gumina, Stefano et al. (2011). "Rupture of the long head biceps tendon treated with tenodesis to the coracoid process. Results at more than 30 years". In: *International orthopaedics* 35.5, pp. 713–716. ISSN: 0341-2695. DOI: 10.1007/s00264-010-1099-0.
- Halder, A. M. et al. (2001). "Dynamic contributions to superior shoulder stability". In: *Journal of orthopaedic research : official publication of the Orthopaedic Research Society* 19.2, pp. 206–212. DOI: 10.1016/S0736-0266(00)00028-0.
- Hashizume, Satoru et al. (2016). "Comparison of the Achilles tendon moment arms determined using the tendon excursion and three-dimensional methods". In: *Physiological Reports* 4.19, e12967. DOI: 10.14814/phy2.12967. eprint: <https://physoc.onlinelibrary.wiley.com/doi/pdf/10.14814/phy2.12967>. URL: <https://physoc.onlinelibrary.wiley.com/doi/abs/10.14814/phy2.12967>.
- Havelková, L. (2016). "Biomechanical musculoskeletal model." PhD thesis. University of West Bohemia, Plzeň.
- Havelková L., Špička J. Vychytil J. Aurbach M. and Z. Krňoul (2018). "Torus-obstacle method used for representing muscle path in musculoskeletal models." In: *In Proceeding of the 8th World Congress of Biomechanics, Dublin, Ireland*.
- Hawi, Nael et al. (2017). "Pulley lesions in rotator cuff tears: prevalence, etiology, and concomitant pathologies". In: *Archives of orthopaedic and trauma surgery* 137.8, pp. 1097–1105. DOI: 10.1007/s00402-017-2721-z.
- Hill, Archibald Vivian (1938). "The heat of shortening and the dynamic constants of muscle". In: *Proceedings of the Royal Society of London. Series B - Biological Sciences* 126.843, pp. 136–195. DOI: 10.1098/rspb.1938.0050. eprint: <https://royalsocietypublishing.org/doi/pdf/10.1098/rspb.1938.0050>. URL: <https://royalsocietypublishing.org/doi/abs/10.1098/rspb.1938.0050>.

- Holmberg, L. Joakim and Anders Klarbring (2012). "Muscle decomposition and recruitment criteria influence muscle force estimates". In: *Multibody System Dynamics* 28.3, pp. 283–289. ISSN: 1384-5640. DOI: 10.1007/s11044-011-9277-4. URL: <https://doi.org/10.1007/s11044-011-9277-4>.
- Hölscher, Thomas et al. (2016a). "Influence of rotator cuff tears on glenohumeral stability during abduction tasks". In: *Journal of orthopaedic research : official publication of the Orthopaedic Research Society* 34.9, pp. 1628–1635. DOI: 10.1002/jor.23161.
- (2016b). "Influence of rotator cuff tears on glenohumeral stability during abduction tasks". In: *Journal of orthopaedic research : official publication of the Orthopaedic Research Society* 34.9, pp. 1628–1635. DOI: 10.1002/jor.23161.
- Howell, S. M. et al. (1986). "Clarification of the role of the supraspinatus muscle in shoulder function". In: *JBJS* 68.3, pp. 398–404. ISSN: 0021-9355. URL: https://journals.lww.com/jbjsjournal/Fulltext/1986/68030/Clarification_of_the_role_of_the_supraspinatus.13.aspx.
- Hurley, Eoghan T. et al. (2018). "Biceps tenodesis versus labral repair for superior labrum anterior-to-posterior tears: a systematic review and meta-analysis". In: *Journal of shoulder and elbow surgery* 27.10, pp. 1913–1919. ISSN: 1058-2746. DOI: 10.1016/j.jse.2018.04.011.
- Itoi, Eiji et al. (1999). "Which is More Useful, the "Full Can Test" or the "Empty Can Test," in Detecting the Torn Supraspinatus Tendon?" In: *The American Journal of Sports Medicine* 27.1. PMID: 9934421, pp. 65–68. DOI: 10.1177/03635465990270011901. eprint: <https://doi.org/10.1177/03635465990270011901>. URL: <https://doi.org/10.1177/03635465990270011901>.
- Juul-Kristensen, B. et al. (2000). "Muscle sizes and moment arms of rotator cuff muscles determined by magnetic resonance imaging". In: *Cells, tissues, organs* 167.2-3, pp. 214–222. ISSN: 1422-6405. DOI: 10.1159/000016784.
- Kai, Yoshihiro et al. (2015). "Electromyographic study of rotator cuff muscle activity during full and empty can tests". In: *Asia-Pacific Journal of Sports Medicine, Arthroscopy, Rehabilitation and Technology* 2.1, pp. 36–41. ISSN: 2214-6873. DOI: <https://doi.org/10.1016/j.asmart.2014.12.001>. URL: <http://www.sciencedirect.com/science/article/pii/S2214687314000752>.
- Keating, J. F. et al. (1993). "The relative strengths of the rotator cuff muscles. A cadaver study". In: *The Journal of bone and joint surgery. British volume* 75.1, pp. 137–140. ISSN: 0301-620X.

- Kerschbaum, Maximilian et al. (2019). "Novel implant-free loop Tenodesis vs. simple Tenotomy of the long biceps tendon - a biomechanical investigation". In: *BMC musculoskeletal disorders* 20.1, p. 522. ISSN: 1471-2474. DOI: 10.1186/s12891-019-2919-z.
- Konrad, Peter (2006). *The ABC of EMG: a practical introduction to kinesiological electromyography*. Version 1.4. Noraxon USA, Inc. ISBN: 0977162214. URL: <http://www.noraxon.com/>.
- Lee, Choon-Key et al. (2014). "Comparison of muscle activity in the empty-can and full-can testing positions using 18 F-FDG PET/CT". In: *Journal of orthopaedic surgery and research* 9, p. 85. DOI: 10.1186/s13018-014-0085-4.
- Leschinger, Tim et al. (2019). "A musculoskeletal shoulder simulation of moment arms and joint reaction forces after medialization of the supraspinatus footprint in rotator cuff repair". In: *Computer Methods in Biomechanics and Biomedical Engineering* 22.6. PMID: 30835541, pp. 595–604. DOI: 10.1080/10255842.2019.1572749. eprint: <https://doi.org/10.1080/10255842.2019.1572749>. URL: <https://doi.org/10.1080/10255842.2019.1572749>.
- Ludewig, Paula M. et al. (2009). "Motion of the shoulder complex during multiplanar humeral elevation". In: *The Journal of bone and joint surgery. American volume* 91.2, pp. 378–389. DOI: 10.2106/JBJS.G.01483.
- Lund, Morten, John Rasmussen, and Michael Andersen (2019). "AnyPyTools: A Python package for reproducible research with the AnyBody Modeling System". In: *Journal of Open Source Software* 4.33, p. 1108. DOI: 10.21105/joss.01108.
- Lund, Morten Enemark et al. (2012). "On validation of multibody musculoskeletal models". In: *Proceedings of the Institution of Mechanical Engineers. Part H, Journal of engineering in medicine* 226.2, pp. 82–94. ISSN: 0954-4119. DOI: 10.1177/0954411911431516.
- Mack, Laurence A et al. (1985). "US evaluation of the rotator cuff." In: *Radiology* 157.1, pp. 205–209.
- Magrers, D.J. et al. (2004a). "Biomechanical analysis of tendon transfers for massive rotator cuff tears". In: *Clinical Biomechanics* 19.4, pp. 350–357. ISSN: 0268-0033. DOI: <https://doi.org/10.1016/j.clinbiomech.2003.11.013>. URL: <http://www.sciencedirect.com/science/article/pii/S0268003303002687>.
- Magrers, D.J et al. (2004b). "Effectiveness of tendon transfers for massive rotator cuff tears: a simulation study". In: *Clinical Biomechanics* 19.2, pp. 116–122. ISSN:

- 0268-0033. DOI: <https://doi.org/10.1016/j.clinbiomech.2003.09.008>. URL: <http://www.sciencedirect.com/science/article/pii/S0268003303002195>.
- Mahaphonchaikul, K. et al. (2010). "EMG signal feature extraction based on wavelet transform". In: *ECTI-CON2010: The 2010 ECTI International Confernce on Electrical Engineering/Electronics, Computer, Telecommunications and Information Technology*, pp. 327–331.
- Mall, Nathan A. et al. (2010). "Symptomatic progression of asymptomatic rotator cuff tears: a prospective study of clinical and sonographic variables". In: *The Journal of bone and joint surgery. American volume* 92.16, pp. 2623–2633. DOI: 10.2106/JBJS.I.00506.
- Man, Kam (2017). "A validation method to find moment arm of the deltoid from MRI images." MA thesis. Ecole de technologie superieure universite du Quebec, Montreal, Canada.
- Mariani, E. M. et al. (1988). "Rupture of the tendon of the long head of the biceps brachii. Surgical versus nonsurgical treatment". In: *Clinical orthopaedics and related research* 228, pp. 233–239. ISSN: 0009-921X.
- Marra, Marco A. et al. (2015). "A subject-specific musculoskeletal modeling framework to predict in vivo mechanics of total knee arthroplasty". In: *Journal of biomechanical engineering* 137.2, p. 020904. ISSN: 0148-0731. DOI: 10.1115/1.4029258.
- Massimini, Daniel F. et al. (2012). "In-vivo glenohumeral translation and ligament elongation during abduction and abduction with internal and external rotation". In: *Journal of orthopaedic surgery and research* 7, p. 29. DOI: 10.1186/1749-799X-7-29.
- Meyer, Markus, Jenny Wenzel, and Antje Schenkel (2018). "Krankheitsbedingte Fehlzeiten in der deutschen Wirtschaft im Jahr 2017". In: *Fehlzeiten-Report 2018: Sinn erleben – Arbeit und Gesundheit*. Ed. by Bernhard Badura et al. Berlin, Heidelberg: Springer Berlin Heidelberg, pp. 331–536. ISBN: 978-3-662-57388-4. DOI: 10.1007/978-3-662-57388-4_29. URL: https://doi.org/10.1007/978-3-662-57388-4_29.
- Minagawa, Hiroshi et al. (2013). "Prevalence of symptomatic and asymptomatic rotator cuff tears in the general population: From mass-screening in one village". In: *Journal of orthopaedics* 10.1, pp. 8–12. ISSN: 0972-978X. DOI: 10.1016/j.jor.2013.01.008.
- Moor, B.K. et al. (2014). "Age, trauma and the critical shoulder angle accurately predict supraspinatus tendon tears". In: *Orthopaedics & Traumatology: Surgery & Research* 100.5, pp. 489–494. ISSN: 1877-0568. DOI: <https://doi.org/10.1016/j.>

- otsr.2014.03.022. URL: <http://www.sciencedirect.com/science/article/pii/S1877056814001236>.
- Moosmayer, Stefan et al. (2013). "The natural history of asymptomatic rotator cuff tears: a three-year follow-up of fifty cases". In: *The Journal of bone and joint surgery. American volume* 95.14, pp. 1249–1255. DOI: 10.2106/JBJS.L.00185.
- Moppes, Floris I van, Onno Veldkamp, and Jan Roorda (1995). "Role of shoulder ultrasonography in the evaluation of the painful shoulder". In: *European journal of radiology* 19.2, pp. 142–146.
- Morrow, Melissa M. B., Kenton R. Kaufman, and Kai-Nan An (2010). "Shoulder model validation and joint contact forces during wheelchair activities". In: *Journal of Biomechanics* 43.13, pp. 2487–2492. ISSN: 00219290. DOI: 10.1016/j.jbiomech.2010.05.026.
- Na, Yuyan et al. (2019). "A meta-analysis comparing tenotomy or tenodesis for lesions of the long head of the biceps tendon with concomitant reparable rotator cuff tears". In: DOI: 10.1186/s13018-019-1429-x.
- Neumann, Donald A. (2002). *Kinesiology of the musculoskeletal system : foundations for physical rehabilitation*. First edition. St. Louis : Mosby, [2002] ©2002. URL: <https://search.library.wisc.edu/catalog/999931373602121>.
- Nikooyan, A. A. et al. (2010). "Validation of the Delft Shoulder and Elbow Model using in-vivo glenohumeral joint contact forces". In: *Journal of Biomechanics* 43.15, pp. 3007–3014. ISSN: 00219290. DOI: 10.1016/j.jbiomech.2010.06.015.
- Nikooyan, A. A. et al. (2012). "An EMG-driven musculoskeletal model of the shoulder". In: *Human movement science* 31.2, pp. 429–447. DOI: 10.1016/j.humov.2011.08.006.
- Nikooyan, A. Asadi et al. (2011). "Development of a comprehensive musculoskeletal model of the shoulder and elbow". In: *Medical & biological engineering & computing* 49.12, pp. 1425–1435. DOI: 10.1007/s11517-011-0839-7.
- Nussbaum, M. A., D. B. Chaffin, and C. J. Rehtien (1995). "Muscle lines-of-action affect predicted forces in optimization-based spine muscle modeling". In: *Journal of Biomechanics* 28.4, pp. 401–409. ISSN: 00219290. DOI: 10.1016/0021-9290(94)00078-i.
- Oh, Joo Han et al. (2011). "Does a critical rotator cuff tear stage exist?: a biomechanical study of rotator cuff tear progression in human cadaver shoulders". In: *The Journal of bone and joint surgery. American volume* 93.22, pp. 2100–2109. DOI: 10.2106/JBJS.J.00032.

- O'Neill, Matthew C. et al. (2013). "A three-dimensional musculoskeletal model of the chimpanzee (*Pan troglodytes*) pelvis and hind limb". In: *Journal of Experimental Biology* 216.19, pp. 3709–3723. ISSN: 0022-0949. DOI: 10.1242/jeb.079665. eprint: <https://jeb.biologists.org/content/216/19/3709.full.pdf>. URL: <https://jeb.biologists.org/content/216/19/3709>.
- Phinyomark, A., C. Limsakul, and P. Phukpattaranont (Jan. 2011). "Application of Wavelet Analysis in EMG Feature Extraction for Pattern Classification". In: *Measurement Science Review* 11.2, pp. 45–52. DOI: 10.2478/v10048-011-0009-y.
- Pope, Daniel P et al. (1997). "Prevalence of shoulder pain in the community: the influence of case definition". In: *Annals of the Rheumatic Diseases* 56.5, pp. 308–312. ISSN: 0003-4967. DOI: 10.1136/ard.56.5.308. eprint: <https://ard.bmj.com/content/56/5/308.full.pdf>. URL: <https://ard.bmj.com/content/56/5/308>.
- Pribicevic, Mario (2012). "The Epidemiology of Shoulder Pain: A Narrative Review of the Literature". In: *Pain in Perspective*. Ed. by Subhamay Ghosh. Rijeka: IntechOpen. Chap. 7. DOI: 10.5772/52931. URL: <https://doi.org/10.5772/52931>.
- Prinold, Joe A. I. et al. (2013). "Musculoskeletal shoulder models: a technical review and proposals for research foci". In: *Proceedings of the Institution of Mechanical Engineers. Part H, Journal of engineering in medicine* 227.10, pp. 1041–1057. ISSN: 0954-4119. DOI: 10.1177/0954411913492303.
- Quinn, Stephen F et al. (1995). "Rotator cuff tendon tears: evaluation with fat-suppressed MR imaging with arthroscopic correlation in 100 patients." In: *Radiology* 195.2, pp. 497–500.
- Raikova, R. T. and B. I. Prilutsky (2001). "Sensitivity of predicted muscle forces to parameters of the optimization-based human leg model revealed by analytical and numerical analyses". In: *Journal of Biomechanics* 34.10, pp. 1243–1255. ISSN: 00219290. DOI: 10.1016/s0021-9290(01)00097-5.
- Rajaratnam, Bala (2014). "A Comparison of EMG Signals from Surface and Fine-Wire Electrodes During Shoulder Abduction". In: *International Journal of Physical Medicine & Rehabilitation* 02.04. DOI: 10.4172/2329-9096.1000206.
- Rasmussen, John et al. (2005). "A General Method for Scaling Musculo-Skeletal Models". In: *2005 International Symposium on Computer Simulation in Biomechanics*.
- Rassier, D. E., B. R. MacIntosh, and W. Herzog (1999). "Length dependence of active force production in skeletal muscle". In: *Journal of applied physiology (Bethesda, Md. : 1985)* 86.5, pp. 1445–1457. ISSN: 0161-7567. DOI: 10.1152/jappl.1999.86.5.1445.

- Reinold, Michael M. et al. (2007a). "Electromyographic analysis of the supraspinatus and deltoid muscles during 3 common rehabilitation exercises". In: *Journal of athletic training* 42.4, pp. 464–469. ISSN: 1062-6050.
- (2007b). "Electromyographic analysis of the supraspinatus and deltoid muscles during 3 common rehabilitation exercises". In: *Journal of athletic training* 42.4, pp. 464–469. ISSN: 1062-6050.
- (2007c). "Electromyographic analysis of the supraspinatus and deltoid muscles during 3 common rehabilitation exercises". In: *Journal of athletic training* 42.4, pp. 464–469. ISSN: 1062-6050.
- Ringelberg, J. A. (1985). "EMG and force production of some human shoulder muscles during isometric abduction". In: *Journal of Biomechanics* 18.12, pp. 939–947. ISSN: 00219290. DOI: 10.1016/0021-9290(85)90037-5.
- Sakaki, Y. et al. (2015). "Electromyographic characteristics of shoulder muscles after rotator cuff repair". In: *Physiotherapy* 101. World Confederation for Physical Therapy Congress 2015 Abstracts, Singapore, 1-4 May 2015, e1319 –e1320. ISSN: 0031-9406. DOI: <https://doi.org/10.1016/j.physio.2015.03.1244>. URL: <http://www.sciencedirect.com/science/article/pii/S0031940615012742>.
- Sakurai, G. et al. (1998). "Morphologic changes in long head of biceps brachii in rotator cuff dysfunction". In: *Journal of orthopaedic science : official journal of the Japanese Orthopaedic Association* 3.3, pp. 137–142. ISSN: 0949-2658. DOI: 10.1007/s007760050033.
- Scapinelli, R. et al. (1999). "Subcutaneous rupture of the tendon of the long head of the biceps brachii in subacromial impingement syndrome". In: *La Chirurgia degli organi di movimento* 84.3, pp. 229–237. ISSN: 0009-4749.
- Schoch, Christian, Michael Geyer, and Björn Drews (2017). "Suprapectoral biceps tenodesis using a suture plate: clinical results after 2 years". In: *Archives of orthopaedic and trauma surgery* 137.6, pp. 829–835. DOI: 10.1007/s00402-017-2664-4.
- Schünke, M., E. Schulte, and U. Schumacher (2007). *Prometheus - LernAtlas der Anatomie: allgemeine Anatomie und Bewegungssystem ; 182 Tabellen*. Vol. Erik Schulte; Udo Schumacher. Unter Mitarb. von Jürgen Rude. Ill. von Markus Voll; Karl Wesker. Prometheus : LernAtlas der Anatomie / Michael Schünke. Thieme. ISBN: 9783131395221. URL: <https://books.google.de/books?id=olMVD14Ao08C>.
- Scovil, Carol Y. and Janet L. Ronsky (2006). "Sensitivity of a Hill-based muscle model to perturbations in model parameters". In: *Journal of Biomechanics* 39.11, pp. 2055 –

2063. ISSN: 0021-9290. DOI: <https://doi.org/10.1016/j.jbiomech.2005.06.005>. URL: <http://www.sciencedirect.com/science/article/pii/S0021929005002770>.
- Sins, Lauranne et al. (2015). "Adaptation of the AnyBody™ Musculoskeletal Shoulder Model to the Nonconforming Total Shoulder Arthroplasty Context". In: *Journal of biomechanical engineering* 137.10, p. 101006. DOI: 10.1115/1.4031330.
- Skipper Andersen, Michael et al. (2017). "Introduction to Force-Dependent Kinematics: Theory and Application to Mandible Modeling". In: *Journal of biomechanical engineering* 139.9. DOI: 10.1115/1.4037100.
- Solomonow, M. et al. (1994). "Surface and wire EMG crosstalk in neighbouring muscles". In: *Journal of Electromyography and Kinesiology* 4.3, pp. 131–142. ISSN: 10506411. DOI: 10.1016/1050-6411(94)90014-0.
- Soslowsky, L. J., D. M. Malicky, and R. B. Blasier (1997). "Active and passive factors in inferior glenohumeral stabilization: a biomechanical model". In: *Journal of shoulder and elbow surgery* 6.4, pp. 371–379. ISSN: 1058-2746. DOI: 10.1016/s1058-2746(97)90005-7.
- Steenbrink, F. et al. (2009). "Glenohumeral stability in simulated rotator cuff tears". In: *Journal of Biomechanics* 42.11, pp. 1740–1745. ISSN: 0021-9290. DOI: <https://doi.org/10.1016/j.jbiomech.2009.04.011>. URL: <http://www.sciencedirect.com/science/article/pii/S0021929009002115>.
- Steenbrink, Frans et al. (2010). "The relation between increased deltoid activation and adductor muscle activation due to glenohumeral cuff tears". In: *Journal of Biomechanics* 43.11, pp. 2049–2054. ISSN: 0021-9290. DOI: <https://doi.org/10.1016/j.jbiomech.2010.04.012>. URL: <http://www.sciencedirect.com/science/article/pii/S0021929010002241>.
- Strzelczak, M. et al. (2018). "A new wrapping approach for the deltoid muscle modelling." In: *The Proceedings of the 20th Biennial Meeting of the Canadian Society for Biomechanics* (2018).
- Timmons, Mark K et al. (2016). "Empty can exercise provokes more pain and has undesirable biomechanics compared with the full can exercise". In: *Journal of shoulder and elbow surgery* 25.4, pp. 548–556.
- van der Helm, F.C.T. (1994a). "A finite element musculoskeletal model of the shoulder mechanism". In: *Journal of Biomechanics* 27.5, pp. 551–569. ISSN: 00219290. DOI: 10.1016/0021-9290(94)90065-5.

- van der Helm, F.C.T. (1994b). "Analysis of the kinematic and dynamic behavior of the shoulder mechanism". In: *Journal of Biomechanics* 27.5, pp. 527–550. ISSN: 0021-9290. DOI: 10.1016/0021-9290(94)90064-7.
- van der Windt, D A et al. (1995). "Shoulder disorders in general practice: incidence, patient characteristics, and management." In: *Annals of the Rheumatic Diseases* 54.12, pp. 959–964. ISSN: 0003-4967. DOI: 10.1136/ard.54.12.959. eprint: <https://ard.bmj.com/content/54/12/959.full.pdf>. URL: <https://ard.bmj.com/content/54/12/959>.
- Veeger, H.E.J. and F.C.T. [van der Helm] (2007). "Shoulder function: The perfect compromise between mobility and stability". In: *Journal of Biomechanics* 40.10, pp. 2119–2129. ISSN: 0021-9290. DOI: <https://doi.org/10.1016/j.jbiomech.2006.10.016>. URL: <http://www.sciencedirect.com/science/article/pii/S0021929006003812>.
- Vidt, Meghan E. et al. (2018). "Modeling a rotator cuff tear: Individualized shoulder muscle forces influence glenohumeral joint contact force predictions". In: *Clinical Biomechanics* 60, pp. 20–29. ISSN: 0268-0033. DOI: <https://doi.org/10.1016/j.clinbiomech.2018.10.004>. URL: <http://www.sciencedirect.com/science/article/pii/S0268003318304418>.
- Voss, Andreas, Andreas B. Imhoff, and Felix Dyrna (2018). "Intra-Articular Tenodesis of the Long Head of the Biceps Tendon". In: *Operative Techniques in Sports Medicine* 26.2, pp. 86–90. ISSN: 1060-1872. DOI: <https://doi.org/10.1053/j.otsm.2018.02.004>. URL: <http://www.sciencedirect.com/science/article/pii/S1060187218300157>.
- Voss, Andreas et al. (2016). "Open Subpectoral Tenodesis of the Proximal Biceps". In: *Clinics in sports medicine* 35.1, pp. 137–152. ISSN: 0278-5919. DOI: 10.1016/j.csm.2015.08.007.
- Voss, Andreas et al. (2017). "Open subpectoral biceps tenodesis in patients over 65 does not result in an increased rate of complications". In: *BMC musculoskeletal disorders* 18.1, p. 430. ISSN: 1471-2474. DOI: 10.1186/s12891-017-1780-1.
- Špička J., Vychytil J. Ryba T. and L. Havelková (2018). "Development of a Personalized Musculoskeletal Human Shoulder Model." In: *In Proceeding of the Computational Mechanics 2018. University of West Bohemia*.
- Walch, Gilles et al. (2005). "Arthroscopic tenotomy of the long head of the biceps in the treatment of rotator cuff tears: clinical and radiographic results of 307 cases". In: *Journal of shoulder and elbow surgery* 14.3, pp. 238–246. ISSN: 1058-2746. DOI: 10.1016/j.jse.2004.07.008.

- Wang, Gang et al. (2014). "The Analysis of Surface EMG Signals with the Wavelet-Based Correlation Dimension Method". In: *Computational and mathematical methods in medicine* 2014, p. 284308. DOI: 10.1155/2014/284308. URL: <https://doi.org/10.1155/2014/284308>.
- Warner, J. J. and P. J. McMahon (1995). "The role of the long head of the biceps brachii in superior stability of the glenohumeral joint". In: *The Journal of bone and joint surgery. American volume* 77.3, pp. 366–372. DOI: 10.2106/00004623-199503000-00006.
- Wataru, Sahara et al. (2005). "Three-dimensional morphological analysis of humeral heads". In: *Acta Orthopaedica* 76.3, pp. 392–396. ISSN: 1745-3674. DOI: 10.1080/00016470510030878.
- Wickham, James et al. (2010). "Quantifying 'normal' shoulder muscle activity during abduction". In: *Journal of electromyography and kinesiology : official journal of the International Society of Electrophysiological Kinesiology* 20.2, pp. 212–222. DOI: 10.1016/j.jelekin.2009.06.004.
- Wiener, Stephen N and William H Seitz Jr (1993). "Sonography of the shoulder in patients with tears of the rotator cuff: accuracy and value for selecting surgical options." In: *AJR. American journal of roentgenology* 160.1, pp. 103–107.
- Witte, P. B. de et al. (2014a). "The Supraspinatus and the Deltoid - not just two arm elevators". In: *Human movement science* 33, pp. 273–283. DOI: 10.1016/j.humov.2013.08.010.
- Witte, PB de et al. (2014b). "Cranial humerus translation, deltoid activation, adductor co-activation and rotator cuff disease—Different patterns in rotator cuff tears, subacromial impingement and controls". In: *Clinical Biomechanics* 29.1, pp. 26–32.
- Witte, Pieter Bas de et al. (2012). "Arm Adductor with arm Abduction in rotator cuff tear patients vs. healthy—Design of a new measuring instrument". In: *Human movement science* 31.2, pp. 461–471.
- Wolf, Anthony D. and Bruce Pflieger (2003). "Burden of major musculoskeletal conditions". In: *Bulletin of the World Health Organization* 81.9, pp. 646–656. ISSN: 0042-9686.
- World Health Organization (2016). *World health statistics 2016: monitoring health for the SDGs, sustainable development goals*. World Health Organization, 121 p.
- Wuelker, N. et al. (1994a). "Function of the supraspinatus muscle. Abduction of the humerus studied in cadavers". In: *Acta orthopaedica Scandinavica* 65.4, pp. 442–446. ISSN: 0001-6470. DOI: 10.3109/17453679408995490.

Wuelker, Nikolaus et al. (1994b). "Function of the supraspinatus muscle: Abduction of the humerus studied in cadavers". In: *Acta Orthopaedica Scandinavica* 65.4, pp. 442–446. DOI: 10.3109/17453679408995490. eprint: <https://www.tandfonline.com/doi/pdf/10.3109/17453679408995490>. URL: <https://www.tandfonline.com/doi/abs/10.3109/17453679408995490>.

Yamamoto, Atsushi et al. (2010). "Prevalence and risk factors of a rotator cuff tear in the general population". In: *Journal of shoulder and elbow surgery* 19.1, pp. 116–120. ISSN: 1058-2746. DOI: 10.1016/j.jse.2009.04.006.

Appendix A

Supplementary material to chapter 5

A.1 Activity of the deltoids and GH joint reaction force of the ellipsoid model

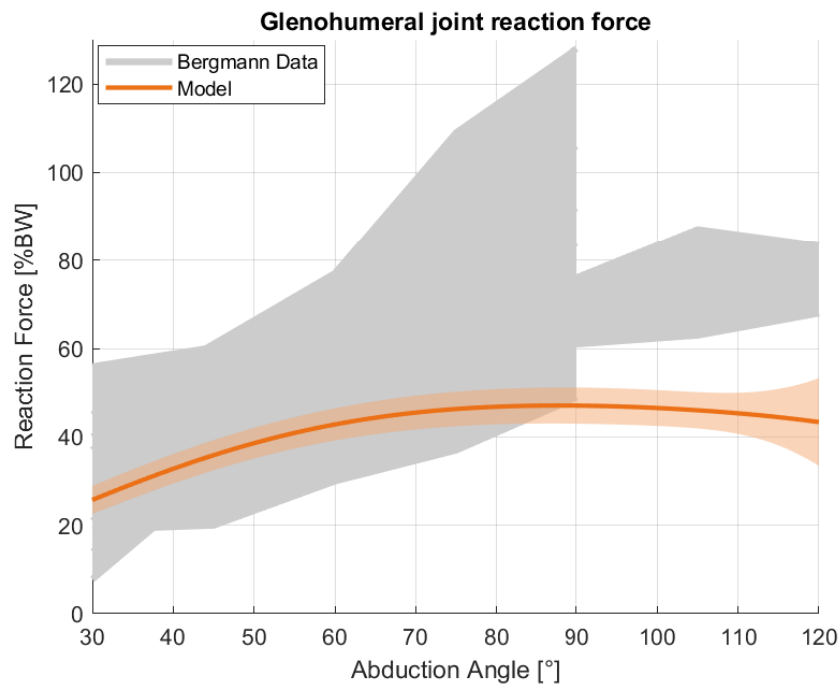


FIGURE A.1: Resultant GHJF in the range of 20 – 120° humeral abduction. The grey shaded area is an envelope of the in-vivo data obtained by Bergmann et al. The orange line is the average calculated GHJF from the motion capture models with ellipsoid wrapping and $p = 5$, with the orange shaded area representing the standard deviation.

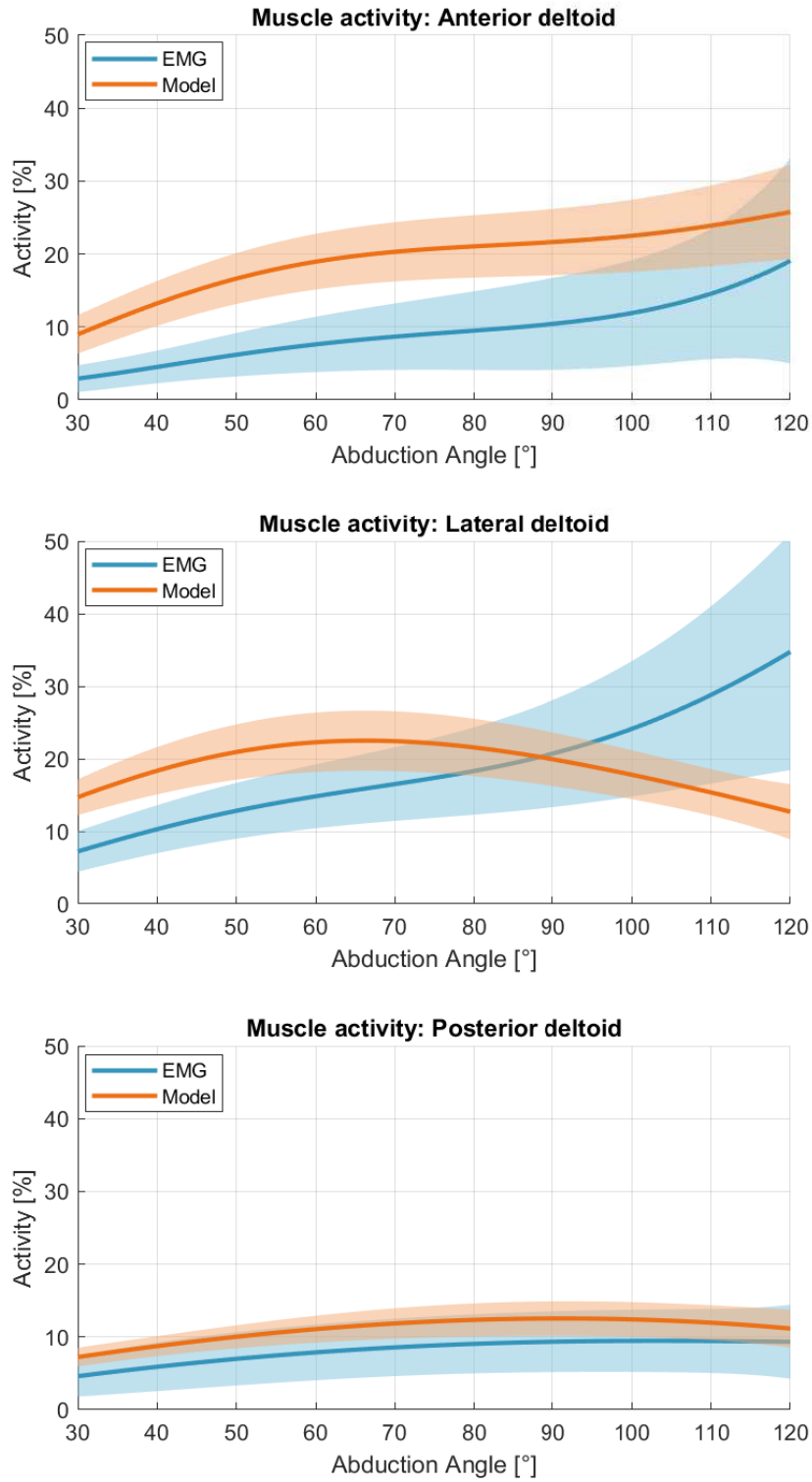


FIGURE A.2: Activity of the anterior, lateral and posterior deltoid groups during abduction between 30-120° of the EMG mean (blue) and the ellipsoid model with $p = 5$ (orange). Standard deviations are provided by the corresponding shaded areas

A.2 Lateral and posterior momentarm comparison

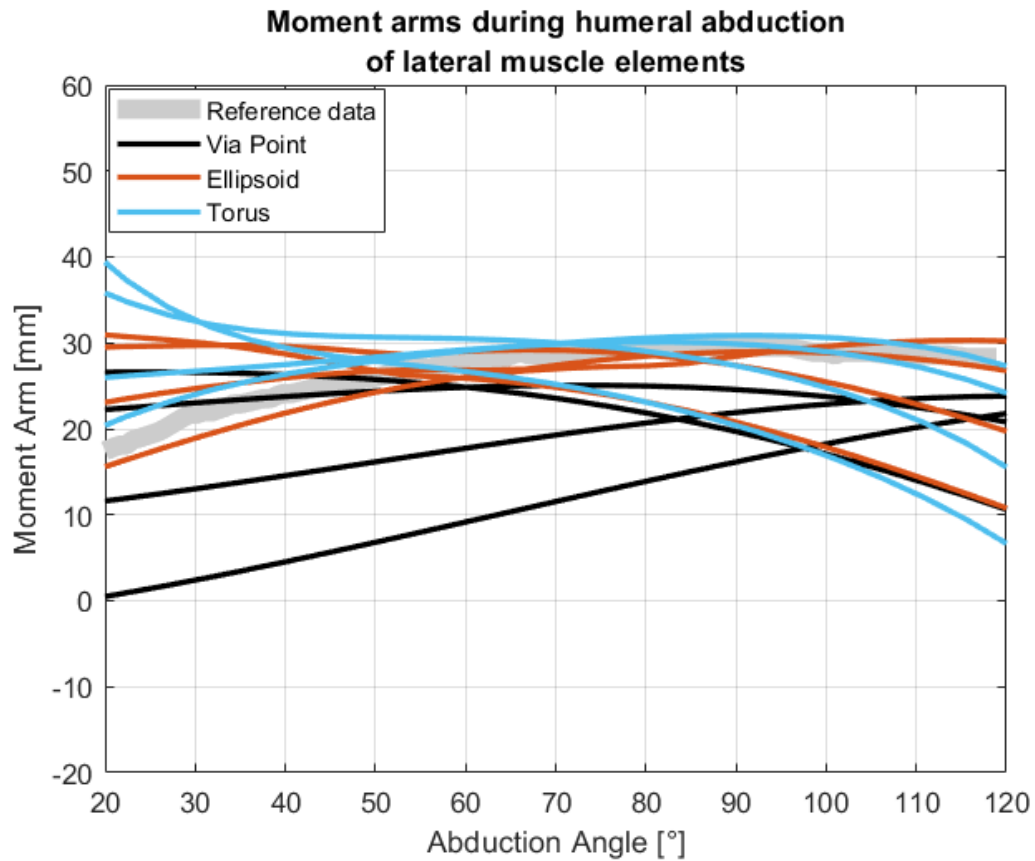


FIGURE A.3: Moment arms during glenohumeral abduction in the range 20 – 120° of the lateral deltoid elements. Grey: moment arms from a cadaver study by Ackland et al., 2008 Black: lateral deltoid moment arms of the via point model, 4 associated model elements. Orange: lateral deltoid moment arms of the ellipsoid model, 4 associated model elements. Blue: lateral deltoid moment arms of the torus model, 4 associated model elements.

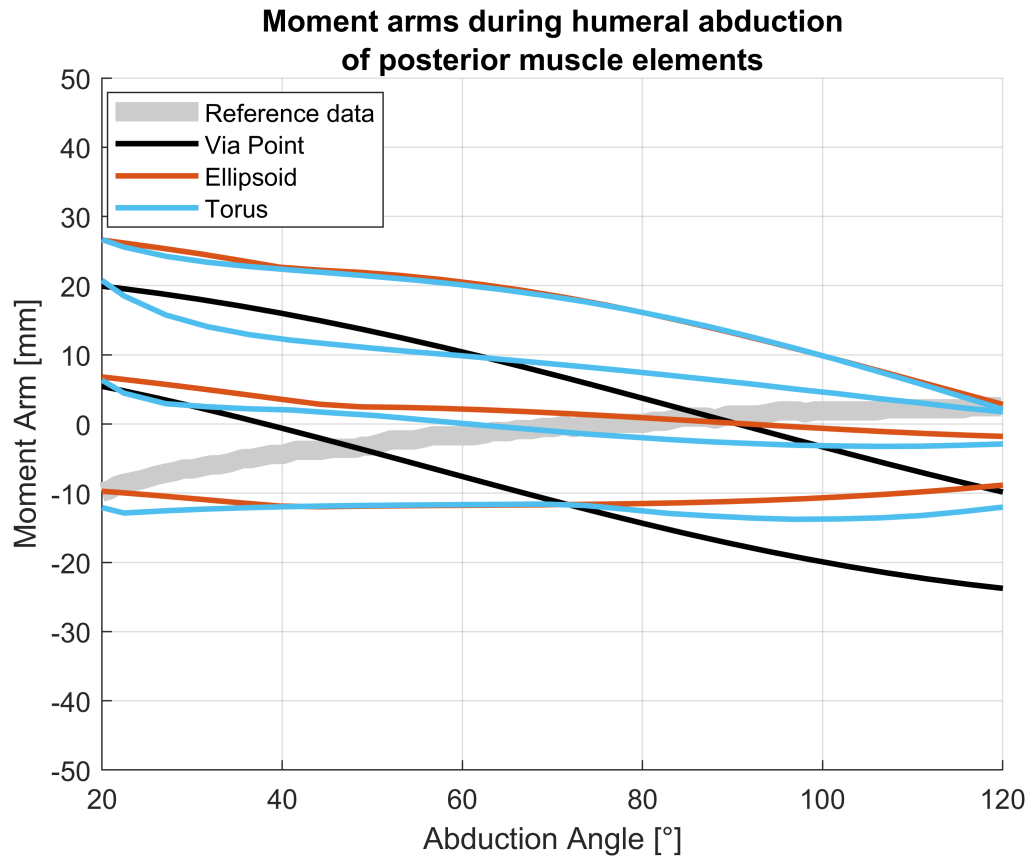


FIGURE A.4: Moment arms during glenohumeral abduction in the range 20 – 120° of the posterior deltoid elements. Grey: moment arms from a cadaver study by Ackland et al., 2008 Black: posterior deltoid moment arms of the via point model, 2 associated model elements. Orange: posterior deltoid moment arms of the ellipsoid model, 4 associated model elements. Blue: posterior deltoid moment arms of the torus model, 4 associated model elements.

A.3 Moments transmitted onto the humerus from the tori

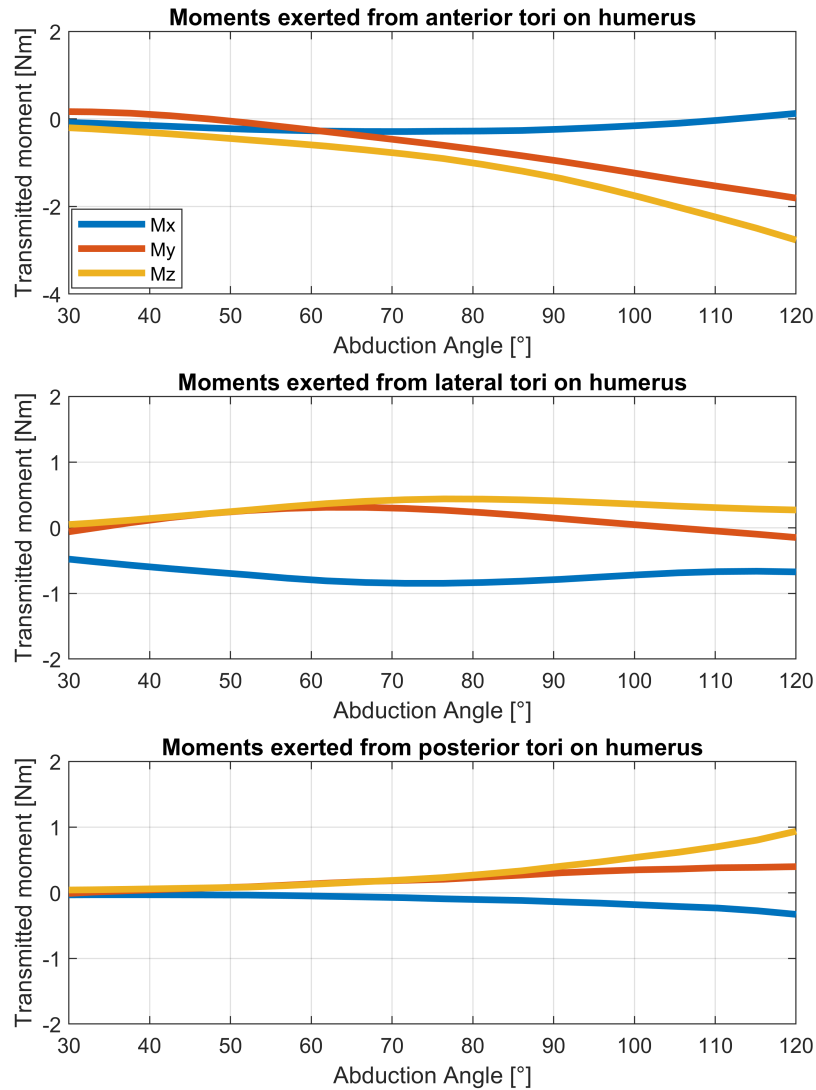


FIGURE A.5: Moments transmitted from the anterior, lateral and posterior tori carrier elements onto the humerus from the ALLFM model (see 5.2.3) during abduction of the humerus in the range 30-120°. X,Y and Z components are expressed in the humerus coordinate frame (Figure 5.3, green coordinate system).

A.4 Muscle activities and joint reaction force of the torus model with $p = 3$ and all forces / moments transmitted

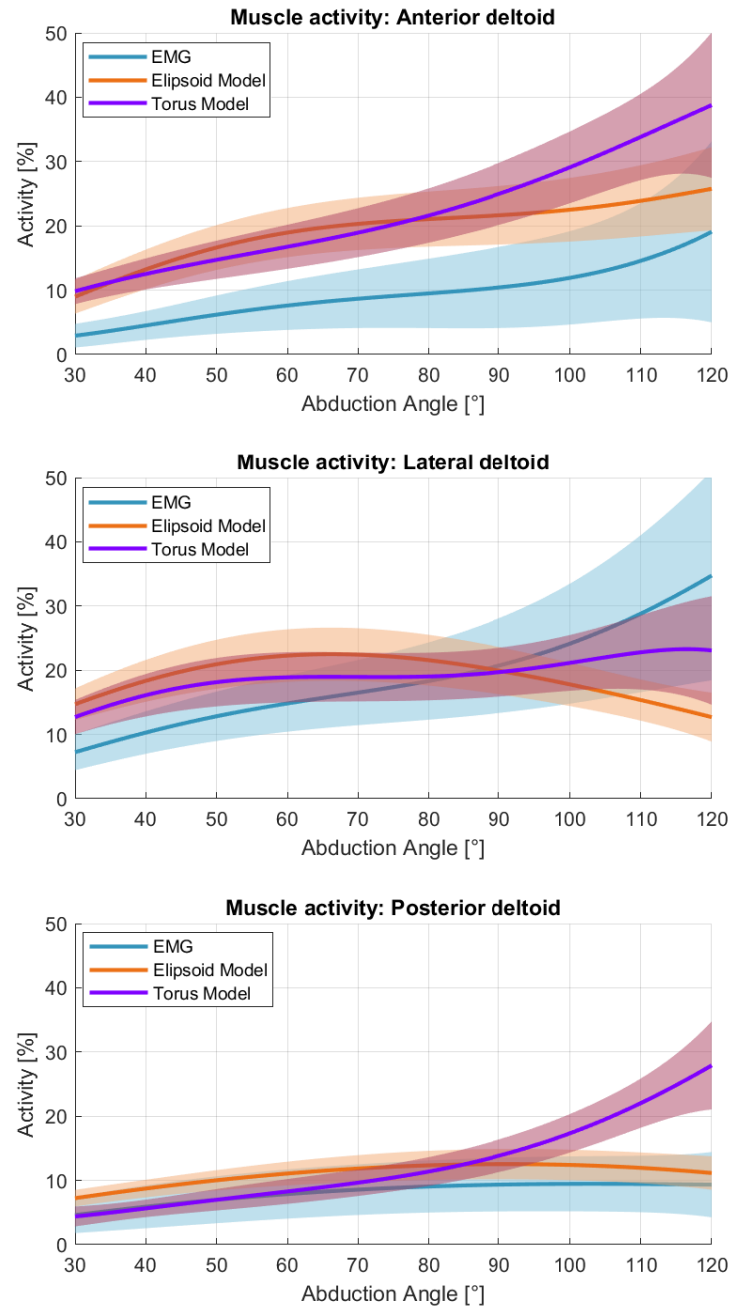


FIGURE A.6: Activity of the anterior, lateral and posterior deltoid groups during abduction between 30-120° of the EMG mean (blue), the ellipsoid (orange) and the torus model (purple) with $p = 3$.

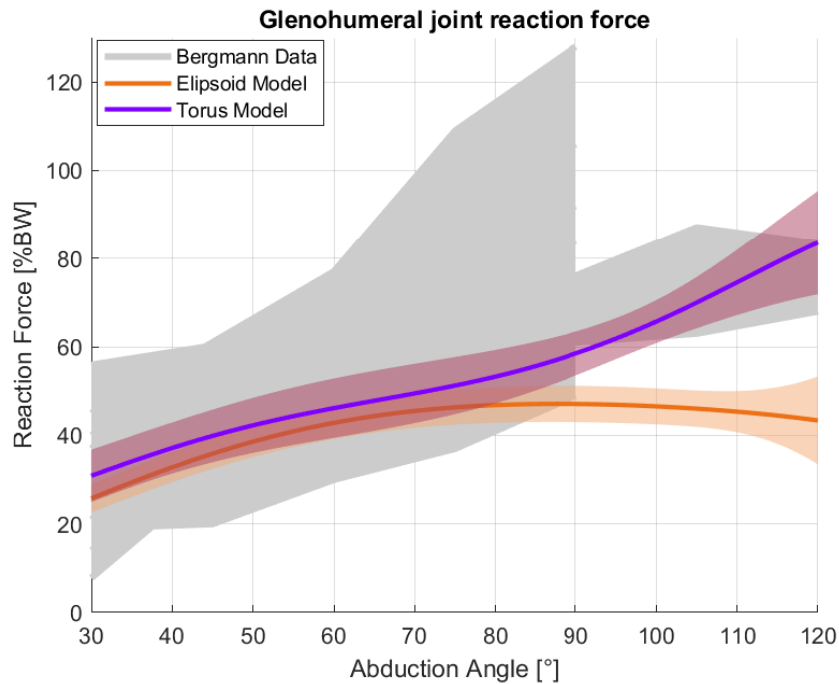
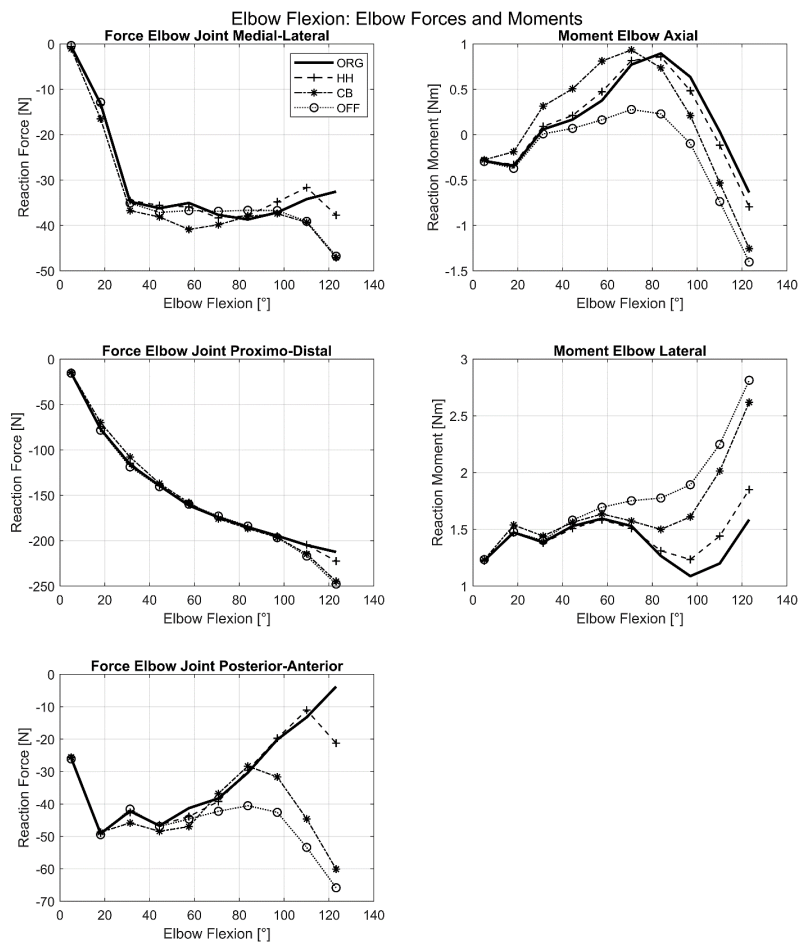


FIGURE A.7: Resultant GH joint reaction force in %BW over the abduction angle of the humerus. Grey depicts an envelope of the in-vivo data (Retrieved 15. May, 2018 from <http://www.OrthoLoad.com>, files: s1r_210206_1_42, s2r_040408_1_2, s2r_270306_1_86, s3l_190308_1_48, s4r_140207_1_70, s5r_131108_1_40, s8r_161208_1_17, s8r_161208_1_31) in comparison to the the ellipsoid (orange) and the torus model (purple) with $p = 3$.

Appendix B

Supplementary material to chapter 6

B.0.1 Joint reaction forces and moments on the elbow joint for the flexion, pronation and pouring motion



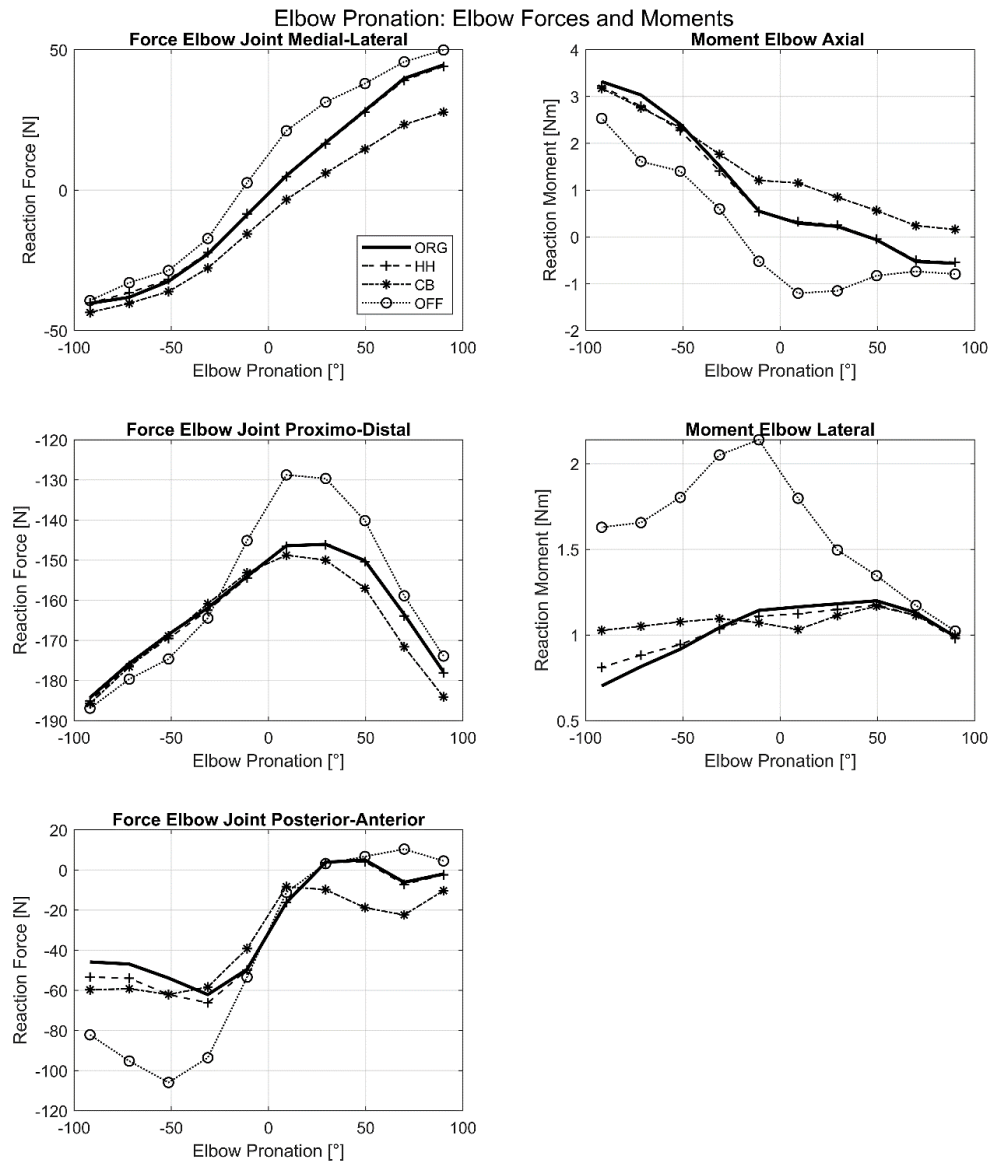


FIGURE B.2: Forces and moments acting on the EL joint over the EL pronation angle during pronation for the ORG, HH, CB and OFF model

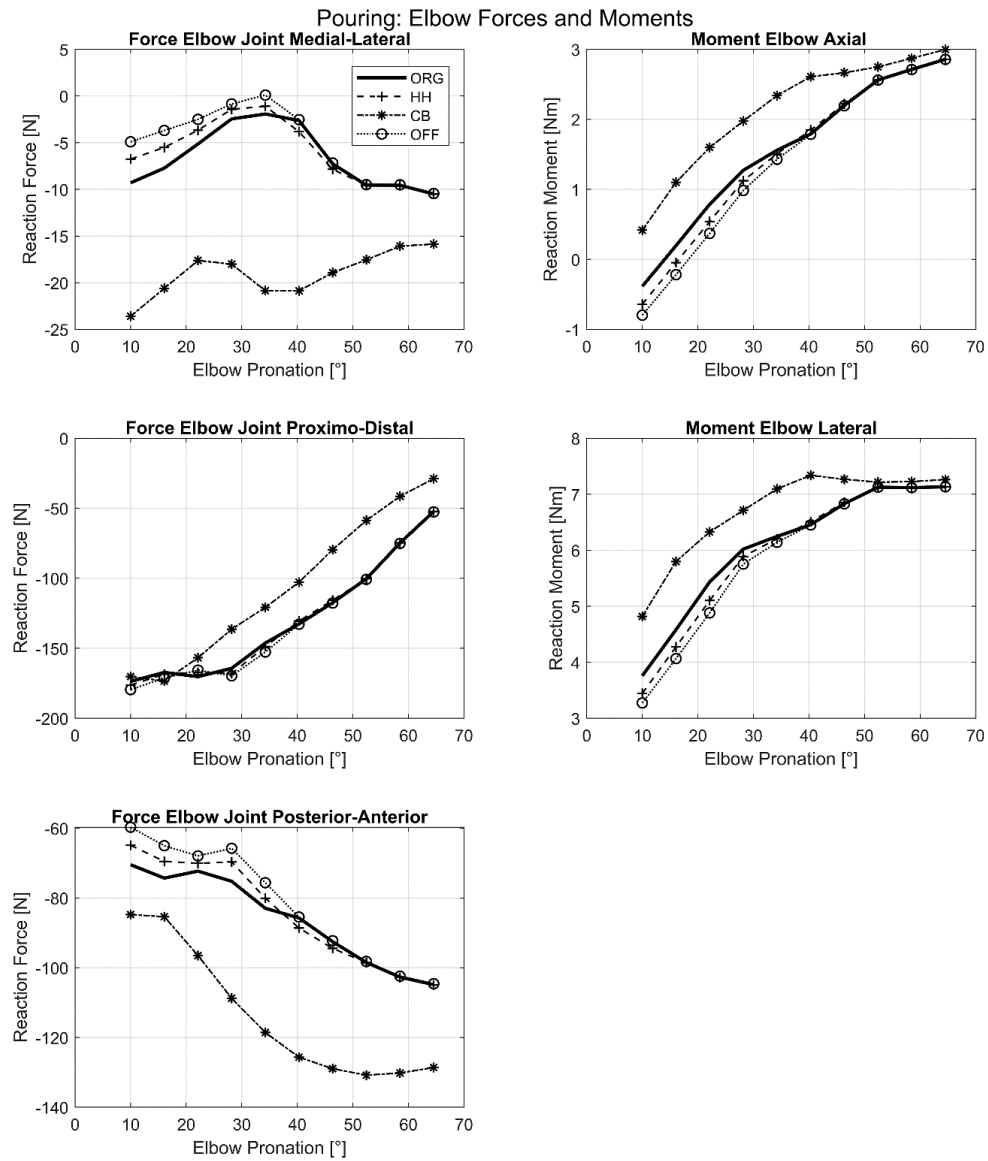


FIGURE B.3: Forces and moments acting on the EL joint over the EL pronation angle during the pouring motion for the ORG, HH, CB and OFF model

B.0.2 Joint reaction forces on the glenohumeral joint for the flexion, pronation and pouring motion

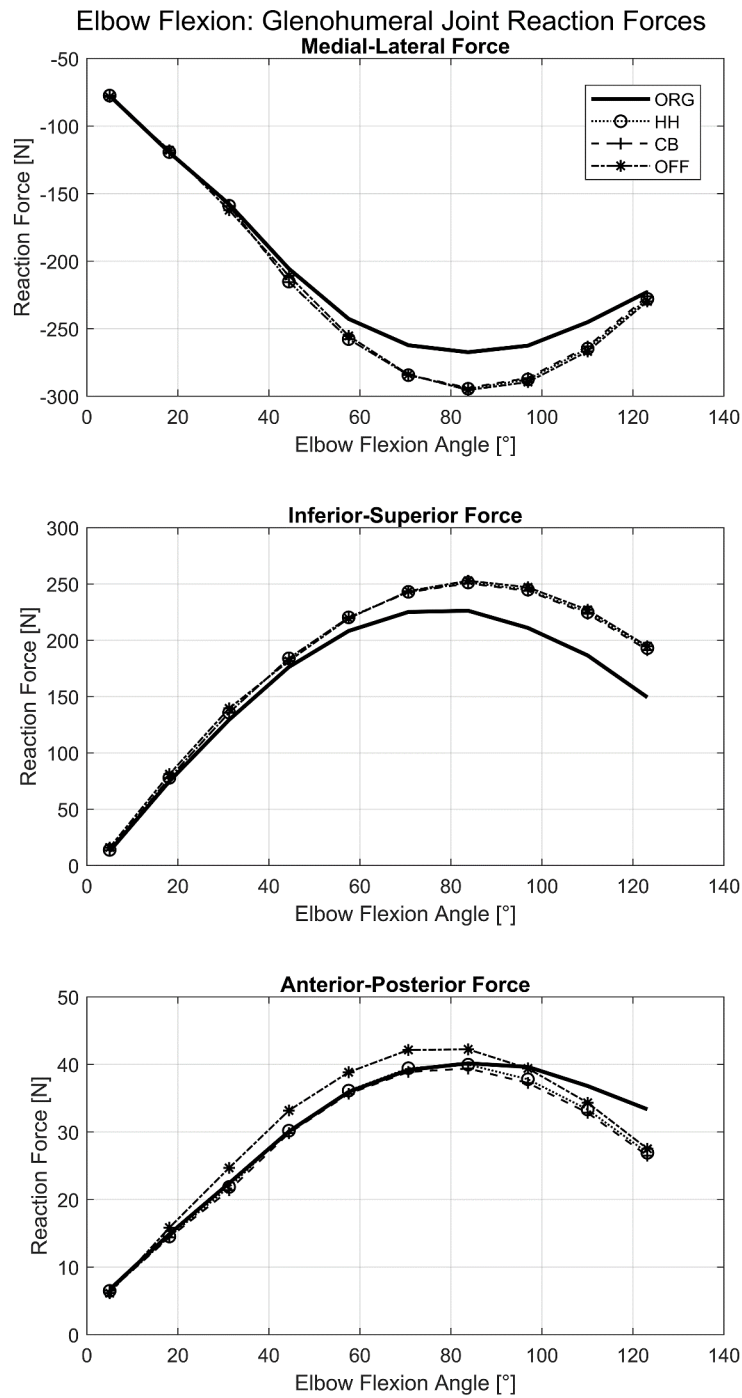


FIGURE B.4: Forces in the GH joint over the EL flexion angle during flexion for the ORG, HH, CB and OFF model

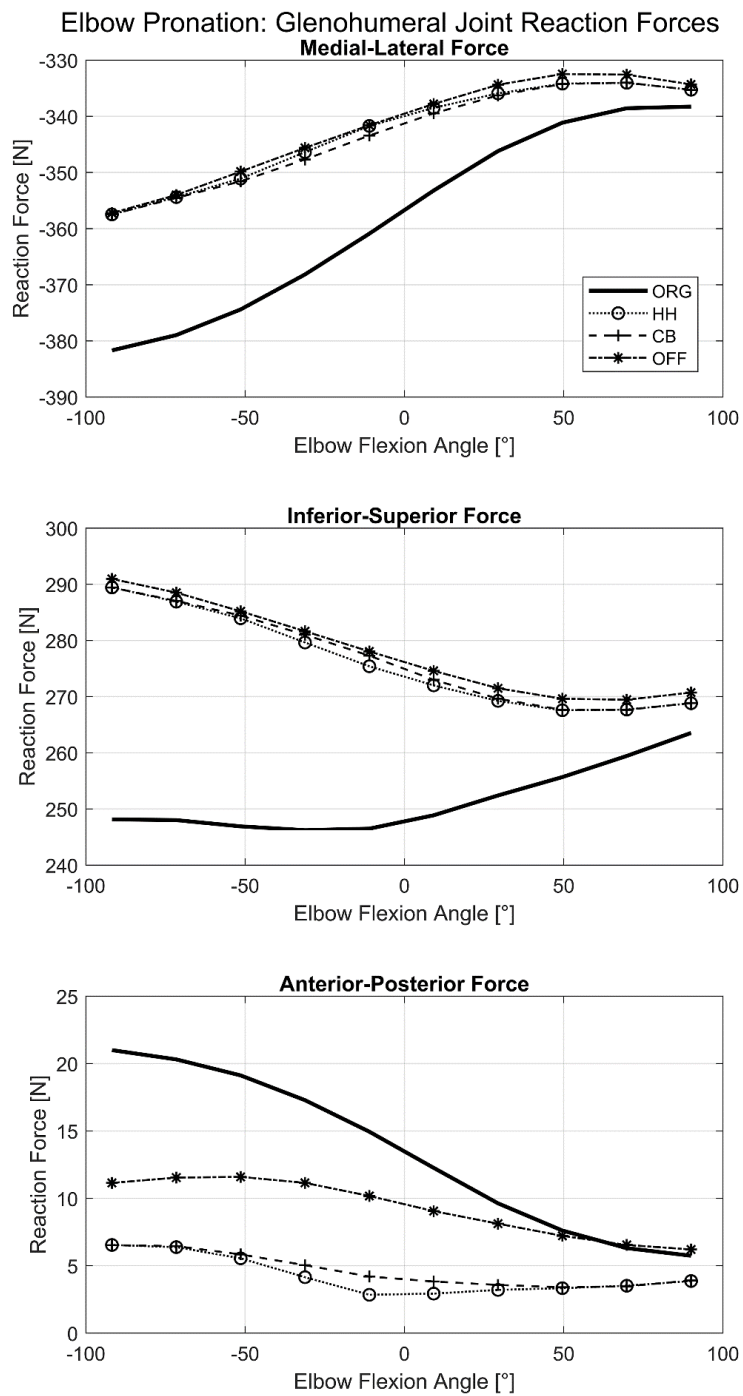


FIGURE B.5: Forces in the GH joint over the EL pronation angle during pronation for the ORG, HH, CB and OFF model

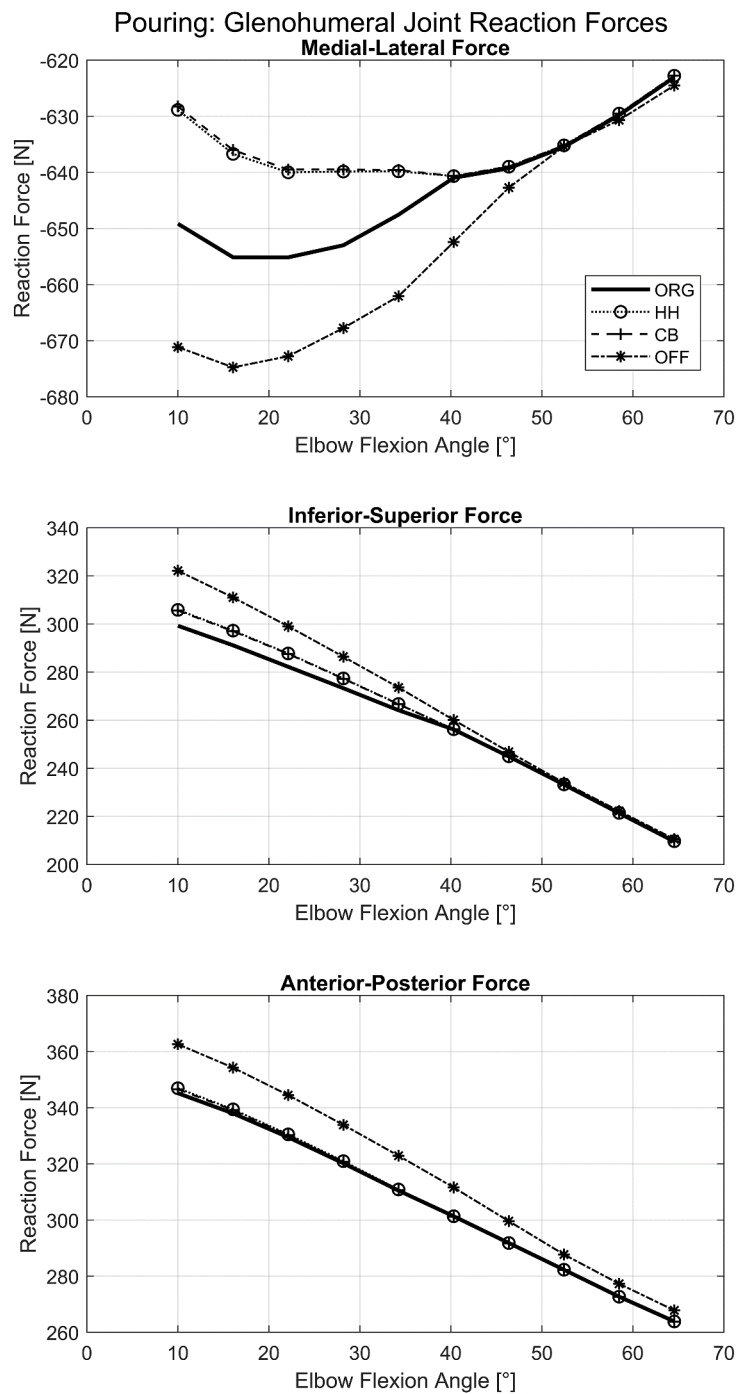


FIGURE B.6: Forces in the GH joint over the EL pronation angle during the pouring motion for the ORG, HH, CB and OFF model

Appendix C

Supplementary material to chapter 7

C.0.1 Muscle activities of intact models and pathological models of the healthy subject group

Neutral position

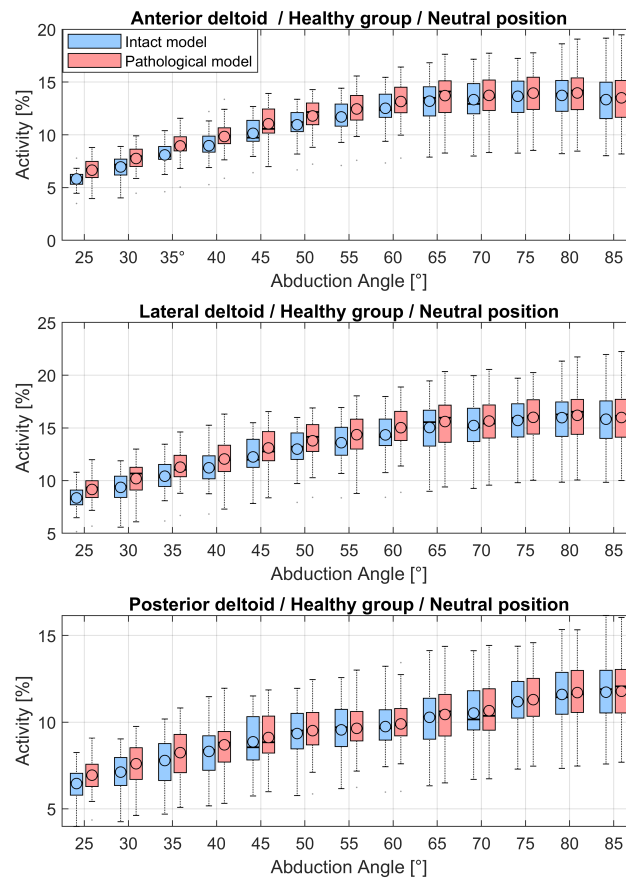


FIGURE C.1: Computed muscle activities of the anterior, posterior and lateral deltoids over the abduction angle in 5° increments during the neutral position trial. Blue depicts the activities of the intact model and red the modelled tear of the m. supraspinatus. Blue depicts the activities of the intact model and red the modelled tear of the m. supraspinatus of the healthy subject cohort.

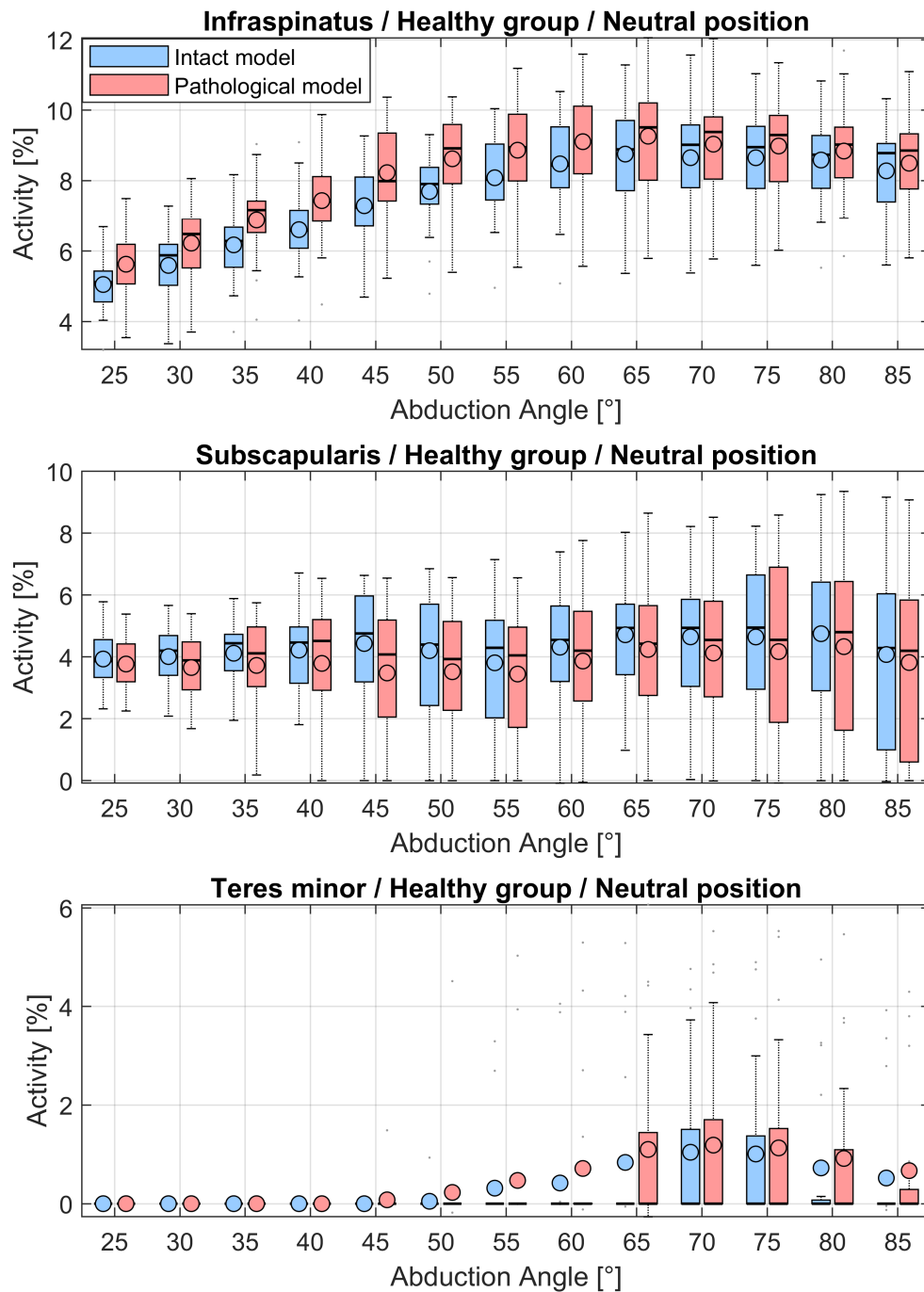


FIGURE C.2: Computed muscle activities of infraspinatus, subscapularis and teres minor over the abduction angle in 5° increments during the neutral position trial with 5 N load in hand. Blue depicts the activities of the intact model and red the modelled tear of the m. supraspinatus of the healthy subject cohort.

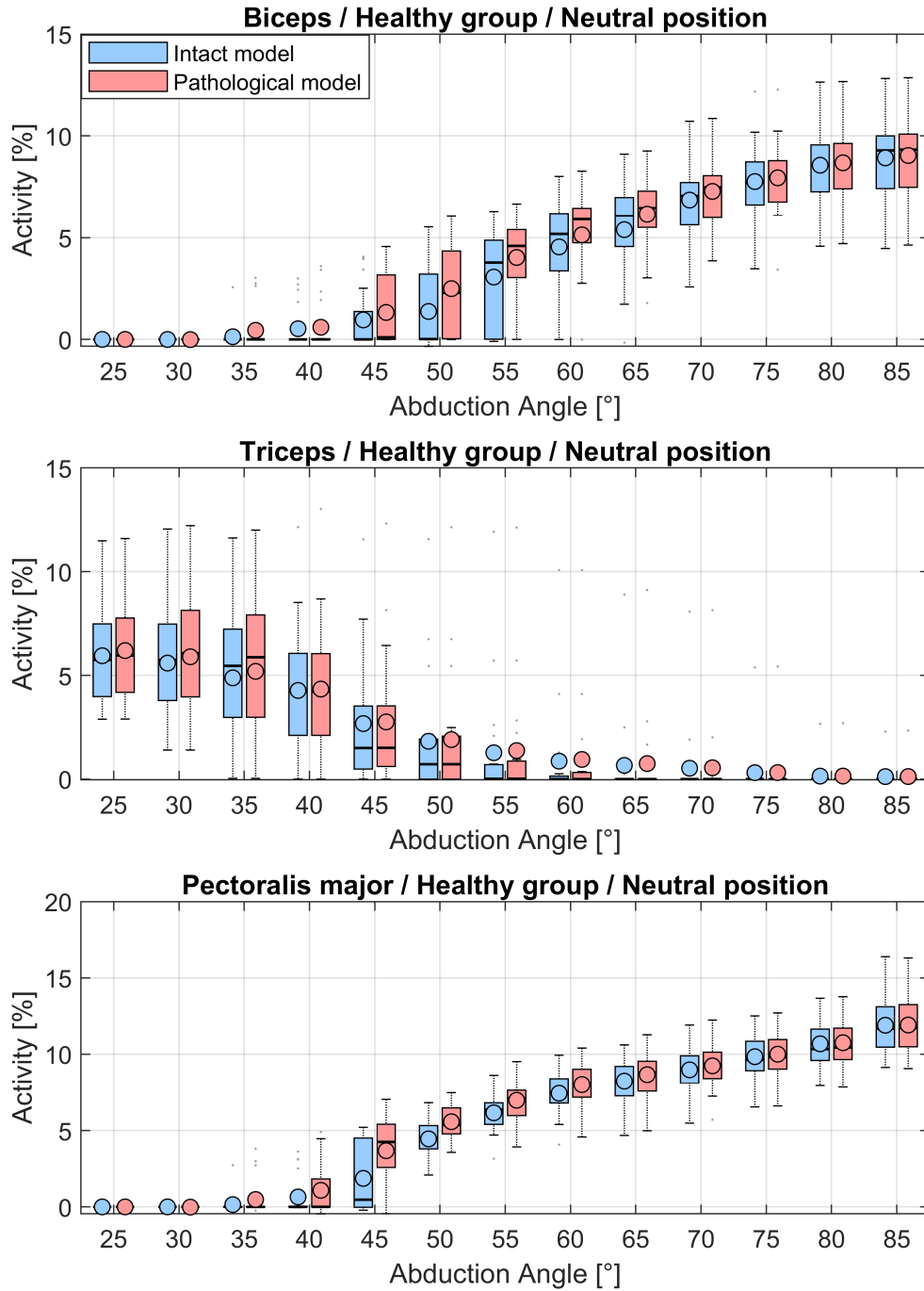


FIGURE C.3: Computed muscle activities of the biceps, triceps and pectoralis major over the abduction angle in 5° increments during the neutral position trial. Blue depicts the activities of the intact model and red the modelled tear of the m. supraspinatus of the healthy subject cohort.

Neutral position with 5N in hand

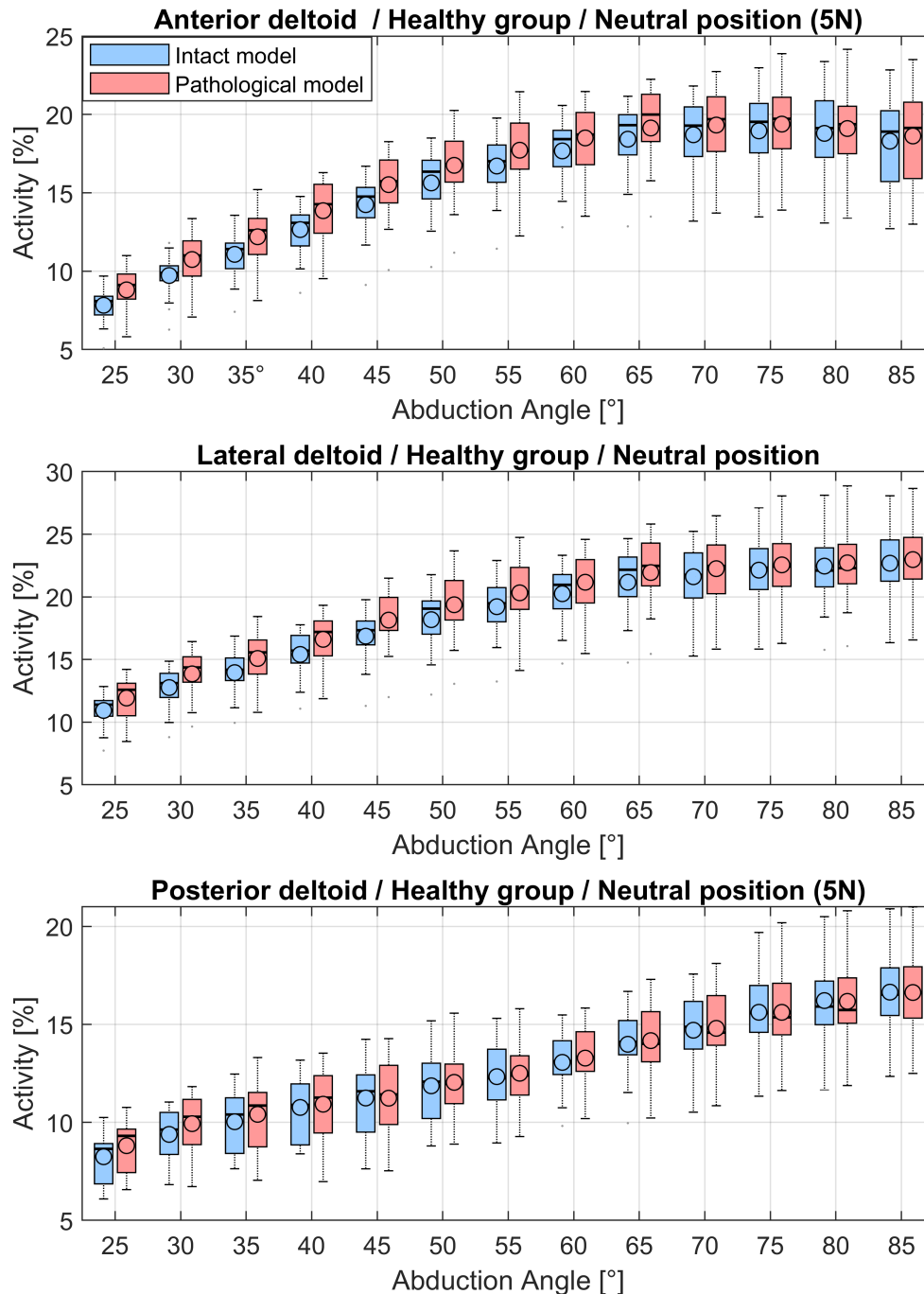


FIGURE C.4: Computed muscle activities of the anterior, posterior and lateral deltoids over the abduction angle in 5° increments during the neutral position trial with 5 N load in hand. Blue depicts the activities of the intact model and red the modelled tear of the m. supraspinatus. Blue depicts the activities of the intact model and red the modelled tear of the m. supraspinatus of the healthy subject cohort.

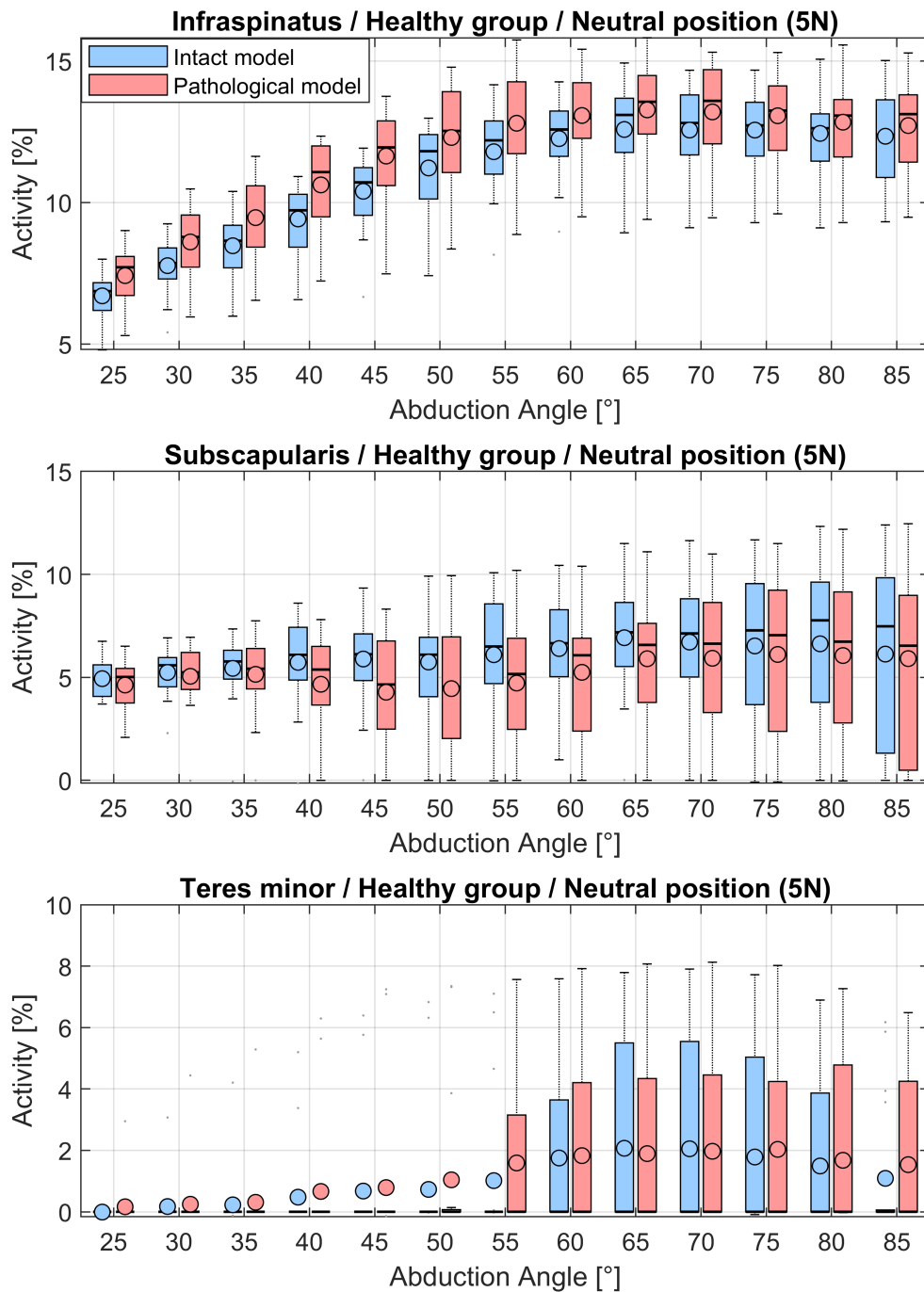


FIGURE C.5: Computed muscle activities of infraspinatus, subscapularis and teres minor over the abduction angle in 5° increments during the neutral position trial with 5 N load in hand. Blue depicts the activities of the intact model and red the modelled tear of the m. supraspinatus of the healthy subject cohort.

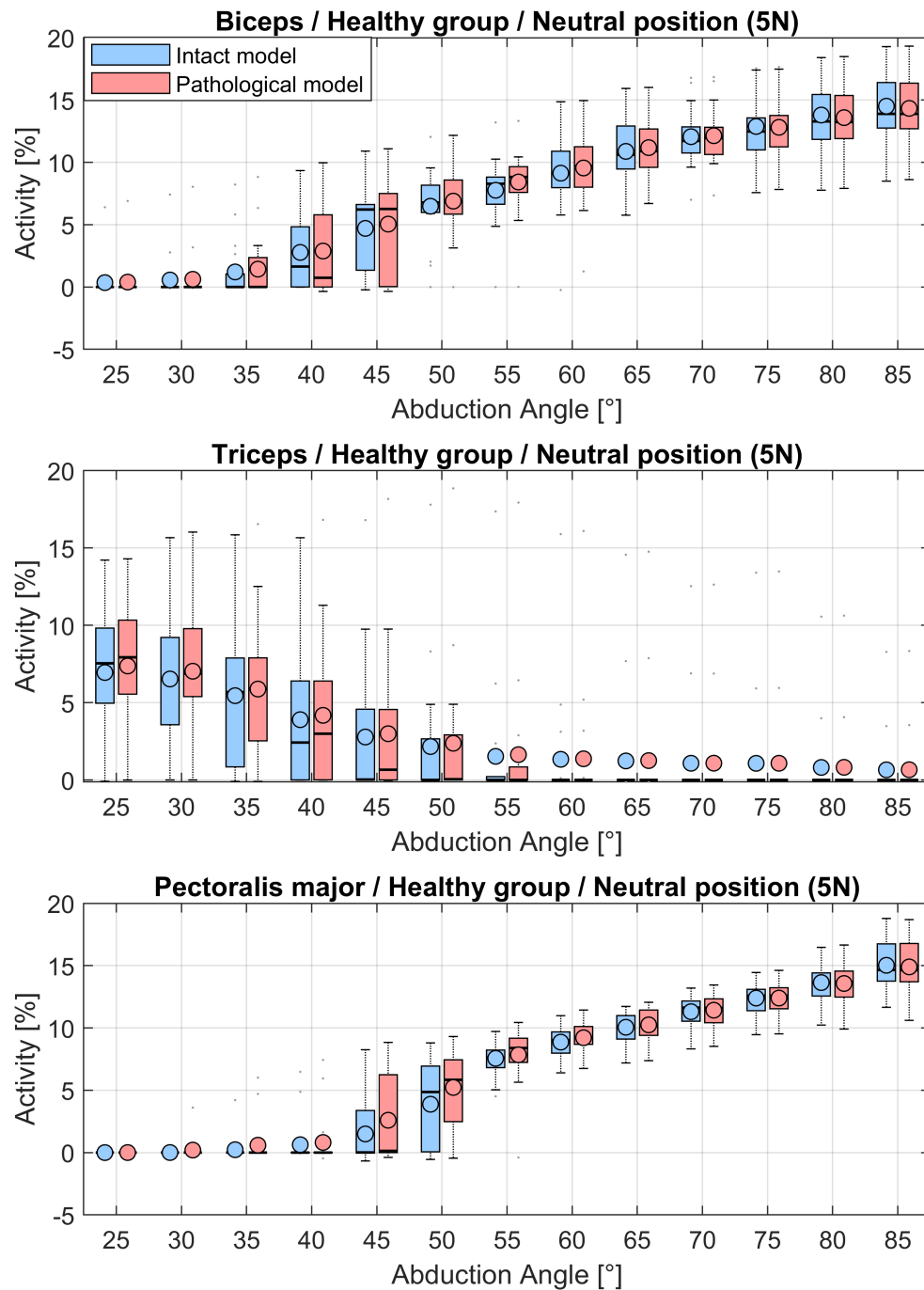


FIGURE C.6: Computed muscle activities of the biceps, triceps and pectoralis major over the abduction angle in 5° increments during the neutral position trial with 5 N load in hand. Blue depicts the activities of the intact model and red the modelled tear of the m. supraspinatus of the healthy subject cohort.

Internal rotation

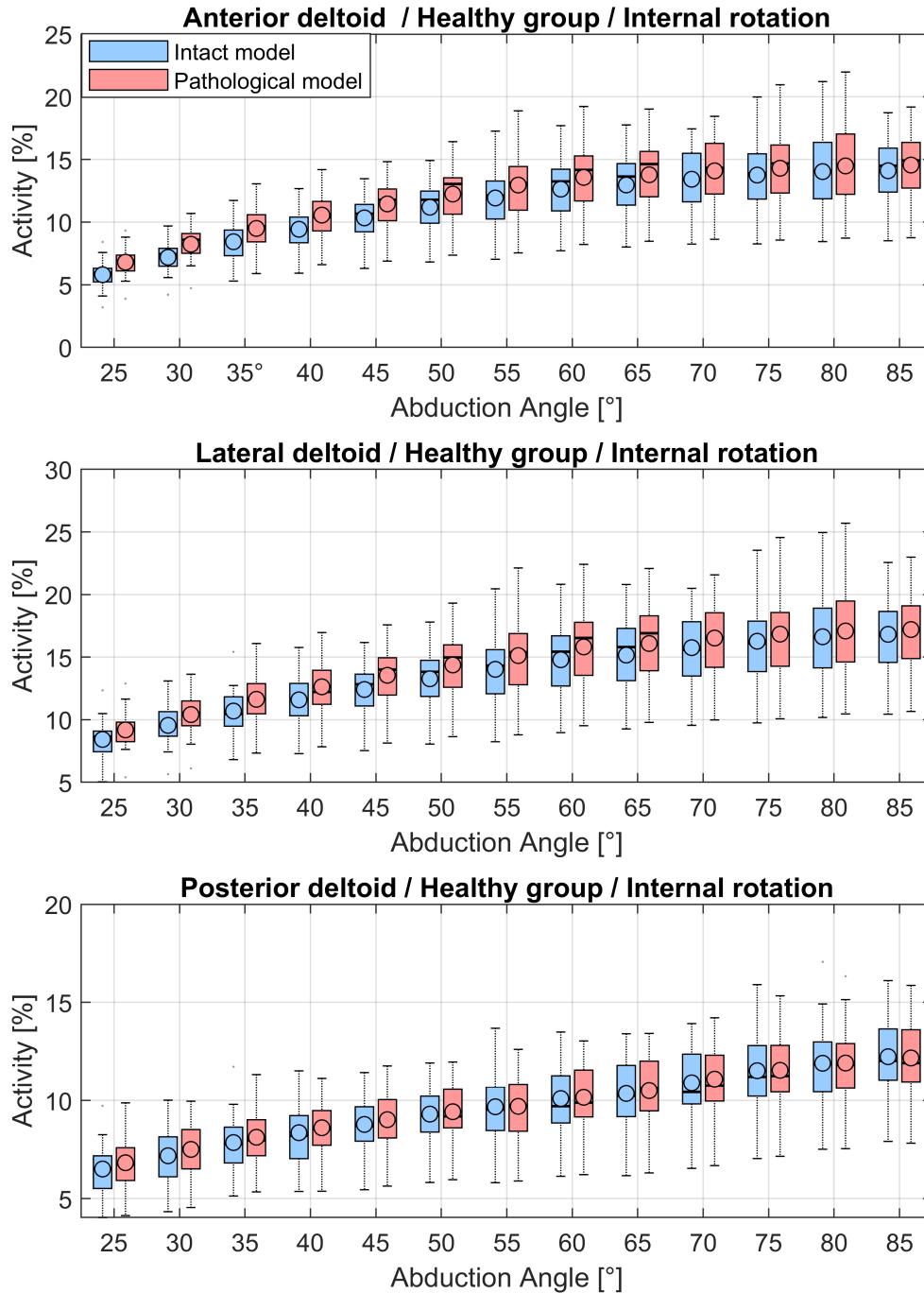


FIGURE C.7: Computed muscle activities of the anterior, posterior and lateral deltoids over the abduction angle in 5° increments during the internal rotation trial. Blue depicts the activities of the intact model and red the modelled tear of the m. supraspinatus. Blue depicts the activities of the intact model and red the modelled tear of the m. supraspinatus of the healthy subject cohort.

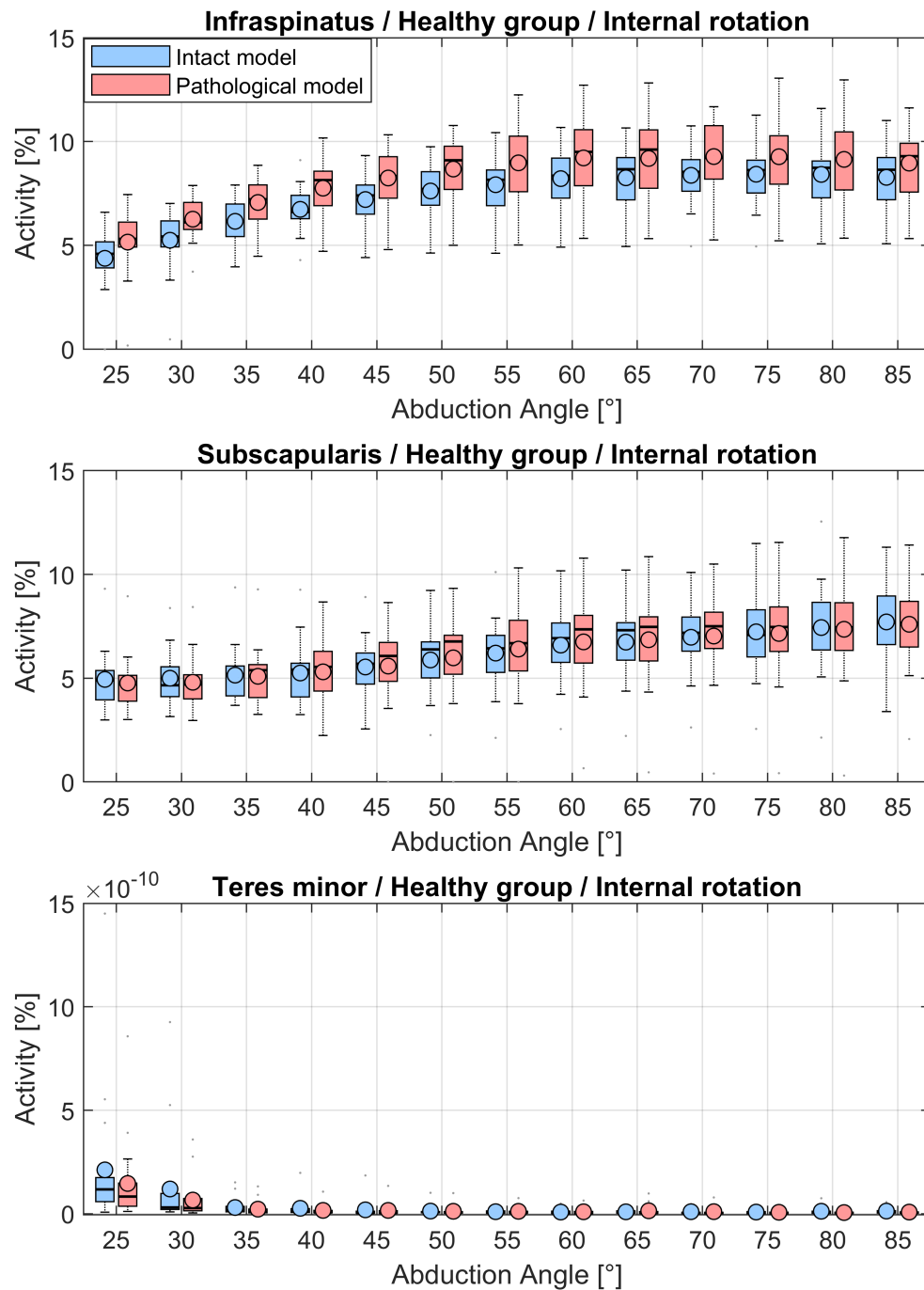


FIGURE C.8: Computed muscle activities of infrapinatus, subscapularis and teres minor over the abduction angle in 5° increments during the internal rotation trial. Blue depicts the activities of the intact model and red the modelled tear of the m. supraspinatus of the healthy subject cohort.

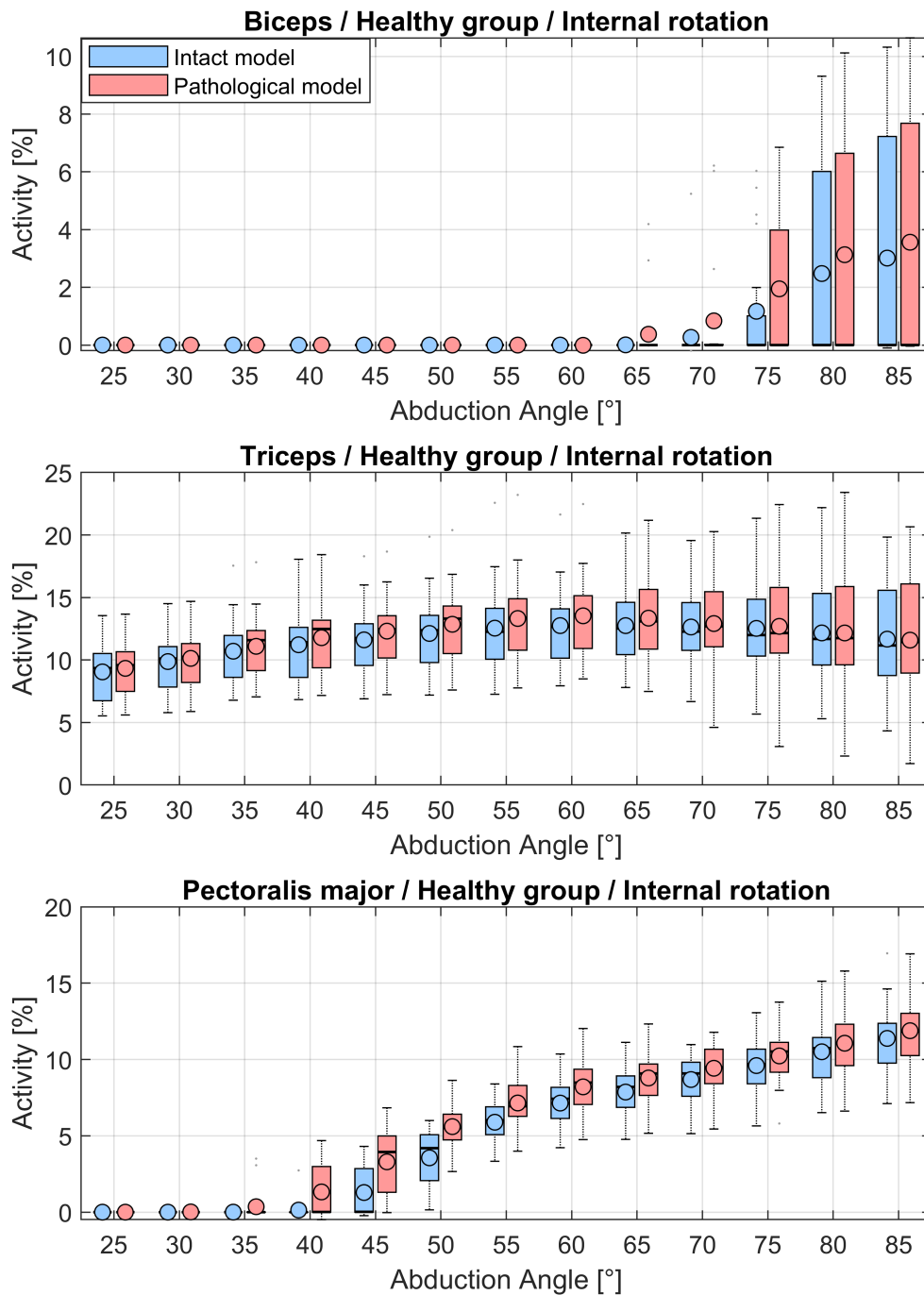


FIGURE C.9: Computed muscle activities of the biceps, triceps and pectoralis major over the abduction angle in 5° increments during the internal rotation trial. Blue depicts the activities of the intact model and red the modelled tear of the m. supraspinatus of the healthy subject cohort.

External rotation

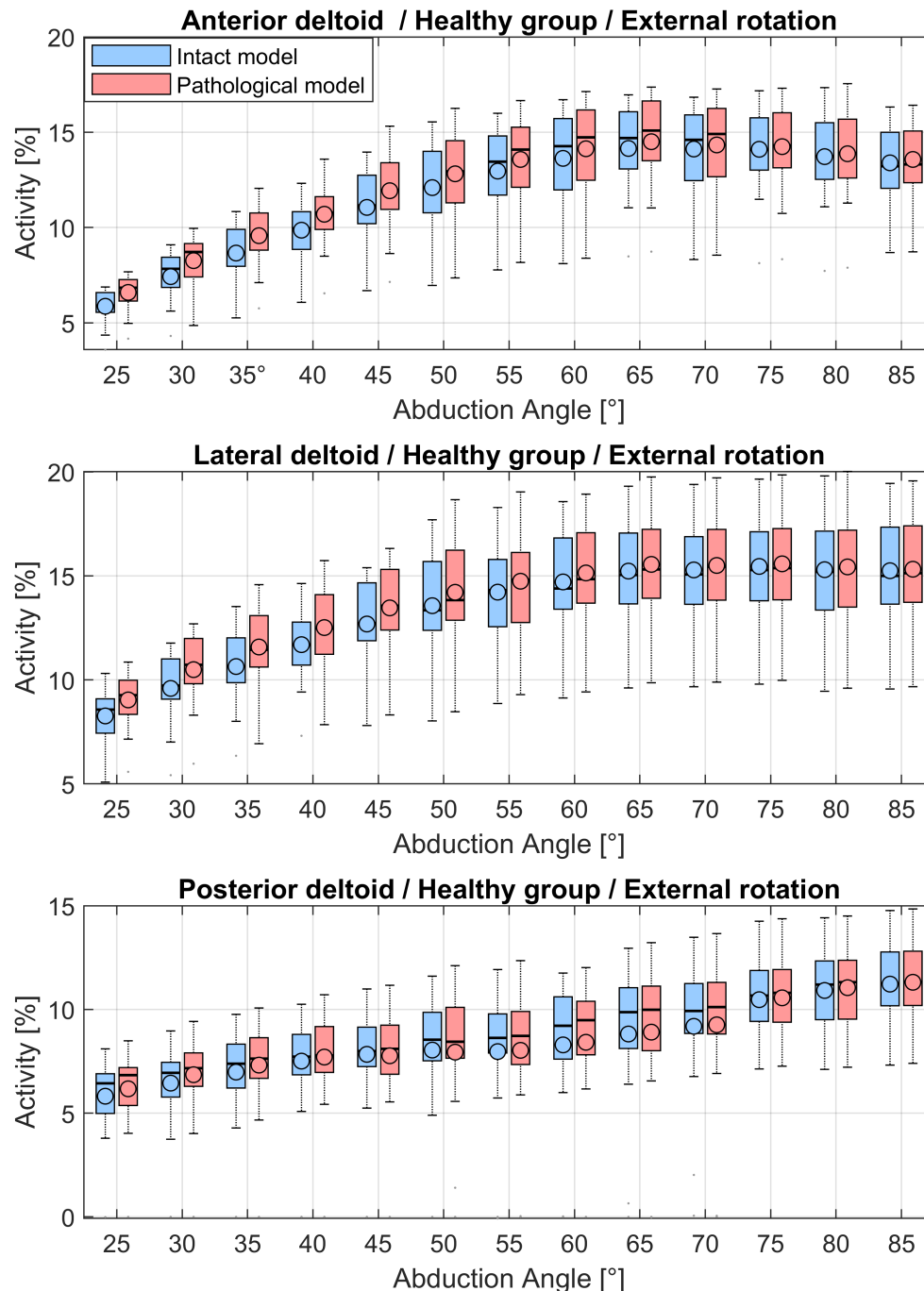


FIGURE C.10: Computed muscle activities of the anterior, posterior and lateral deltoids over the abduction angle in 5° increments during the external rotation trial. Blue depicts the activities of the intact model and red the modelled tear of the m. supraspinatus. Blue depicts the activities of the intact model and red the modelled tear of the m. supraspinatus of the healthy subject cohort.

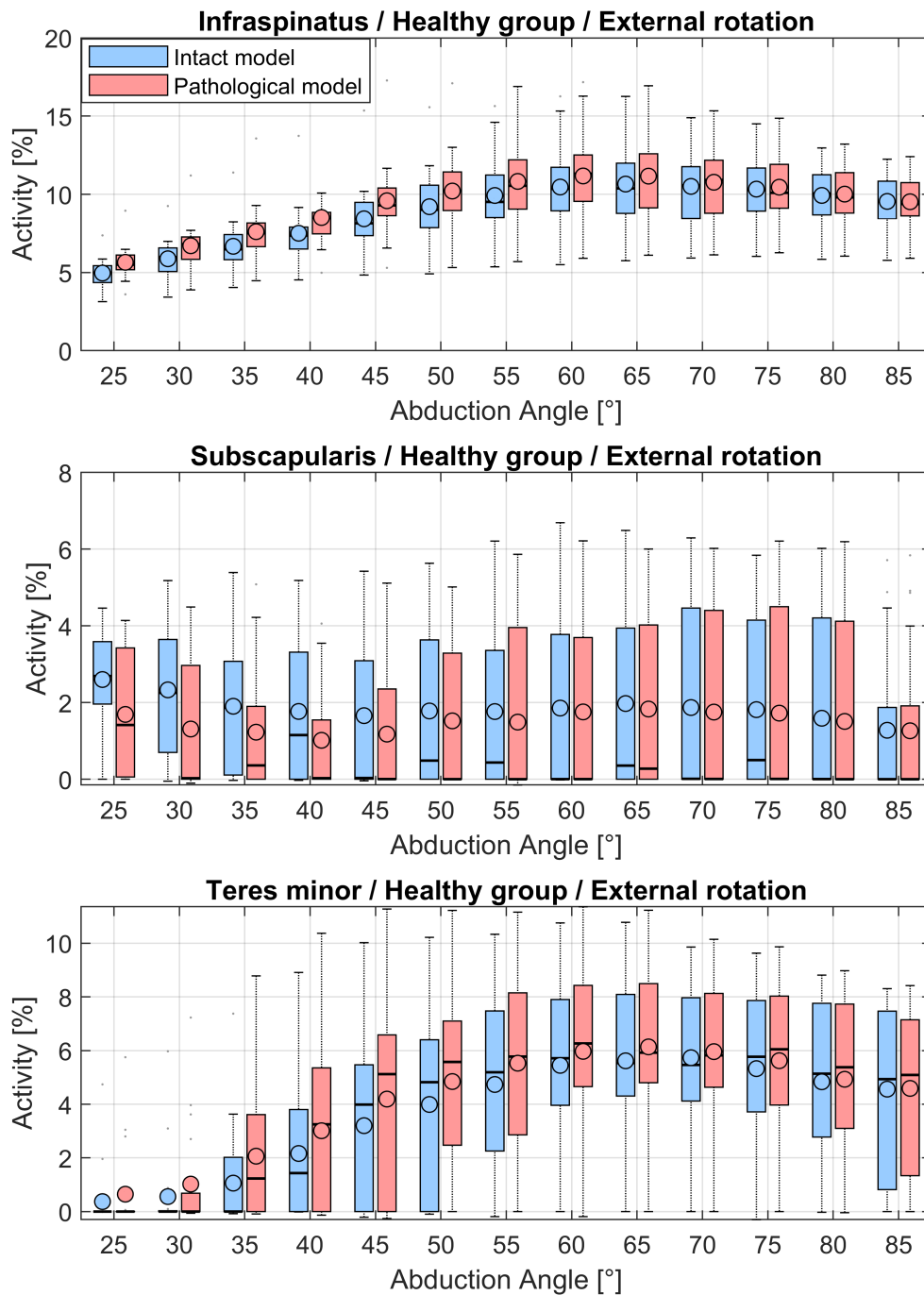


FIGURE C.11: Computed muscle activities of infraspinatus, subscapularis and teres minor over the abduction angle in 5° increments during the external rotation trial. Blue depicts the activities of the intact model and red the modelled tear of the m. supraspinatus of the healthy subject cohort.

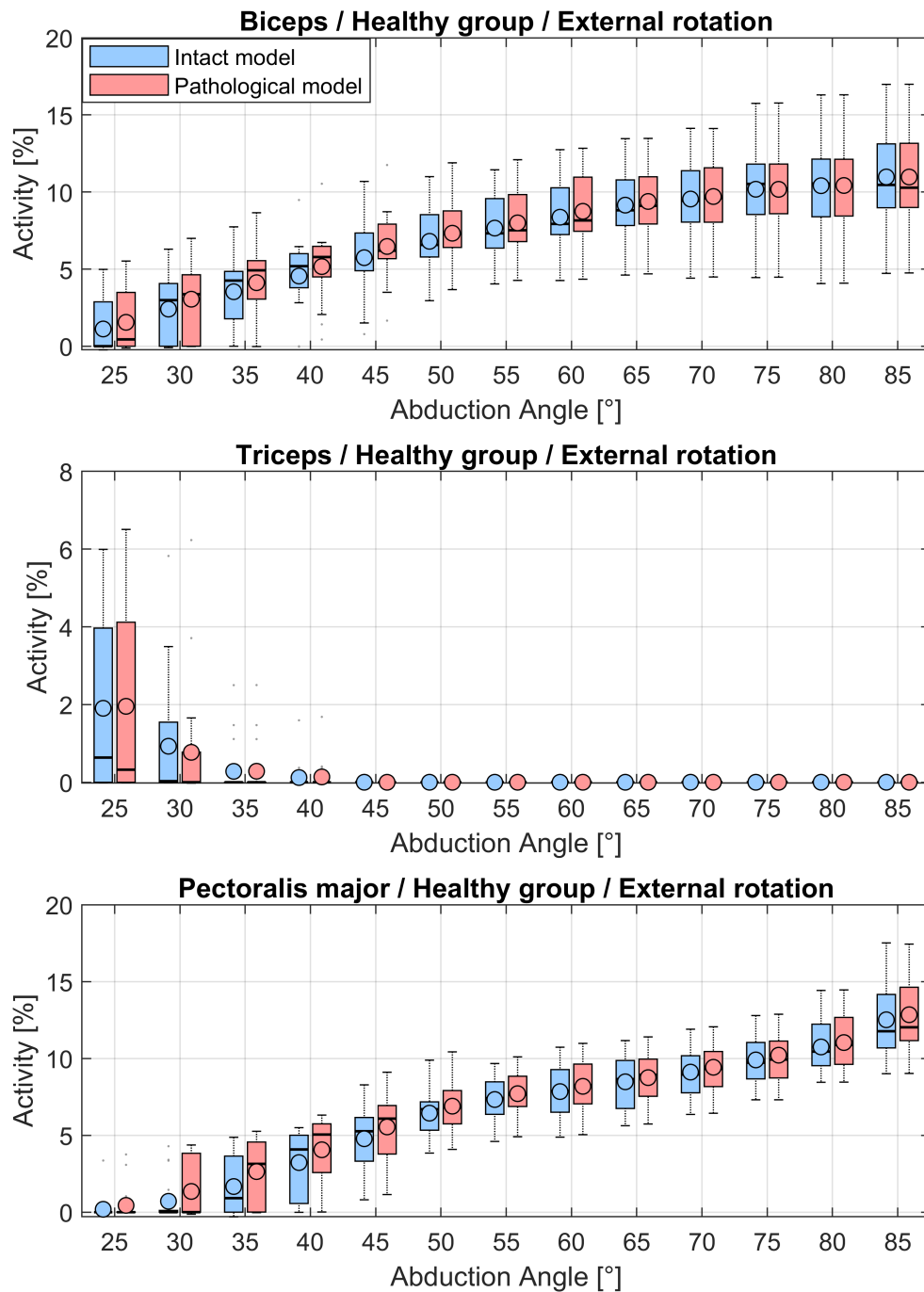


FIGURE C.12: Computed muscle activities of the biceps, triceps and pectoralis major over the abduction angle in 5° increments during the external rotation trial. Blue depicts the activities of the intact model and red the modelled tear of the m. supraspinatus of the healthy subject cohort.

External rotation with 5N in hand

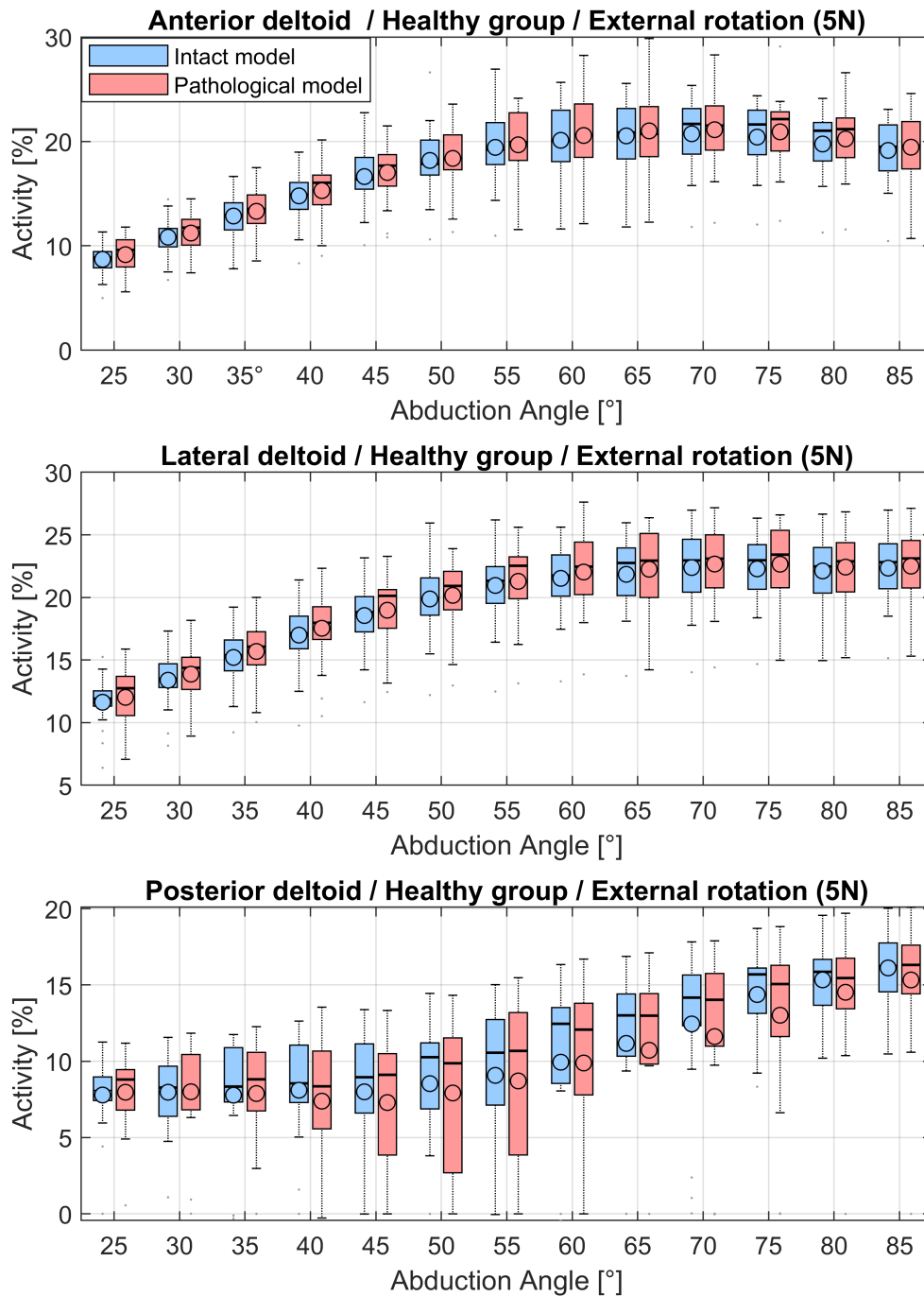


FIGURE C.13: Computed muscle activities of the anterior, posterior and lateral deltoids over the abduction angle in 5° increments during the external rotation trial with 5 N load in hand. Blue depicts the activities of the intact model and red the modelled tear of the m. supraspinatus. Blue depicts the activities of the intact model and red the modelled tear of the m. supraspinatus of the healthy subject cohort.

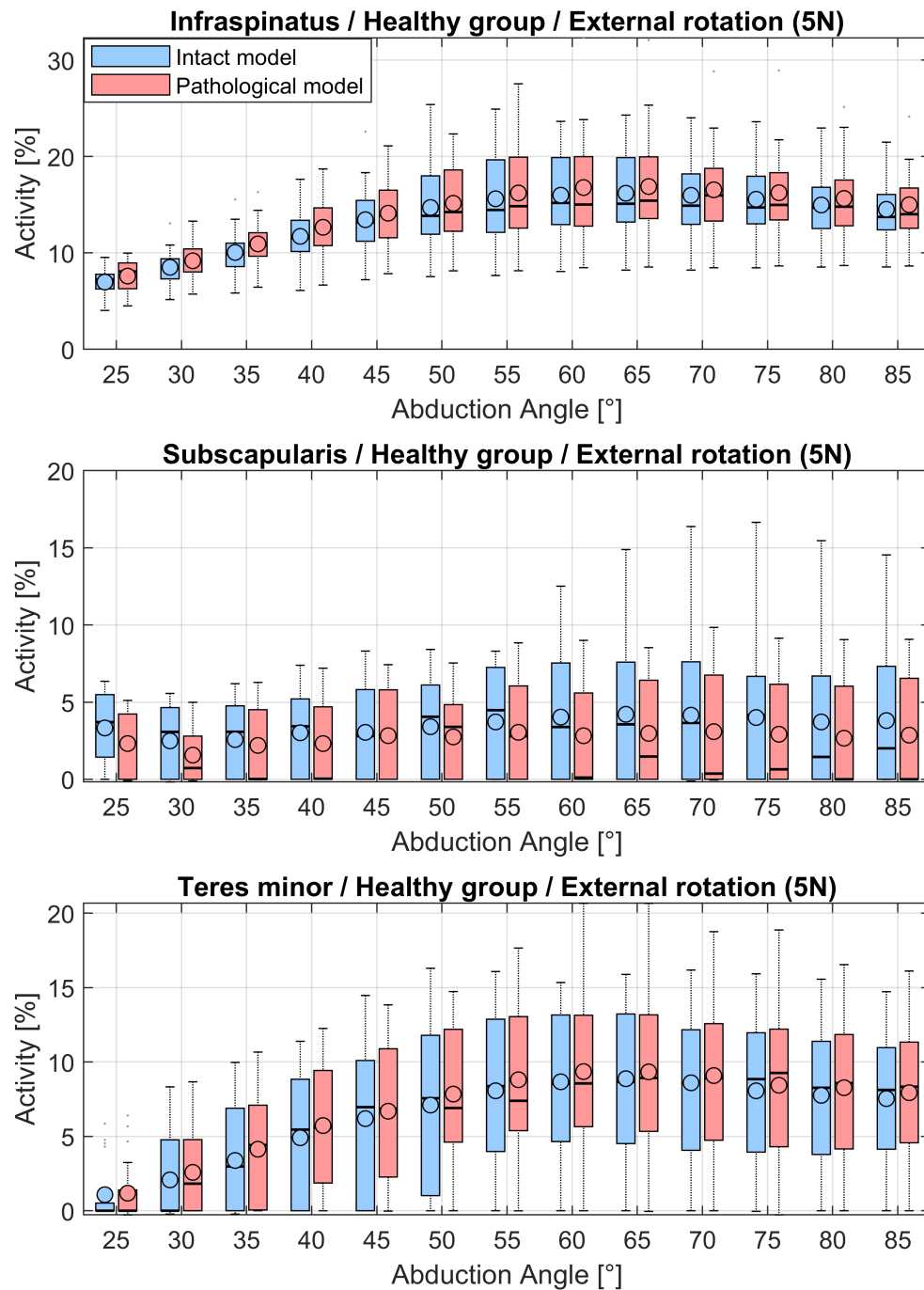


FIGURE C.14: Computed muscle activities of infraspinatus, subscapularis and teres minor over the abduction angle in 5° increments during the external rotation trial with 5 N load in hand. Blue depicts the activities of the intact model and red the modelled tear of the m. supraspinatus of the healthy subject cohort.

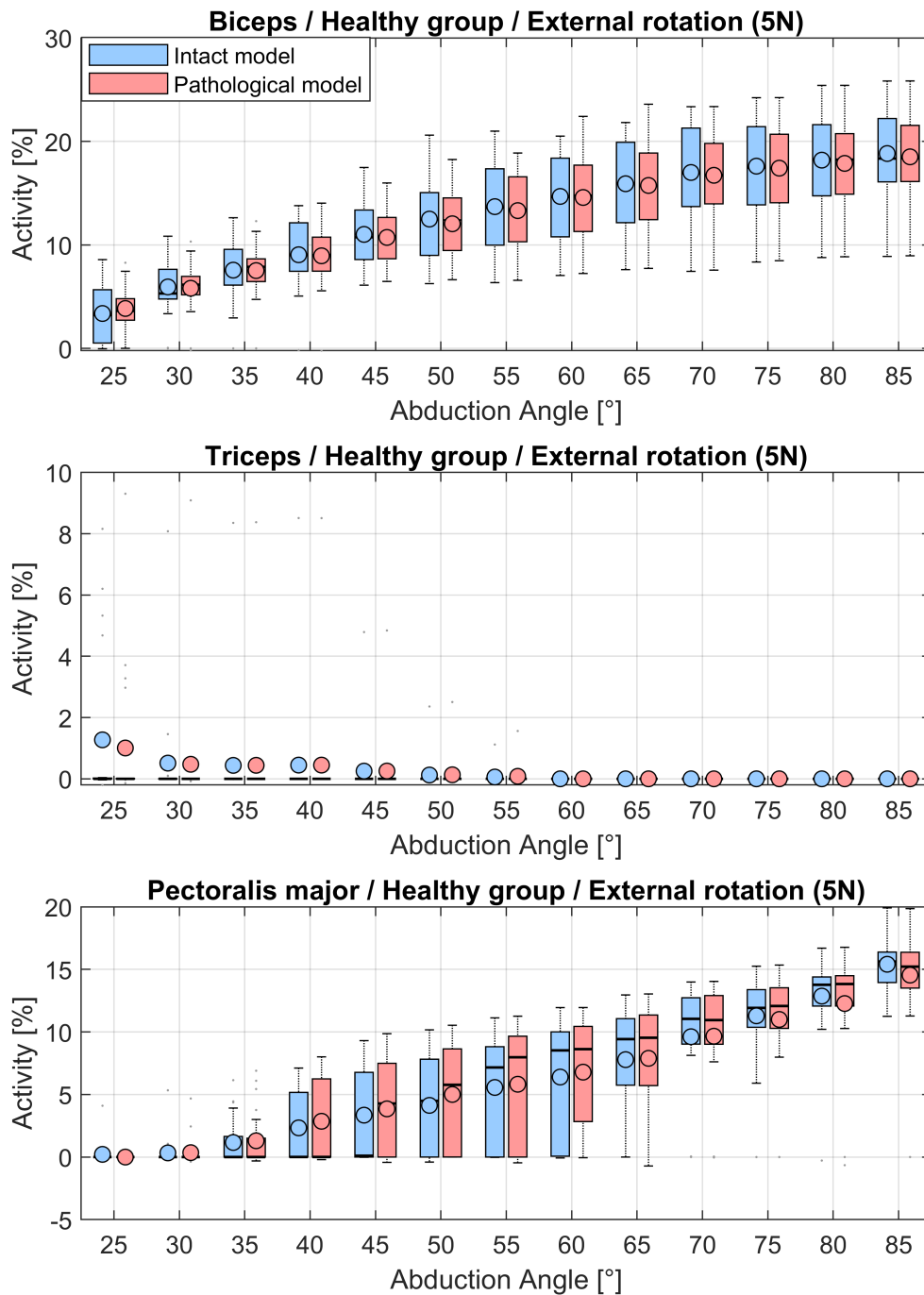


FIGURE C.15: Computed muscle activities of the biceps, triceps and pectoralis major over the abduction angle in 5° increments during the external rotation trial with 5 N load in hand. Blue depicts the activities of the intact model and red the modelled tear of the m. supraspinatus of the healthy subject cohort.

C.0.2 Forces acting on the glenoid of intact models and pathological models of the healthy subject group

Neutral position

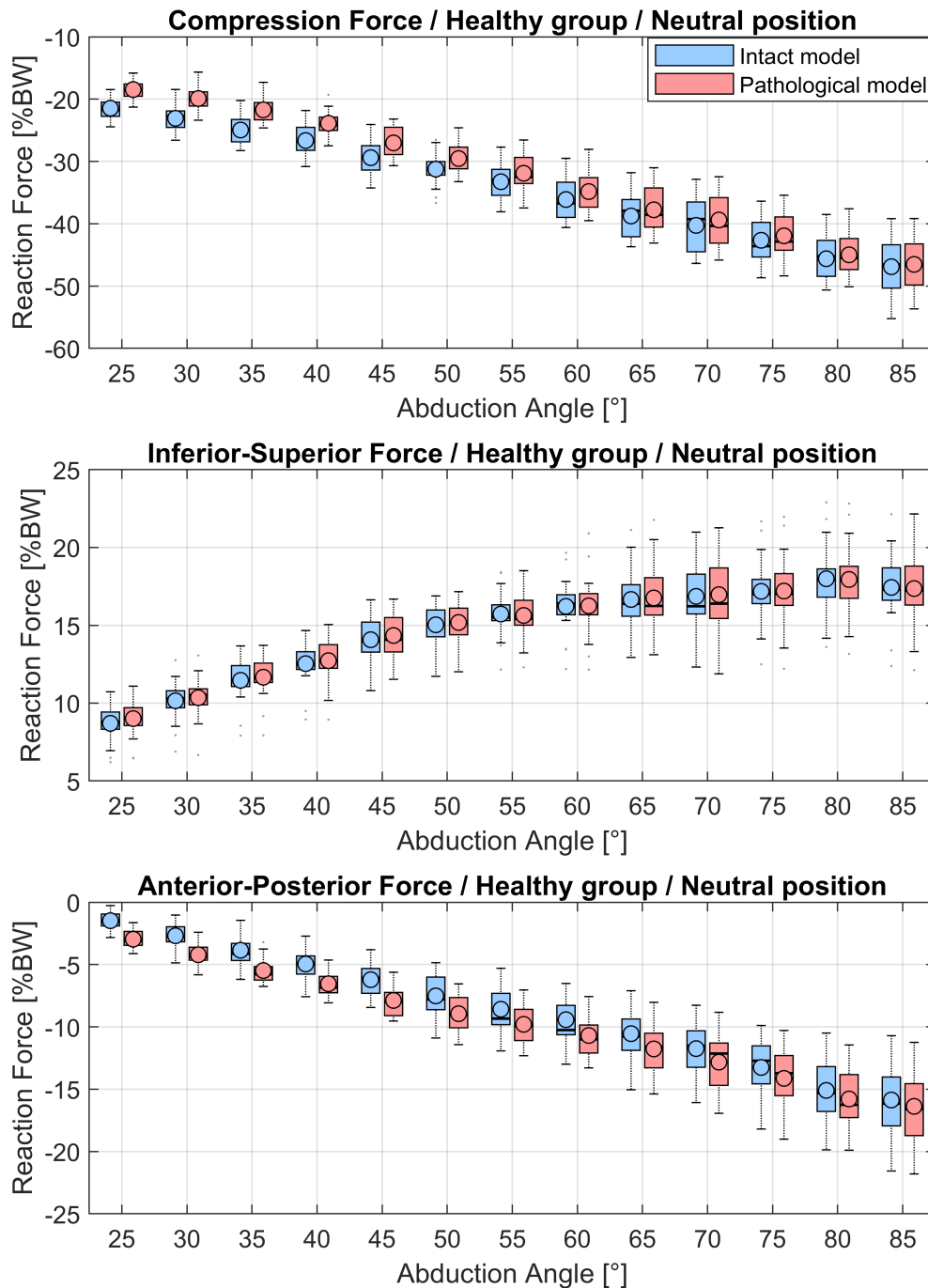


FIGURE C.16: Compression force, inferior-superior force and anterior-posterior force of intact (blue) and pathological (red) models of the healthy subject cohort during the neutral position trial over the abduction angle in 5° increments.

Forces on the glenoid of intact model vs. pathological model

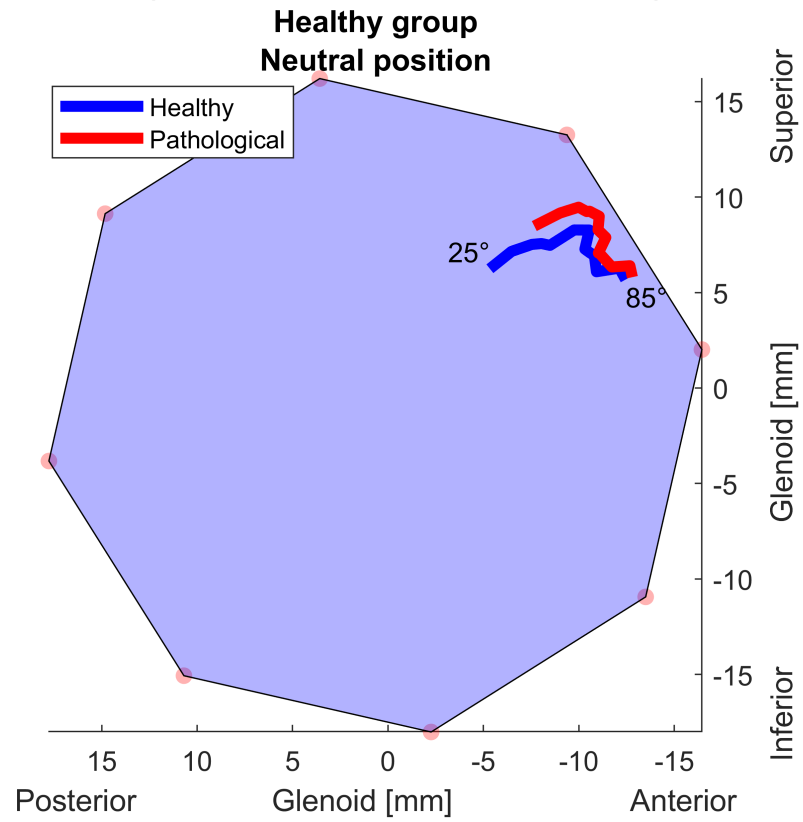


FIGURE C.17: Projected median GH joint reaction force of all models onto the glenoid of intact and pathological models of the healthy subject cohort during the neutral position trial. Intact/healthy models (blue) and pathological models (red) with their starting value at 25° abduction and the progression up to 85° abduction.

Neutral position with 5N in hand

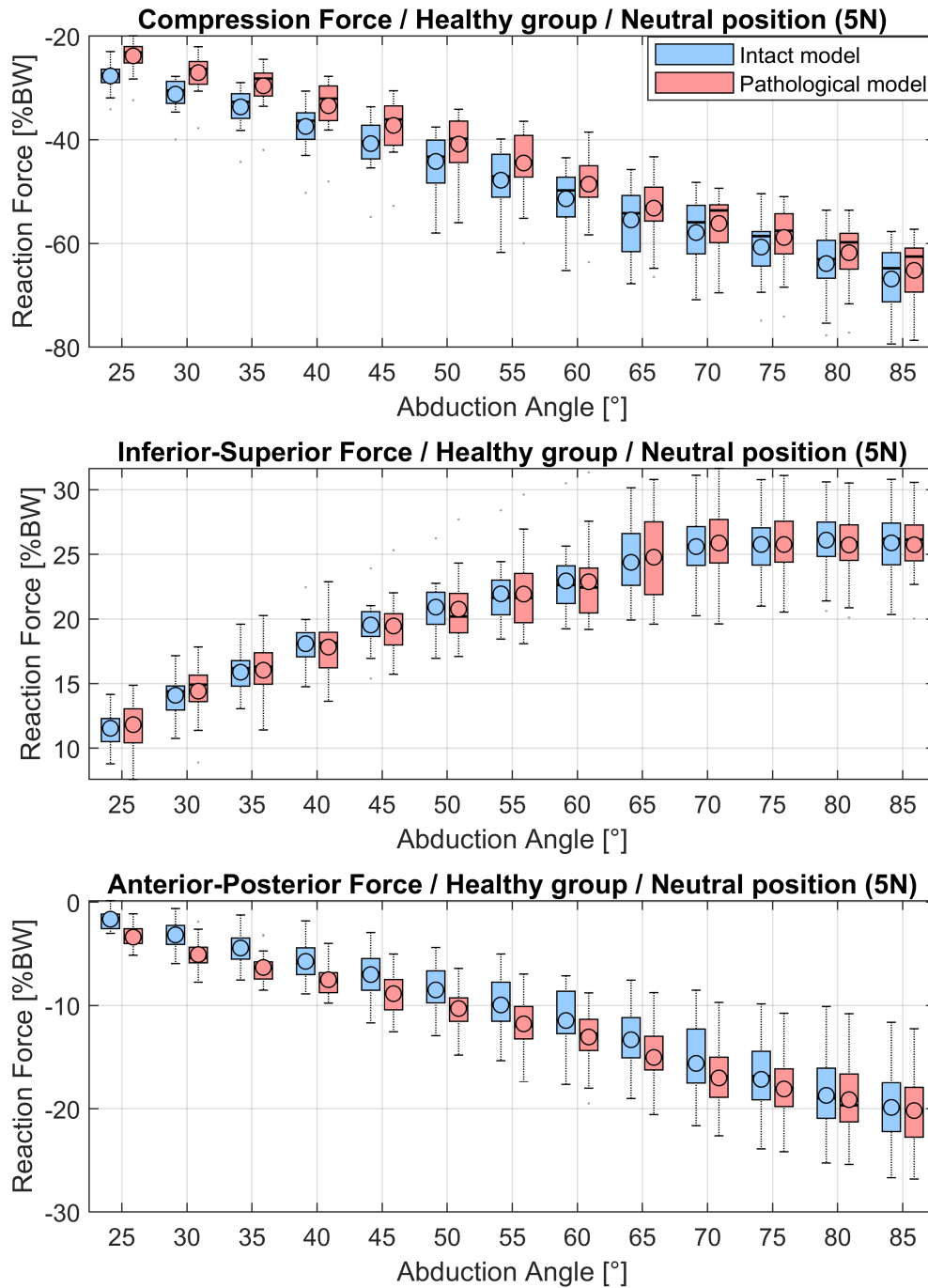


FIGURE C.18: Compression force, inferior-superior force and anterior-posterior force of intact (blue) and pathological (red) models of the healthy subject cohort during the neutral position trial with 5 N load in hand over the abduction angle in 5° increments.

Forces on the glenoid of intact model vs. pathological model

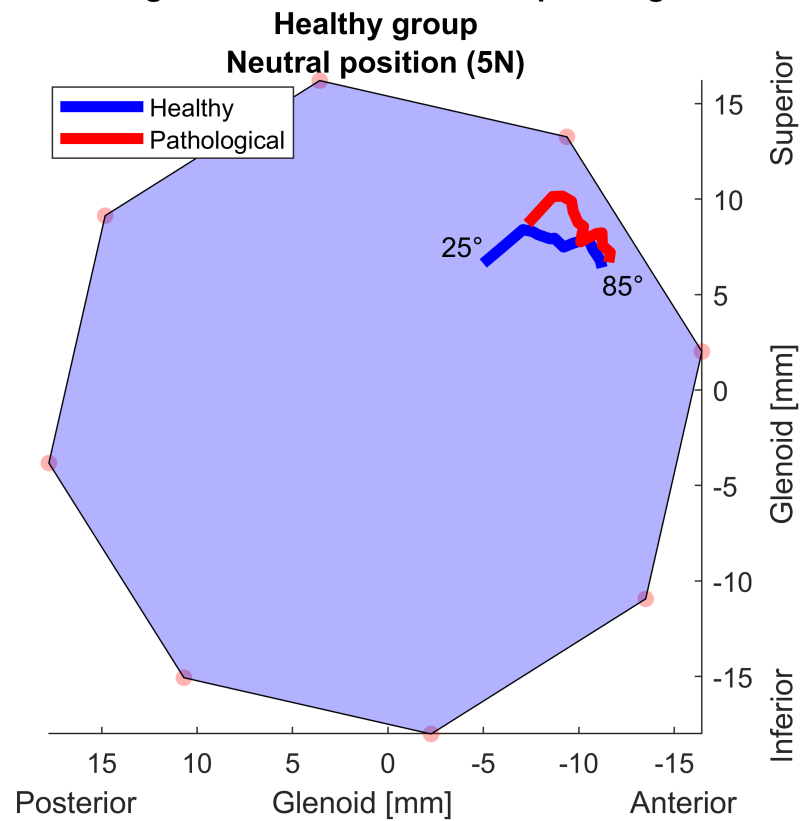


FIGURE C.19: Projected median GH joint reaction force of all models onto the glenoid of intact and pathological models of the healthy subject cohort during the neutral position trial with 5 N load in hand. Intact/healthy models (blue) and pathological models (red) with their starting value at 25° abduction and the progression up to 85° abduction.

Internal rotation

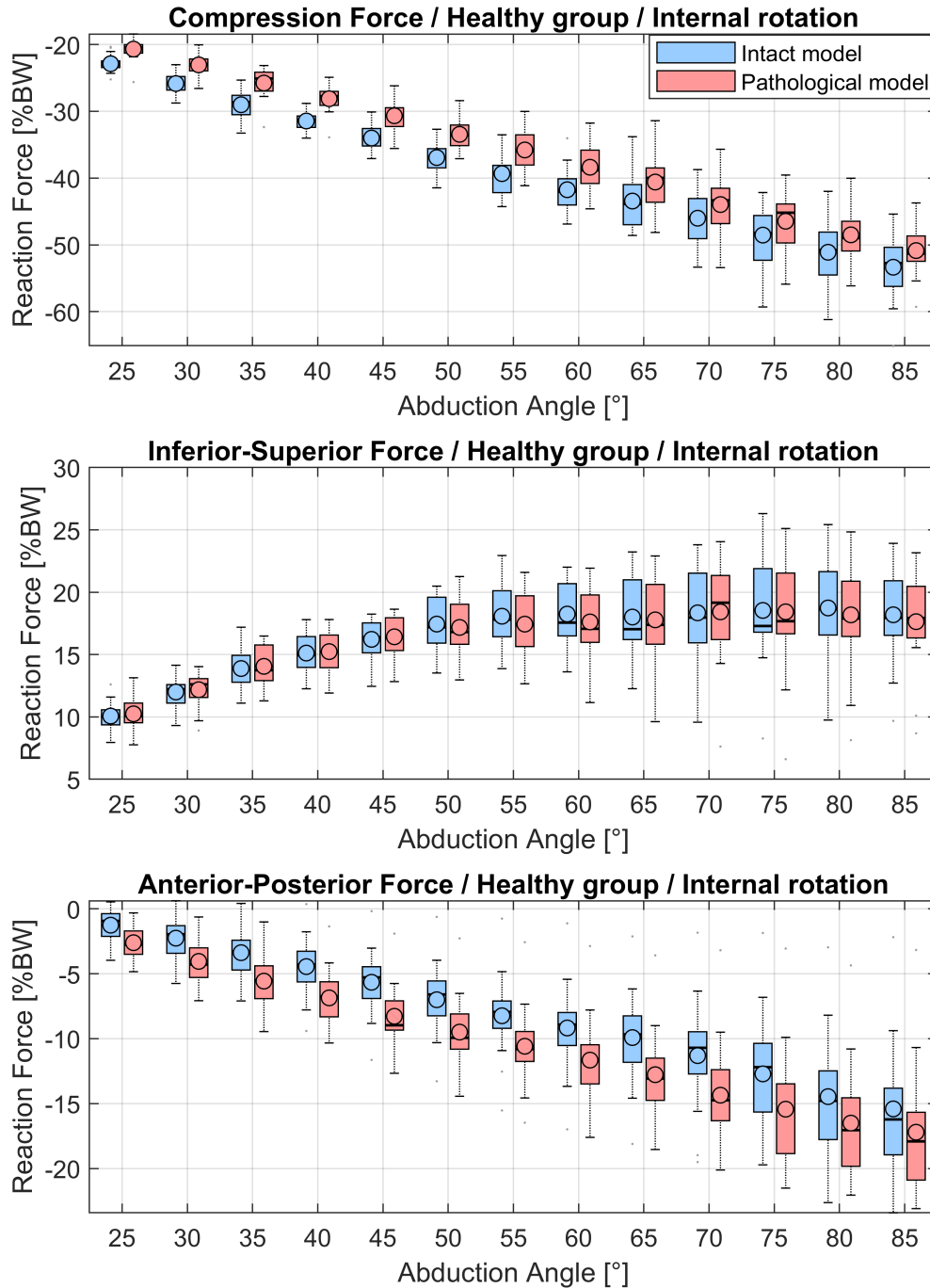


FIGURE C.20: Compression force, inferior-superior force and anterior-posterior force of intact (blue) and pathological (red) models of the healthy subject cohort during the internal rotation trial over the abduction angle in 5° increments.

Forces on the glenoid of intact model vs. pathological model

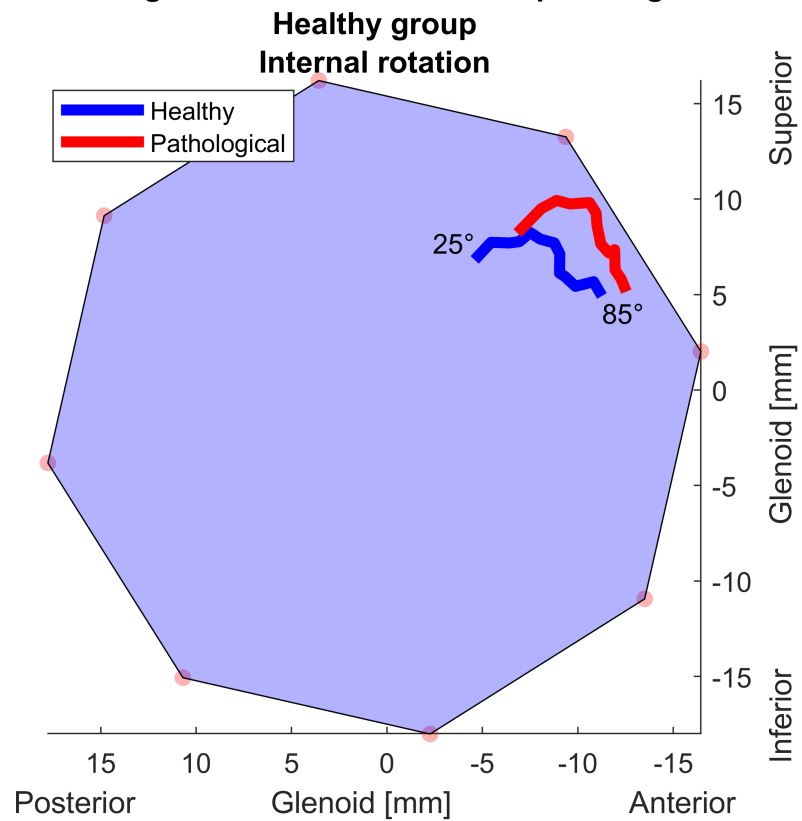


FIGURE C.21: Projected median GH joint reaction force of all models onto the glenoid of intact and pathological models of the healthy subject cohort during the internal rotation trial. Intact/healthy models (blue) and pathological models (red) with their starting value at 25° abduction and the progression up to 85° abduction.

External rotation

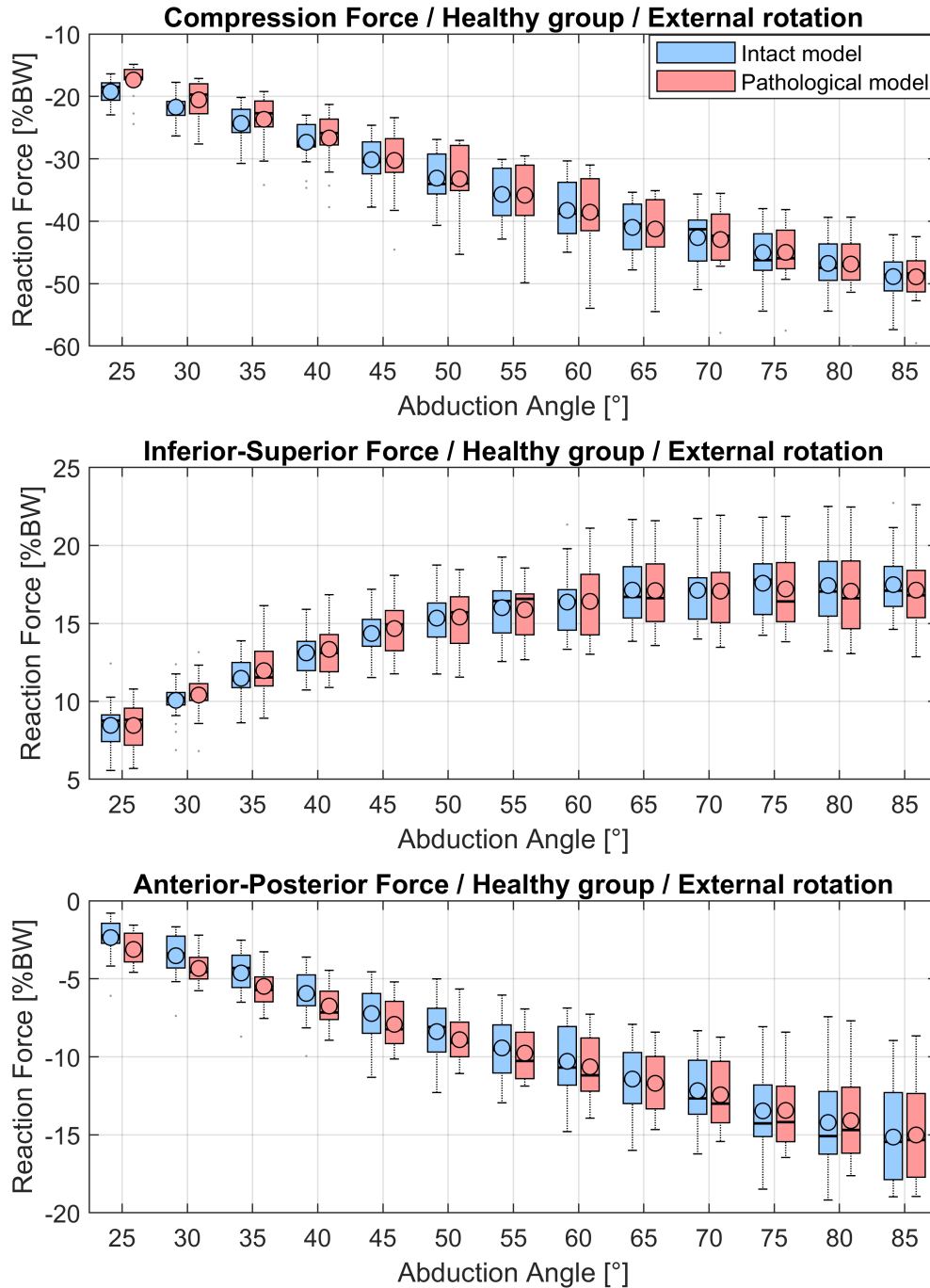


FIGURE C.22: Compression force, inferior-superior force and anterior-posterior force of intact (blue) and pathological (red) models of the healthy subject cohort during the external rotation trial over the abduction angle in 5° increments.

Forces on the glenoid of intact model vs. pathological model

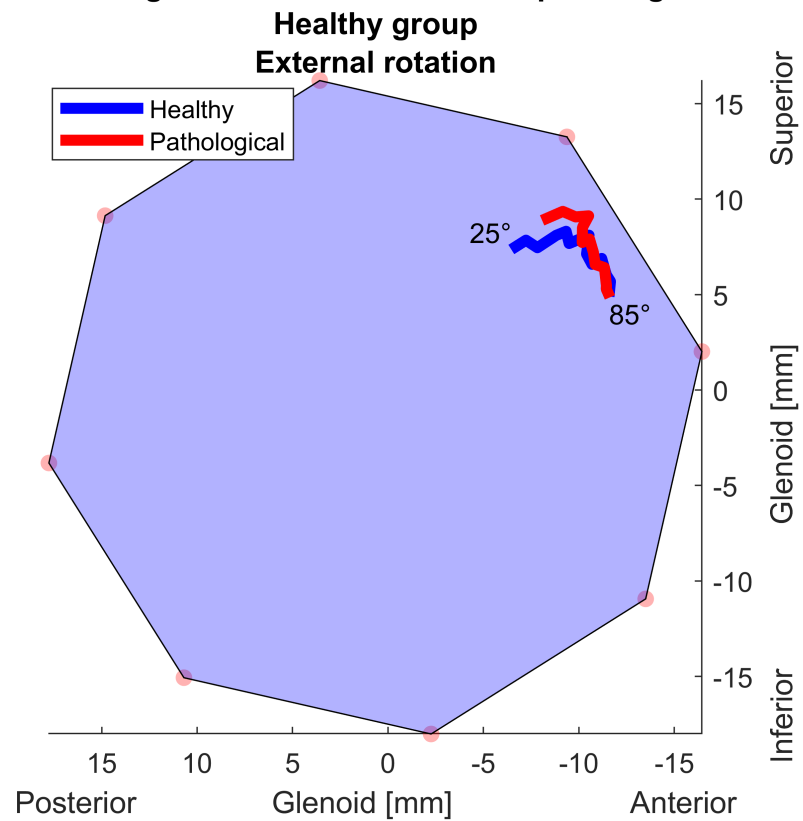


FIGURE C.23: Projected median GH joint reaction force of all models onto the glenoid of intact and pathological models of the healthy subject cohort during the external rotation trial. Intact/healthy models (blue) and pathological models (red) with their starting value at 25° abduction and the progression up to 85° abduction.

External rotation with 5N in hand

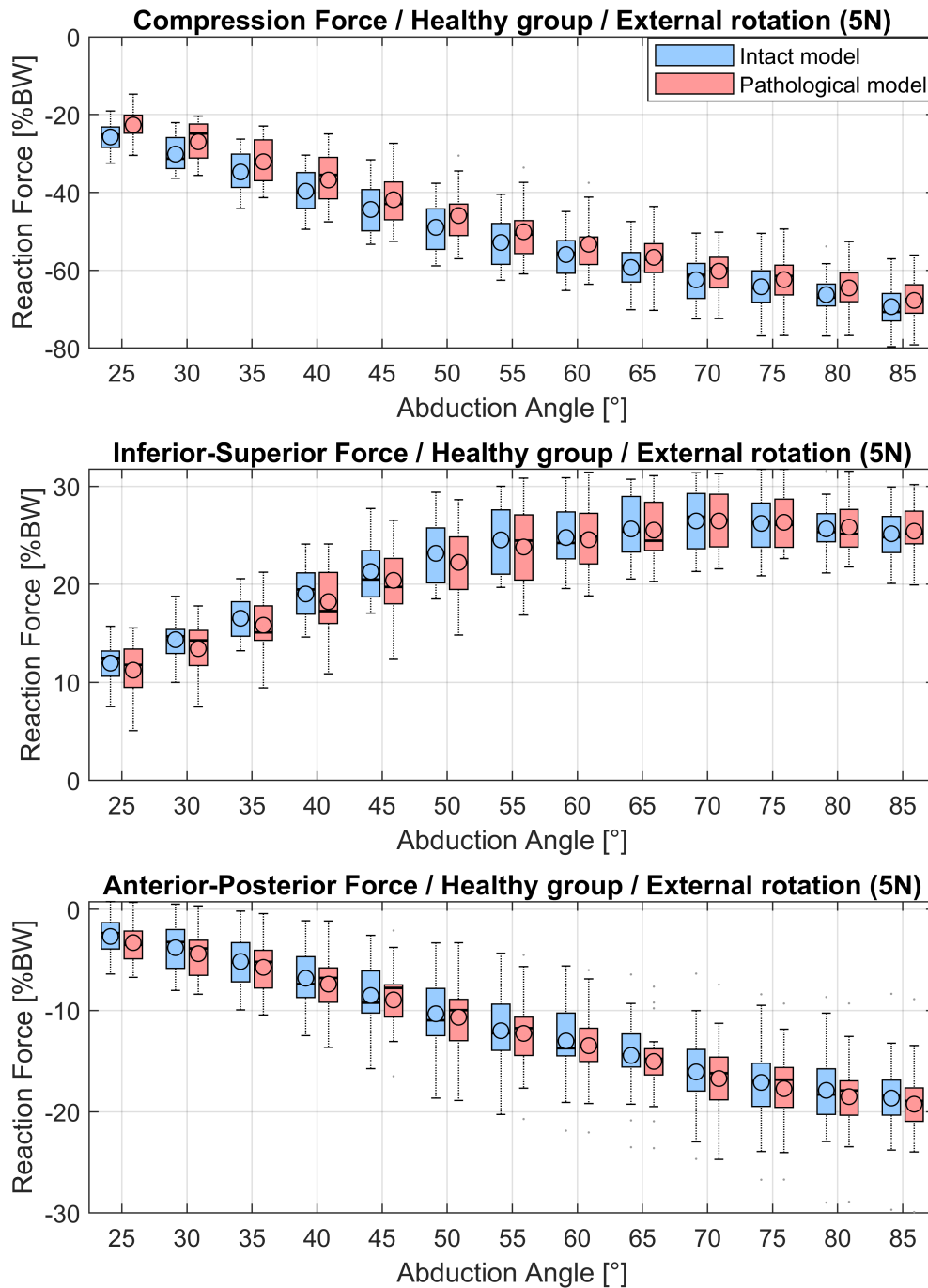


FIGURE C.24: Compression force, inferior-superior force and anterior-posterior force of intact (blue) and pathological (red) models of the healthy subject cohort during the external rotation trial with 5 N load in hand over the abduction angle in 5° increments.

Forces on the glenoid of intact model vs. pathological model

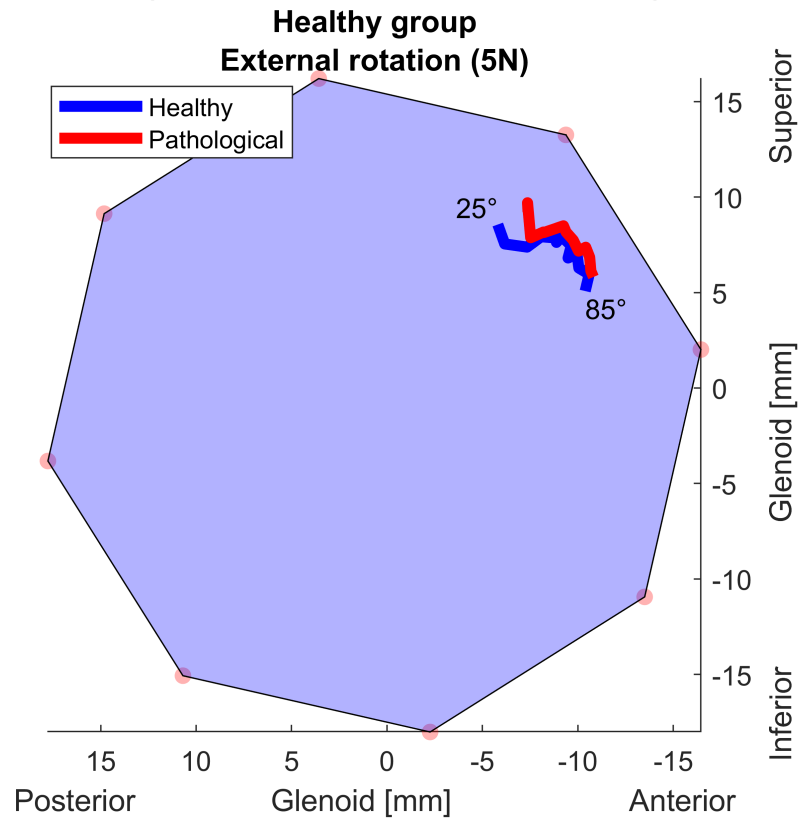


FIGURE C.25: Projected median GH joint reaction force of all models onto the glenoid of intact and pathological models of the healthy subject cohort during the external rotation trial with 5 N in hand. Intact/healthy models (blue) and pathological models (red) with their starting value at 25° abduction and the progression up to 85° abduction.

C.0.3 Numeric comparison of forces and muscle activities of intact models and pathological models of the healthy subject group

Neutral position

Abduction [°]	AD [%]	LD [%]	PD [%]	INF [%]	SS [%]	BIC [%]	TRI [%]	TM [%]	PM [%]	CF [%BW]	ISF [%BW]	APF [%BW]
25	0.8*	1.1	0.3	0.5*	-0.1	0.0	0.2	0.0	0.0	-3.0***	-0.3	1.5***
30	0.8	1.2	0.5	0.6*	-0.3	0.0	0.3	0.0	0.0	-2.6***	-0.2	1.6***
35	1.0	0.7	0.4	0.9*	-0.3	0.0	0.4	0.0	0.0	-3.2***	-0.2	1.6***
40	0.9	0.8	0.4	0.8*	0.1	0.0	0.0	0.0	0.0	-2.7**	-0.2	2.0***
45	0.8	0.8	0.3	0.8*	-0.7	0.1	0.0	0.0	3.8*	-2.0*	-0.1	1.9***
50	1.0	0.9	0.0	1.0*	-0.5	2.3	0.0	0.0	0.9*	-1.9	-0.1	1.3**
55	0.9	0.9	-0.1	0.9	-0.2	0.8	0.0	0.0	0.7*	-0.5	0.1	0.6*
60	0.6	0.9	0.2	0.7	-0.3	0.7	0.0	0.0	0.6	-1.9	0.2	0.7*
65	0.6	0.4	0.3	0.6	-0.5	0.4	0.0	0.0	0.6	0.7	0.1	0.8
70	0.6	0.4	0.2	0.4	-0.4	0.4	0.0	0.0	0.3	1.1	-0.2	0.6
75	0.3	0.2	0.1	0.3	-0.4	0.3	0.0	0.0	0.2	-0.7	0.0	1.0
80	0.3	0.2	0.2	0.3	0.0	0.1	0.0	0.0	0.1	0.3	0.0	0.9
85	0.1	0.2	0.2	0.1	-0.1	0.0	0.0	0.0	0.0	0.2	0.1	0.4

TABLE C.1: Differences in median values of muscle activities, GH joint reaction forces and kinematics between intact and pathological models of the healthy subject cohort during the neutral position trial in 5° increments. Asterisks indicate the significance level. AD = anterior deltoid, LD = lateral deltoid, PD = posterior deltoid, INF = infraspinatus, SS = subscapularis, BIC = biceps, TRI = triceps, TM = teres minor, PM = pectoralis major, CF = compression force, ISF = inferior-superior force, APF = anterior-posterior force, FLX = Flexion angle, ER = external rotation angle

Neutral position with 5N in hand

Abduction [°]	AD [%]	LD [%]	PD [%]	INF [%]	SS [%]	BIC [%]	TRI [%]	TM [%]	PM [%]	CF [%BW]	ISF [%BW]	APF [%BW]
25	1.0*	1.2*	0.7	0.8*	0.1	0.0	0.4	0.0	0.0	-4.2***	-0.2	2.0***
30	1.1*	1.2*	0.7	0.9*	-0.3	0.0	0.4	0.0	0.0	-4.1***	-0.5	2.2***
35	1.2	1.4	0.5	0.9*	-0.4	0.0	0.2	0.0	0.0	-4.5***	-0.1	1.9***
40	1.2	1.5	0.4	1.3*	-0.7	-0.9	0.6	0.0	0.0	-4.3**	-0.1	1.8**
45	1.0*	0.9	-0.2	1.2*	-1.5	0.0	0.6	0.0	0.1	-4.2*	0.2	2.0*
50	0.5	0.3	-0.1	0.7	-1.6	0.1	0.0	0.0	1.0	-3.5	0.6	1.5*
55	0.7	0.9	0.1	0.6	-1.3	0.5	0.0	0.0	0.8	-2.9	0.0	2.2*
60	0.3	0.2	0.2	0.4	-0.6	0.6	0.0	0.0	0.2	-1.7	0.2	1.3
65	0.7	0.3	-0.1	0.5	-0.6	0.3	0.0	0.0	0.1	-1.4	-0.3	1.7
70	0.4	0.7	-0.3	0.8	-0.5	0.2	0.0	0.0	0.0	-2.3	-0.1	1.2
75	0.2	0.1	-0.2	0.5	-0.2	0.2	0.0	0.0	0.0	-1.0	-0.1	1.1
80	0.2	0.2	-0.2	0.4	-1.0	-0.1	0.0	0.0	0.1	-3.3	0.2	0.7
85	0.2	0.3	0.1	0.7	-0.9	0.0	0.0	0.0	0.0	-2.2	0.1	0.3

TABLE C.2: Differences in median values of muscle activities, GH joint reaction forces and kinematics between intact and pathological models of the healthy subject cohort during the neutral position trial with 5 N load in hand in 5° increments. Asterisks indicate the significance level. AD = anterior deltoid, LD = lateral deltoid, PD = posterior deltoid, INF = infraspinatus, SS = subscapularis, BIC = biceps, TRI = triceps, TM = teres minor, PM = pectoralis major, CF = compression force, ISF = inferior-superior force, APF = anterior-posterior force, FLX = Flexion angle, ER = external rotation angle

Internal rotation

Abduction [°]	AD [%]	LD [%]	PD [%]	INF [%]	SS [%]	BIC [%]	TRI [%]	TM [%]	PM [%]	CF [%BW]	ISF [%BW]	APF [%BW]
25	1.0**	0.6	0.2	0.7	-0.2	0.0	0.2	0.0	0.0	-2.6***	-0.1	1.8**
30	1.1**	1.1	0.4	0.7	0	0.0	0.1	0.0	0.0	-2.9***	-0.4	2.3**
35	1.1*	1.2	0.2	1.1	0.2	0.0	0.8	0.0	0.0	-3.6***	0.1	2.2**
40	1.0	0.5	0.3	1.5	0.1	0.0	1.1	0.0	0.0	-3.5***	-0.3	2.4**
45	1.1*	1.2	0.3	0.9	0.4	0.0	0.7	0.0	3.9**	-3.1***	0.1	3.7***
50	1.3	1.1	0.0	1.4	0.4	0.0	0.9	0.0	1.3**	-3.3***	0.4	3.3**
55	1.0	1.1	0.2	0.9	0.2	0.0	1.1	0.0	0.9*	-3.4**	0.5	2.9**
60	0.9	1.1	0.2	1.1	0.4	0.0	1.0	0.0	1.1	-3.2**	0.5	2.8*
65	1.0	1.1	0.4	0.9	0.2	0.0	0.6	0.0	0.9	-3.9*	-0.3	3.4**
70	0.9	1.0	0.3	0.7	0.3	0.0	0.4	0.0	0.4	-2.5	-1.2	4.0**
75	0.8	0.8	0.0	0.5	0.4	0.0	0.2	0.0	0.8	-3.0	-0.4	3.3
80	0.5	0.5	0.0	0.5	0.0	0.0	0.1	0.0	0.3	-1.8	0.7	2.3
85	0.4	0.5	-0.1	0.7	0.0	0.0	0.3	0.0	0.5	-1.4	0.0	1.7

TABLE C.3: Differences in median values of muscle activities, GH joint reaction forces and kinematics between intact and pathological models of the healthy subject cohort during the internal rotation trial in 5° increments. Asterisks indicate the significance level. AD = anterior deltoid, LD = lateral deltoid, PD = posterior deltoid, INF = infraspinatus, SS = subscapularis, BIC = biceps, TRI = triceps, TM = teres minor, PM = pectoralis major, CF = compression force, ISF = inferior-superior force, APF = anterior-posterior force, FLX = Flexion angle, ER = external rotation angle

External rotation

Abduction [°]	AD [%]	LD [%]	PD [%]	INF [%]	SS [%]	BIC [%]	TRI [%]	TM [%]	PM [%]	CF [%BW]	ISF [%BW]	APF [%BW]
25	0.9*	0.7	0.4	0.5*	-1.3	0.4	-0.3	0.0	0.0	-1.5**	-0.1	0.9*
30	0.9*	1.0	0.2	0.8	-2.2	0.4	0.0	0.0	0.0	-1.9	-0.2	1.2*
35	0.9	0.8	0.2	1.0*	-1.5	0.7	0.0	1.2	2.2	-1.9	-0.2	1.4*
40	0.8	0.8	0.1	1.1*	-1.1	0.6	0.0	1.8	1.0	-2.0	0.1	1.1
45	0.8	0.8	0.1	1.1*	0.0	0.5	0.0	1.1	0.8	-0.3	-0.5	1.0
50	0.8	0.5	-0.1	1.2	-0.5	0.7	0.0	0.8	0.1	-0.1	-0.5	1.0
55	0.6	0.5	0.1	1.0	-0.4	0.2	0.0	0.6	0.2	0.2	-0.1	0.7
60	0.5	0.4	0.3	1.0	0.0	0.2	0.0	0.6	0.3	0.1	0.1	0.5
65	0.4	0.3	0.1	0.8	-0.1	0.3	0.0	0.4	0.3	0.8	0.1	0.2
70	0.3	0.4	0.2	0.4	0.0	0.2	0.0	0.4	0.4	1.1	0.3	0.3
75	0.2	0.1	0.1	-0.2	-0.5	-0.3	0.0	0.3	0.2	-0.3	1.4	-0.1
80	0.2	0.2	0.1	-0.2	0.0	-0.1	0.0	0.2	0.4	-0.3	0.4	-0.4
85	0.1	0.1	0.1	-0.1	0.0	-0.2	0.0	0.2	0.3	-0.2	0.3	-0.1

TABLE C.4: Differences in median values of muscle activities, GH joint reaction forces and kinematics between intact and pathological models of the healthy subject cohort during the external rotation trial in 5° increments. Asterisks indicate the significance level. AD = anterior deltoid, LD = lateral deltoid, PD = posterior deltoid, INF = infraspinatus, SS = subscapularis, BIC = biceps, TRI = triceps, TM = teres minor, PM = pectoralis major, CF = compression force, ISF = inferior-superior force, APF = anterior-posterior force, FLX = Flexion angle, ER = external rotation angle

Eternal rotation with 5N in hand

Abduction [°]	AD [%]	LD [%]	PD [%]	INF [%]	SS [%]	BIC [%]	TRI [%]	TM [%]	PM [%]	CF [%BW]	ISF [%BW]	APF [%BW]
25	0.7	0.8	0.7	0.8	-1.3	0.4	0.0	0.0	0.0	-2.6*	0.7	1.2
30	0.9	0.9	-0.2	0.7	-2.3	0.8	0.0	1.8	0.0	-6.5*	0.4	0.6
35	0.6	0.7	0.5	0.9	-3.1	0.3	0.0	1.4	0.0	-2.8	1.3	-0.1
40	1.1	0.8	-0.2	1.2	-3.4	0.0	0.0	0.1	0.0	-4.4	2.2	-0.6
45	1.3	1.3	0.2	0.7	-0.1	0.1	0.0	-0.1	4.2	-1.5	0.8	-1.5
50	0.6	1.0	-0.4	0.4	-0.7	0.0	0.0	-0.7	1.3	-3.2	0.9	-1.0
55	0.7	1.2	0.1	0.4	-1.7	-0.2	0.0	-1	0.8	-1.7	0.1	-0.5
60	0.5	0.7	-0.4	-0.2	-3.3	0.1	0.0	0.1	0.1	-2.3	-0.7	-0.1
65	-0.1	0.2	0.0	0.3	-2.1	-0.2	0.0	0.3	0.1	-1.6	0.9	0.4
70	-0.2	0.1	-0.1	1.1	-3.3	-0.2	0.0	0.3	-0.1	-1.7	0.3	0.1
75	0.5	0.4	-0.6	0.3	-3.5	0.0	0.0	0.4	0.2	-3.2	0.2	-0.1
80	0.2	0.4	-0.4	0.1	-1.4	0.0	0.0	0.3	0.1	-2.3	0.2	-0.4
85	0.1	0.3	0.1	0.3	-2	0.0	0.0	0.2	-0.4	-3.3	-0.4	0.5

TABLE C.5: Differences in median values of muscle activities, GH joint reaction forces and kinematics between intact and pathological models of the healthy subject cohort during the external rotation trial with 5 N load in hand in 5° increments. Asterisks indicate the significance level. AD = anterior deltoid, LD = lateral deltoid, PD = posterior deltoid, INF = infraspinatus, SS = subscapularis, BIC = biceps, TRI = triceps, TM = teres minor, PM = pectoralis major, CF = compression force, ISF = inferior-superior force, APF = anterior-posterior force, FLX = Flexion angle, ER = external rotation angle

C.0.4 Kinematics of the humerus of healthy and pathological subjects

Neutral position

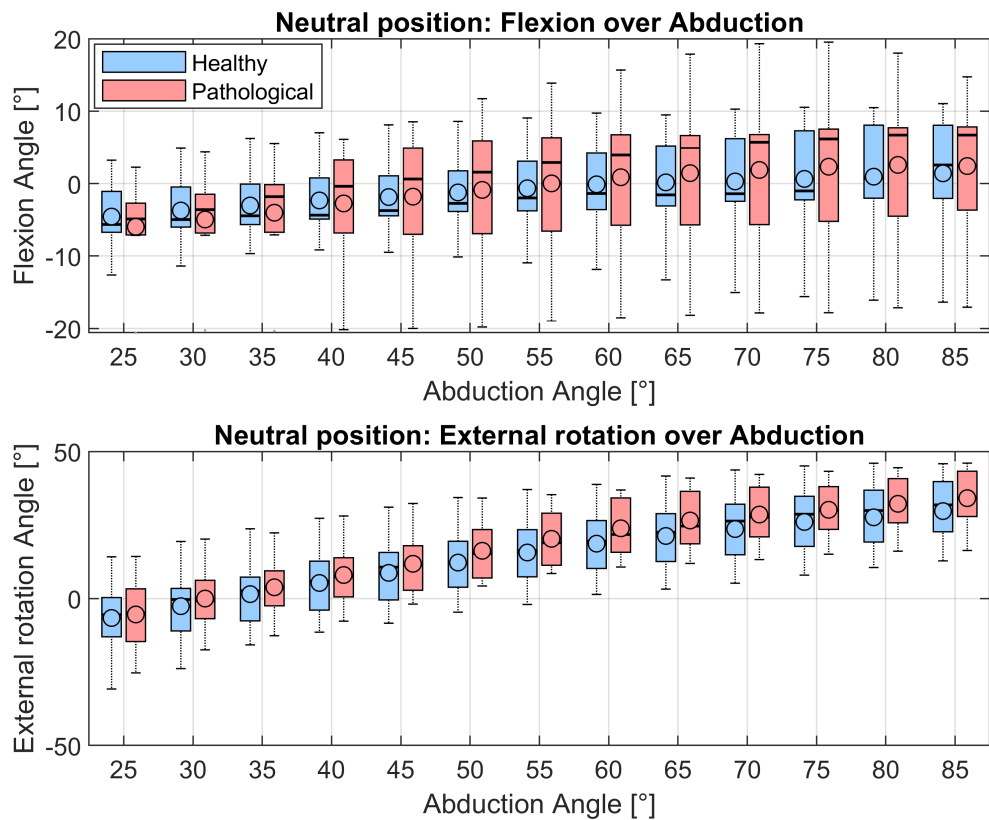


FIGURE C.26: Flexion and external rotation angle over abduction of the healthy cohort (blue) and pathological cohort (red) during the neutral position trial.

Neutral position with 5 N in hand

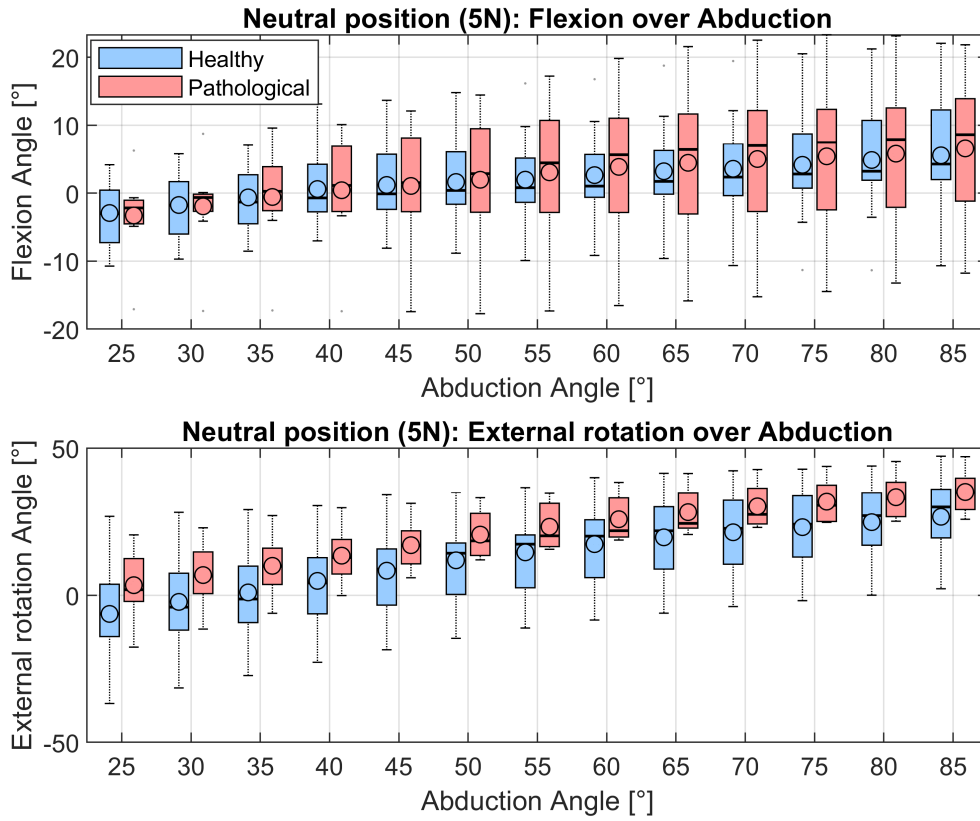


FIGURE C.27: Flexion and external rotation angle over abduction of the healthy cohort (blue) and pathological cohort (red) during the neutral position trial with 5 N load in hand.

Internal rotation

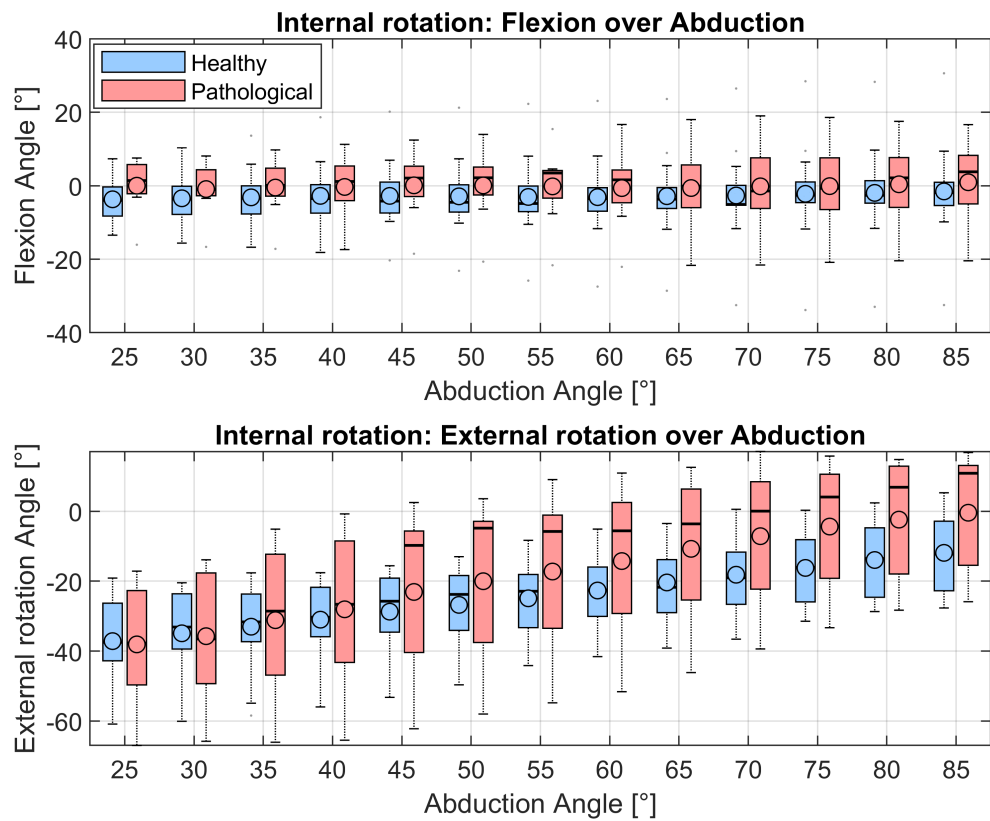


FIGURE C.28: Flexion and external rotation angle over abduction of the healthy cohort (blue) and pathological cohort (red) during the internal rotation trial.

External rotation

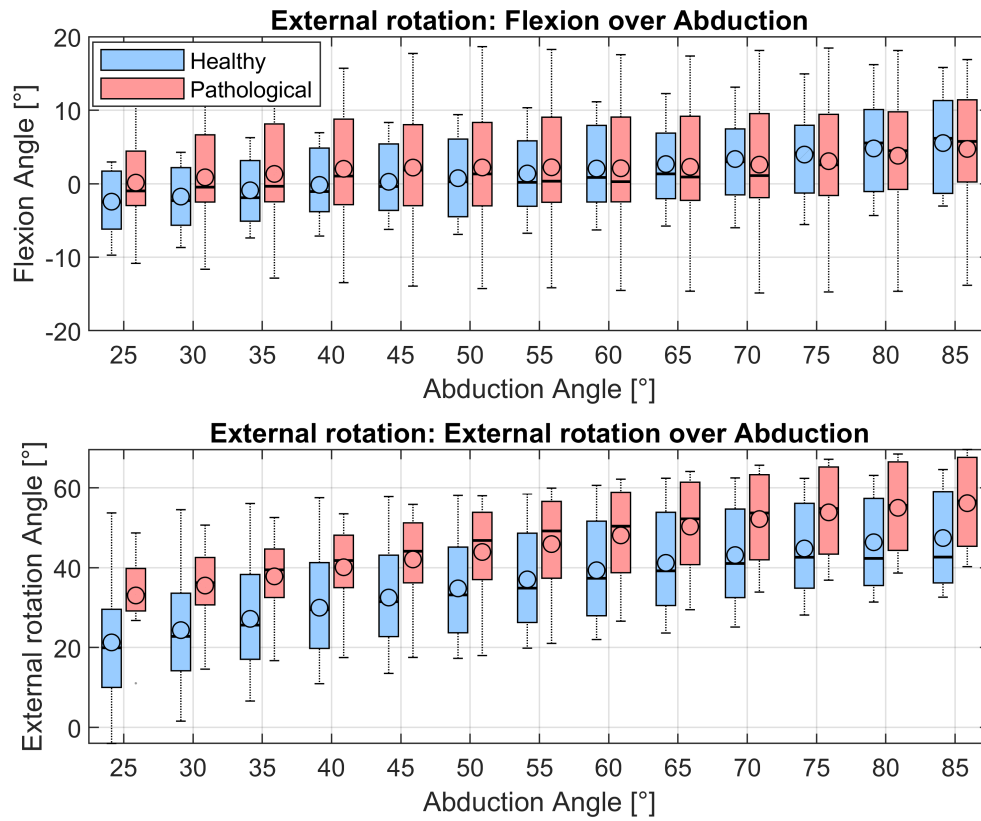


FIGURE C.29: Flexion and external rotation angle over abduction of the healthy cohort (blue) and pathological cohort (red) during the external rotation trial.

External rotation with 5N in hand

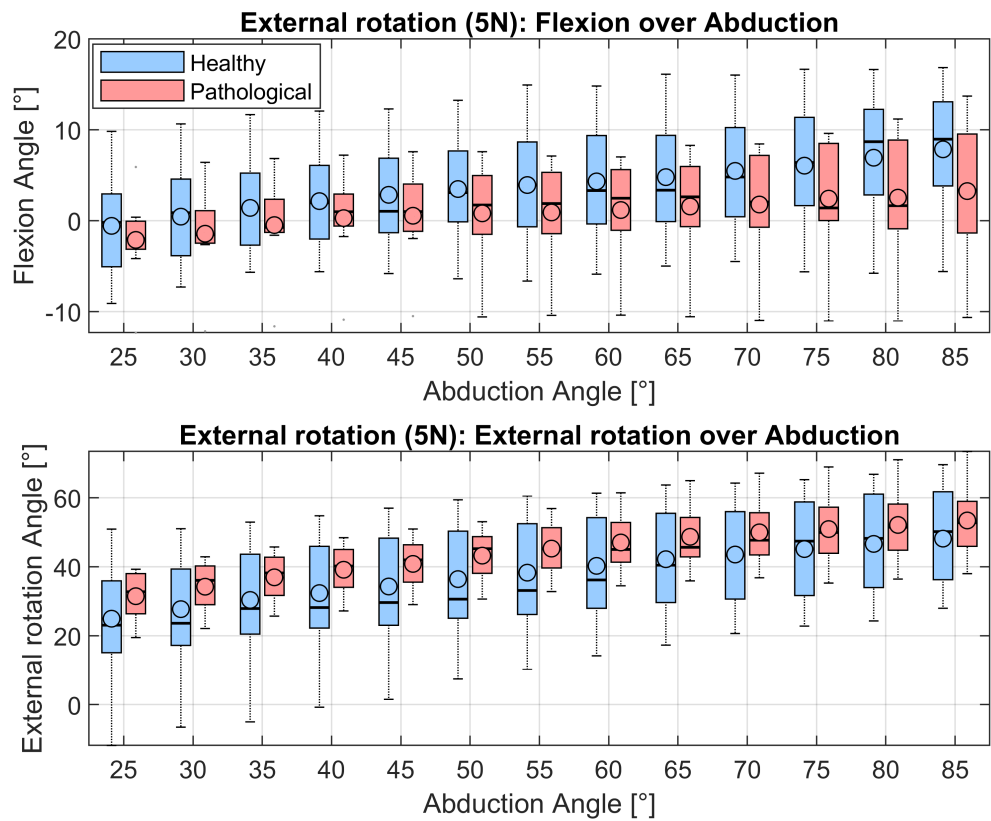


FIGURE C.30: Flexion and external rotation angle over abduction of the healthy cohort (blue) and pathological cohort (red) during the external rotation trial with 5 N load in hand.

C.0.5 Muscle activities of intact models and pathological models of the healthy vs. the pathological group

Neutral position

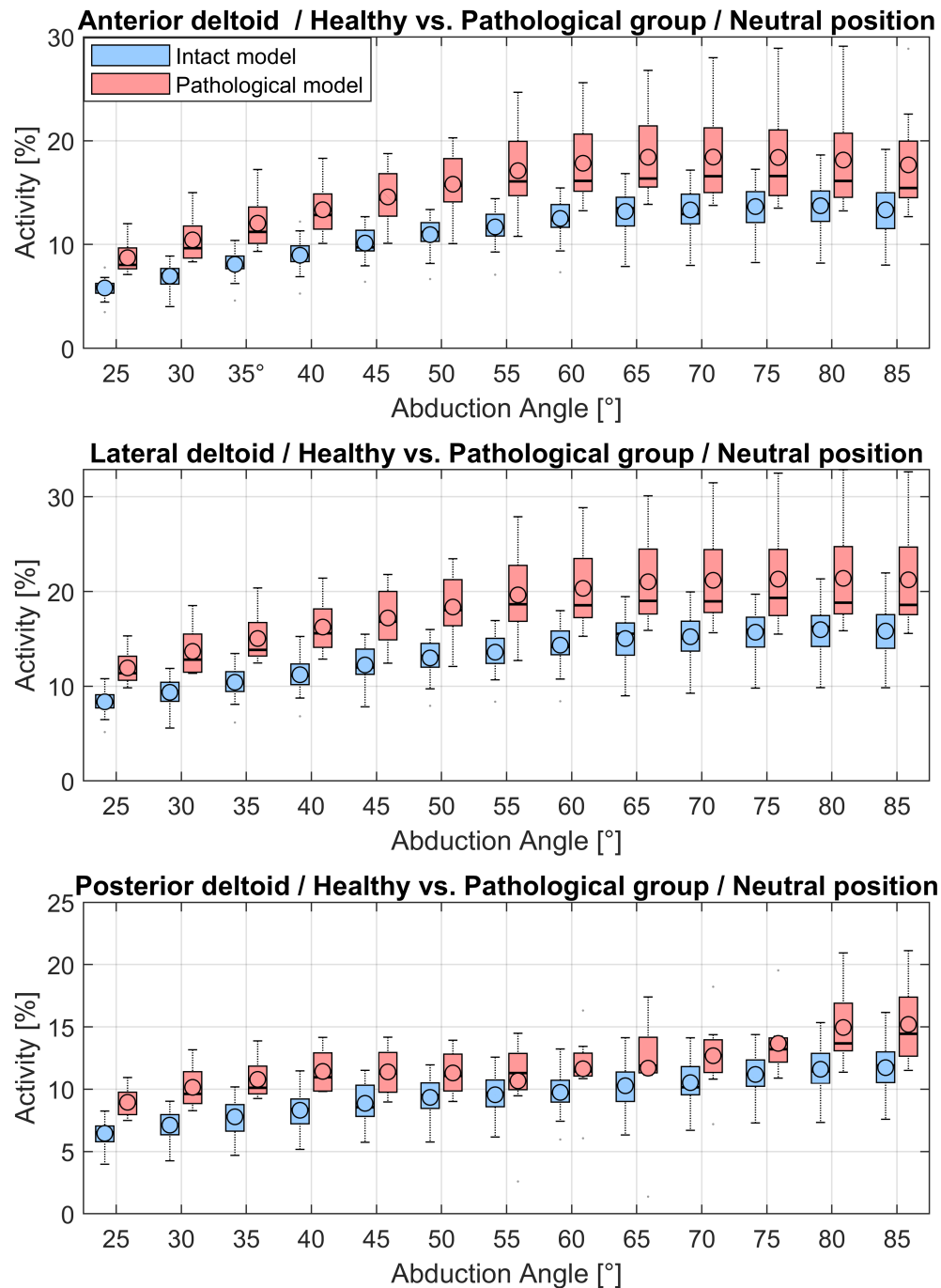


FIGURE C.31: Computed muscle activities of the anterior, posterior and lateral deltoids over the abduction angle in 5° increments during the neutral position trial. Blue depicts the activities of the intact model of the healthy subject group and red the modelled tear of the m. supraspinatus of the patient group.

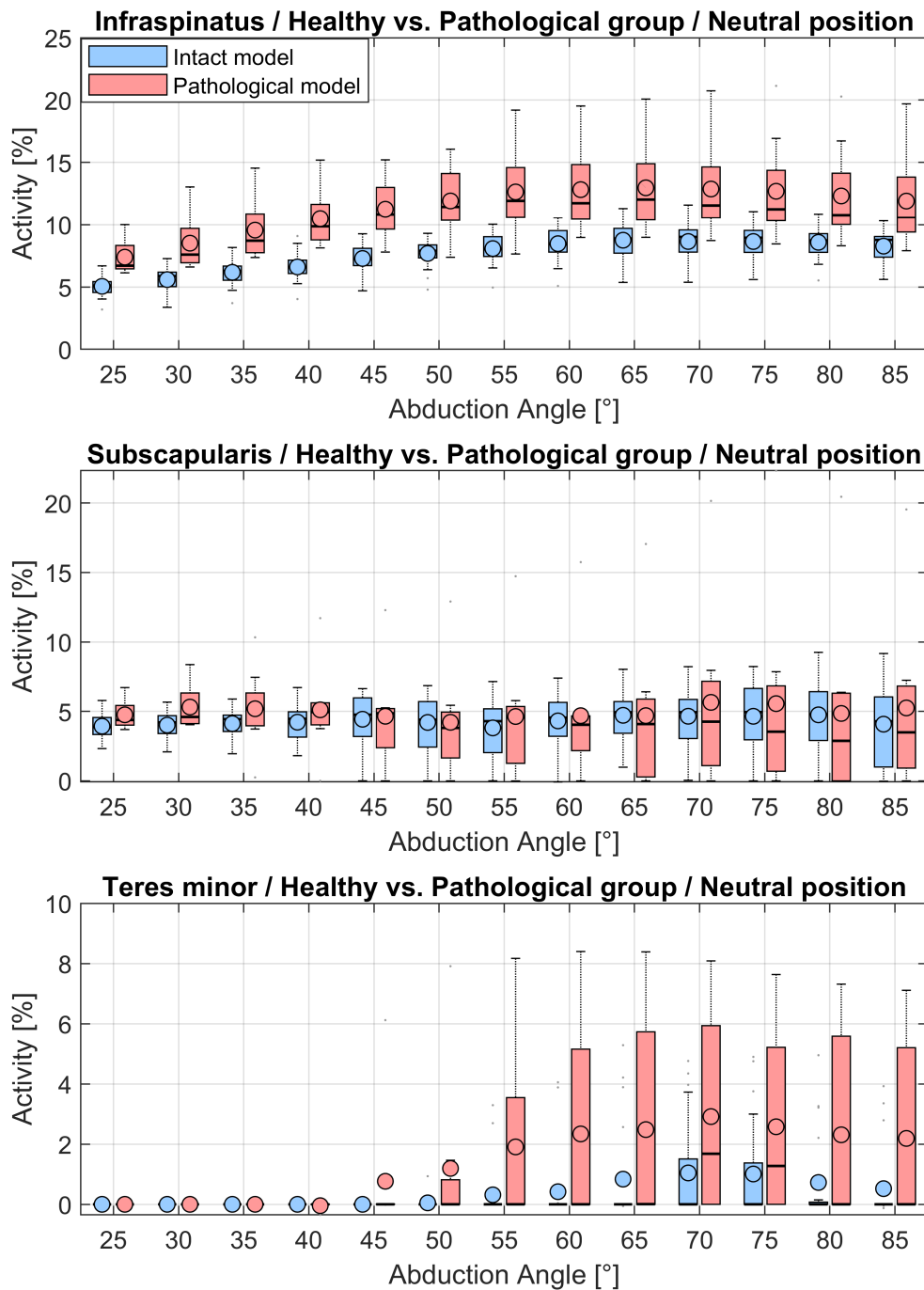


FIGURE C.32: Computed muscle activities of the infraspinatus, subscapularis and teres minor over the abduction angle in 5° increments during the neutral position trial. Blue depicts the activities of the intact model of the healthy subject group and red the modelled tear of the m. supraspinatus of the patient group.

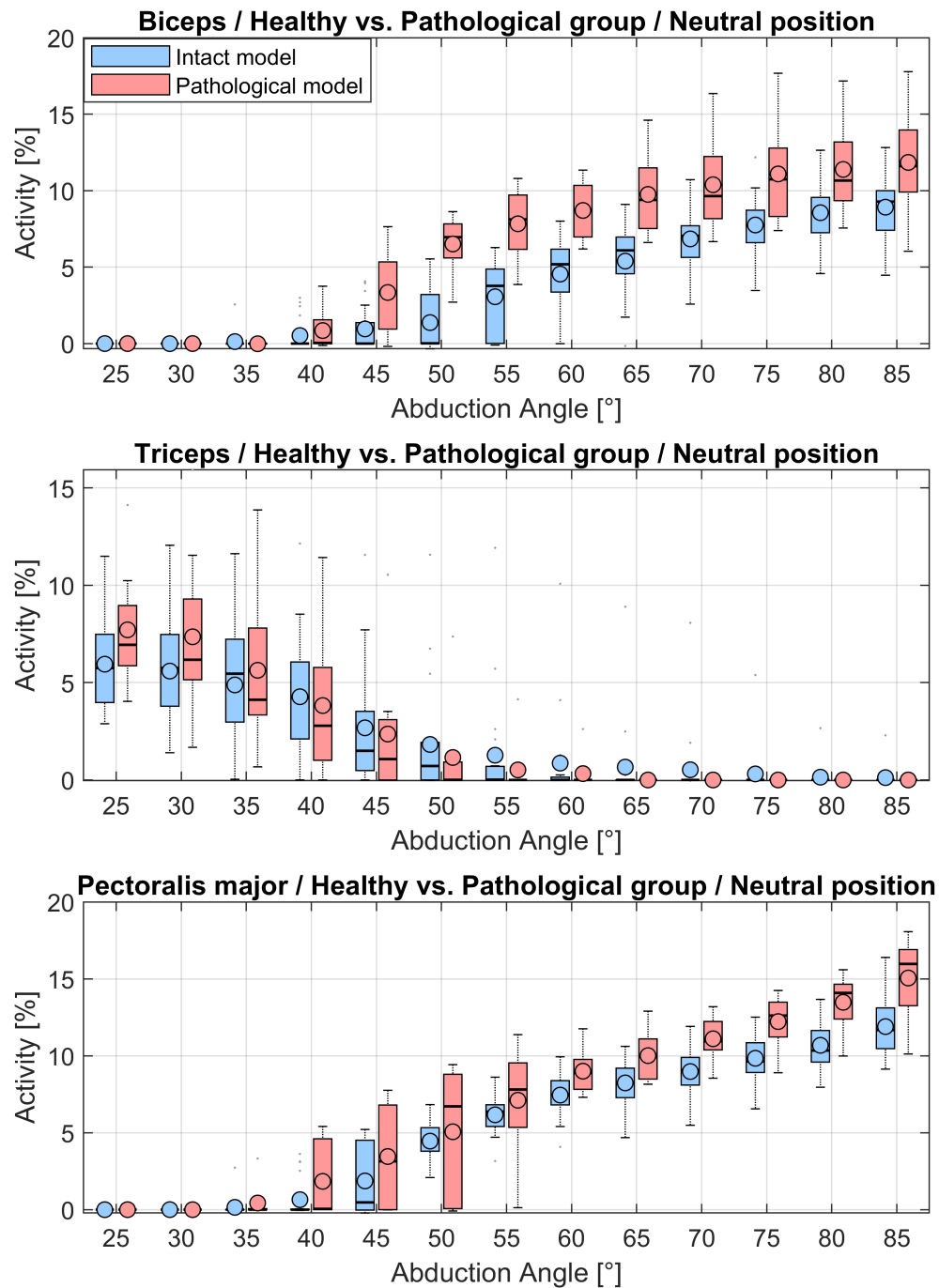


FIGURE C.33: Computed muscle activities of the biceps, triceps and pectoralis major over the abduction angle in 5° increments during the neutral position trial. Blue depicts the activities of the intact model of the healthy subject group and red the modelled tear of the m. supraspinatus of the patient group.

Neutral position with 5N in hand

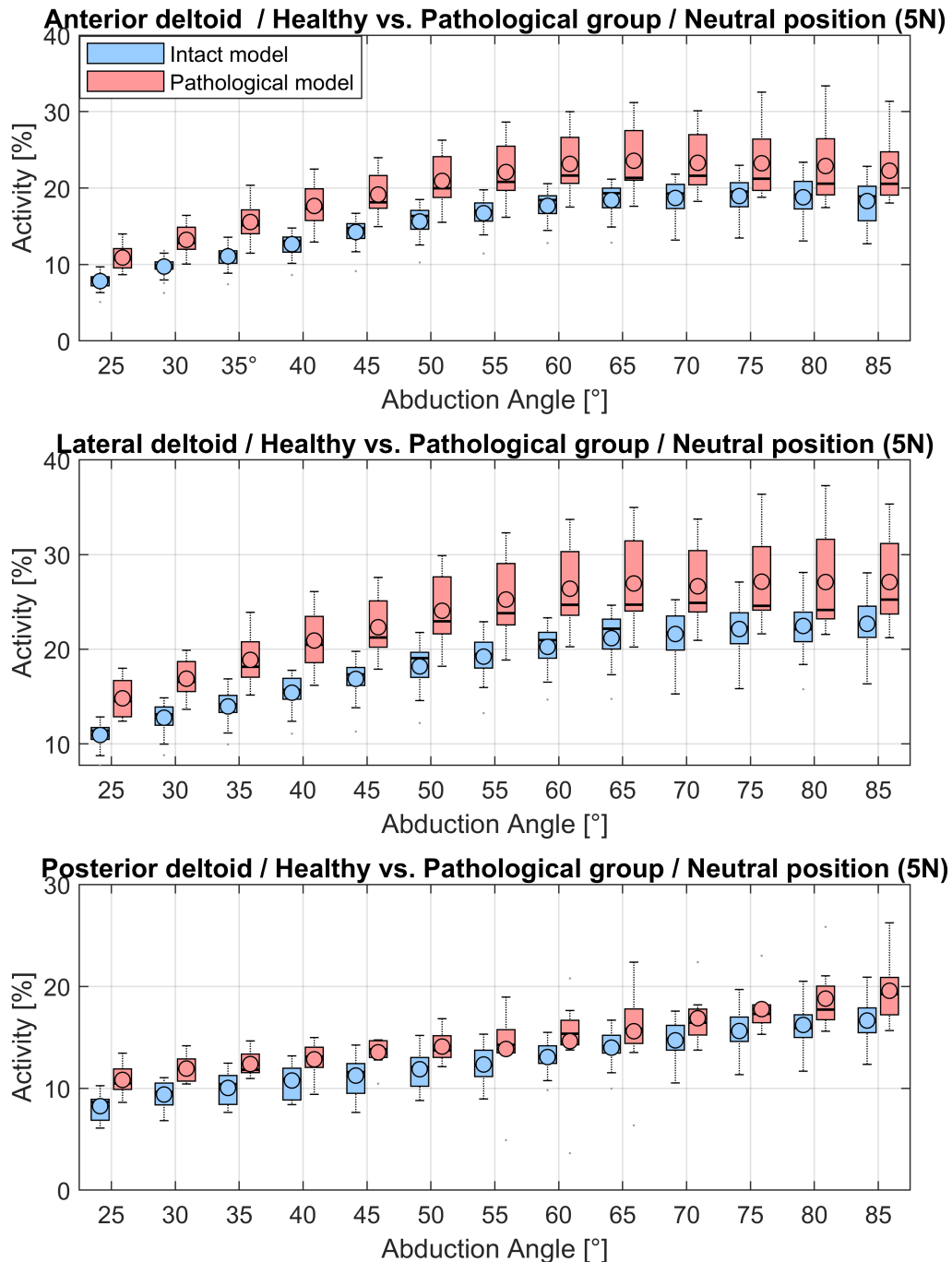


FIGURE C.34: Computed muscle activities of the anterior, posterior and lateral deltoids over the abduction angle in 5° increments during the neutral position trial with 5 N load in hand. Blue depicts the activities of the intact model of the healthy subject group and red the modelled tear of the m. supraspinatus of the patient group.

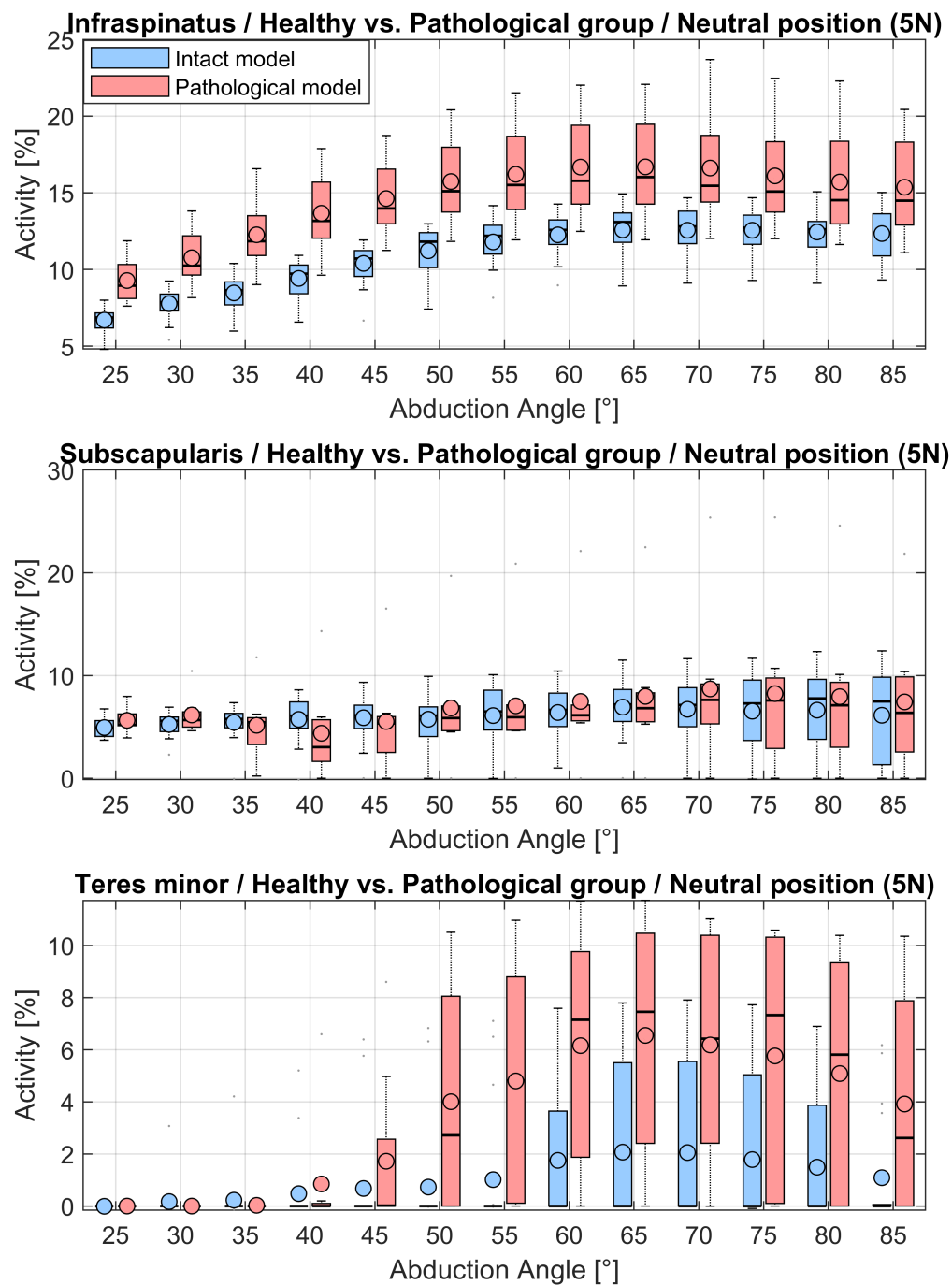


FIGURE C.35: Computed muscle activities of the infraspinatus, subscapularis and teres minor over the abduction angle in 5° increments during the neutral position trial with 5 N load in hand. Blue depicts the activities of the intact model of the healthy subject group and red the modelled tear of the m. supraspinatus of the patient group.

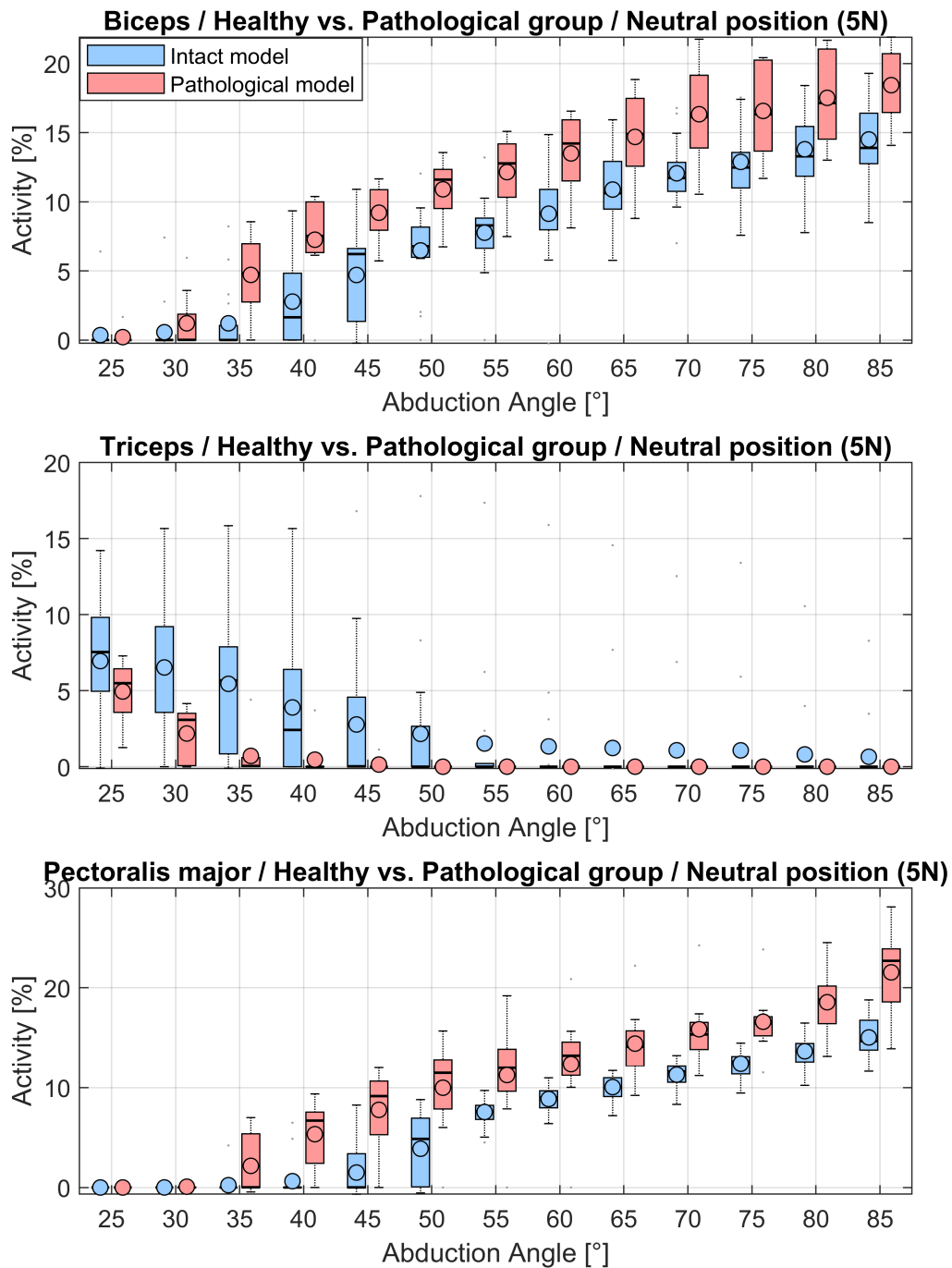


FIGURE C.36: Computed muscle activities of the biceps, triceps and pectoralis major over the abduction angle in 5° increments during the neutral position trial with 5 N load in hand. Blue depicts the activities of the intact model of the healthy subject group and red the modelled tear of the m. supraspinatus of the patient group.

Internal rotation

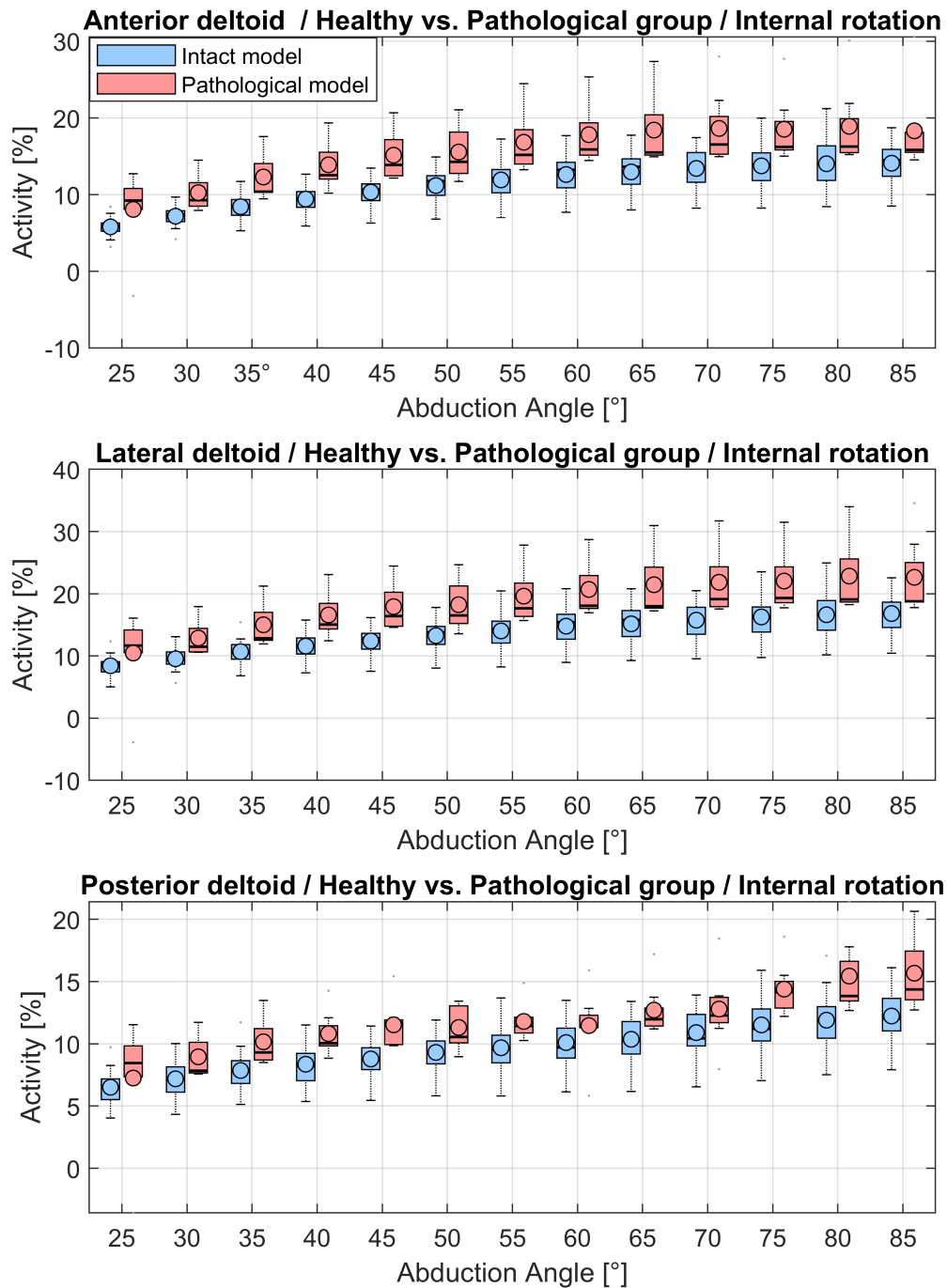


FIGURE C.37: Computed muscle activities of the anterior, posterior and lateral deltoids over the abduction angle in 5° increments during the internal rotation trial. Blue depicts the activities of the intact model of the healthy subject group and red the modelled tear of the m. supraspinatus of the patient group.

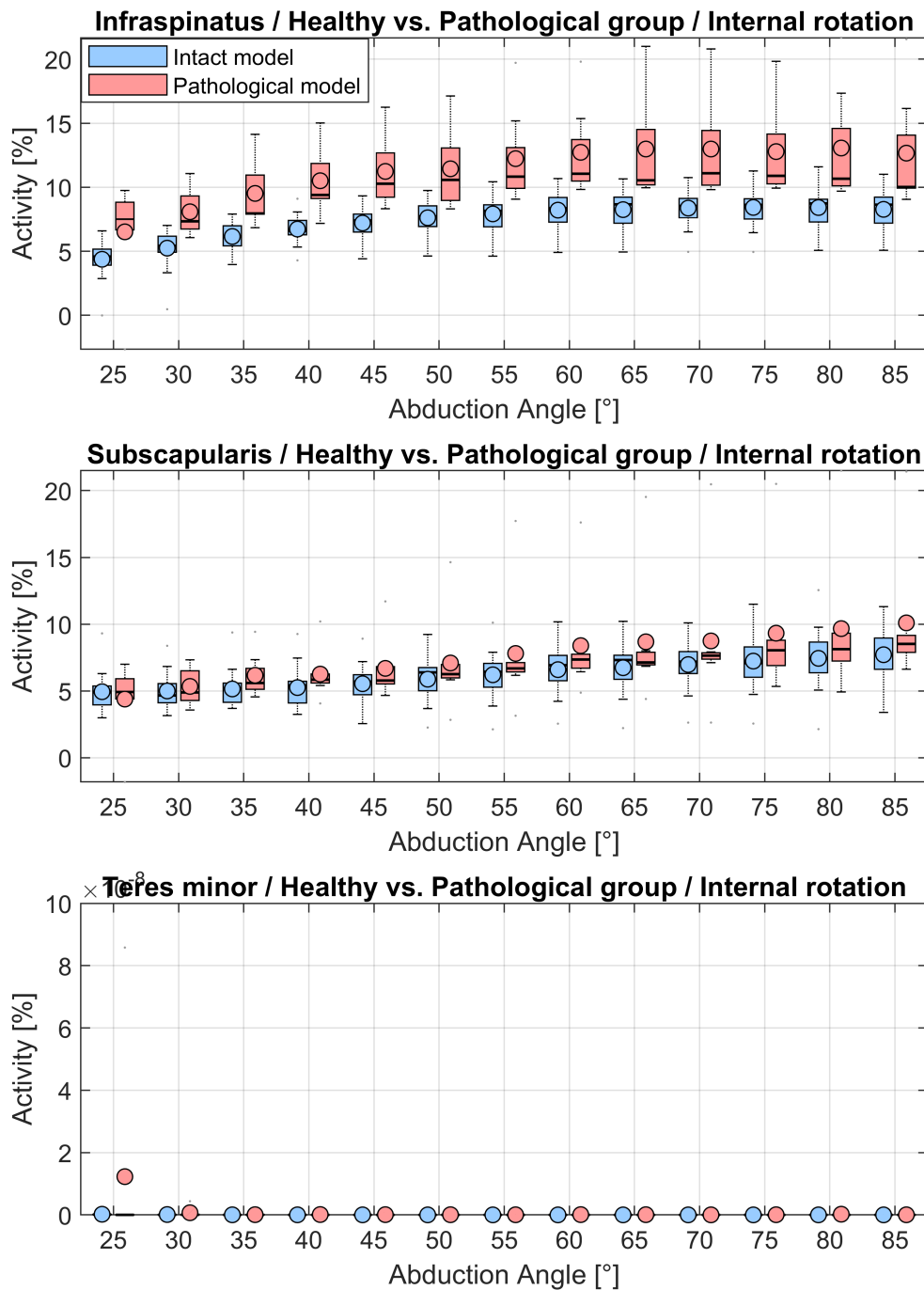


FIGURE C.38: Computed muscle activities of the infraspinatus, subscapularis and teres minor over the abduction angle in 5° increments during the internal rotation trial. Blue depicts the activities of the intact model of the healthy subject group and red the modelled tear of the m. supraspinatus of the patient group.

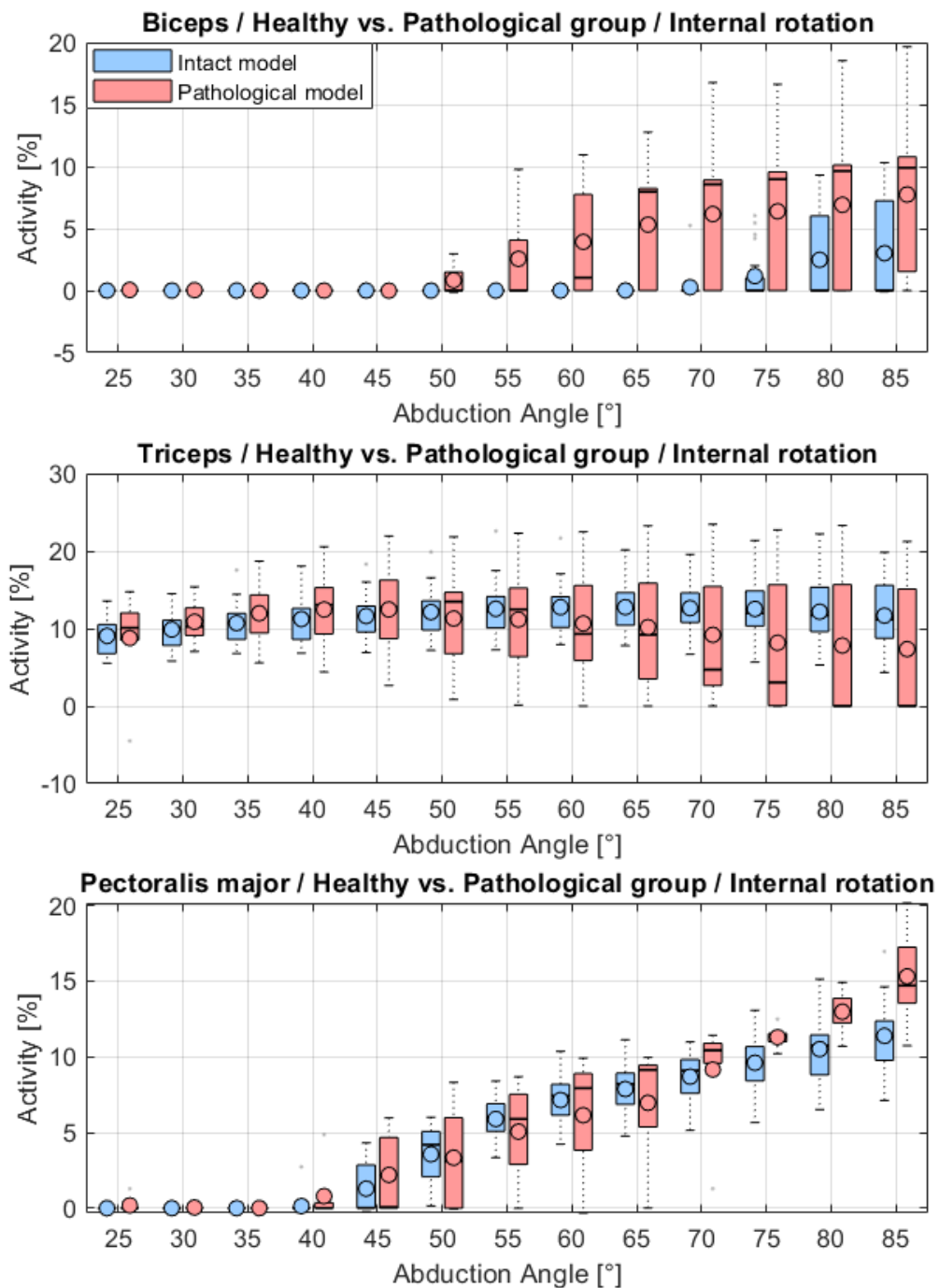


FIGURE C.39: Computed muscle activities of the biceps, triceps and pectoralis major over the abduction angle in 5° increments during the internal rotation trial. Blue depicts the activities of the intact model of the healthy subject group and red the modelled tear of the m. supraspinatus of the patient group.

External rotation

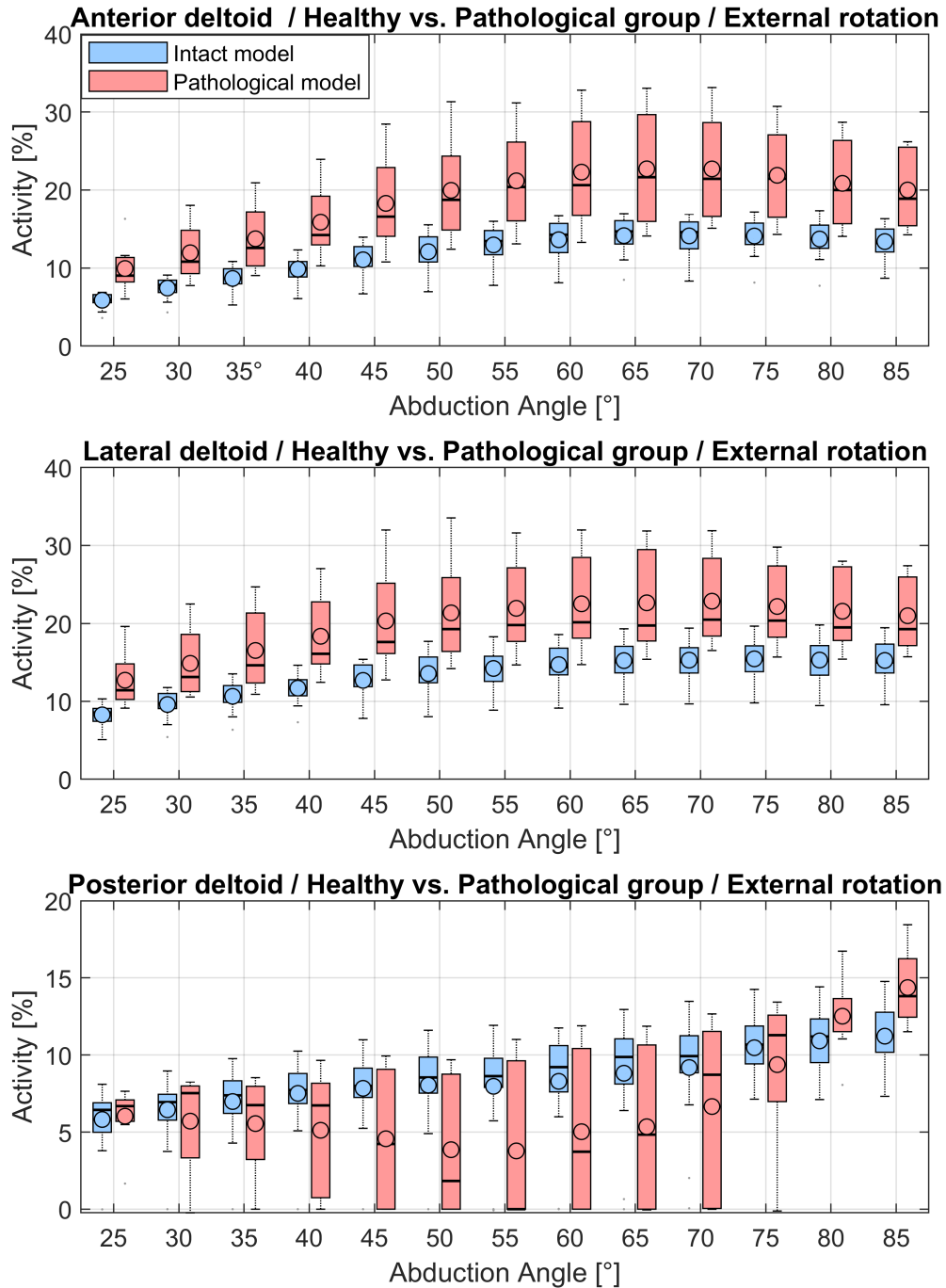


FIGURE C.40: Computed muscle activities of the anterior, posterior and lateral deltoids over the abduction angle in 5° increments during the external rotation trial. Blue depicts the activities of the intact model of the healthy subject group and red the modelled tear of the m. supraspinatus of the patient group.

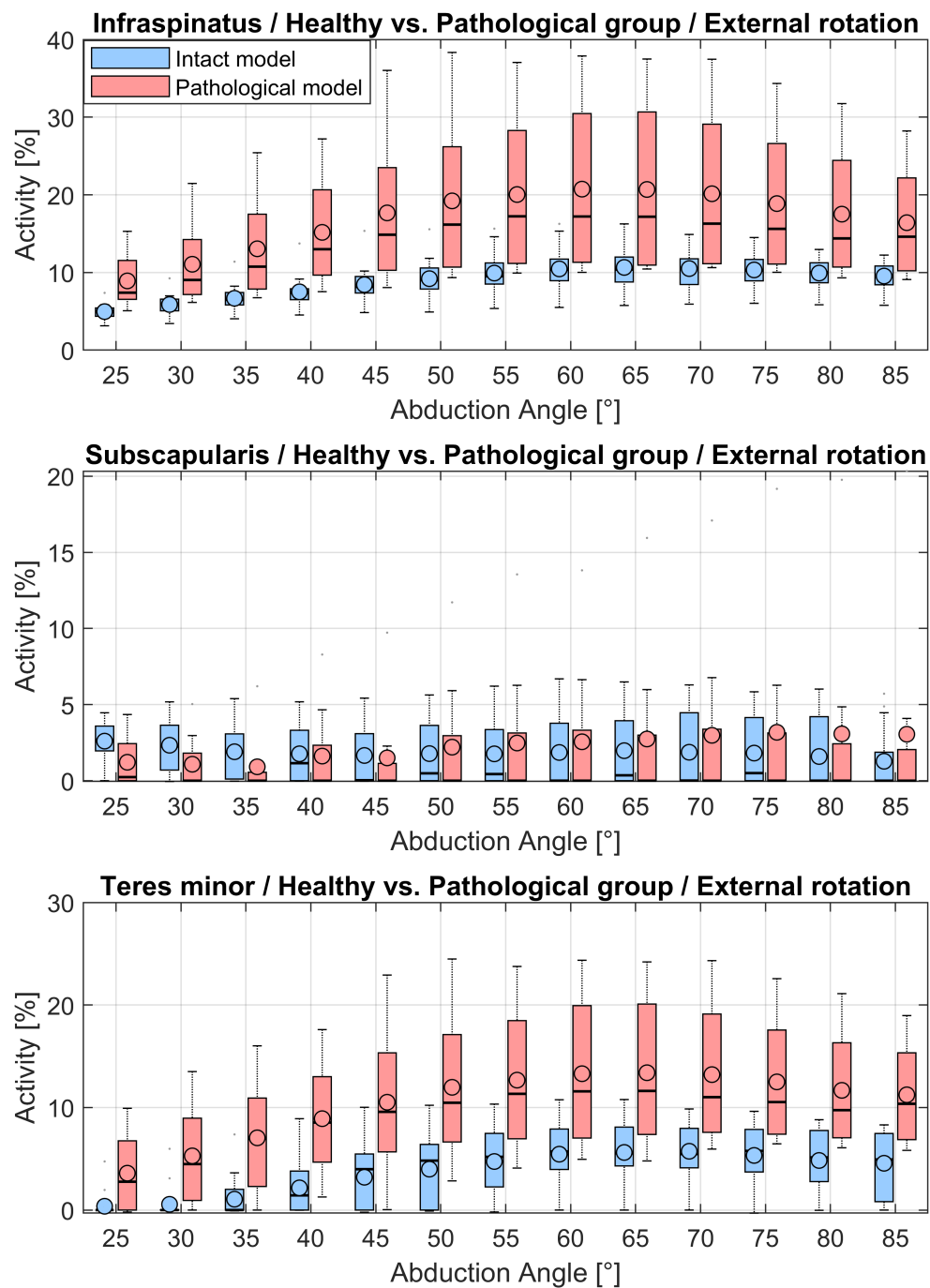


FIGURE C.41: Computed muscle activities of the infraspinatus, subscapularis and teres minor over the abduction angle in 5° increments during the external rotation trial. Blue depicts the activities of the intact model of the healthy subject group and red the modelled tear of the m. supraspinatus of the patient group.

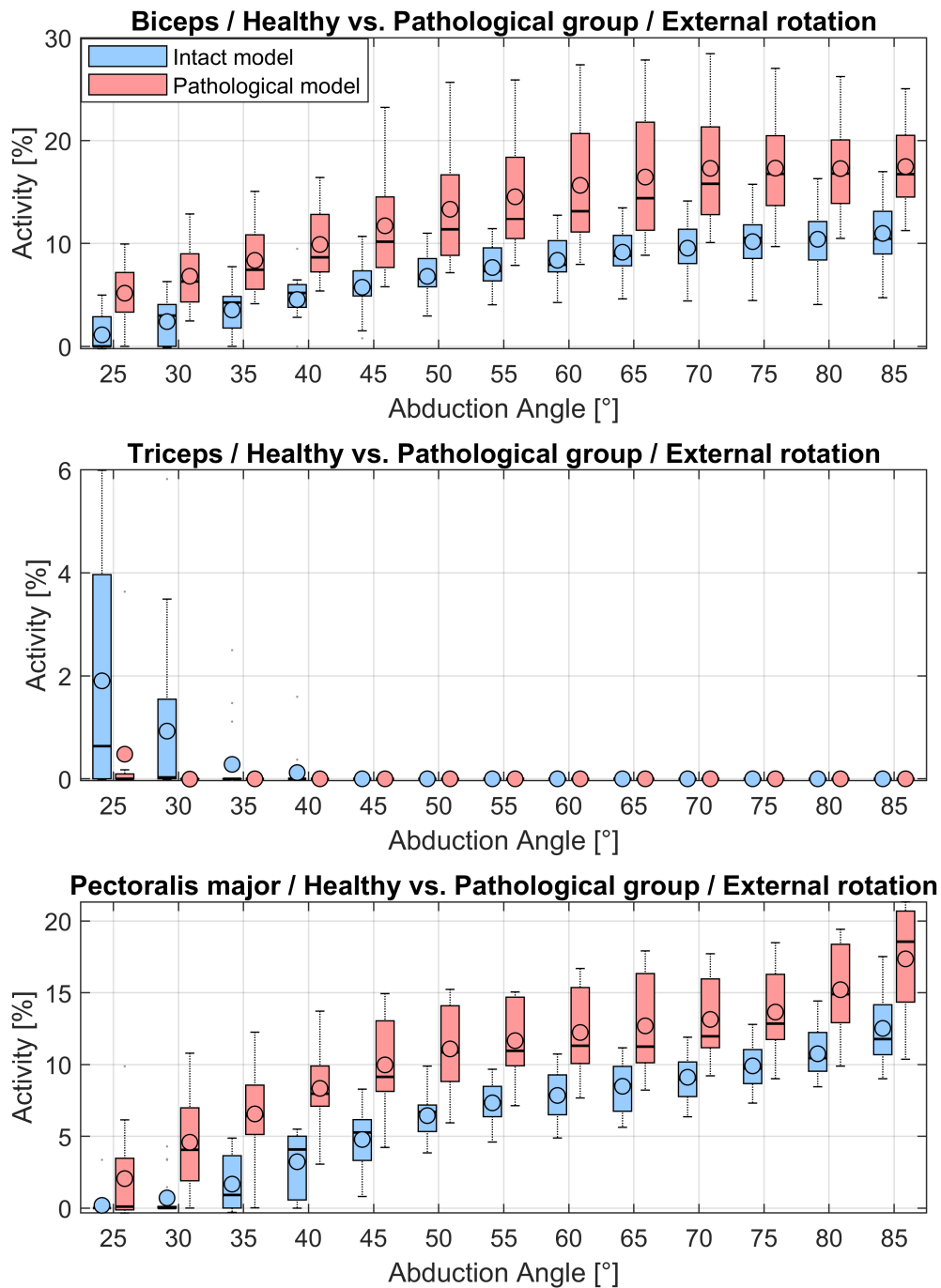


FIGURE C.42: Computed muscle activities of the biceps, triceps and pectoralis major over the abduction angle in 5° increments during the external rotation trial. Blue depicts the activities of the intact model of the healthy subject group and red the modelled tear of the m. supraspinatus of the patient group.

External rotation with 5N in hand

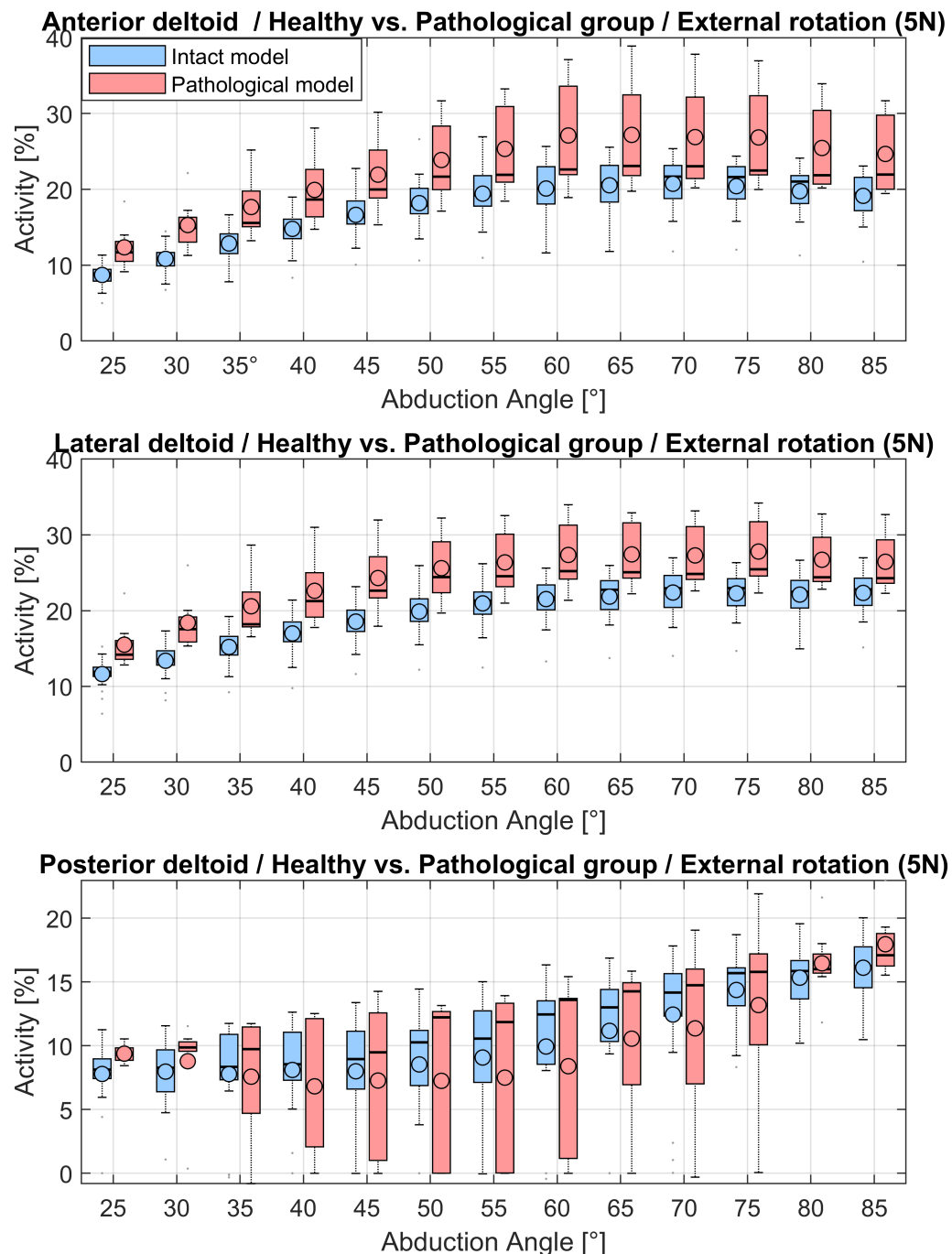


FIGURE C.43: Computed muscle activities of the anterior, posterior and lateral deltoids over the abduction angle in 5° increments during the external rotation trial with 5 N load in hand. Blue depicts the activities of the intact model of the healthy subject group and red the modelled tear of the m. supraspinatus of the patient group.

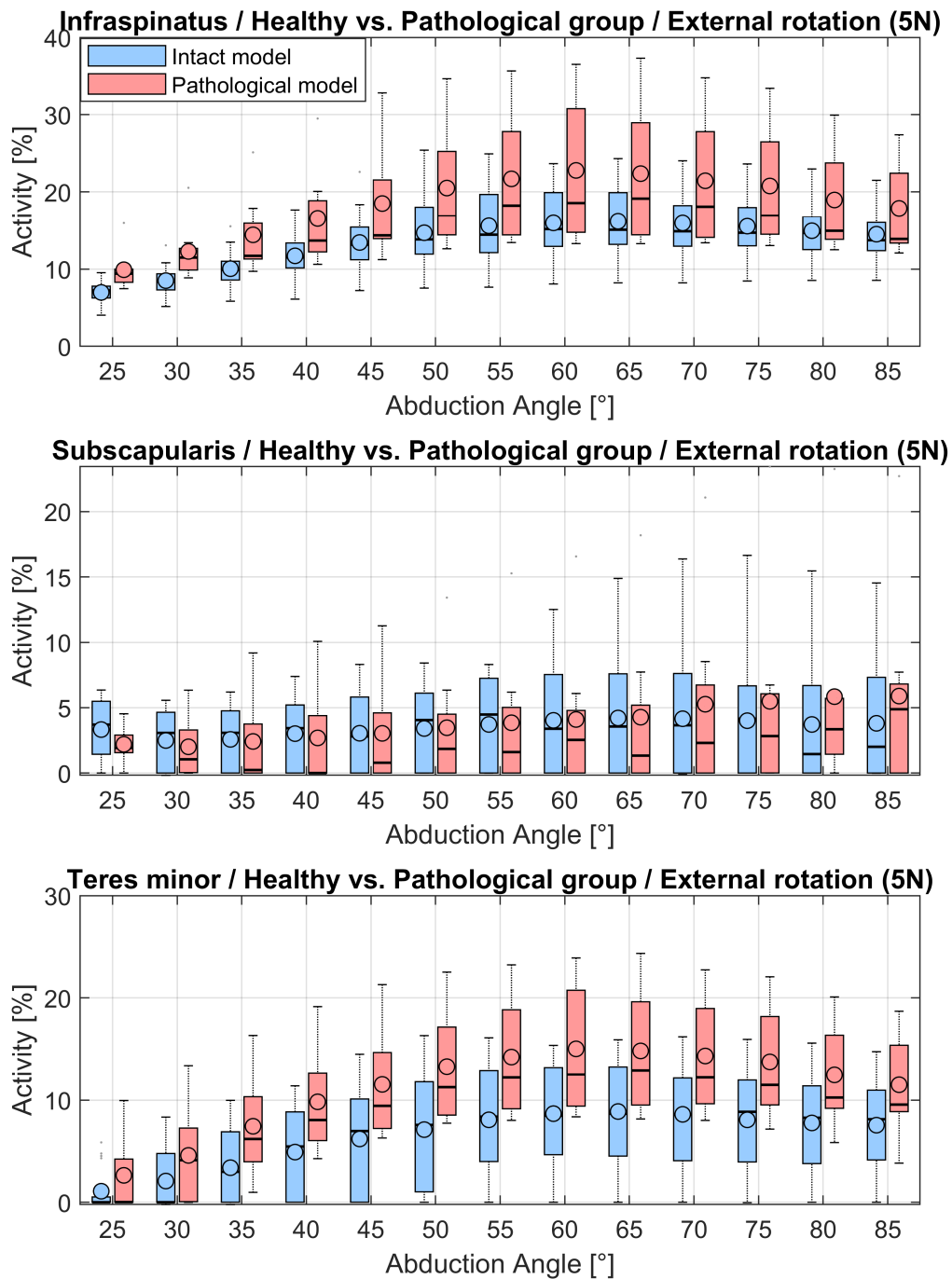


FIGURE C.44: Computed muscle activities of the infraspinatus, subscapularis and teres minor over the abduction angle in 5° increments during the external rotation trial with 5 N load in hand. Blue depicts the activities of the intact model of the healthy subject group and red the modelled tear of the m. supraspinatus of the patient group.

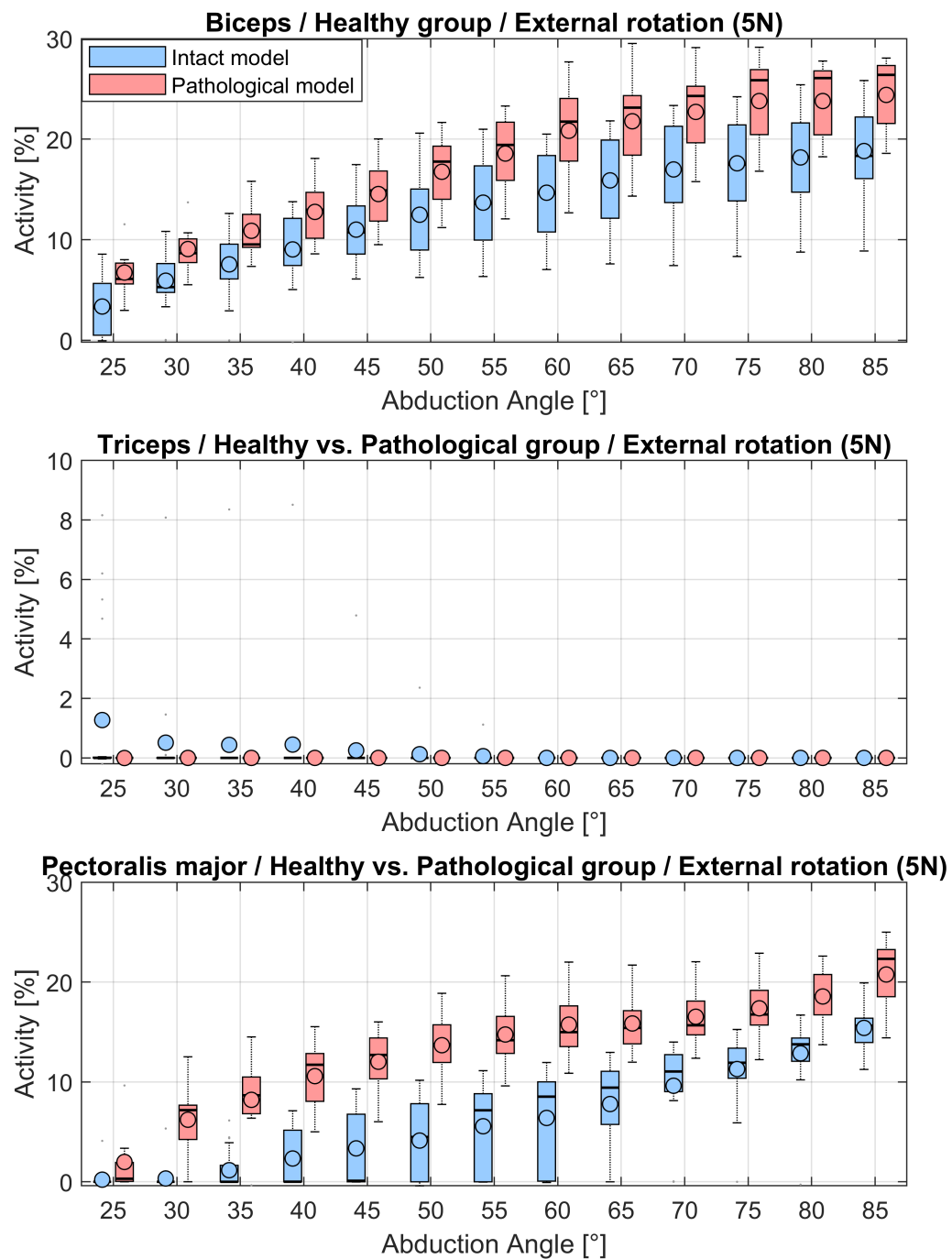


FIGURE C.45: Computed muscle activities of the biceps, triceps and pectoralis major over the abduction angle in 5° increments during the external rotation trial with 5 N load in hand. Blue depicts the activities of the intact model of the healthy subject group and red the modelled tear of the m. supraspinatus of the patient group.

C.0.6 Forces acting on the glenoid of intact models and pathological models of the healthy vs. the pathological group

Neutral position

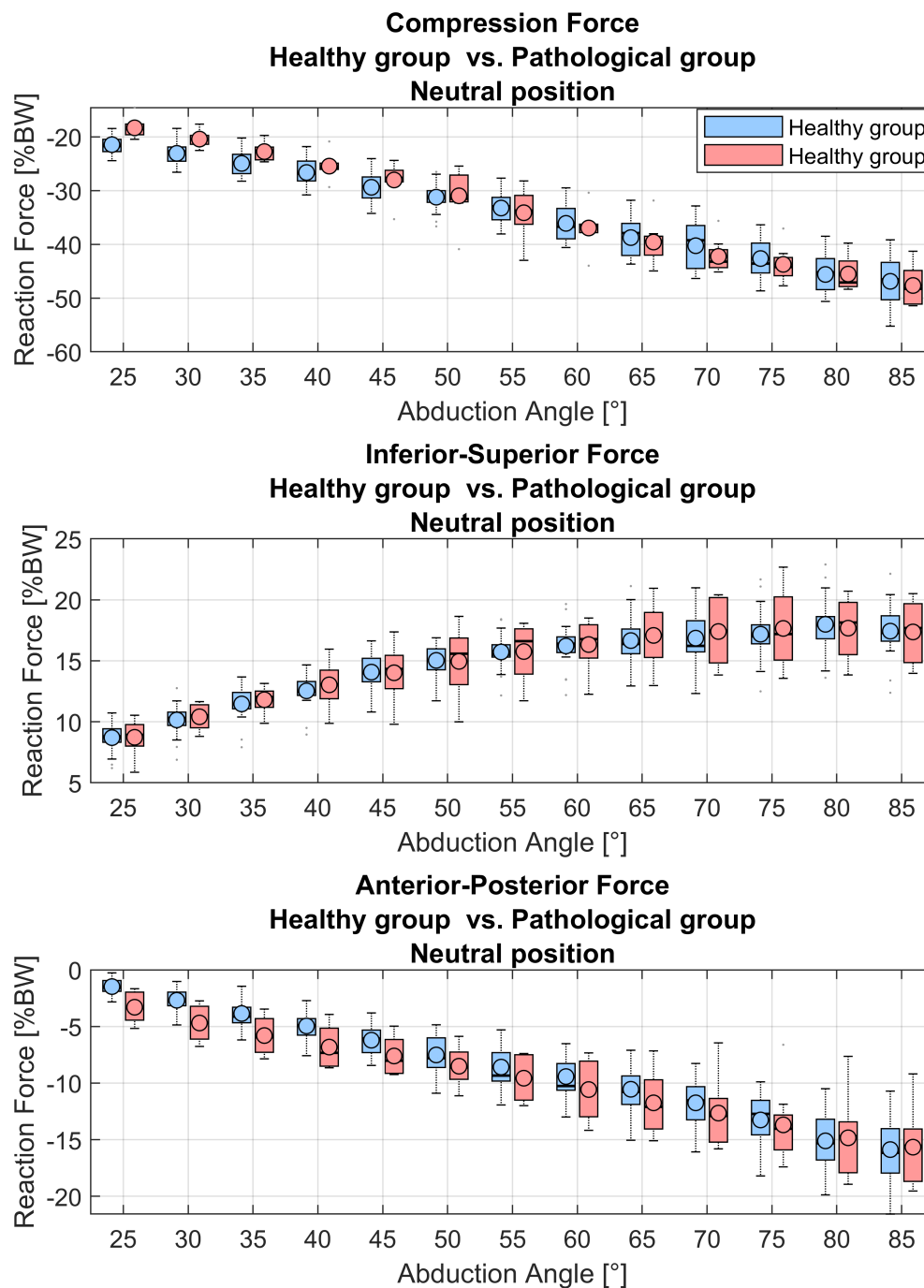


FIGURE C.46: Compression force, inferior-superior force and anterior-posterior force of intact models of the healthy control (blue) and pathological models of the patient group (red) during the neutral position trial over the abduction angle in 5° increments.

**Forces on the glenoid of intact model vs. pathological model
Healthy group vs. Pathological group**

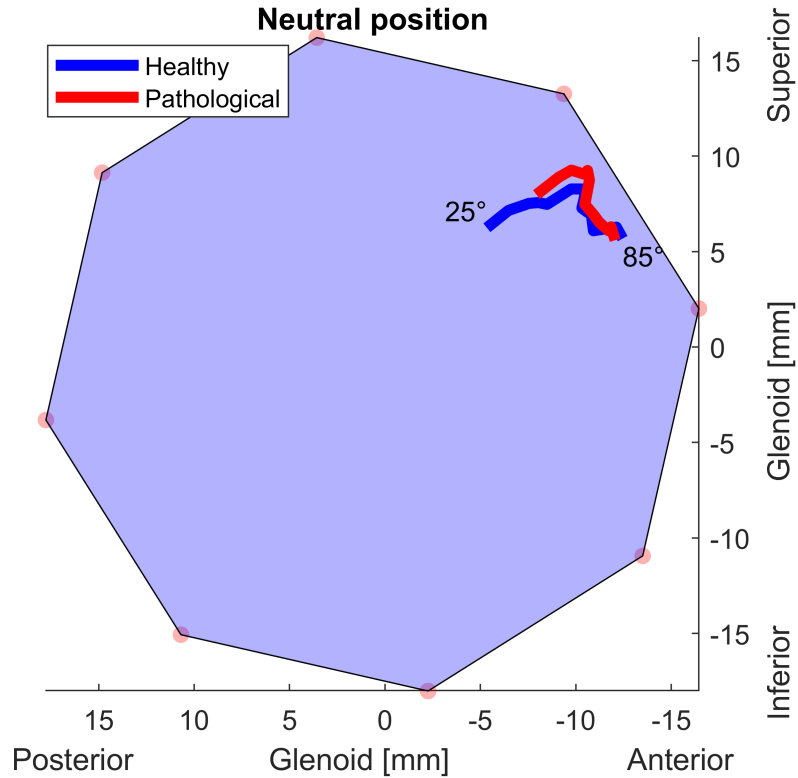


FIGURE C.47: Projected median GH joint reaction force of all models onto the glenoid of intact models of the healthy subject cohort and pathological models of the patient group during the neutral position trial. Intact models of the healthy control (blue) and pathological models of the patient group (red) with their starting value at 25° abduction and the progression up to 85° abduction.

Neutral position with 5N in hand

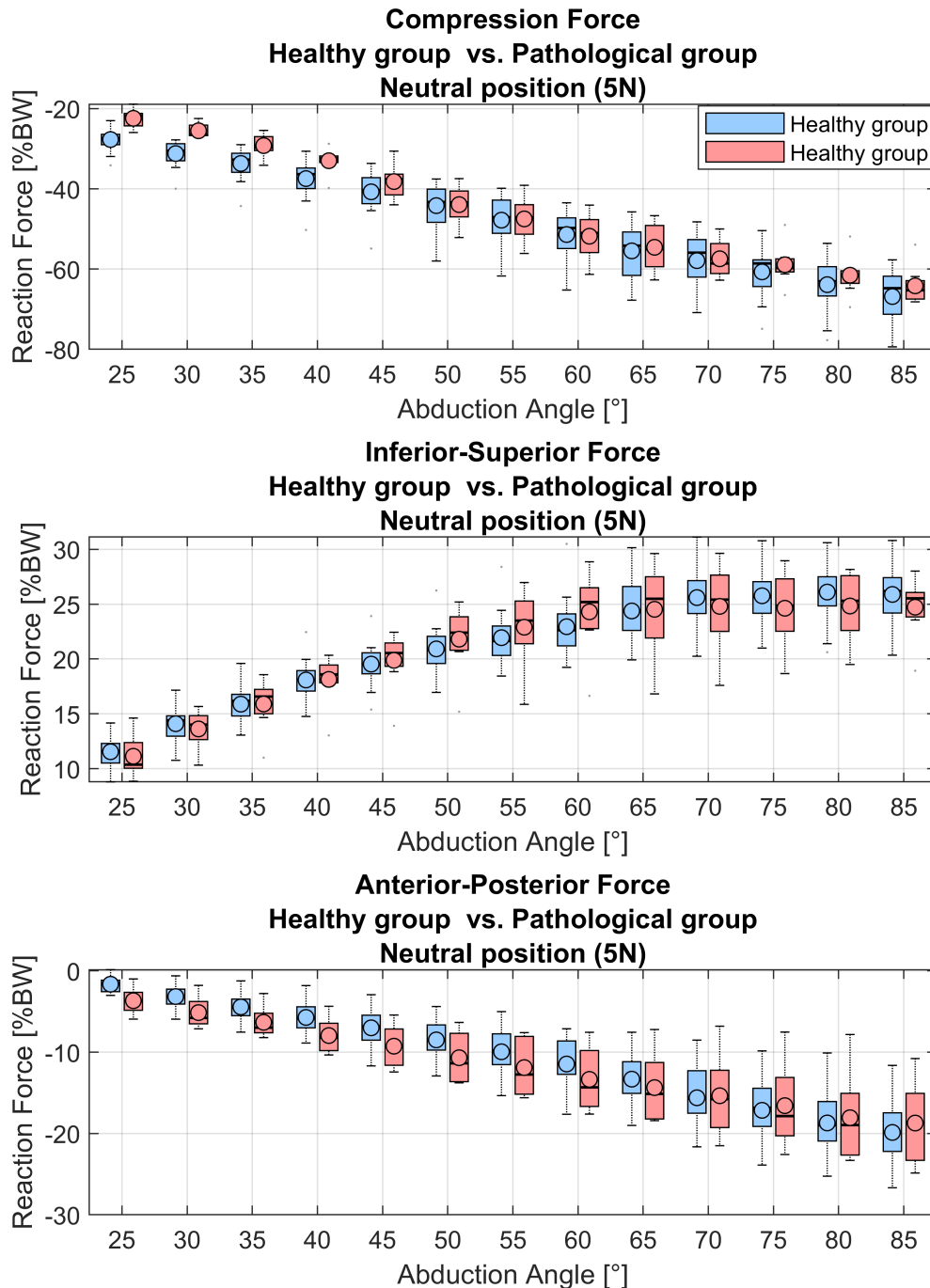


FIGURE C.48: Compression force, inferior-superior force and anterior-posterior force of intact models of the healthy control (blue) and pathological models of the patient group (red) during the neutral position trial with 5 N load in hand over the abduction angle in 5° increments.

**Forces on the glenoid of intact model vs. pathological model
Healthy group vs. Pathological group
Neutral position (5N)**

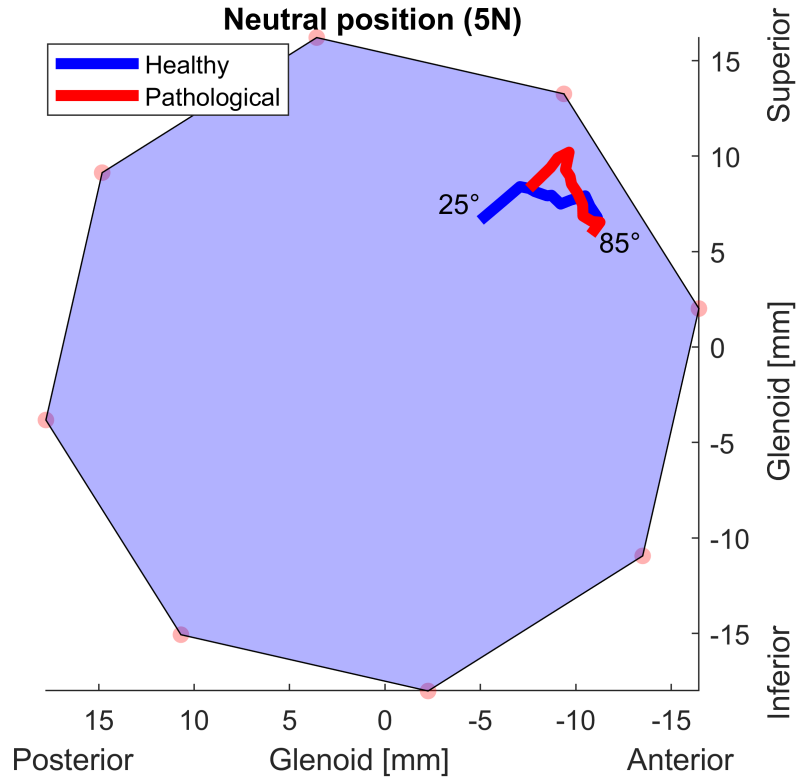


FIGURE C.49: Projected median GH joint reaction force of all models onto the glenoid of intact models of the healthy subject cohort and pathological models of the patient group during the neutral position trial with 5 N load in hand. Intact models of the healthy control (blue) and pathological models of the patient group (red) with their starting value at 25° abduction and the progression up to 85° abduction.

Internal rotation

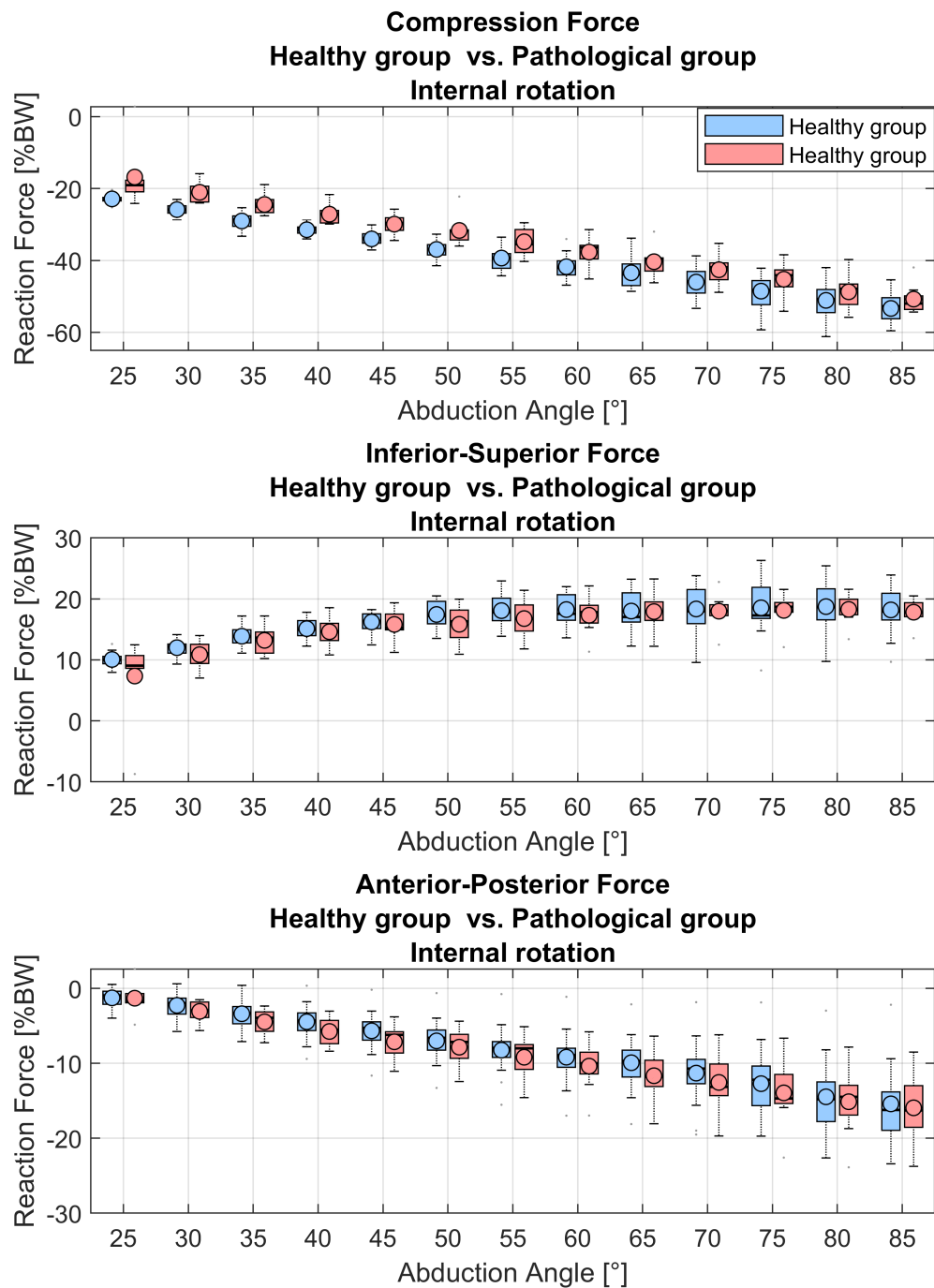


FIGURE C.50: Compression force, inferior-superior force and anterior-posterior force of intact models of the healthy control (blue) and pathological models of the patient group (red) during the internal rotation trial over the abduction angle in 5° increments.

**Forces on the glenoid of intact model vs. pathological model
Healthy group vs. Pathological group**

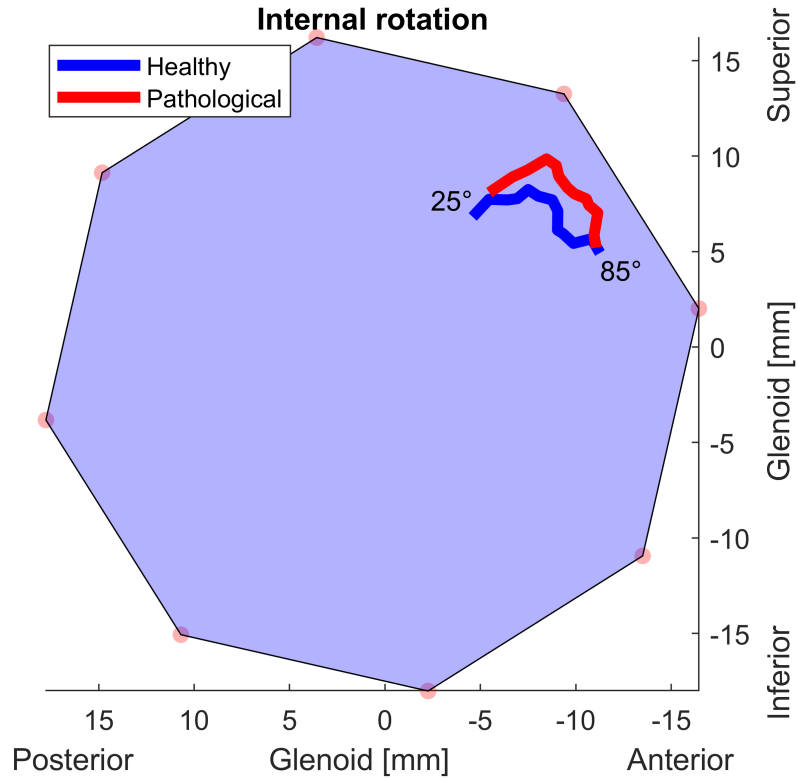


FIGURE C.51: Projected median GH joint reaction force of all models onto the glenoid of intact models of the healthy subject cohort and pathological models of the patient group during the internal rotation trial. Intact models of the healthy control (blue) and pathological models of the patient group (red) with their starting value at 25° abduction and the progression up to 85° abduction.

External rotation

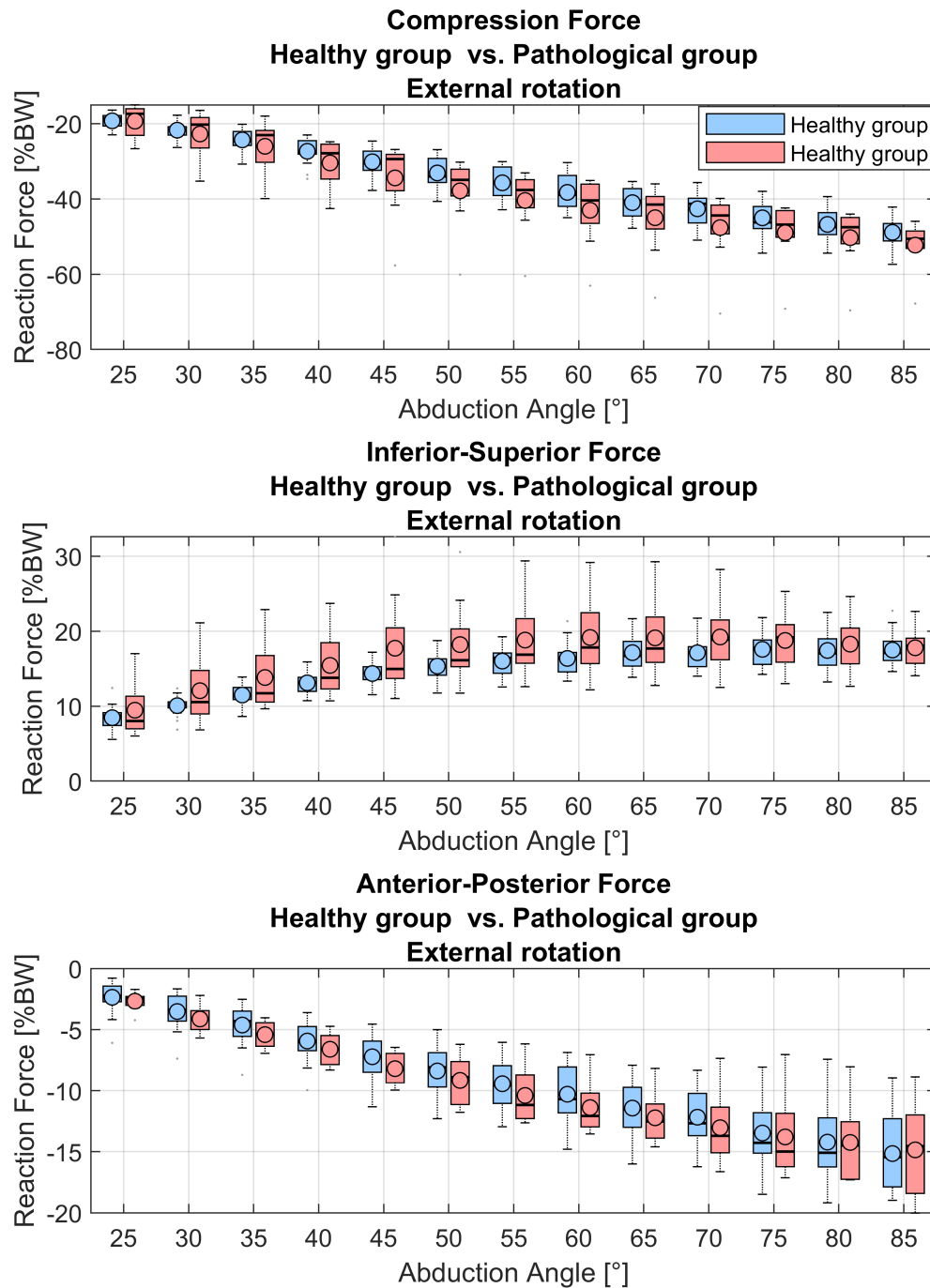


FIGURE C.52: Compression force, inferior-superior force and anterior-posterior force of intact models of the healthy control (blue) and pathological models of the patient group (red) during the external rotation trial over the abduction angle in 5° increments.

**Forces on the glenoid of intact model vs. pathological model
Healthy group vs. Pathological group
External rotation**

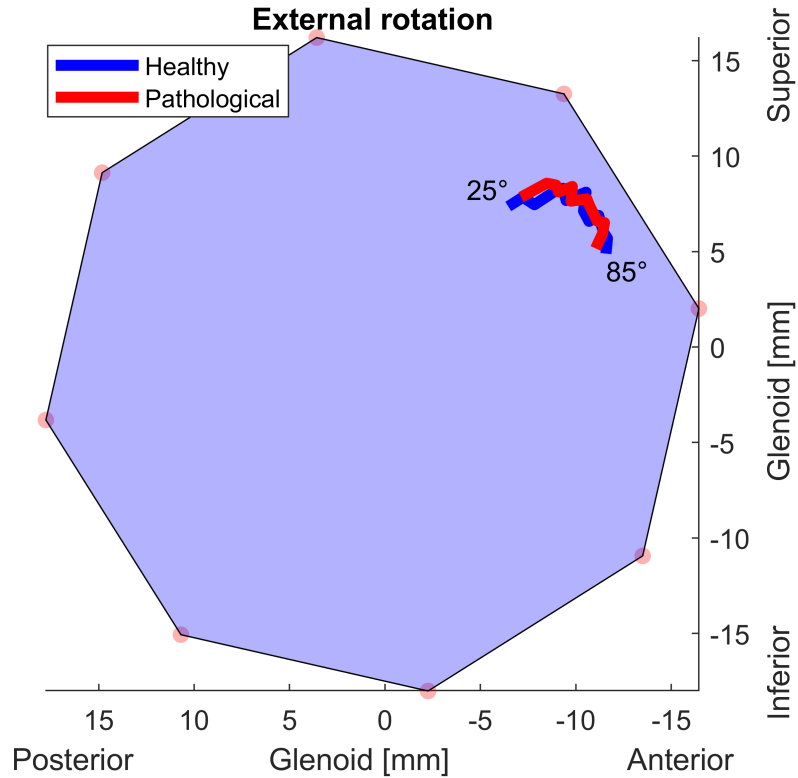


FIGURE C.53: Projected median GH joint reaction force of all models onto the glenoid of intact models of the healthy subject cohort and pathological models of the patient group during the external rotation trial. Intact models of the healthy control (blue) and pathological models of the patient group (red) with their starting value at 25° abduction and the progression up to 85° abduction.

External rotation with 5N in hand

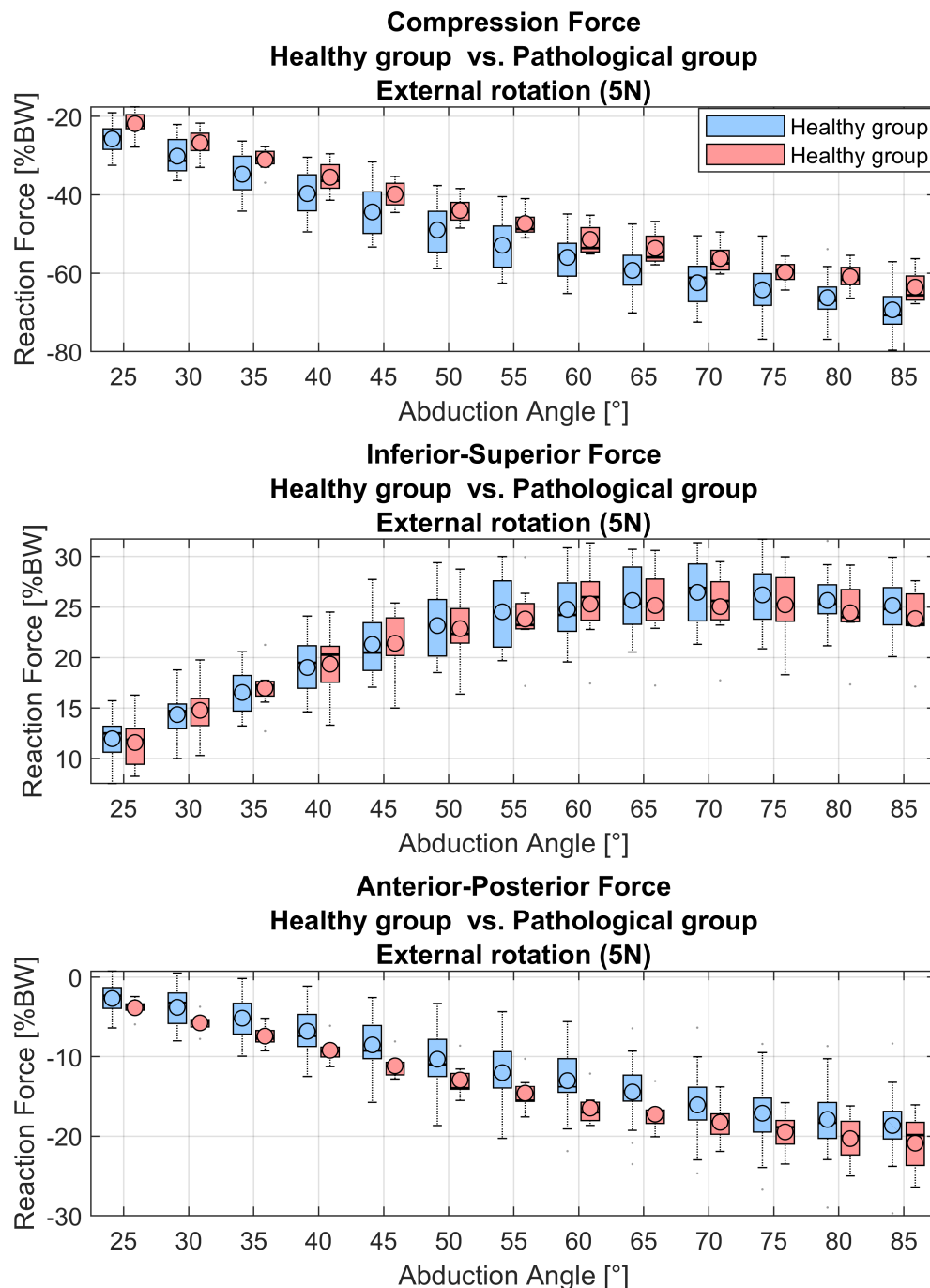


FIGURE C.54: Compression force, inferior-superior force and anterior-posterior force of intact models of the healthy control (blue) and pathological models of the patient group (red) during the external rotation trial with 5 N load in hand over the abduction angle in 5° increments.

**Forces on the glenoid of intact model vs. pathological model
Healthy group vs. Pathological group
External rotation (5N)**

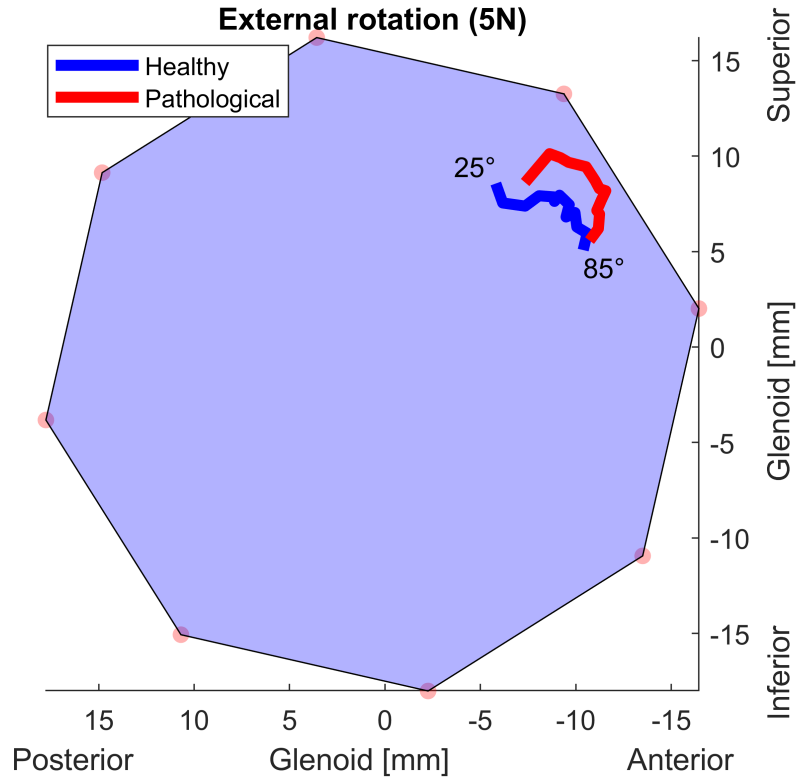


FIGURE C.55: Projected median GH joint reaction force of all models onto the glenoid of intact models of the healthy subject cohort and pathological models of the patient group during the external rotation trial with 5 N load in hand. Intact models of the healthy control (blue) and pathological models of the patient group (red) with their starting value at 25° abduction and the progression up to 85° abduction.

Numeric comparison of forces and muscle activities of intact models and pathological models of the healthy vs. the pathological group

Neutral position

Abduction [°]	AD [%]	LD [%]	PD [%]	INF [%]	SS [%]	BIC [%]	TRI [%]	TM [%]	PM [%]	CF [%BW]	ISF [%BW]	APF [%BW]	FLX [°]	ER [°]
25	2.1***	3.1***	2.3***	1.6***	0.5	0.0	1.2	0.0	0.0	-3.2**	-0.1	1.8**	-0.8	-0.6
30	2.5***	3.3***	2.5***	1.7***	0.4	0.0	0.4	0.0	0.0	-2.2**	-0.2	1.9**	-1.4	0.4
35	3.2***	3.5***	2.3***	2.4***	0.7	0.0	-1.3	0.0	0.0	-2.2*	-0.6	1.8*	-2.6	-0.9
40	3.9***	4.5***	2.6***	3.3***	0.5	0.0	-1.4	0.0	0.1	-1.1	-0.6	2.4*	-4.0	-1.4
45	4.6***	4.8***	2.7**	3.6***	0.1	3.4*	-0.4	0.0	2.7	-1.6	-0.4	2.0*	-4.4	-0.6
50	4.5***	4.8**	1.6*	3.5***	-0.6	6.9***	-0.7	0.0	2.2	0.3	-0.5	0.8	-4.3	-3.3
55	4.4**	5.1**	1.6	3.9***	0.3	4.3***	0.0	0.0	1.4	0.8	-1.1	0.2	-4.9	-2.7
60	3.8***	4.4***	1.8*	3.3***	-0.5	3.6***	0.0	0.0	1.4*	-0.1	-0.4	0.2	-5.3	-2.3
65	2.9**	3.5**	1.6*	3.1***	-0.9	3.3***	0.0	0.0	1.7*	1.5	-0.7	1.3	-6.6	-2.1
70	3.7**	3.9**	2.6*	2.5***	-0.7	2.6**	0.0	1.7*	1.9**	4.0	-1.2	1.4	-7.1	-1.3
75	3.0**	3.4**	2.0*	2.3***	-1.4	3.0*	0.0	1.3	3.0**	0.6	-0.2	1.3	-7.2	-1.3
80	2.2*	2.5**	2.2**	2.0**	-1.9	2.1*	0.0	0.0	3.7**	1.9	-0.2	-0.6	-6.0	-2.1
85	1.9*	2.7*	2.5*	1.8**	-0.8	2.3*	0.0	0.0	4.3*	1.8	-0.4	-0.6	-4.1	-2.3

TABLE C.6: Differences in median values of muscle activities, GH joint reaction forces and kinematics between intact models of the healthy subject cohort and pathological models of the patient group during the internal rotation trial with 5 N load in hand in 5° increments. Asterisks indicate the significance level. AD = anterior deltoid, LD = lateral deltoid, PD = posterior deltoid, INF = infraspinatus, SS = subscapularis, BIC = biceps, TRI = triceps, TM = teres minor, PM = pectoralis major, CF = compression force, ISF = inferior-superior force, APF = anterior-posterior force, FLX = Flexion angle, ER = external rotation angle

Neutral position with 5N in hand

Abduction [°]	AD [%]	LD [%]	PD [%]	INF [%]	SS [%]	BIC [%]	TRI [%]	TM [%]	PM [%]	CF [%BW]	ISF [%BW]	APF [%BW]	FLX [°]	ER [°]
25	2.6***	3.1***	1.8***	2.1***	0.3	0.0	-2.0	0.0	0.0	-5.6***	1.2	2.2**	-0.9	-8.2
30	2.9***	3.4***	2.2***	2.4***	0.1	0.0	-3.4**	0.0	0.0	-4.1***	0.4	2.6*	-1.1	-10.5
35	3.7***	4.0***	1.4**	3.2***	-0.3	4.8*	-5.6*	0.0	0.0	-3.0**	-0.4	2.5*	-1.6	-11.1
40	4.2***	4.8***	2.2**	3.4***	-3.1	5.9**	-2.4*	0.0	6.7**	-3.9**	-0.5	2.4*	-1.8	-8.6
45	3.4***	3.9***	2.2**	3.3***	-0.8	3.1**	0.0	0.0	9.1**	-2.7	-1	2.5	-1.6	-8.0
50	3.6***	3.9***	1.6**	3.3***	-0.2	4.8***	0.0	2.7***	6.6**	0.1	-1.6	2.8	-2.5	-4.2
55	3.8***	4.3***	2.0*	3.3***	-0.6	4.5**	0.0	4.8**	4.4**	0.0	-1.9	2.9	-3.7	-2.8
60	3.2***	3.7***	2.2*	3.2***	-0.5	5.1**	0.0	7.1*	4.2**	1.2	-2.6	2.9	-4.6	-1.9
65	2.0**	2.5**	1.7	2.9**	-0.4	4.3*	0.0	7.5*	4.0**	0.9	-1.1	1.7	-4.7	-2.5
70	2.3*	3.1**	1.6*	2.6***	0.5	4.4**	0.0	6.4**	3.7***	2.7	0.3	0.1	-4.7	-4.8
75	1.7*	2.3*	1.7*	2.4**	0.3	3.8*	0.0	7.3*	3.8***	1.2	0.8	1.0	-4.6	-6.4
80	1.4	2.0*	1.8*	1.9*	-0.7	3.9*	0.0	5.8	5.2**	-1.6	0.9	0.0	-4.6	-5.8
85	1.7	2.6*	2.7*	2.1*	-1.1	4.7**	0.0	2.6	8.0**	0.5	0.7	-1.2	-4.3	-5.0

TABLE C.7: Differences in median values of muscle activities, GH joint reaction forces and kinematics between intact models of the healthy subject cohort and pathological models of the patient group during the neutral position trial with 5 N load in hand in 5° increments. Asterisks indicate the significance level. AD = anterior deltoid, LD = lateral deltoid, PD = posterior deltoid, INF = infraspinatus, SS = subscapularis, BIC = biceps, TRI = triceps, TM = teres minor, PM = pectoralis major, CF = compression force, ISF = inferior-superior force, APF = anterior-posterior force, FLX = Flexion angle, ER = external rotation angle

Internal rotation

Abduction [°]	AD [%]	LD [%]	PD [%]	INF [%]	SS [%]	BIC [%]	TRI [%]	TM [%]	PM [%]	CF [%BW]	ISF [%BW]	APF [%BW]	FLX [°]	ER [°]
25	3.3**	3.0*	1.9*	2.9**	0.0	0.0	0.7	0.0	0.0	-4.0**	1.0	0.8	-5.4	0.2
30	1.8***	2.0**	0.7	1.9***	0.2	0.0	0.1	0.0	0.0	-4.7***	1.1	1.0	-2.6	3.4
35	1.9***	2.4**	1.5**	1.8***	0.4	0.0	1.3	0.0	0.0	-3.6***	0.2	0.6	-3.5	-3.1
40	3.1***	3.4**	1.8**	2.8***	0.4	0.0	1.7	0.0	0.0	-4.2***	0.3	1.2	-4.6	-3.7
45	3.2***	3.6***	3.0***	2.9***	0.1	0.0	1.0	0.0	0.0	-4.2**	1.1	0.9	-6.3	-16
50	2.5**	2.7**	1.3*	2.9**	-0.1	0.0	1.1	0.0	-1.1	-5.1**	0.9	0.5	-6.7	-18.9
55	3.1**	3.3**	1.9*	2.7***	0.2	0.0	0.2	0.0	-0.1	-3.9*	1.1	0.0	-8.3	-17.1
60	2.6**	2.6***	1.6	2.7***	0.4	1.0	-3.3	0.0	0.5	-5.6*	-0.3	1.1	-5.1	-17.0
65	1.9***	2.2***	1.7*	1.9***	-0.2	8.0	-3.3	0.0	0.9	-4.1	-0.9	2.1	-3.6	-18.1
70	3.1**	3.6**	1.8	2.6***	0.5	8.6*	-7.6	0.0	1.3	-4.0	-0.1	2.4	-3.7	-19.1
75	2.3**	3.2**	3.0**	2.3***	1.0	9.0	-8.9	0.0	1.6**	-4.1	-1.4	2.5	-1.9	-20.1
80	2.2*	2.5*	2.0**	1.9***	0.7	9.6	-11.7	0.0	2.3*	-2.9	0.4	-0.3	-4.8	-20.4
85	1.3*	2.0*	2.3*	1.4***	0.8	9.9	-11.2	0.0	3.3**	-0.7	0.2	0.1	-5.7	-23.1

TABLE C.8: Differences in median values of muscle activities, GH joint reaction forces and kinematics between intact models of the healthy subject cohort and pathological models of the patient group during the internal rotation trial in 5° increments. Asterisks indicate the significance level. AD = anterior deltoid, LD = lateral deltoid, PD = posterior deltoid, INF = infraspinatus, SS = subscapularis, BIC = biceps, TRI = triceps, TM = teres minor, PM = pectoralis major, CF = compression force, ISF = inferior-superior force, APF = anterior-posterior force, FLX = Flexion angle, ER = external rotation angle

External rotation

Abduction [°]	AD [%]	LD [%]	PD [%]	INF [%]	SS [%]	BIC [%]	TRI [%]	TM [%]	PM [%]	CF [%BW]	ISF [%BW]	APF [%BW]	FLX [°]	ER [°]
25	3.1***	2.9***	0.2	2.4***	-2.5	5.2**	-0.6	2.8*	0.1	-1.1	0.7	0.2	-1.5	-13.4*
30	3.0***	3.4***	0.6	3.1**	-2.3	3.3**	0.0	4.5*	4.1**	-1.3	-0.3	0.8	-1.8	-13.4*
35	3.9**	4.0**	-0.6	4.3**	-1.9	3.2**	0.0	6.9**	5.5***	-1.6	-0.4	1.0	-1.6	-13.8*
40	4.3***	4.4***	-1.0	5.6***	-1.2	3.5***	0.0	7.1**	3.9***	0.0	-0.6	0.6	-2.1	-12.3
45	5.4***	4.9***	-3.8	6.7**	0.0	4.5**	0.0	5.6**	3.9***	-1.1	-0.6	1.1	-2.2	-12.6
50	6.6***	5.9***	-6.7	7.2***	-0.5	4.8**	0.0	5.6**	4.1**	0.9	-0.9	0.8	-1.1	-13.6
55	6.9***	5.5***	-8.6	7.7**	-0.4	5.1***	0.0	6.1**	3.5***	2.0	-0.4	1.6	-0.2	-14.3
60	6.4***	5.8***	-5.5	6.9**	0.0	5.2***	0.0	5.9**	3.4***	1.5	-1.4	1.4	0.6	-13.0
65	6.9**	4.7**	-5.0	6.8**	-0.4	5.6**	0.0	6.1**	2.6**	1.1	-1.0	1.0	0.4	-13.0
70	6.8***	5.4***	-1.2	5.7**	0.0	6.4***	0.0	5.5**	3.0***	3.1	-1.7	1.0	1.9	-12.6
75	7.4**	5.1**	0.6	5.3**	-0.5	6.2***	0.0	4.8**	3.1**	0.60	-1.4	0.7	1.6	-12.2
80	6.3**	4.3**	1.3	4.3*	0.0	6.3***	0.0	4.6**	4.5**	0.0	-1.3	-0.6	1.0	-13.3
85	5.7**	4.3**	2.6**	5.1*	0.0	6.3***	0.0	5.4**	6.8**	2.0	-0.9	-0.9	0.4	-14.0

TABLE C.9: Differences in median values of muscle activities, GH joint reaction forces and kinematics between intact models of the healthy subject cohort and pathological models of the patient group during the external rotation trials in 5° increments. Asterisks indicate the significance level. AD = anterior deltoid, LD = lateral deltoid, PD = posterior deltoid, INF = infraspinatus, SS = subscapularis, BIC = biceps, TRI = triceps, TM = teres minor, PM = pectoralis major, CF = compression force, ISF = inferior-superior force, APF = anterior-posterior force, FLX = Flexion angle, ER = external rotation angle

External rotation with 5N in hand

Abduction [°]	AD [%]	LD [%]	PD [%]	INF [%]	SS [%]	BIC [%]	TRI [%]	TM [%]	PM [%]	CF [%BW]	ISF [%BW]	APF [%BW]	FLX [°]	ER [°]
25	2.8**	2.3**	1.2*	2.2**	-1.8	2.9*	0.0	0.0	0.3	-2.8*	0.6	1.2	1.8	-9.7
30	4.0**	4.1***	1.6	3.1**	-2.0	3.4*	0.0	4.1	7.2***	-4.9	-0.3	2.3	2.4	-12.4
35	2.6**	2.8***	1.4	1.8*	-2.8	2.0*	0.0	3.2	8.7**	-4.0	-0.8	2.5*	2.1	-10.3
40	3.7*	4.1**	-1.7	2.2	-3.4	4.0*	0.0	2.6	11.7***	-3.5	-0.8	2.0*	1.0	-12.0
45	3.6*	3.8**	0.5	1.2	-2.0	4.2	0.0	2.5	12.6***	-4.7	-0.8	1.9*	0.0	-12.4
50	3.8*	4.5**	2.0	3.0	-2.2	5.3*	0.0	3.7*	9.3***	-4.5	0.8	3.0*	1.4	-14.6
55	2.7*	3.2*	1.3	3.7	-2.9	5.8*	0.0	3.8	7.0***	-3.8*	1.3	3.3	2.0	-12.1
60	2.5	3.5*	1.1	3.3	-0.9	7.1*	0.0	4.0	6.5***	-1.9	-1.8	3.3*	0.8	-8.9
65	2.2*	2.3*	1.3	4.0	-2.2	7.2*	0.0	4.2	6.0***	-2.9*	0.0	3.0*	0.7	-5.2
70	1.4	1.9*	0.6	3.2	-1.4	7.4*	0.0	3.7	4.6***	-3.7*	1.3	2.1	2.8	-4.4
75	0.9	2.5*	0.1	2.2	-1.3	8.4*	0.0	2.6	4.8***	-5.3	1.0	1.9	5.0	-2.5
80	0.8	1.9*	0.1	0.3	1.9	7.8*	0.0	2.0	4.9**	-5.4	1.3	1.7	7.0	-3.2
85	2.5*	1.5*	0.9	0.2	2.9	8.1**	0.0	1.4	6.7**	-5.1	1.5	1.4	5.6	-2.6

TABLE C.10: Differences in median values of muscle activities, GH joint reaction forces and kinematics between intact models of the healthy subject cohort and pathological models of the patient group during the external rotation trial with 5 N load in hand in 5° increments. Asterisks indicate the significance level. AD = anterior deltoid, LD = lateral deltoid, PD = posterior deltoid, INF = infraspinatus, SS = subscapularis, BIC = biceps, TRI = triceps, TM = teres minor, PM = pectoralis major, CF = compression force, ISF = inferior-superior force, APF = anterior-posterior force, FLX = Flexion angle, ER = external rotation angle

C.0.7 EMG comparison between the healthy vs. the pathological group

Neutral position

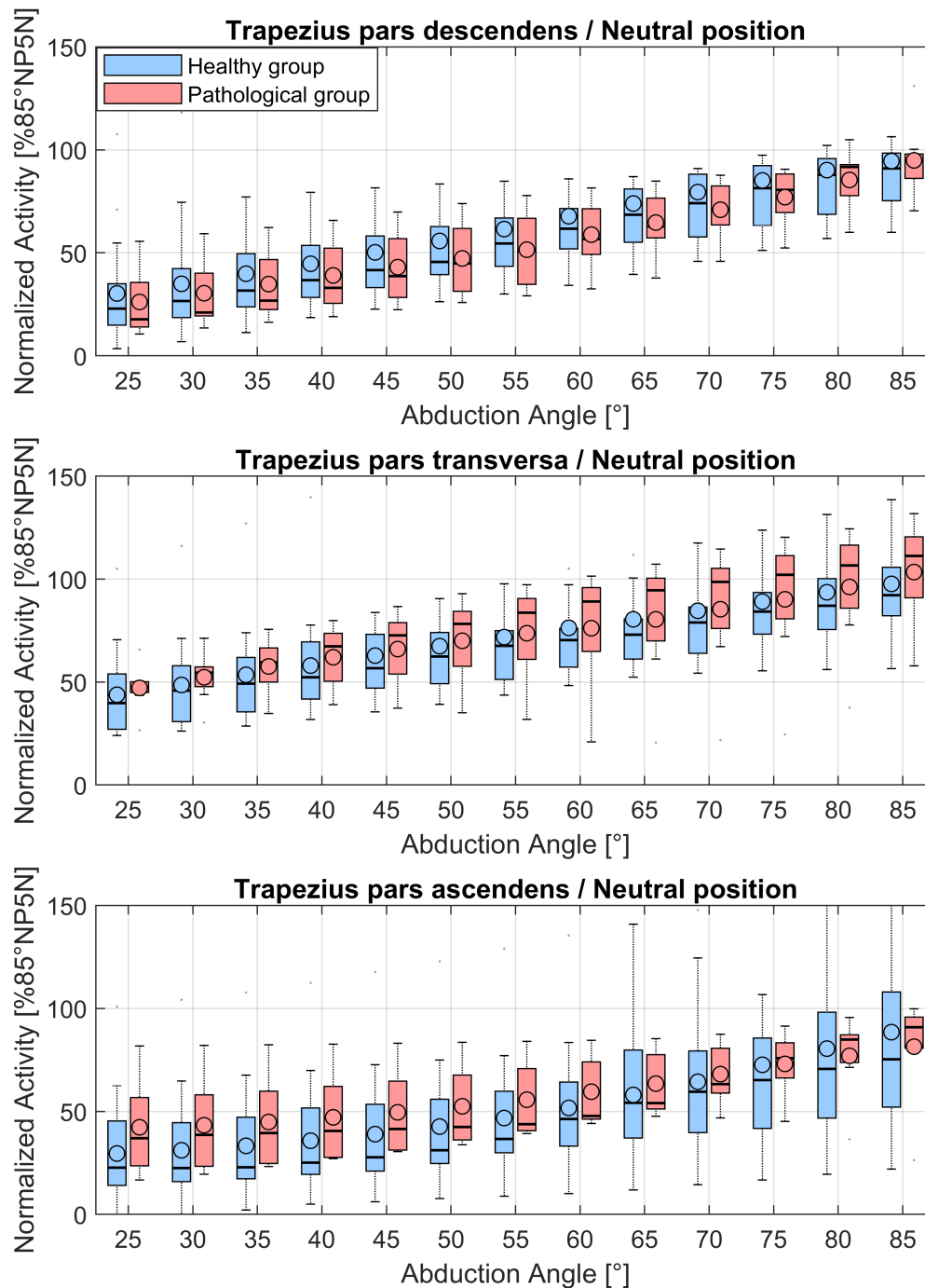


FIGURE C.56: EMG muscle activities normalized to the 85° position of the neutral position trial with 5 N load in hand of the trapezius pars descendens, trapezius pars transversa and trapezius pars ascendens over the abduction angle in 5° increments during the neutral position trial. Blue depicts the EMG activities of the healthy subject group and red of

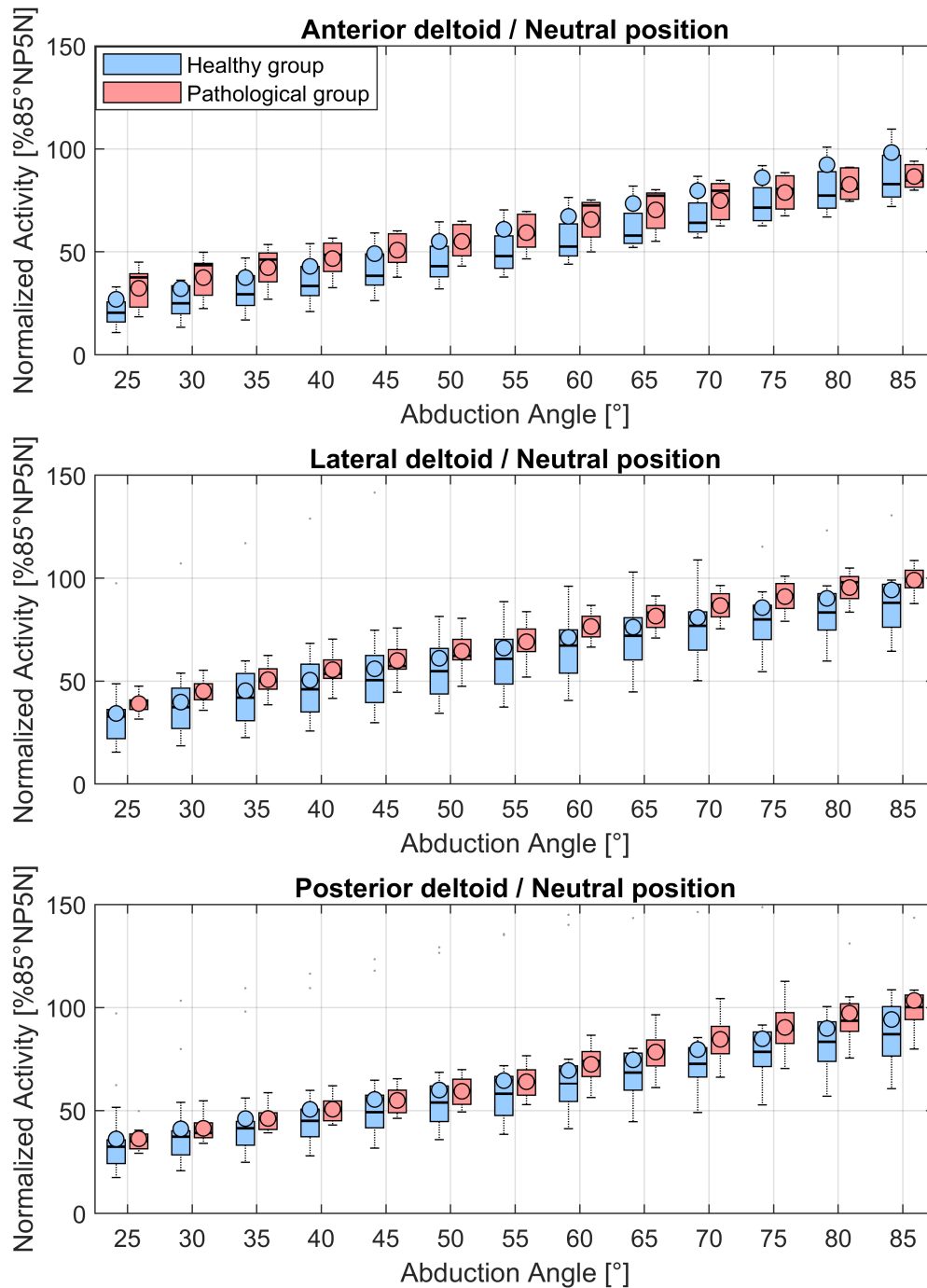


FIGURE C.57: EMG muscle activities normalized to the 85° position of the neutral position trial with 5 N load in hand of the anterior deltoid, lateral deltoid and posterior deltoid over the abduction angle in 5° increments during the neutral position trial. Blue depicts the EMG activities of the healthy subject group and red of the patient group.

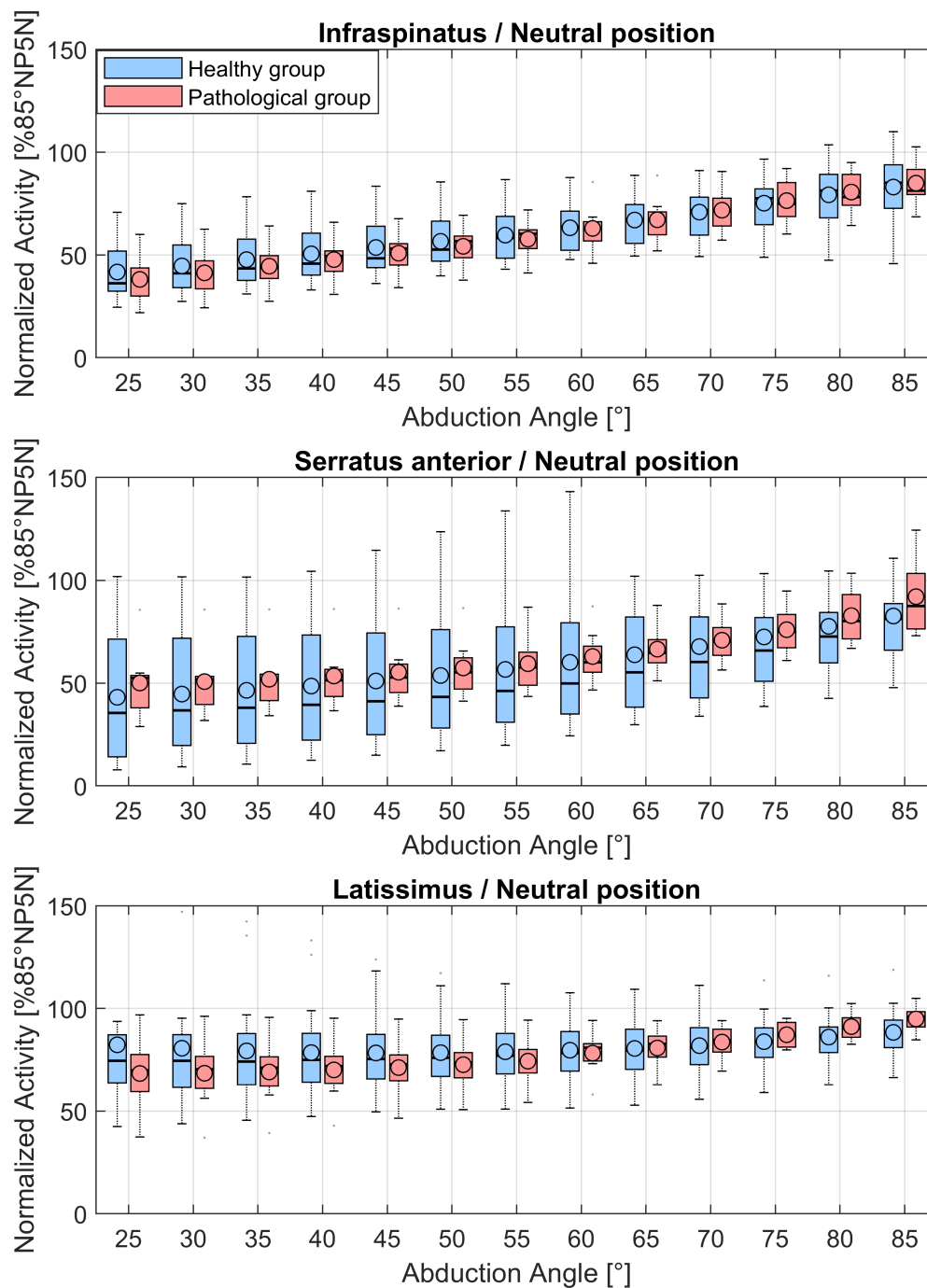


FIGURE C.58: EMG muscle activities normalized to the 85° position of the neutral position trial with 5 N load in hand of the infraspinatus, serratus anterior and latissimus over the abduction angle in 5° increments during the neutral position trial. Blue depicts the EMG activities of the healthy subject group and red of the patient group.

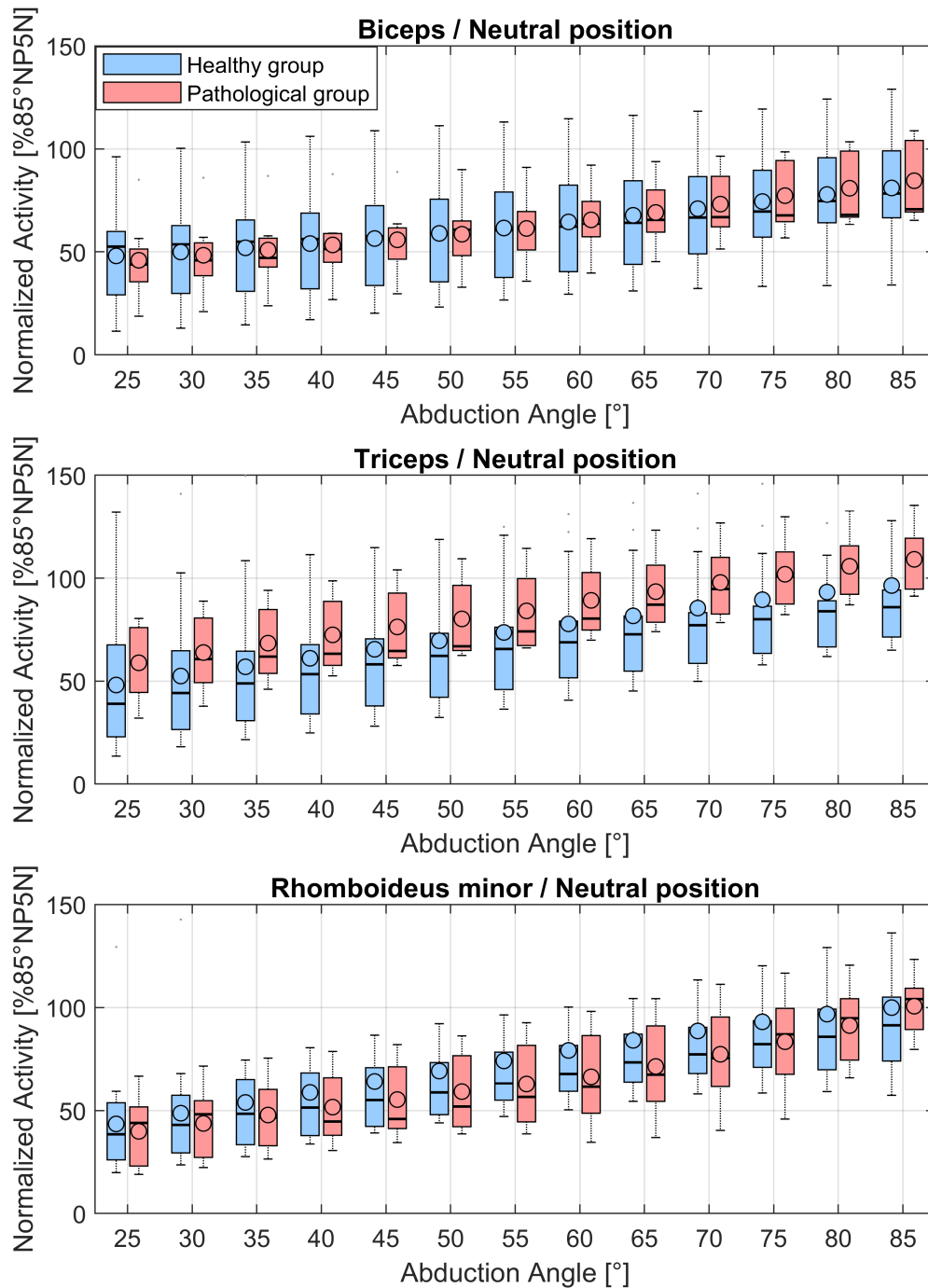


FIGURE C.59: EMG muscle activities normalized to the 85° position of the neutral position trial with 5 N load in hand of the biceps, triceps and rhomboideus minor over the abduction angle in 5° increments during the neutral position trial. Blue depicts the EMG activities of the healthy subject group and red of the patient group.

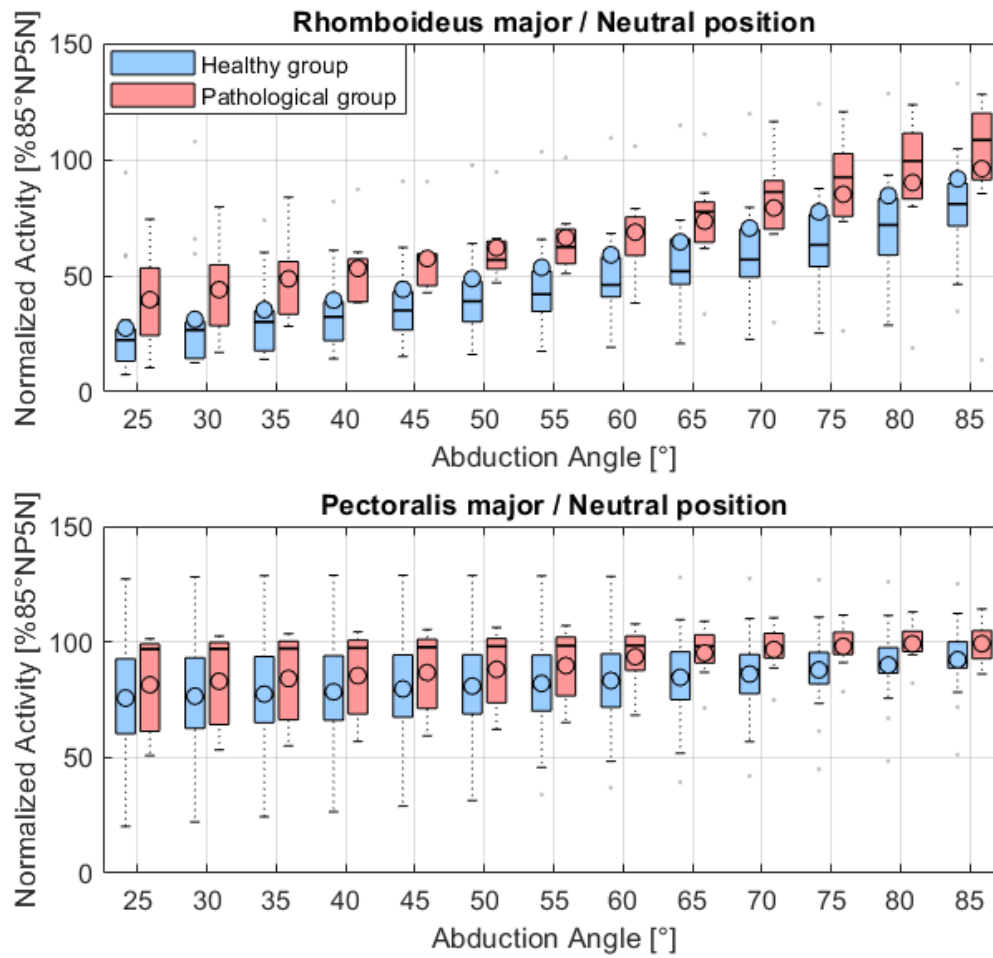


FIGURE C.60: EMG muscle activities normalized to the 85° position of the neutral position trial with 5 N load in hand of the rhomboideus major and pectoralis major over the abduction angle in 5° increments during the neutral position trial. Blue depicts the EMG activities of the healthy subject group and red of the patient group.

Neutral position 5N in hand

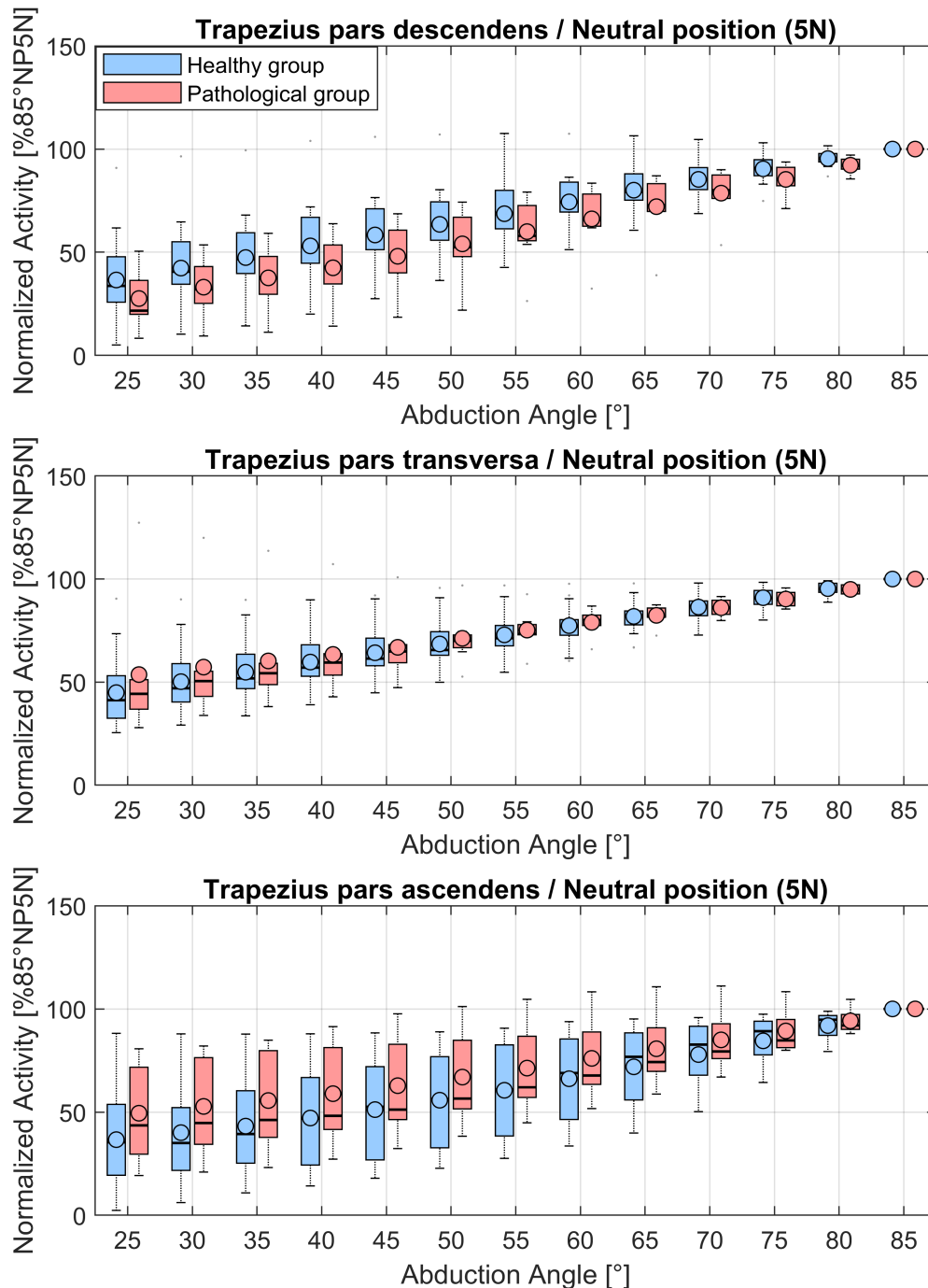


FIGURE C.61: EMG muscle activities normalized to the 85° position of the neutral position trial with 5 N load in hand of the trapezius pars descendens, trapezius pars transversa and trapezius pars ascendens over the abduction angle in 5° increments during the neutral position trial with 5 N load in hand. Blue depicts the EMG activities of the healthy subject group and red of the patient group.

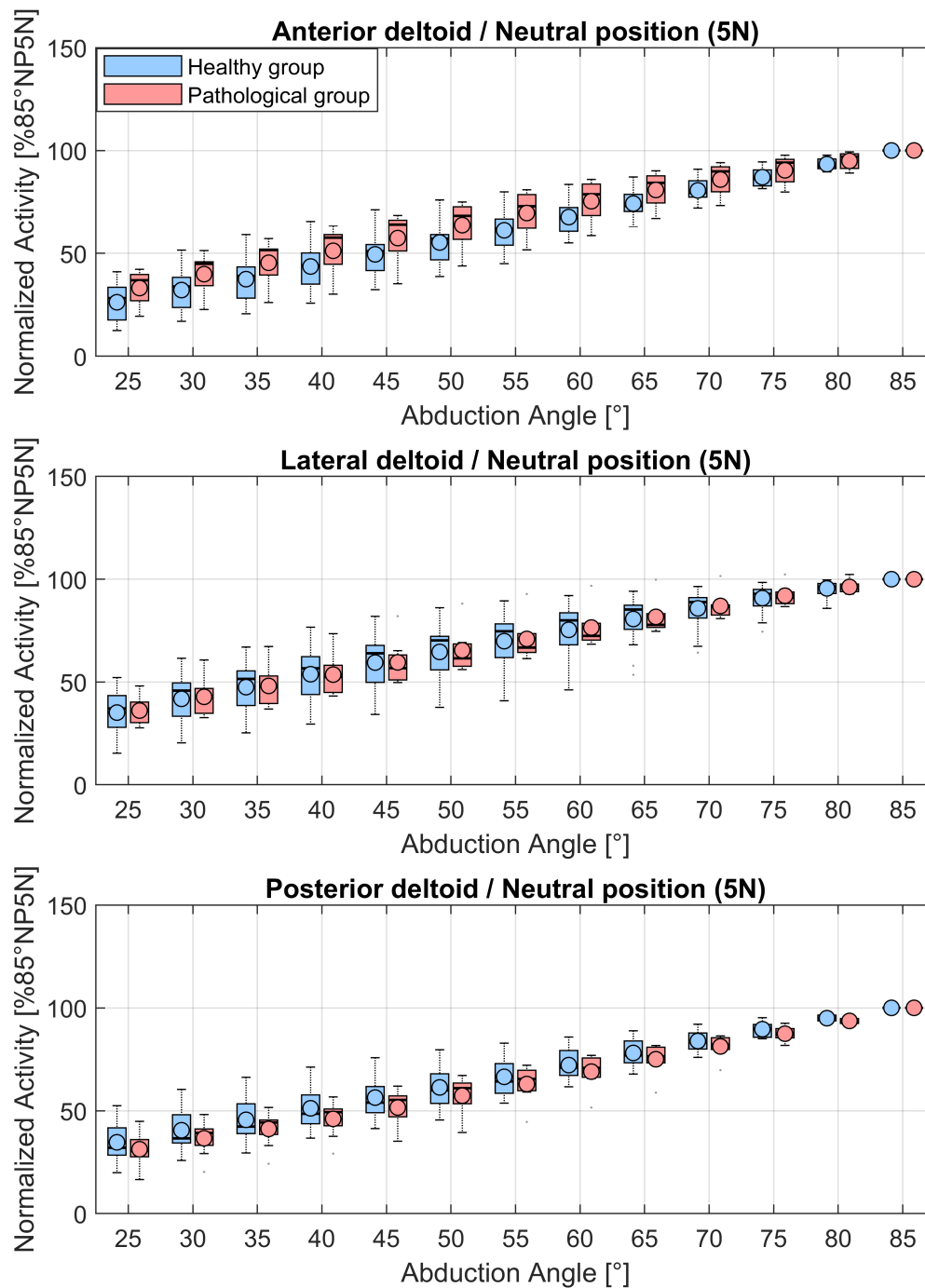


FIGURE C.62: EMG muscle activities normalized to the 85° position of the neutral position trial with 5 N load in hand of the anterior deltoid, lateral deltoid and posterior deltoid over the abduction angle in 5° increments during the neutral position trial with 5 N load in hand. Blue depicts the EMG activities of the healthy subject group and red of the patient group.

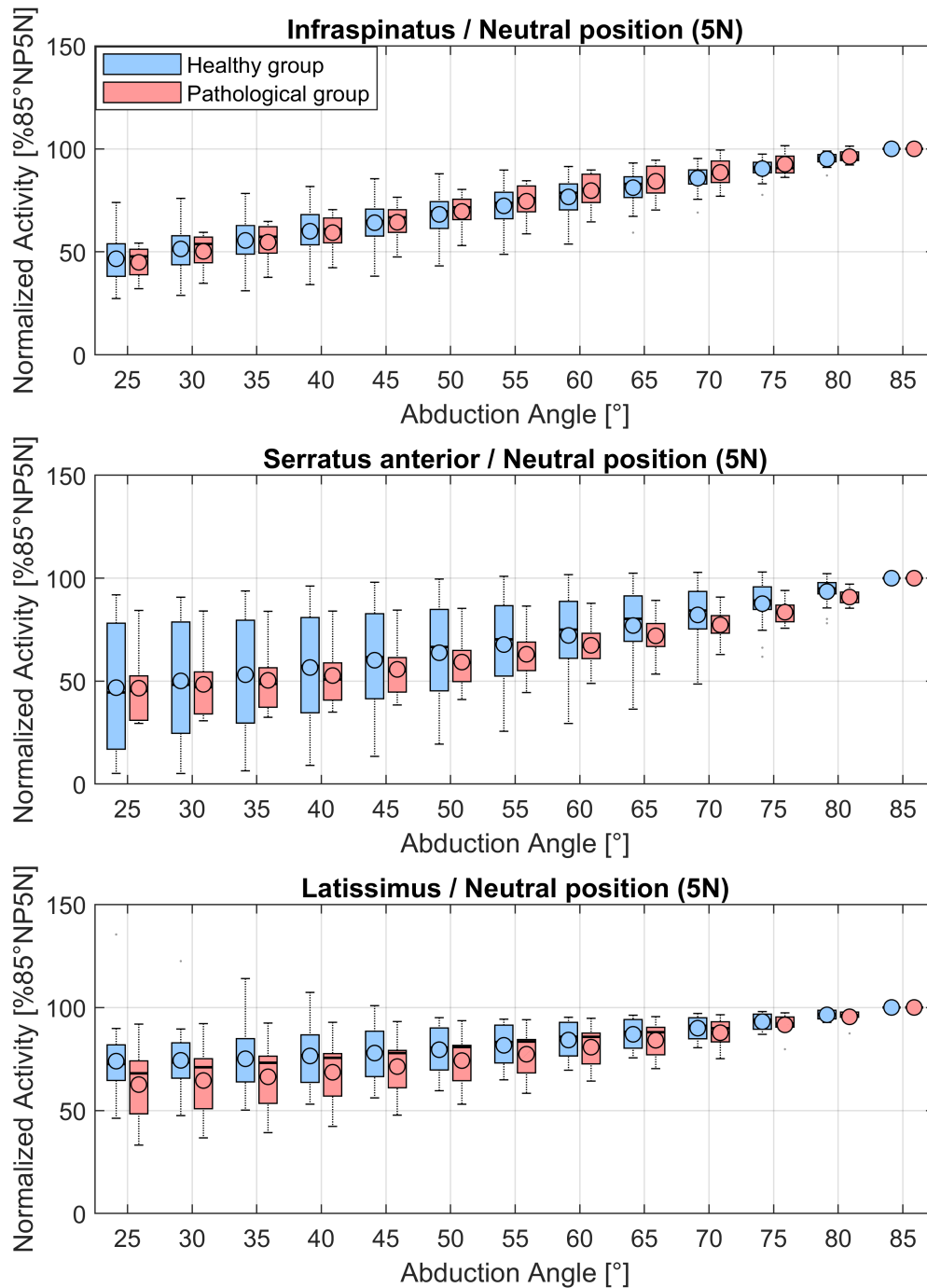


FIGURE C.63: EMG muscle activities normalized to the 85° position of the neutral position trial with 5 N load in hand of the infraspinatus, serratus anterior and latissimus over the abduction angle in 5° increments during the neutral position trial with 5 N load in hand. Blue depicts the EMG activities of the healthy subject group and red of the patient group.

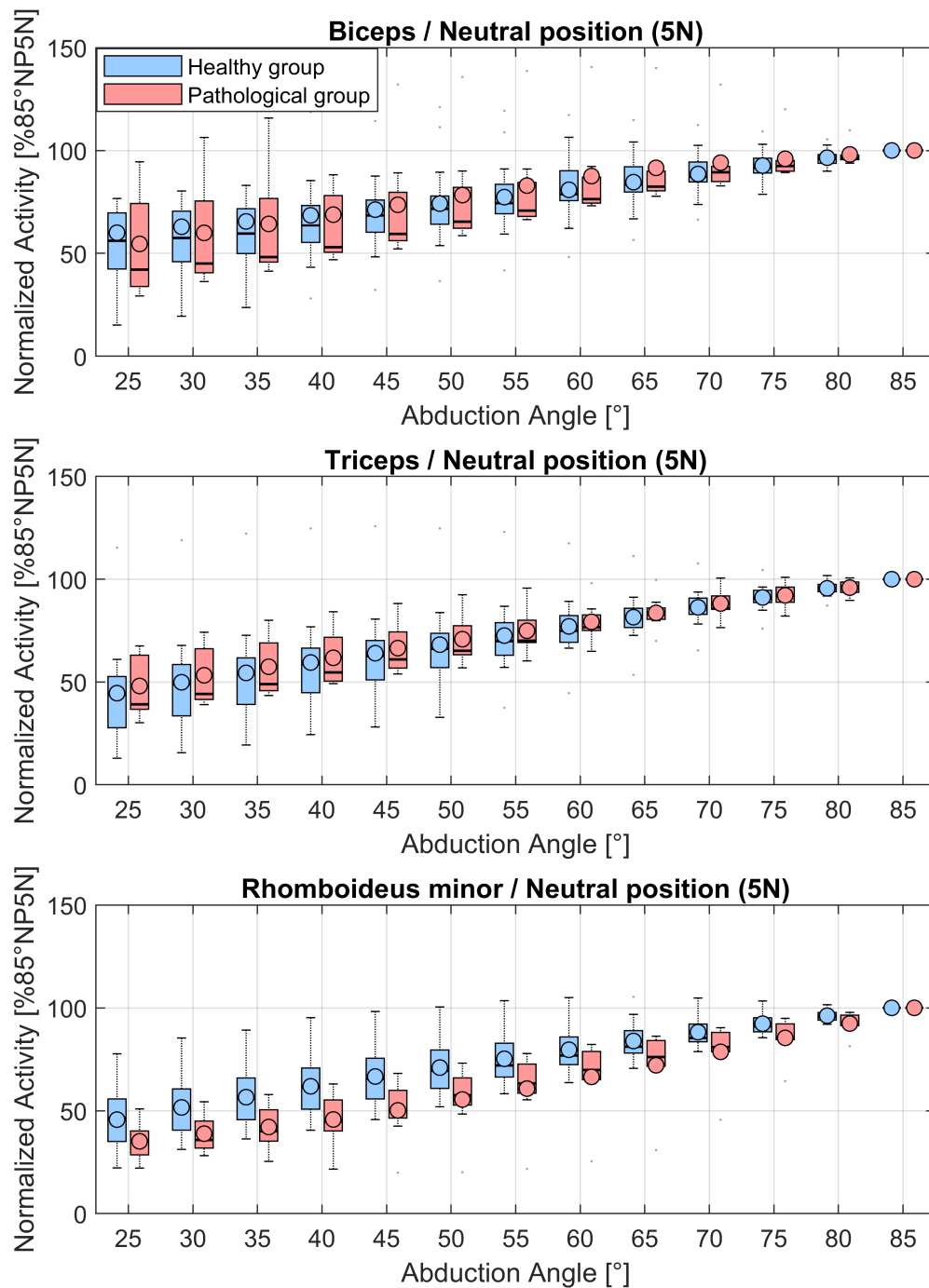


FIGURE C.64: EMG muscle activities normalized to the 85° position of the neutral position trial with 5 N load in hand of the biceps, triceps and rhomboideus minor over the abduction angle in 5° increments during the neutral position trial with 5 N load in hand. Blue depicts the EMG activities of the healthy subject group and red of the patient group.

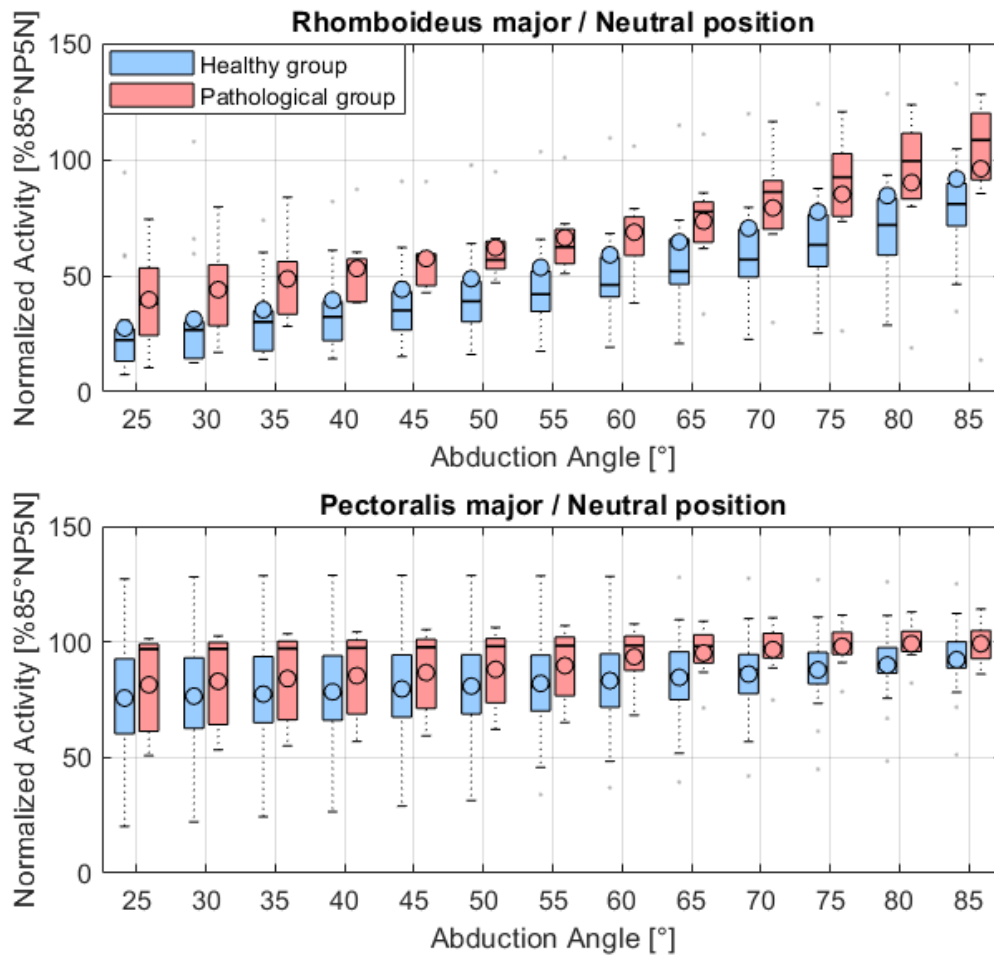


FIGURE C.65: EMG muscle activities normalized to the 85° position of the neutral position trial with 5 N load in hand of the rhomboideus major and pectoralis major over the abduction angle in 5° increments during the neutral position trial with 5 N load in hand. Blue depicts the EMG activities of the healthy subject group and red of the patient group.

Internal rotation

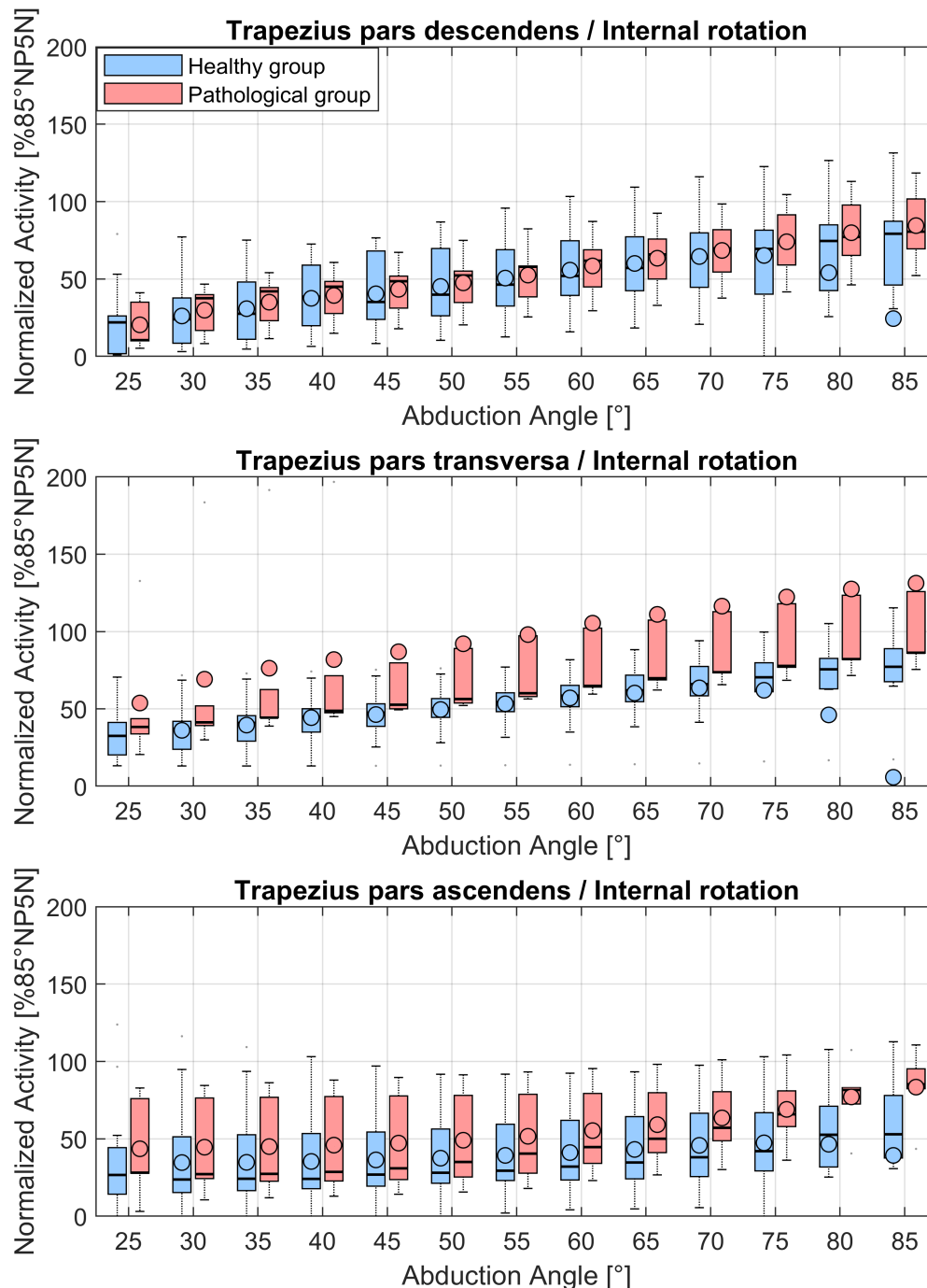


FIGURE C.66: EMG muscle activities normalized to the 85° position of the neutral position trial with 5 N load in hand of the trapezius pars descendens, trapezius pars transversa and trapezius pars ascendens over the abduction angle in 5° increments during the internal rotation trial. Blue depicts the EMG activities of the healthy subject group and red of the patient group.

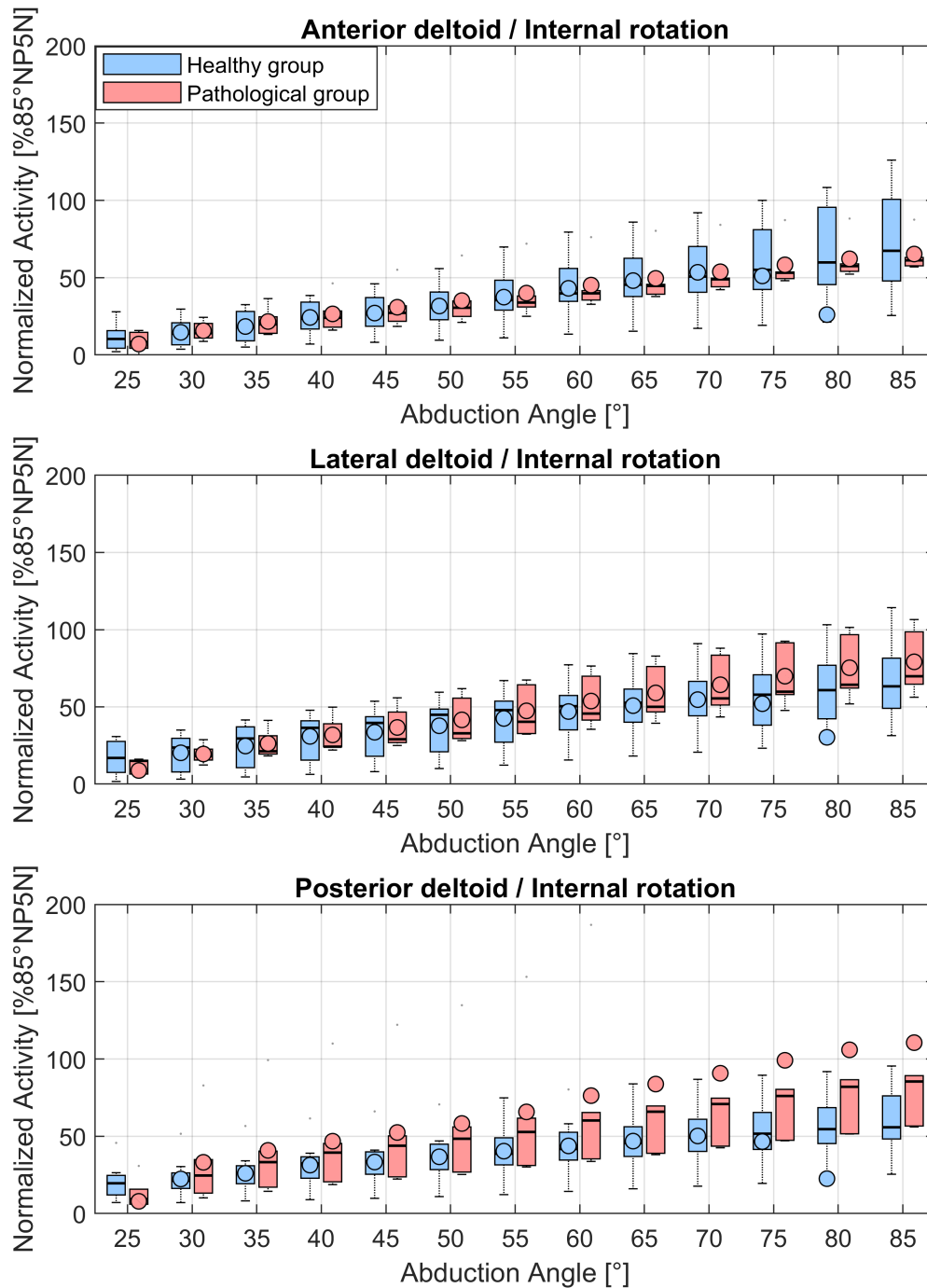


FIGURE C.67: EMG muscle activities normalized to the 85° position of the neutral position trial with 5 N load in hand of the anterior deltoid, lateral deltoid and posterior deltoid over the abduction angle in 5° increments during the internal rotation trial. Blue depicts the EMG activities of the healthy subject group and red of the patient group.

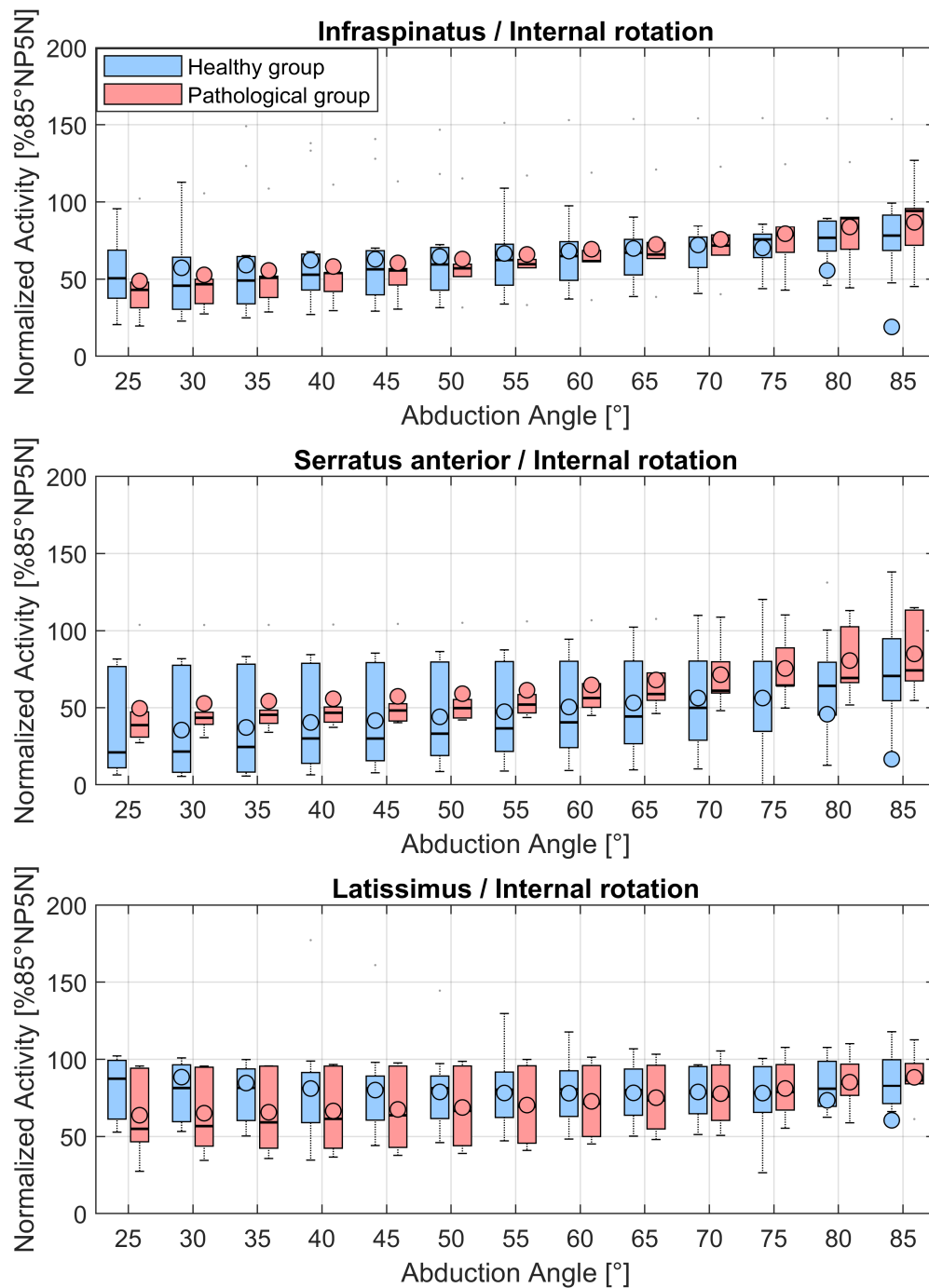


FIGURE C.68: EMG muscle activities normalized to the 85° position of the neutral position trial with 5 N load in hand of the infraspinatus, serratus anterior and latissimus over the abduction angle in 5° increments during the internal rotation trial. Blue depicts the EMG activities of the healthy subject group and red of the patient group.

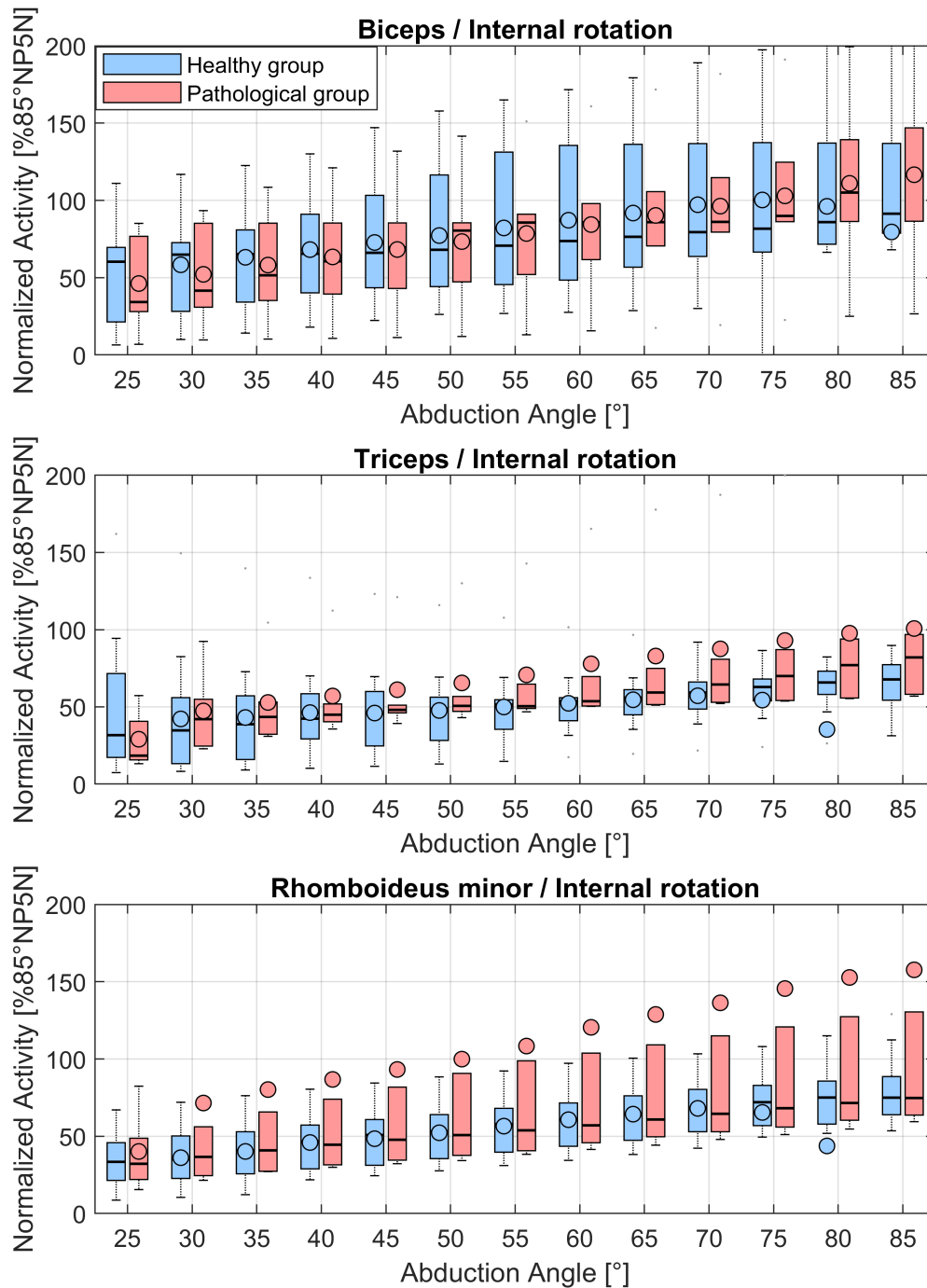


FIGURE C.69: EMG muscle activities normalized to the 85° position of the neutral position trial with 5 N load in hand of the biceps, triceps and rhomboideus minor over the abduction angle in 5° increments during the internal rotation trial. Blue depicts the EMG activities of the healthy subject group and red of the patient group.

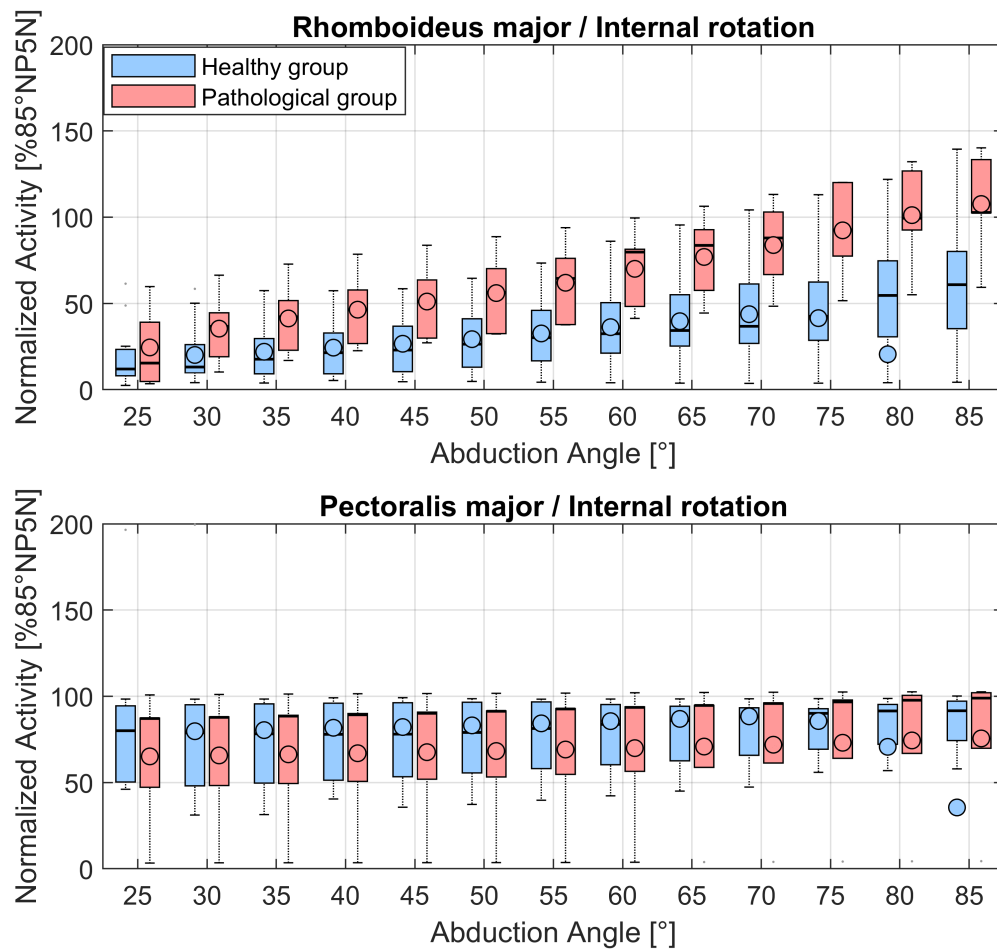


FIGURE C.70: EMG muscle activities normalized to the 85° position of the neutral position trial with 5 N load in hand of the rhomboideus major and pectoralis major over the abduction angle in 5° increments during the internal rotation trial. Blue depicts the EMG activities of the healthy subject group and red of the patient group.

External rotation

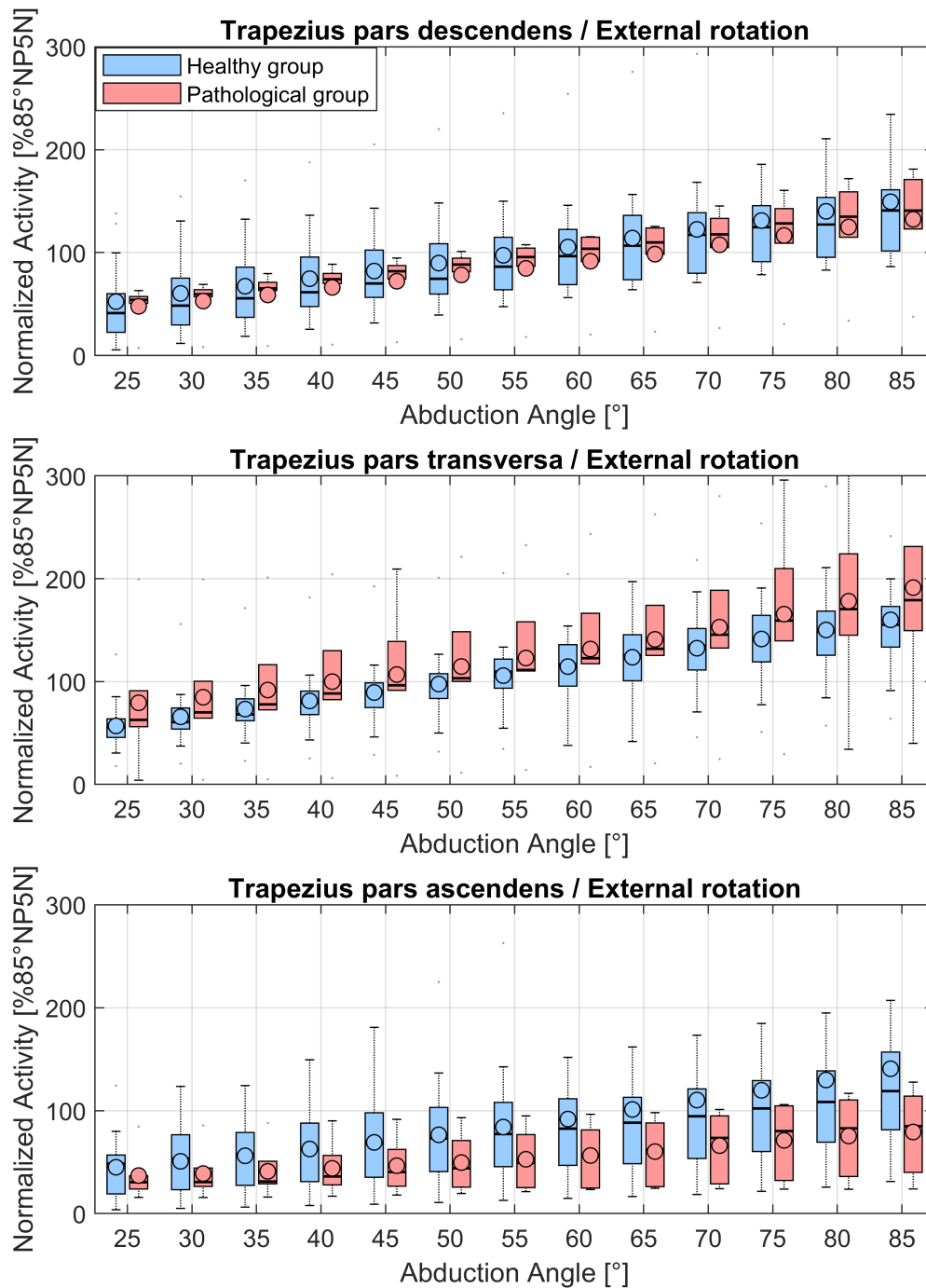


FIGURE C.71: EMG muscle activities normalized to the 85° position of the neutral position trial with 5 N load in hand of the trapezius pars descendens, trapezius pars transversa and trapezius pars ascendens over the abduction angle in 5° increments during the external rotation trial. Blue depicts the EMG activities of the healthy subject group and red of the patient group.

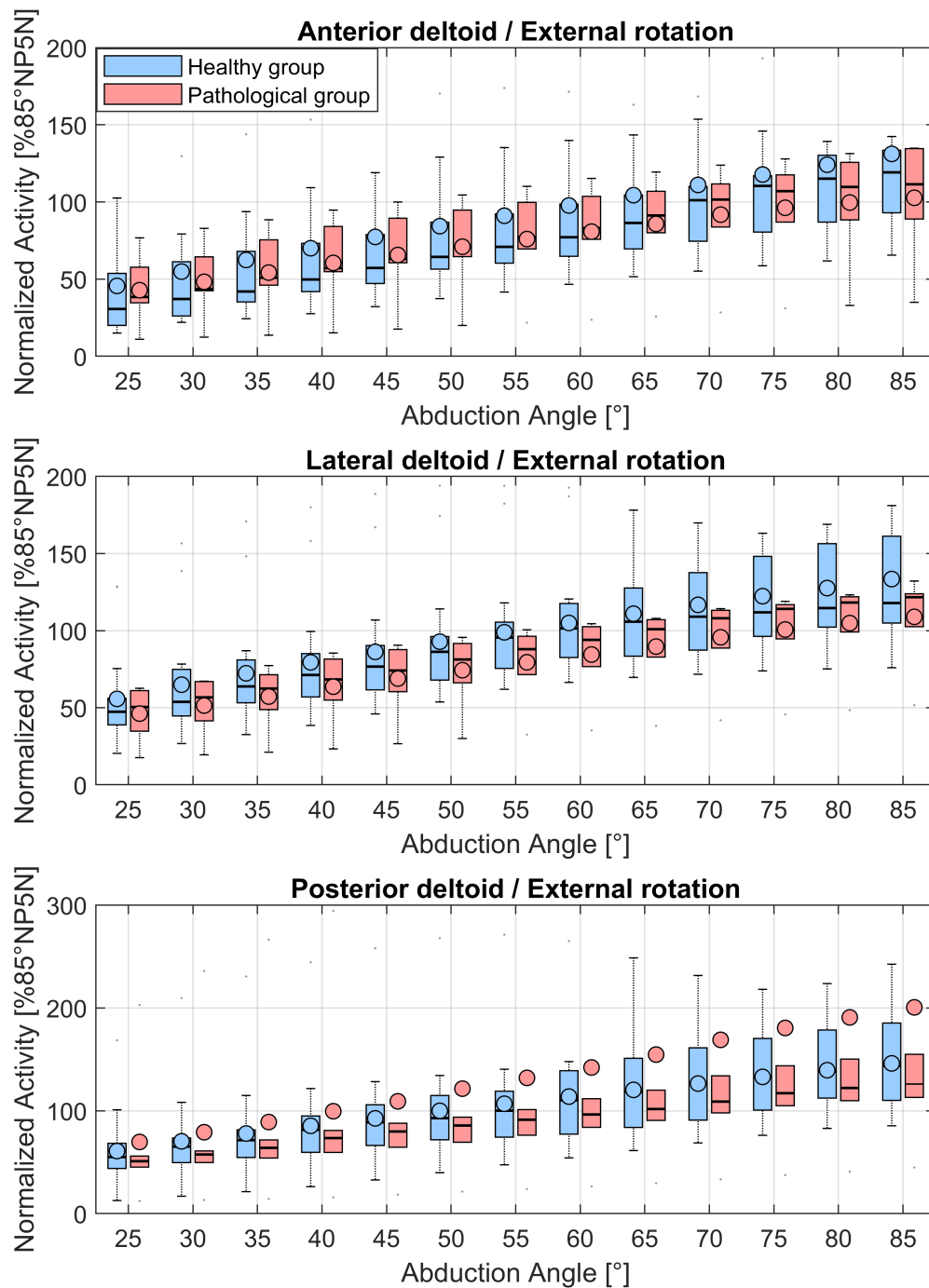


FIGURE C.72: EMG muscle activities normalized to the 85° position of the neutral position trial with 5 N load in hand of the anterior deltoid, lateral deltoid and posterior deltoid over the abduction angle in 5° increments during the external rotation trial. Blue depicts the EMG activities of the healthy subject group and red of the patient group.

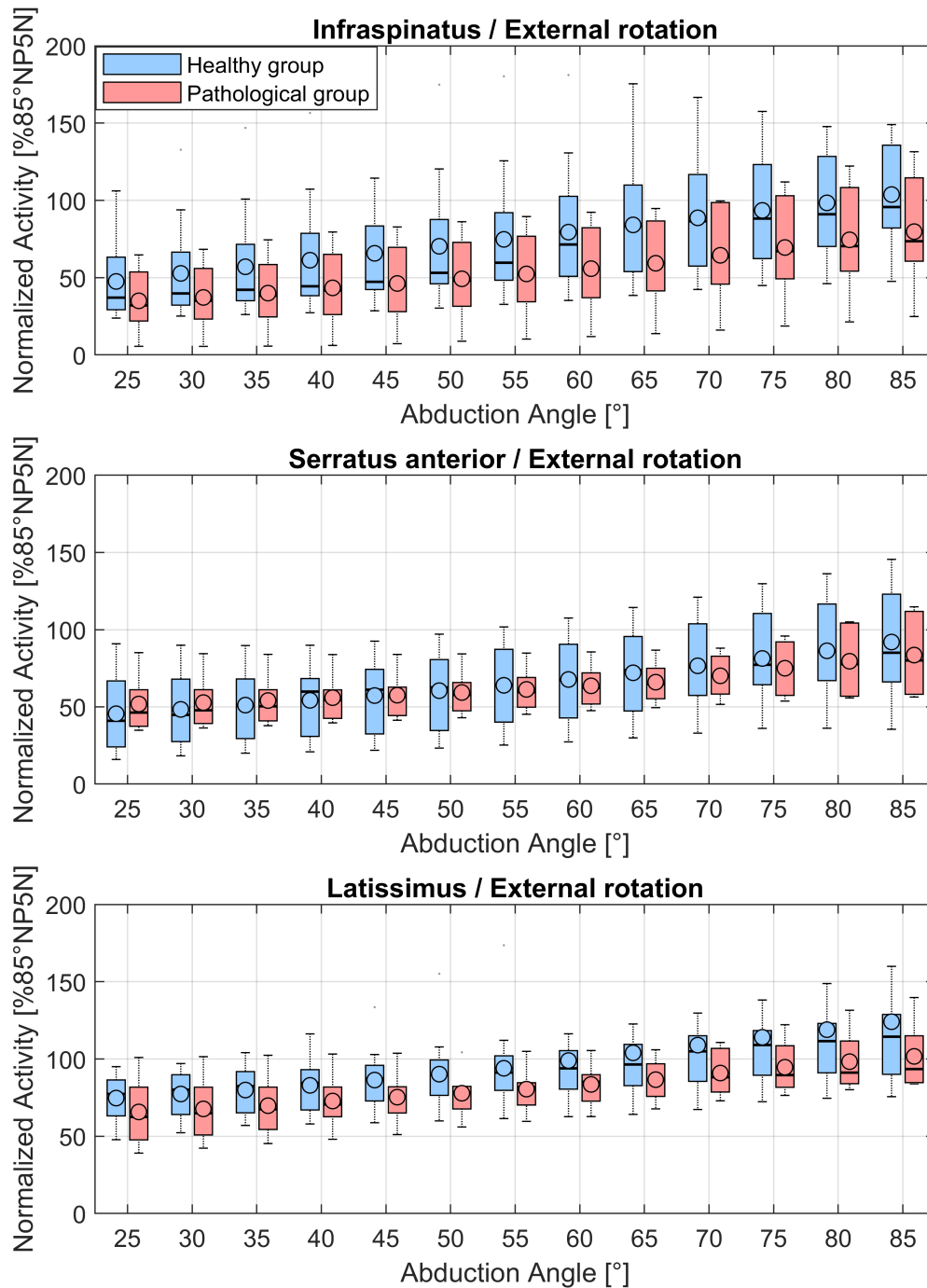


FIGURE C.73: EMG muscle activities normalized to the 85° position of the neutral position trial with 5 N load in hand of the infraspinatus, serratus anterior and latissimus over the abduction angle in 5° increments during the external rotation trial. Blue depicts the EMG activities of the healthy subject group and red of the patient group.

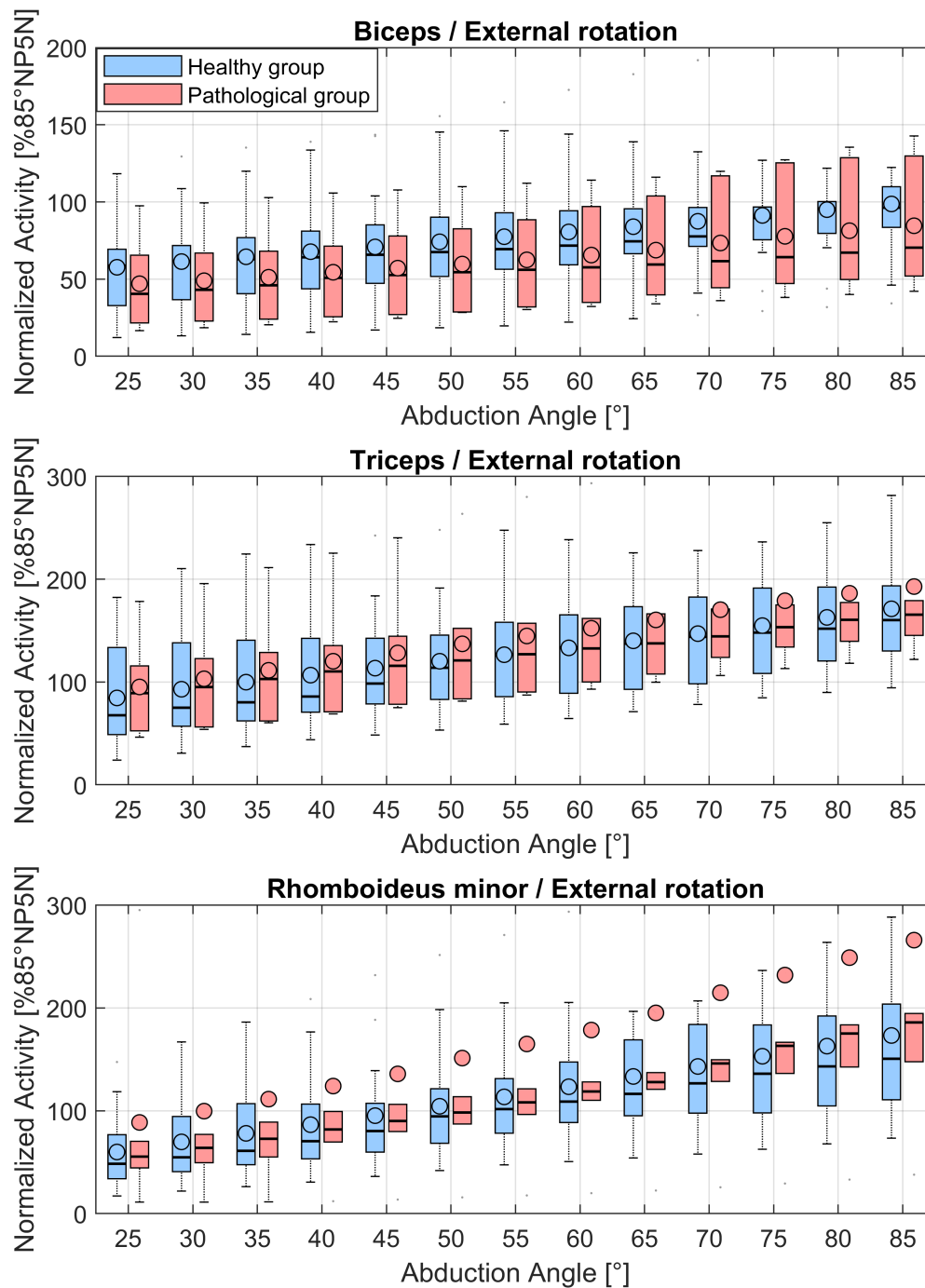


FIGURE C.74: EMG muscle activities normalized to the 85° position of the neutral position trial with 5 N load in hand of the biceps, triceps and rhomboideus minor over the abduction angle in 5° increments during the external rotation trial. Blue depicts the EMG activities of the healthy subject group and red of the patient group.

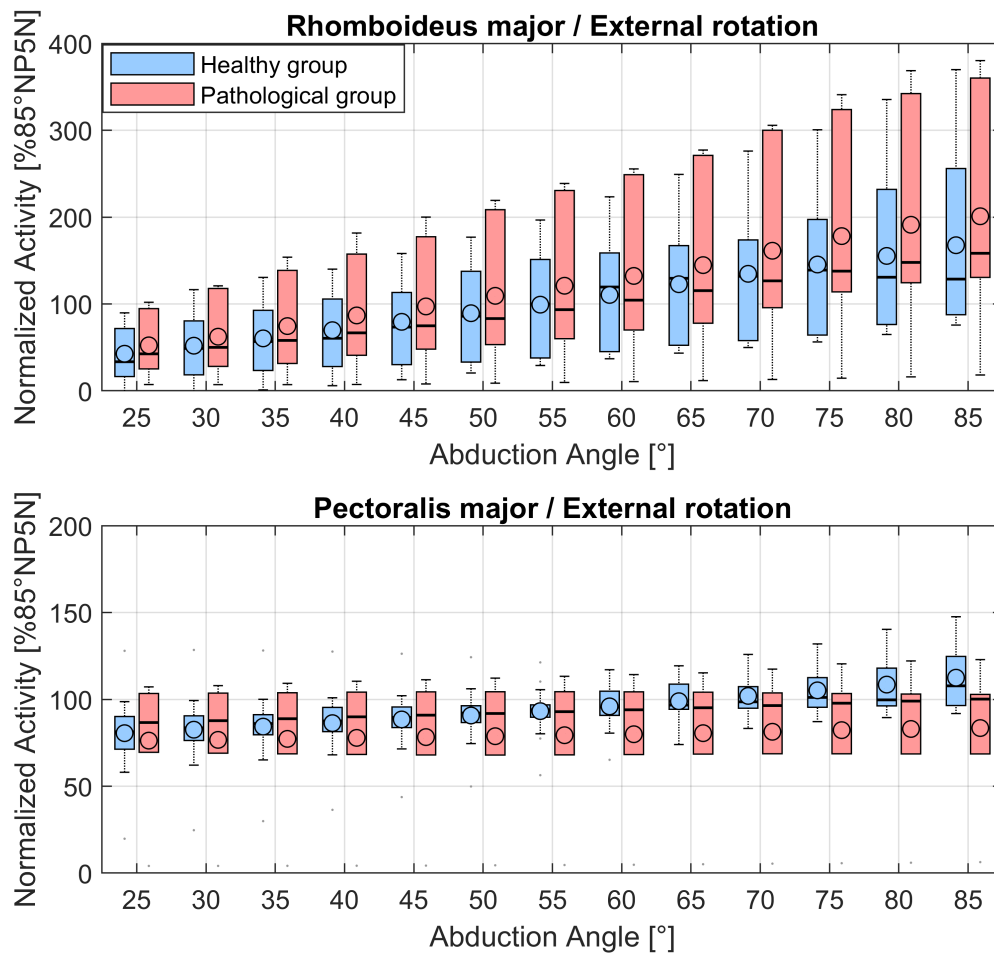


FIGURE C.75: EMG muscle activities normalized to the 85° position of the neutral position trial with 5 N load in hand of the rhomboideus major and pectoralis major over the abduction angle in 5° increments during the external rotation trial. Blue depicts the EMG activities of the healthy subject group and red of the patient group.

External rotation 5N in hand

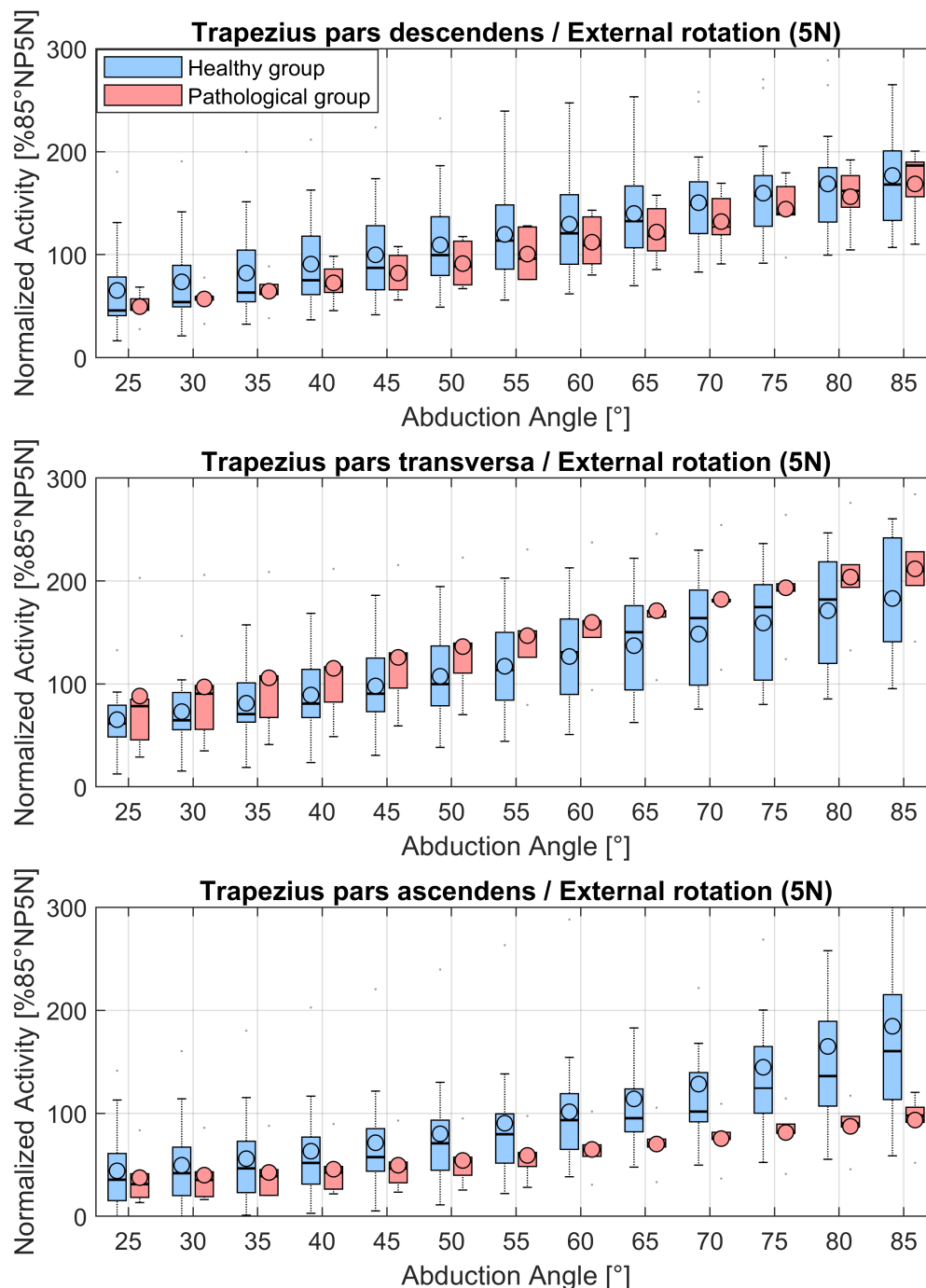


FIGURE C.76: EMG muscle activities normalized to the 85° position of the neutral position trial with 5 N load in hand of the trapezius pars descendens, trapezius pars transversa and trapezius pars ascendens over the abduction angle in 5° increments during the external rotation trial with 5 N load in hand. Blue depicts the EMG activities of the healthy subject group and red of the patient group.

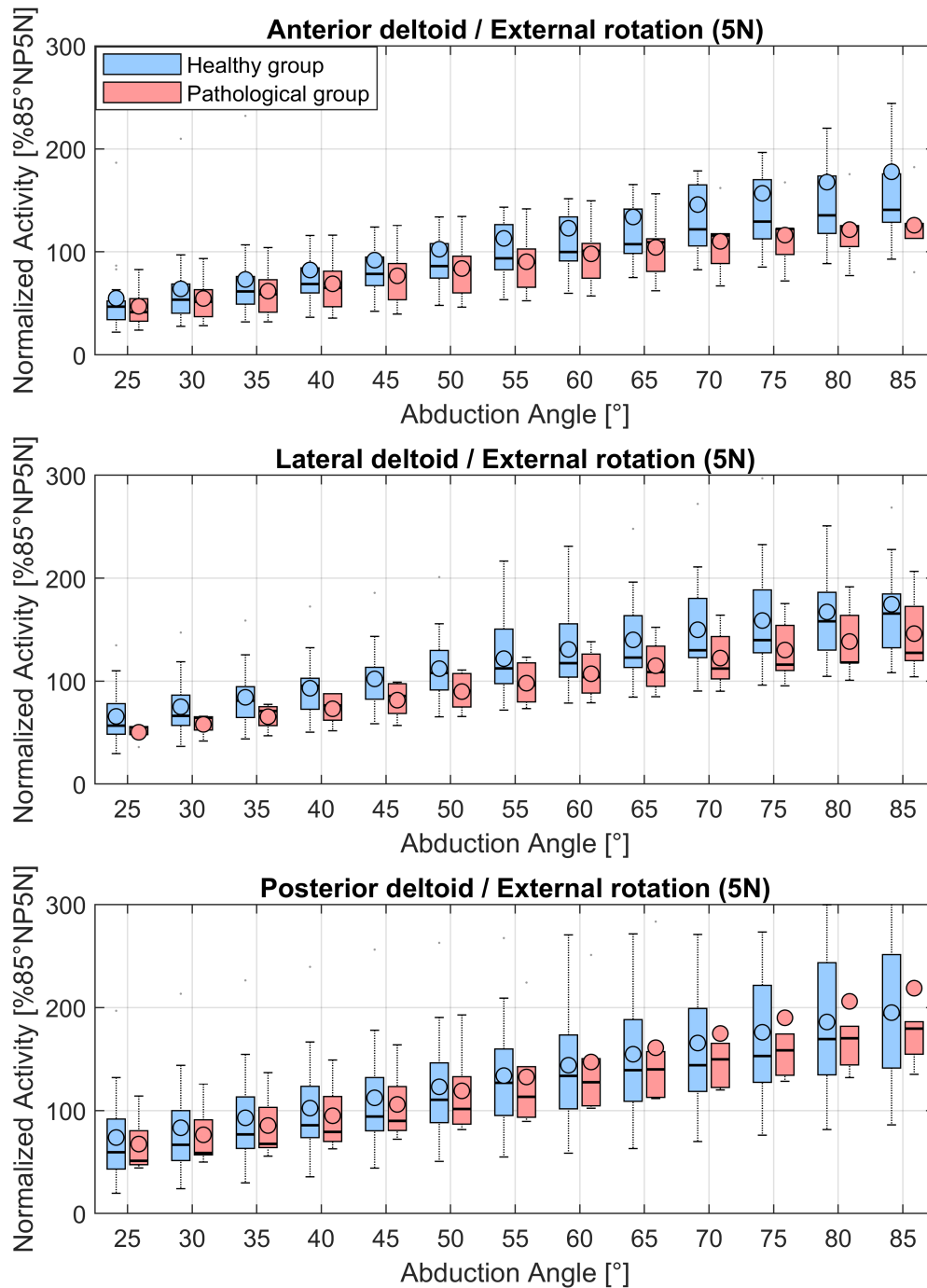


FIGURE C.77: EMG muscle activities normalized to the 85° position of the neutral position trial with 5 N load in hand of the anterior deltoid, lateral deltoid and posterior deltoid over the abduction angle in 5° increments during the external rotation trial with 5 N load in hand. Blue depicts the EMG activities of the healthy subject group and red of the patient group.

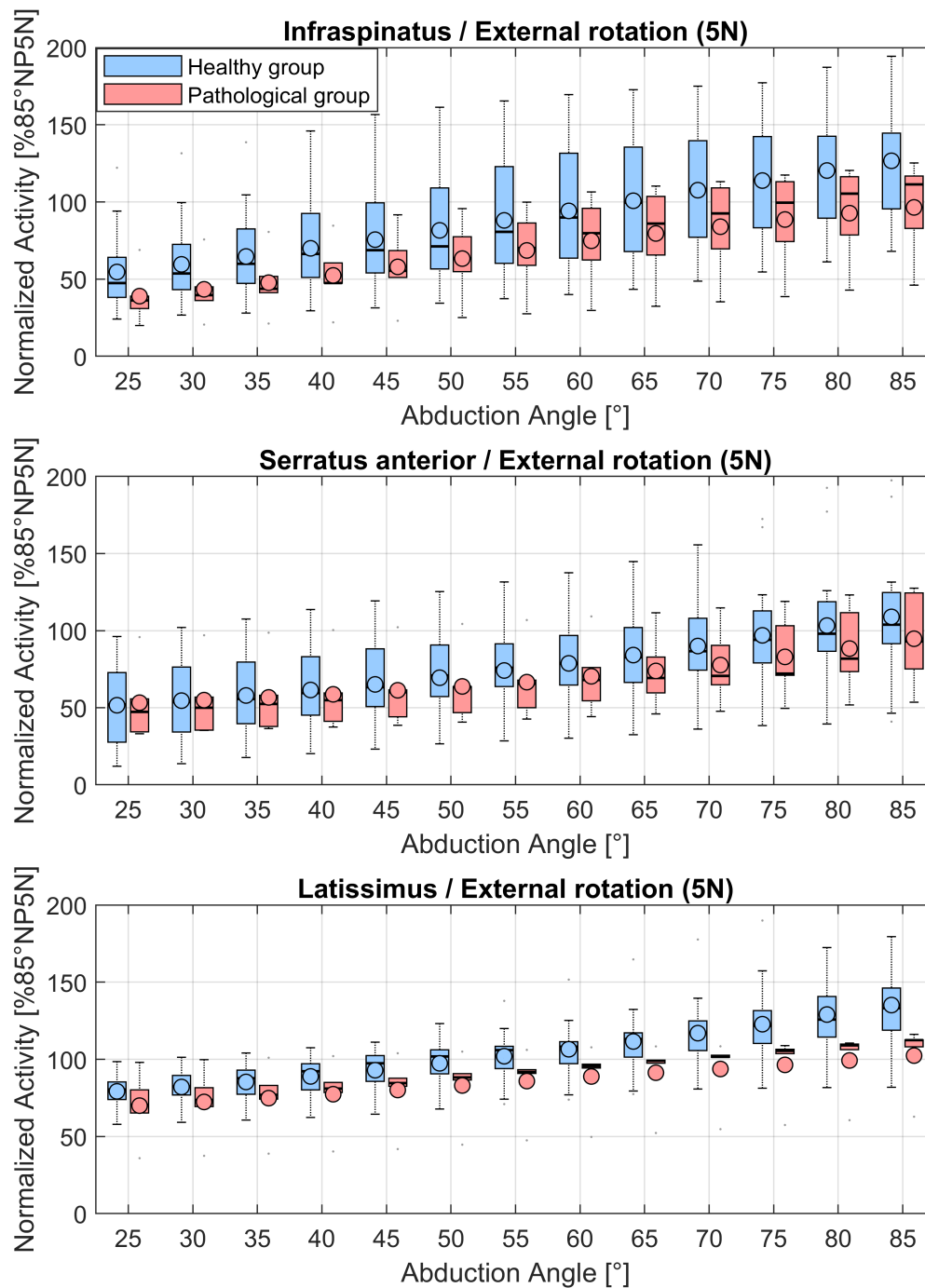


FIGURE C.78: EMG muscle activities normalized to the 85° position of the neutral position trial with 5 N load in hand of the infraspinatus, serratus anterior and latissimus over the abduction angle in 5° increments during the external rotation trial with 5 N load in hand. Blue depicts the EMG activities of the healthy subject group and red of the patient group.

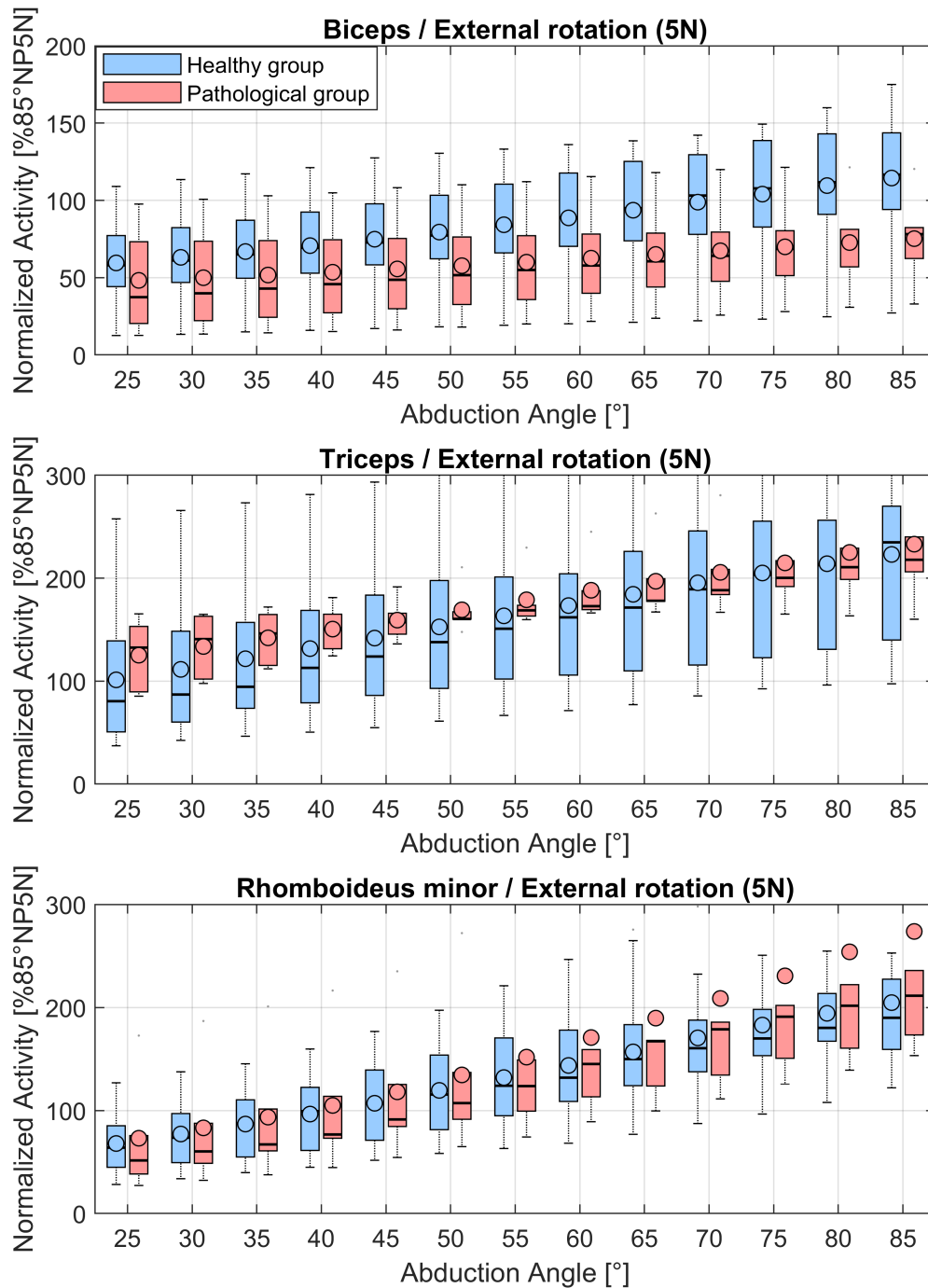


FIGURE C.79: EMG muscle activities normalized to the 85° position of the neutral position trial with 5 N load in hand of the biceps, triceps and rhomboideus minor over the abduction angle in 5° increments during the external rotation trial with 5 N load in hand. Blue depicts the EMG activities of the healthy subject group and red of the patient group.

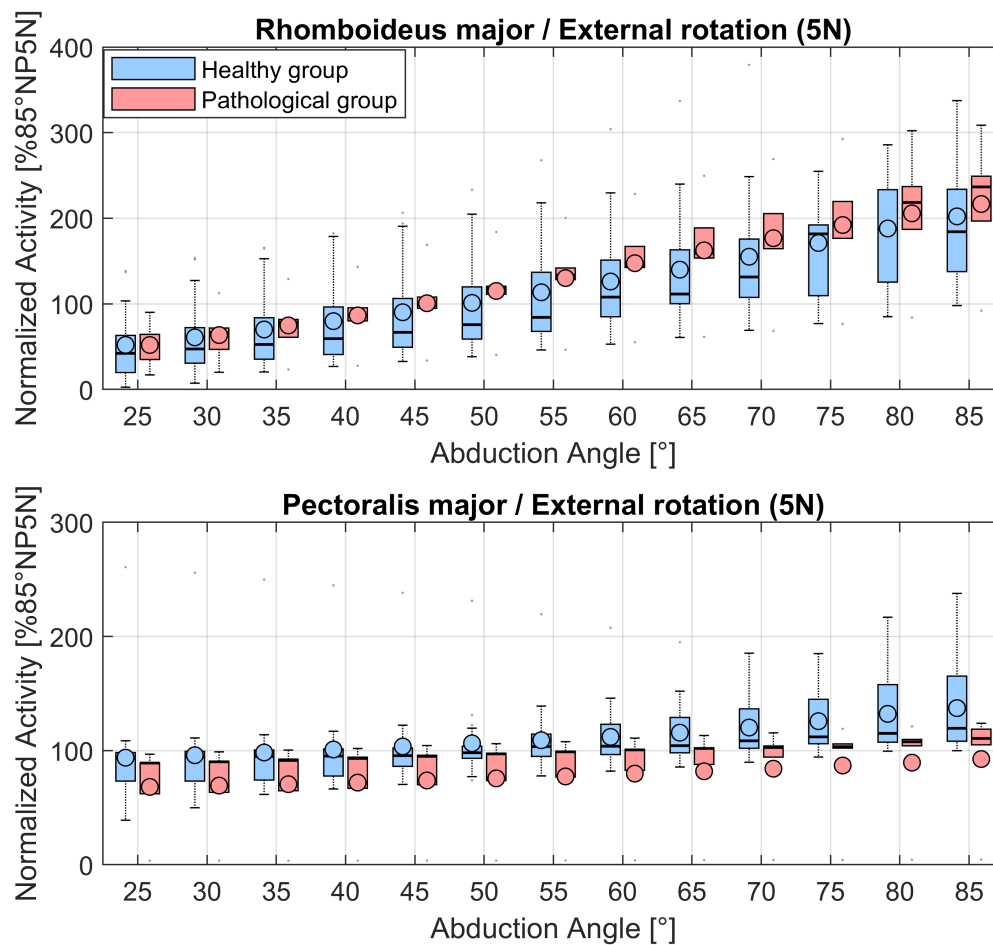


FIGURE C.80: EMG muscle activities normalized to the 85° position of the neutral position trial with 5 N load in hand of the rhomboideus major and pectoralis major over the abduction angle in 5° increments during the external rotation trial with 5 N load in hand. Blue depicts the EMG activities of the healthy subject group and red of the patient group.

C.0.8 Median differences in the EMG between the healthy and pathological group

Neutral position

Abduction [°]	TD [%85°]	TT [%85°]	TA [%85°]	AD [%85°]	LD [%85°]	PD [%85°]	INF [%85°]	SER [%85°]	LAT [%85°]	BIC [%85°]	TRI [%85°]	RMA [%85°]	RMI [%85°]	PEC [%85°]
25	-5.2	7.7	14.3	17.2*	7.5	2.7	1.3	17.0	-4.7	-8.7	19.8	15.6	5.5	21.5
30	-5.6	8.7	16.1	18.5*	8.3	1.8	-0.2	15.1	-4.1	-7.7	16.5	18.3	5.2	21.0
35	-4.9	10.4	16.6	16.9*	7.9	4.4	0.3	13.6	-3.0	-7.8	13.0	19.6	-1.9	20.4
40	-3.8	15.0	15.4	15.1*	7.5	5.2	3.7	11.9	-3.0	-4.8	9.9	21.9*	-6.8	19.8
45	-2.9	16.0	13.7	12.4*	6.9	5.9	4.7	11.6	-2.6	-1.2	6.5	23.3*	-9.2	18.8
50	-0.7	15.8	11.3	11.9*	7.4	5.9	4.1	11.9	-2.3	1.9	4.7	17.8*	-6.9	18.4
55	-3.6	16.1	7.2	10.2	8.1	5.8	2.0	11.4	-2.4	1.4	8.5	20.3*	-6.4	17.5
60	-5.0	18.7	1.5	20.0	9.1	11.2	-0.8	10.2	2.6	1.1	11.5	23.4	-6.2	15.7
65	-5.7	21.6	-0.1	19.4	11.3	10.9	0.7	9.5	3.3	1.4	14.4	25.7	-6.0	12.4
70	-3.1	19.7	3.7	15.6	10.9	11.9	-0.5	9.9	3.6	0.2	17.6	29.1	-1.8	10.0
75	-0.9	17.9	10.6	9.0	12.0	10.6	-2.7	9.1	2.9	-1.9	20.7*	29.1	4.8	10.0
80	3.8	19.6	14.3	3.4	14.7*	10.2	-3.2	7.6	3.6	-6.7	21.3*	27.5	9.0	7.6
85	3.6	19.1	15.6	1.8	10.6*	13.1	-3.9	6.3	7.4	-7.6	23.4*	27.6	12.7	7.6

TABLE C.11: Differences in median values of EMG activities normalized to the 85° position of the neutral position trial with 5 N load in hand between the healthy subject cohort and patient group during the neutral position trial in 5° increments. Asterisks indicate the significance level. TD = trapezius descendens, TT = trapezius transversa, TA = trapezius ascendens, AD = anterior deltoid, LD = lateral deltoid, PD = posterior deltoid, INF = infraspinatus, SER = serratus anterior, LAT = latissimus, BIC = biceps, TRI = triceps, RMA = rhomboideus major, RMI = rhomboideus minor, PEC = pectoralis major

Neutral position 5N in hand

Abduction [°]	TD [%85°]	TT [%85°]	TA [%85°]	AD [%85°]	LD [%85°]	PD [%85°]	INF [%85°]	SER [%85°]	LAT [%85°]	BIC [%85°]	TRI [%85°]	RMA [%85°]	RMI [%85°]	PEC [%85°]
25	-12.0	3.1	8.2	8.7	-1.1	-1.6	0.9	0.7	-4.5	-14.0	-4.6	0.6	-11.1	14.3
30	-8.6	3.5	9.7	11.0	-2.8	2.6	3.0	-1.2	-2.4	-12.4	-4.8	2.5	-16.1*	13.4
35	-9.2	2.5	6.8	12.6	-3.9	2.0	1.6	-4.4	-2.0	-11.4	-4.9	2.2	-15.8*	12.5
40	-9.7	2.5	1.3	13.5	-4.2	0.8	0.1	-6.6	-1.3	-10.5	-4.0	1.1	-16.6*	10.5
45	-10.4	3.4	-1.4	12.9	-7.3	1.3	1.8	-6.8	-0.6	-9.0	-1.6	1.2	-15.1*	8.5
50	-10.6	4.5	0.2	11.1	-8.7	1.0	2.0	-7.6	0.3	-6.3	-1.0	3.3	-11.9	6.4
55	-11.1	2.1	1.2	10.9	-7.9	1.2	2.3	-8.0	0.2	-3.7	0.2	3.9	-8.7	4.9
60	-8.5	3.2	-1.2	11.6	-7.6	-0.2	1.9	-8.3	0.0	-2.4	1.7	4.0	-7.1	6.2
65	-6.5	-0.5	-2.5	11.2	-7.5	-0.5	1.8	-8.5	-0.1	-1.0	0.8	2.4	-5.0	4.4
70	-5.1	-0.9	-3.3	10.4	-2.3	-1.1	1.6	-6.8	-1.2	2.2	-0.7	1.4	-4.4	3.3
75	-5.4	-0.7	-4.5	8.0	-1.8	-2.7	-0.3	-5.9	-1.9	0.8	1.4	-1.7	-5.9	1.7
80	-3.5	-0.4	-2.8	4.7	-0.9	-1.8	-0.8	-4.3	-0.5	0.2	0.9	-2.0	-4.1	0.5
85	0.0	0.0	0.0	0.0	0.0	0.0	0.0	0.0	0.0	0.0	0.0	0.0	0.0	0.0

TABLE C.12: Differences in median values of EMG activities normalized to the 85° position of the neutral position trial with 5 N load in hand between the healthy subject cohort and patient group during the neutral position trial with 5 N load in hand in 5° increments. Asterisks indicate the significance level. TD = trapezius descendens, TT = trapezius transversa, TA = trapezius ascendens, AD = anterior deltoid, LD = lateral deltoid, PD = posterior deltoid, INF = infraspinatus, SER = serratus anterior, LAT = latissimus, BIC = biceps, TRI = triceps, RMA = rhomboideus major, RMI = rhomboideus minor, PEC = pectoralis major

Internal rotation

Abduction	TD	TT	TA	AD	LD	PD	INF	SER	LAT	BIC	TRI	RMA	RMI	PEC
[°]	[%85°]	[%85°]	[%85°]	[%85°]	[%85°]	[%85°]	[%85°]	[%85°]	[%85°]	[%85°]	[%85°]	[%85°]	[%85°]	[%85°]
25	-11.5	5.8	1.5	-2.0	-1.9	-10.2	-7.5	17.7	-32.5	-26.1	-13.3	3.4	-1.3	7.1
30	13.6	4.3	3.5	0.2	-5.5	3.3	1.0	21.9	-24.7	-23.3	7.3	23.6	1.6	9.0
35	14.5	3.4	3.1	1.9	-8.2	7.1	1.7	20.9	-22.3	-13.6	4.7	24.6	0.10	10.3
40	6.5	3.9	4.5	0.7	-12.2	7.0	1.1	16.7	-20.0	-4.9	2.6	24.9*	-2.1	11.3
45	13.4	5.1	4.0	0.9	-10.6	10.2	-0.7	18.2	-17.4	3.5	2.4	28.1*	-3.1	12.1
50	12.4	6.0	7.0	0.0	-12	11.7	-2.5	16.6	-14.7	12.4	1.8	30.0*	-2.4	12.3
55	11.5	5.8	11.1	-1.6	-7.6	14.1	-2.7	15.4	-10.9	15.0	-1.1	34.3*	-4.0	11.3
60	9.8	6.3	12.6	0.1	-4.8	18.5	-3.3	15.8	-9.3	12.1	0.0	47.3*	-4.1	9.8
65	8.7	7.8	15.3	-0.8	-2.6	20.3	-1.2	14.5	-6.6	9.5	3.3	49.3*	-3.5	8.7
70	6.2	7.7	19.0	-1.8	0.6	21.7	0.0	11.1	-2.6	6.6	5.2	51.2*	-3.8	7.8
75	4.1	7.3	23.8	-1.9	1.9	24.4	2.8	7.9	0.4	8.3	7.1	50.0**	-3.9	6.6
80	2.6	6.6	29.0	-2.4	3.5	27.4	12.7	5.1	2.5	19.1	11.2	44.8**	-3.5	6.2
85	1.3	9.1	32.3	-6.2	6.5	29.6	15.9	3.6	3.4	24.7	14.3	41.9*	-0.20	7.3

TABLE C.13: Differences in median values of EMG activities normalized to the 85° position of the neutral position trial with 5 N load in hand between the healthy subject cohort and patient group during the internal rotation trial in 5° increments. Asterisks indicate the significance level. TD = trapezius descendens, TT = trapezius transversa, TA = trapezius ascendens, AD = anterior deltoid, LD = lateral deltoid, PD = posterior deltoid, INF = infraspinatus, SER = serratus anterior, LAT = latissimus, BIC = biceps, TRI = triceps, RMA = rhomboideus major, RMI = rhomboideus minor, PEC = pectoralis major

External rotation

Abduction [°]	TD [%85°]	TT [%85°]	TA [%85°]	AD [%85°]	LD [%85°]	PD [%85°]	INF [%85°]	SER [%85°]	LAT [%85°]	BIC [%85°]	TRI [%85°]	RMA [%85°]	RMI [%85°]	PEC [%85°]
25	12.9	7.5	-18.0	7.8	3.1	-4.1	-5.0	5.3	-14.9	-18.2	21.5	9.1	7.0	5.3
30	11.1	9.4	-22.8	6.5	2.9	-7.6	-4.7	3.0	-15.2	-18.7	20.1	1.2	9.2	4.1
35	9.6	9.7	-26.7	8.9	-1.4	-7.5	-3.8	-0.50	-15.0	-16.9	22.7	1.3	11.7	2.7
40	12.7	9.0	-26.1	7.3	-2.9	-8.0	-2.7	-5.6	-14.	-13.3	24.4	6.2	11.4	2.3
45	11.9	6.0	-27.7	5.8	-2.6	-8.9	-2.5	-4.7	-12.4	-13.1	17.2	1.5	9.8	1.3
50	13.8	4.0	-29.0	6.7	-5.0	-7.2	-5.1	-4.9	-11.3	-13.0	7.1	-2.7	3.8	-0.3
55	9.4	1.7	-28.1	6.4	-7.6	-8.8	-7.9	-4.6	-9.4	-13.4	0.4	-6.6	6.5	-1.1
60	7.2	6.0	-26.3	6.0	-7.4	-13.9	-15.7	-5.0	-8.7	-14.1	-0.8	-15.1	9.8	-1.5
65	3.1	6.0	-26.0	4.9	-4.9	-16.6	-23.8	-9.1	-9.7	-15.0	0.3	-14.2	11.4	-1.5
70	0.4	10.6	-21.0	0.40	-1.0	-17.6	-23.1	-5.6	-16.8	-16.0	0.5	-5.3	19.3	-2.2
75	3.7	17.3	-22.0	-3.4	2.2	-15.7	-21.1	-1.8	-19.5	-25.4	5.3	-1.2	27.1	-3.3
80	7.7	22.1	-25.6	-5.4	3.6	-16.2	-20.6	-8.3	-20.4	-28.6	8.6	17.1	32.0	-0.7
85	0.0	23.9	-34.0	-7.7	3.8	-18.2	-22.1	-5.0	-20.9	-25.9	5.3	29.7	35.3	-7.6

TABLE C.14: Differences in median values of EMG activities normalized to the 85° position of the neutral position trial with 5 N load in hand between the healthy subject cohort and patient group during the external rotation trial in 5° increments. Asterisks indicate the significance level. TD = trapezius descendens, TT = trapezius transversa, TA = trapezius ascendens, AD = anterior deltoid, LD = lateral deltoid, PD = posterior deltoid, INF = infraspinatus, SER = serratus anterior, LAT = latissimus, BIC = biceps, TRI = triceps, RMA = rhomboideus major, RMI = rhomboideus minor, PEC = pectoralis major

External rotation 5N in hand

Abduction [°]	TD [%85°]	TT [%85°]	TA [%85°]	AD [%85°]	LD [%85°]	PD [%85°]	INF [%85°]	SER [%85°]	LAT [%85°]	BIC [%85°]	TRI [%85°]	RMA [%85°]	RMI [%85°]	PEC [%85°]
25	2.4	16.9	-4.3	-5.3	-1.6	-8.3	-11.3	-4.8	-9.9	-20.6	52.1	11.2	-12.4	-4.0
30	5.2	25.9	-6.6	-2.0	-1.8	-8.0	-14.0	-3.6	-8.8	-21.2	53.8	19.3	-13.3	-4.3
35	0.2	33.8	-7.6	-2.7	-10.0	-9.2	-16.2	-3.2	-10.8	-22.1	51.8	26.2	-20.3	-3.4
40	-5.4	35.1	-9.3	-3.7	-19.1	-6.5	-18.9	-4.6	-11.2	-23.5	37.7	26.8	-22.6	-2.0
45	-5.7	37.8	-11.0	-2.5	-17.0	-4.3	-13.4	-3.2	-12.8	-24.1	33.3	31.4	-15.4	-0.6
50	-11.1	38.4	-17.6	-3.6	-17.3	-8.9	-7.8	-7.3	-13.6	-25.6	22.5	43.2	-8.3	-1.0
55	-17.5	33.4	-20.0	-4.3	-16.5	-13.6	-10.4	-10.4	-14.2	-28.3	17.8	49.4	-0.4	-4.6
60	-11.6	30.3	-28.7	1.2	-13.6	-6.2	-10.2	-10.6	-12.5	-31.0	10.9	36.3	13.3	-3.2
65	-14.5	19.6	-25.2	1.9	-14.1	0.8	-13.5	-13.4	-14.1	-34.4	6.6	47.7	17.3	-2.4
70	-22.1	16.3	-26.5*	-6.0	-17.8	5.7	-15.8	-16.0	-15.6*	-39.0	-0.9	44.7	18.3	-5.8
75	-17.4	16.8	-43.6*	-7.1	-23.8	5.5	-14.8	-21.9	-16.2*	-39.2	-3.1	13.4	21.1	-8.6
80	-4.7	19.1	-45.9*	-10.5	-40.0	0.8	-14.8	-16.2	-16.7*	-38.7	-2.1	31.4	21.5	-7.4
85	18.5	28.1	-62.5*	-14.7	-38.2	-13.3	-15.4	-10.9	-20.7*	-38.5*	-17.0	52.4	21.4	-8.9

TABLE C.15: Differences in median values of EMG activities normalized to the 85° position of the neutral position trial with 5 N load in hand between the healthy subject cohort and patient group during the external rotation trial with 5 N load in hand in 5° increments. Asterisks indicate the significance level. TD = trapezius descendens, TT = trapezius transversa, TA = trapezius ascendens, AD = anterior deltoid, LD = lateral deltoid, PD = posterior deltoid, INF = infraspinatus, SER = serratus anterior, LAT = latissimus, BIC = biceps, TRI = triceps, RMA = rhomboideus major, RMI = rhomboideus minor, PEC = pectoralis major